Age-related Remodeling is Associated with Altered Cardiac Resident and Circulation-derived Macrophage Phenotype and Function

by

Martin John Haschak

Bachelor of Science, University of Pittsburgh, 2015

Submitted to the Graduate Faculty of the

Swanson School of Engineering in partial fulfillment

of the requirements for the degree of

Doctor of Philosophy

University of Pittsburgh

2021

UNIVERSITY OF PITTSBURGH

SWANSON SCHOOL OF ENGINEERING

This dissertation was presented

by

Martin John Haschak

It was defended on

September 13, 2021

and approved by

Sanjeev Shroff, PhD, Distinguished Professor, Department of Bioengineering

Harvey Borovetz, PhD, Distinguished Professor, Department of Bioengineering

Cecelia Yates, PhD, Associate Professor, Department of Health Promotion and Development

Dissertation Director: Bryan Brown, PhD, Associate Professor, Department of Bioengineering

Age-related Remodeling is Associated with Altered Cardiac Resident and Circulation-derived Macrophage Phenotype and Function

Martin John Haschak, PhD

University of Pittsburgh, 2021

Increased age is associated with an increased risk of cardiovascular disease incidence. This increased risk can be attributed to several processes which occur with increasing age - including an accumulation of intracellular damage, altered resident cell metabolism, increased secretion of cytokines characteristic of the senescence-associated cell phenotype, and altered deposition of matrix proteins within the extracellular microenvironment. Considering the limited regenerative therapeutic availability for heart failure patients coupled with the limited availability of donor organs, understanding the mechanisms by which these processes induce altered cardiac cell function will be important to attenuate the cardiovascular disease risk which faces the aging United States population. Cardiac resident macrophages have been identified as both essential mediators of cardiac homeostasis as well as important regulators of the cardiac tissue remodeling response. Given the numerous changes which occur in the aging cardiac microenvironment coupled with the importance of microenvironmental stimuli in inducing macrophage phenotype, *in vitro* and *in vivo* models of differing cardiac microenvironments were developed to better understand the consequences of this remodeling on cardiac macrophage phenotype and function. Significant alterations in macrophage morphology and function were observed in response to the differing *in vitro* culture conditions, with substrates of increased stiffness promoting increasingly inflammatory functional responses. Additionally, macrophage culture with decellularized cardiac extracellular matrix isolated from aged individuals was found to attenuate macrophage functional

capacity. An *in vivo* model of cardiac microenvironmental remodeling was then developed and flow cytometry was utilized to characterize any changes in cardiac resident macrophage regulation. The developed *in vivo* model was found to recapitulate several hallmark cardiac tissue remodeling features observed in aged individuals, including cardiomyocyte hypertrophy and increased perivascular fibrosis. These microenvironmental alterations were found to promote CX3CR1+ macrophage subset expansion and increased pro-inflammatory CD86 expression in all characterized subsets. Cardiac microenvironmental remodeling was also found to induce increased expression of pro-inflammatory, pro-fibrotic, and stress response-associated genes. Murine echocardiographic assessment also suggested some impaired ventricular relaxation resultant of the experimentally induced cardiac remodeling. These models help elucidate the impact that age-related cardiac microenvironmental biochemical and biomechanical change plays in promoting altered macrophage phenotype and function.

Table of Contents

List of Tables

List of Figures

Preface

I would like to first acknowledge the contributions in mentorship and professional development that Dr. Bryan Brown has provided me during my time working with his laboratory group. I would also like to acknowledge the mentorship provided by my additional dissertation committee members - Dr. Sanjeev Shroff, Dr. Harvey Borovetz, and Dr. Cecelia Yates.

I would like to acknowledge several core facilities which assisted with tissue processing or experimental data collection for the subsequently described studies. First, I would like to acknowledge the McGowan Institute for Regenerative Medicine Histology Core, which assisted with the processing and sectioning of fixed tissue samples for future experimental analysis. I would also like to acknowledge the McGowan Institute for Regenerative Medicine Flow Cytometry Core which assisted with flow cytometry data collection and cytometer training. Finally, I would like to acknowledge Brenda McMahon from the Small Animal Sonography Core at the Vascular Medicine Institute within the University of Pittsburgh School of Medicine who collected murine echocardiographic data and performed the analysis of the acquired images.

I would also like to acknowledge additional sources of mentorship that have aided me in my professional development. I would like to acknowledge Dr. Fabrisia Ambrosio for the undergraduate research opportunity and mentorship which allowed me to successfully transition to my graduate training. I would also like to acknowledge Dr. Rick Shaub for the opportunity to work in the Artificial Heart Program at the University of Pittsburgh Medical Center and for all of the training provided to me within this program. I finally would like to acknowledge past and present members of the Brown lab group, who have helped tremendously with my professional development and with the review of my dissertation work.

Abbreviations and definitions: αSMA = alpha smooth muscle actin, μm = micrometer, ACE = angiotensin converting enzyme, ADAMTS = a disintegrin and metalloprotease with thrombospondin-like motif, AET = aortic ejection time, AGE = advanced glycation end product, Ald = D-Aldosterone, Ald+Salt = D-Aldosterone osmotic minipump and 1% NaCl drinking water experimental treatment, Ald+Salt+BAPN = D-Aldosterone osmotic minipump and 1% NaCl drinking water experimental treatment with BAPN pre-treatment, ANOVA = analysis of variance, Arg = arginase, AV = atrioventricular, BAPN = β-aminopropionitrile, BMP = bone morphogenic protein, Ca = calcium, CCL2 = C-C motif chemokine ligand 2, CCR2 = C-C motif chemokine receptor 2, CCN2 = cellular communication network factor 2 (also known as CTGF), CD163 = high affinity scavenger receptor for hemoglobin-haptoglobin complex, cECM = cardiac extracellular matrix, cMoP = common monocyte progenitor, Col1a1 = collagen type I alpha I, CSF-1R = colony stimulating factor-1 receptor, CTGF = connective tissue growth factor (also known as CCN2), CVD = cardiovascular disease, CX3CR1 = C-X3-C motif chemokine receptor 1, DAMP = damage-associated molecular pattern, DAPI = 4',6-diamidino-2-phenylindole nuclear stain, DC = dendritic cell, DNA= deoxyribonucleic acid, DCP = dendritic cell precursor, ECM = extracellular matrix, EGF = epidermal growth factor, EMP = erythromyeloid progenitor, FGF2 = fibroblast growth factor 2, Gapdh = glyceraldehyde 3-phosphate dehydrogenase, GCS = global circumferential strain, GLS = global longitudinal strain, IFN-γ = interferon-gamma, IGF-1 = insulin-like growth factor 1, IIS = insulin and insulin-like growth factor 1 signaling, IL-1β = interleukin 1 beta, IL-4 = interleukin-4, IL-6 = interleukin-6, iNOS = inducible nitric oxide synthase protein, IQR = interquartile range, IVRT = isovolumic relaxation time, kPA = kilopascals, LAP = latency associated protein, LOX = lysyl oxidase, LPS = lipopolysaccharide, LV = left ventricle, LVAD = left ventricular assist device, LVAW = left

ventricular anterior wall, LVFW = left ventricular free wall, LVPW = left ventricular posterior wall, LYVE1 = lymphatic vessel endothelial hyaluronan receptor 1, MCP-1 = monocyte chemoattractant protein-1, MDP = macrophage-DC precursor, mm = millimeter, MMP = matrix metalloprotease, MPS = mononuclear phagocyte system, mtDNA = mitochondrial DNA, mTOR = mammalian target of rapamycin, MV = mitral valve, NaCl = sodium chloride, Nos2 = nitric oxide synthase 2, PAMP = pathogen-associated molecular pattern, PBS = phosphate buffered saline, PDGF = platelet derived growth factor, PDMS = poly-dimethyl-siloxane, PRR = pattern recognition receptor, qRT-PCR = quantitative real time polymerase chain reaction, RNA = ribonucleic acid, RV= right ventricle, SASP = senescence associated secretory phenotype, SLRP = small leucine rich protein, Sod3 = superoxide dismutase 3, SPARC = secreted protein acidic and rich in cysteine, TAC = transverse aortic constriction, TCP = tissue culture plastic, TGFβ = transforming growth factor beta, TIMD4 = t-cell immunoglobulin and mucin domain containing 4, TIMP = tissue inhibitor of metalloprotease, TLR = toll-like receptor, TNFα = tumor necrosis factor alpha, TSP = thrombospondin, Xbp1 = x-box binding protein 1.

1.0 Background

1.1 The Hallmarks of Physiological Aging

The physiological aging process can be characterized by numerous changes in resident cell function and tissue microenvironment, which together can contribute to attenuated organ function (Lopez-Otin, Blasco, Partridge, Serrano, & Kroemer, 2013). Considering these changes in cellular function observed in aged individuals are often resultant of an accumulation of cellular damage over time, several hallmarks of physiological aging have been identified (Lopez-Otin et al., 2013). With increasing age, there is an increased risk of cellular stress resultant of cellular DNA damage including somatic nuclear DNA mutation accumulation, mitochondrial DNA (mtDNA) mutation or loss, and nuclear envelope architectural defects (Dechat et al., 2008; Lopez-Otin et al., 2013; Moskalev et al., 2013; Park & Larsson, 2011). Another mechanism of age-related chromosomal instability is the loss of protective terminal telomere sequences due to a lack of somatic cell telomerase expression coupled with extended periods of DNA replication (Blackburn, Greider, & Szostak, 2006; Blasco, 2007; Lopez-Otin et al., 2013). Epigenetic changes in chromosome methylation patterns and histone posttranslational modifications have also been observed in aged individuals, and can contribute to altered expression of genes required for homeostatic tissue function (Lopez-Otin et al., 2013; Talens et al., 2012).

In addition to cellular functional attenuation resultant of dysregulated homeostatic gene expression, aging is also associated with a dysregulation of proper cellular protein homeostasis (Koga, Kaushik, & Cuervo, 2011; Lopez-Otin et al., 2013; Powers, Morimoto, Dillin, Kelly, & Balch, 2009). Aging can result in a loss of chaperone protein expression and a subsequent increase

in misfolded protein aggregation (Calderwood, Murshid, & Prince, 2009; Lopez-Otin et al., 2013). Aging is also associated with a progressive decline in the competency of misfolded protein degradation pathways, including the lysosome-autophagocytic pathway and the ubiquitin-mediated proteolytic pathway (Lopez-Otin et al., 2013; Rubinsztein, Marino, & Kroemer, 2011; Tomaru et al., 2012).

Aging can also lead to dysregulation of nutrient sensing cellular pathways (Lopez-Otin et al., 2013). This dysregulation can subsequently alter cell metabolomics as well as promote altered body composition which is often characterized by increased deposition of deleterious, pro-inflammatory visceral fat (Barzilai, Huffman, Muzumdar, & Bartke, 2012). One important cellular pathway associated with nutrient sensing as well as longevity is the insulin and insulin-like growth factor-1 (IGF-1) signaling (IIS) pathway (Barzilai et al., 2012). Attenuation of IIS pathway signaling intensity, and subsequent reduction in activation of proteins associated with cell growth such as protein kinase B (Akt) or mechanistic target of rapamycin (mTOR), has been shown to be associated with increased longevity (Barzilai et al., 2012; Lopez-Otin et al., 2013). Paradoxically, IGF-1 expression levels have generally been observed to decrease with increasing age (Barzilai et al., 2012; Tatar, Bartke, & Antebi, 2003). This decline is IIS pathway activator expression is hypothesized to be a evolutionarily conserved mechanism for the promotion of cellular longevity by preventing the deleterious consequences associated with excess nutrient uptake (Garinis, van der Horst, Vijg, & Hoeijmakers, 2008; Lopez-Otin et al., 2013). However, as with other aging-associated alterations in cellular function, this initially beneficial alteration in cellular function can promote cell dysfunction and contribute to tissue functional decline over extended periods of time (Lopez-Otin et al., 2013).

Aging has also been correlated with increased mitochondrial dysfunction and reduced respiratory chain efficacy (Green, Galluzzi, & Kroemer, 2011; Lopez-Otin et al., 2013). Age-related mitochondrial dysfunction can lead to increased cellular apoptotic signaling pathway activation following mitochondrial permeabilization in response to intracellular stress signals (Kroemer, Galluzzi, & Brenner, 2007). This mitochondrial permeabilization can also lead to radical oxidative species-mediated or mitochondrial permeabilization associated factor-mediated inflammasome activation (Green et al., 2011). Mitochondrial permeabilization with subsequent radical oxidant release, initially known as the mitochondrial free radical theory of aging, has also been proposed as a mechanism underlying physiological aging; although recent evidence has suggested a more nuanced role for radical oxidants in the aging process (Harman, 1965; Hekimi, Lapointe, & Wen, 2011; Lopez-Otin et al., 2013; Ristow & Schmeisser, 2011; Y. Zhang et al., 2009).

Cellular senescence, which is the arrest of cellular mitosis resultant of either telomeric shortening or other extrinsic senescence-associated stimuli, has been increasingly observed in some organs with increasing age (Campisi & d'Adda di Fagagna, 2007; Lopez-Otin et al., 2013). Cellular senescence induces a change in cellular phenotype and secretome, known as the senescence associated secretory phenotype (SASP), which is characterized by increased pro-inflammatory cytokine and matrix metalloprotease (MMP) secretion (Kuilman, Michaloglou, Mooi, & Peeper, 2010; Lopez-Otin et al., 2013). Although - as with the case of radical oxidant secretion - the function of the senescence-associated secretory phenotype has not been fully elucidated, and this cellular phenotype may ultimately serve a protective role through the promotion of immune cell-mediated degradation of dysfunctional cells (Lopez-Otin et al., 2013). However, the increase in observed senescent cells in aged tissue microenvironments may suggest

a dysfunction in the immune cell mediated clearance of senescent cells in advanced age individuals (Lopez-Otin et al., 2013).

Additionally, a decline in progenitor cell population size with increasing age has been observed and demonstrated to be responsible for the age-related attenuation of regenerative potential in many organ systems (Lopez-Otin et al., 2013). For example, aging has been shown to be associated with a reduction in hematopoietic stem cell (HSC) population cell cycle activity, which correlates with increased rates of hematopoietic stem cell DNA damage (Lopez-Otin et al., 2013; Rossi et al., 2007). Similar exhaustion of progenitor cell populations has been characterized in other tissue microenvironments, including in the forebrain, in skeletal muscle, and in bone (Conboy & Rando, 2012; Lerma, Zukin, & Bennett, 1991; Lopez-Otin et al., 2013; Molofsky et al., 2006). While this exhaustion in progenitor cell populations with increasing age has been observed in many tissue microenvironments, it remains unclear whether the mechanism underlying progenitor cell cycle decline is entirely due to a cell intrinsic accumulation of damage associated signaling cues or if cell extrinsic cues – such as age-related microenvironmental remodeling – plays a role in promoting the attenuation of progenitor cell population function; although recent evidence has increasingly supported the latter cell extrinsic hypothesis (Cerletti, Jang, Finley, Haigis, & Wagers, 2012; Conboy & Rando, 2012; Lavasani et al., 2012; Lopez-Otin et al., 2013).

Aging has also been shown to alter several important neuroendocrine signaling axes as well as promote increased secretion of pro-inflammatory factors into tissue extracellular microenvironments (Laplante & Sabatini, 2012; Lopez-Otin et al., 2013; Pedersen, Wan, & Mattson, 2001; Russell & Kahn, 2007; Salminen, Kaarniranta, & Kauppinen, 2012; G. Zhang et al., 2013). This increased secretion of pro-inflammatory factors, generally termed "inflamm-aging", is hypothesized to result from several mechanisms including the age-related accumulation

of tissue damage, the reduced ability of immune cells to clear necrotic or apoptotic cells, and an increase in the number of senescent cells within tissue microenvironments (Lopez-Otin et al., 2013; Salminen et al., 2012). Tissue resident immune cells consequently exhibit increased inflammasome activation with accompanying secretion of pro-inflammatory factors such as interleukin-1β (IL-1β) or tumor necrosis factor alpha (TNFα) (Lopez-Otin et al., 2013; Salminen et al., 2012). This increased pro-inflammatory factor secretion can then promote additional deleterious tissue remodeling or even contribute to pathology development (Barzilai et al., 2012; Lopez-Otin et al., 2013; Salminen et al., 2012).

1.2 The Aging Cardiovascular System

1.2.1 Age as a Risk Factor for the Acquisition of Cardiovascular Pathology

Aging was first identified as an independent risk factor for the acquisition of cardiovascular disease by the Framingham epidemiological study (Dawber, Meadors, & Moore, 1951). The Framingham study was one of the first epidemiological studies seeking to understand the risk factors underlying cardiovascular disease in order to develop better interventions to prevent cardiovascular disease acquisition (D'Agostino, Pencina, Massaro, & Coady, 2013; Dawber & Kannel, 1958). The Framingham study represented a significant advance in applying statistical modeling of the identified Framingham risk factors for the prediction of ten year cardiovascular disease acquisition risk (D'Agostino et al., 2013). Some of the preliminary Framingham factors utilized in the coronary heart disease risk model included patient blood pressure, total cholesterol level, HDL cholesterol level, diabetes status, smoking status, and age (Truett, Cornfield, & Kannel,

1967). However, while the importance of age as a risk factor for cardiovascular disease acquisition was identified, the mechanisms by which physiological aging induces altered resident cardiac cell functionality and how this altered function subsequently contributes to cardiovascular system dysfunction remain to be fully elucidated (North & Sinclair, 2012).

1.2.2 Age-related Changes to the Cardiac Tissue Microenvironment

In order to better understand how cardiovascular disease develops in aged populations, one can examine how aging alters the cardiac microenvironment, with a subsequent focus on how these microenvironmental changes in turn reduce cardiac functionality. Aged cardiac tissue can generally be characterized by several hallmark alterations, including cardiomyocyte hypertrophy, altered left ventricular diastolic function, reduced endothelial cell function, and increased fibrotic matrix deposition (Lakatta & Levy, 2003a, 2003b; North & Sinclair, 2012). These pathological cardiac tissue changes attenuate the function of the cardiovascular system and reduce distal tissue perfusion, further contributing to co-morbidity development (North & Sinclair, 2012). Thus, understanding the mechanisms by which these pathological alterations develop in cardiac cell populations is important for attenuating the age-related cardiovascular disease risk.

1.2.2.1 Cardiac Extracellular Matrix Composition

The cardiac extracellular matrix is a complex set of proteins which serve both as structural and adhesion support network for resident cardiac cell populations. The cardiac extracellular matrix also serves as a means for mechano-transduction of cell proliferation, migration, or other cell signaling cues (C. Chen, Li, Ross, & Manso, 2016; Hein & Schaper, 2001; Horn & Trafford, 2016). Non-myocyte cell populations and signaling proteins embedded in the extracellular

microenvironment are also important components of the extracellular microenvironment (Horn & Trafford, 2016). Cardiomyocytes in cardiac tissue are generally surrounded by basement membrane composed of collagen IV, laminin, and fibronectin (Horn & Trafford, 2016). In addition to these basement membrane proteins, Collagen-I comprises a significant fraction of the total extracellular matrix protein content in cardiac tissue (Horn & Trafford, 2016; Neuman & Logan, 1950). Fibrillar collagen-III comprises a smaller, but still substantial, fraction of total cardiac extracellular matrix protein (Medugorac & Jacob, 1983). Collagen fiber organization in cardiac tissue is complex and anisotropic, linking both individual myocytes through endomysial collagen networks and myocyte bundles through perimysial collagen networks (Horn & Trafford, 2016; Weber, Sun, Bhattacharya, Ahokas, & Gerling, 2013). These collagen networks confer tensile strength to cardiac tissue and help to prevent chamber dilation under physiological pressures commonly experienced in the left ventricle during homeostatic cardiac function (Caulfield, Norton, & Weaver, 1992; Weber et al., 2013). Cardiomyocytes and other resident cardiac cell populations can also experience altered functionality through signal mechano-transduction pathways mediated by integrin binding of fibrillar collagen networks within cardiac tissue (Ross & Borg, 2001).

Collagen in cardiac tissue is synthesized by cardiac fibroblast cell populations, which comprise a large fraction of the non-myocyte cells within cardiac tissue (Horn & Trafford, 2016; Jugdutt, 2003). Collagen is synthesized as a pro-peptide which is secreted into the extracellular space, where it undergoes enzymatic pro-peptide cleavage, matricellular protein association, and fibril formation (Baicu et al., 2012; Horn & Trafford, 2016; Kadler, Holmes, Trotter, & Chapman, 1996; Norris et al., 2007). Collagen fibrils can then be further stabilized by either enzymatic crosslinking by lysyl oxidase (LOX-1) or by non-enzymatic crosslinking through advanced

glycation end product (AGE) formation (Eyre, Paz, & Gallop, 1984; Hartog, Voors, Bakker, Smit, & van Veldhuisen, 2007). Additionally, small fractions of collagen V and collagen VI comprise portions of the total cardiac extracellular matrix protein content (Fan, Takawale, Lee, & Kassiri, 2012). Collagen V provides support to collagen I fibrils in cardiac tissue and forms heterotypic fibrils with collagen I protein (Wenstrup et al., 2006). Collagen VI forms microfilament networks within cardiac tissue that help to anchor basement membrane proteins to fibrillar collagen networks (Keene, Engvall, & Glanville, 1988).

In addition to the various collagen networks within cardiovascular tissue, numerous additional extracellular matrix proteins, proteoglycans, glycoproteins, and glycosaminoglycans comprise smaller fractions of the cardiac extracellular microenvironment. Elastin is a structural protein within cardiac tissue which associates with fibrillin microfibrils to provide elasticity to cardiac tissue (Kielty, Baldock, et al., 2002; Kielty, Sherratt, & Shuttleworth, 2002). Fibronectin protein on the surface of cell populations bind other extracellular matrix proteins, such as collagen or fibrin, providing a mechanism for cellular adherence or extracellular signal transduction (Mao & Schwarzbauer, 2005). Fibronectin has also been shown to bind lysyl oxidase (LOX), an enzyme responsible for collagen fibril crosslinking (Maruhashi, Kii, Saito, & Kudo, 2010). Cardiac tissue also contains numerous matricellular proteins which play a limited structural role within the extracellular microenvironment and instead serve to induce altered cell behavior, which is generally characterized by the promotion of cellular deadhesion from matrix protein structures and the promotion of cellular migration towards regions of tissue remodeling (Bornstein, 2009; Frangogiannis, 2012). Matricellular proteins are generally expressed at low levels in adult cardiac tissue during homeostasis but can exhibit a robust upregulation in expression in response to cardiac tissue injury (Frangogiannis, 2012). Matricellular proteins are often oligomeric proteins with

multiple binding domains which can bind other extracellular matrix proteins, cell surface protein motifs, or growth factors within the cardiac extracellular microenvironment through which they induce altered cell function (Frangogiannis, 2012). Given this vast binding domain heterogeneity and oligomeric subunit diversity, matricellular proteins can often have a variety of, sometimes contradictory, functions within a given tissue site (Frangogiannis, 2012). While historically cardiac remodeling studies have focused on collagen or elastin deposition and degradation dynamics, recent studies have elucidated some interesting functional roles of various cardiac matricellular proteins in the cardiac microenvironmental remodeling response (Bornstein, 2009; Diez, Gonzalez, & Ravassa, 2016; Frangogiannis, 2012; Riley et al., 2021).

1.2.2.2 Collagen

Collagen is the most abundant protein within the human body with numerous of the 28 collagen protein isoforms composing the various fibrillar and basement membrane structures essential for conferring material strength to many tissues (Kisling, Lust, & Katwa, 2019). The diversity in collagen isoforms arises from distinct α-chain domains and the trimeric interactions of these α-chains (Kisling et al., 2019). Collagen's mature structure is a right-handed super helix composed of three left-handed α-chains (Kisling et al., 2019). Each α-chain is generally composed of a three amino acid repeat sequence of glycine-X-Y where X and Y are typically but not always proline and hydroxyproline, respectively (Kisling et al., 2019). This primary α-chain sequence allows for some of the structural properties commonly associated with collagen fibrils. For example, the large number of glycine residues allows for close association of the individual α-chains when forming super helix structures and the relatively large concentration of proline and hydroxyproline allow for tight coiling within the "collagenous domain" (Kisling et al., 2019). In addition to the Gly-X-Y repeats characteristic of the "collagenous domain", collagen peptides

contain N-terminal and a C-terminal pro-peptide domains which have been shown to have some bioactivity following enzymatic cleavage and release of these domains into the tissue microenvironment (Kisling et al., 2019).

Initial formation of collagen fibrils occurs with the enzymatic processing of collagen's N-terminal and C-terminal pro-peptide domains following cellular secretion of collagen α-chains into the extracellular space (Mienaltowski & Birk, 2014). C-terminal pro-peptides are processed by either bone morphogenic protein 1 (BMP-1) or by furin (Mienaltowski & Birk, 2014). N-terminal pro-peptides are cleaved by either BMP-1 or by a-disintegrin-and-metalloprotease-with-thrombospondin-like-motif (ADAMTS) family proteins -2, -3, or -14 (Mienaltowski & Birk, 2014). Following pro-peptide enzymatic cleavage, collagen α-chains self-assemble into heterotypic fibrils often composed of multiple α-chain subunits (Mienaltowski & Birk, 2014). Once collagen fibril self-assembly has occurred, further modification of collagen fibrils can occur through several enzymatic and non-enzymatic mechanisms. Lysyl oxidase (LOX) enzymes can further stabilize collagen fibrils within a tissue microenvironment by converting proline and hydroxyproline amino groups into aldehydes which can form inter- and intra-molecular crosslinks with other collagen amino groups (Mienaltowski & Birk, 2014). Additionally, glycation of collagen either through cell mediated matrix modification or from dietary induced hyperglycemia can non-enzymatically crosslink tissue collagen to promote increased tissue stiffness (Hartog et al., 2007).

While the collagen peptide primary sequence, heterotypic fibril composition, and degree of crosslinking are important determinants of collagen fibril mechanical strength, the organization of the collagen fibrils into higher order structures within tissue microenvironments also plays an important role in dictating tissue mechanical properties. Collagen fibril assembly is highly tissue

specific, but generally has been shown to begin in the extracellular space with the aggregation of nucleator collagen proteins, such as collagen V or IX, at the cell surface (Mienaltowski & Birk, 2014). Interestingly, the ratio of collagen V to collagen I within a given tissue can partially explain differential collagen fibrillogenesis within that tissue. For example, tissues with high collagen V to collagen I ratios, such as the cornea, tend to have a large number of relatively thin collagen fibers due to the high number of available nucleation sites (Birk, 2001). Conversely, tissues which require large collagen fibril assembly for mechanical strength, such as tendons, generally express lower levels of collagen V (Birk, 2001). With fewer nucleation sites available, collagen I assembly is more likely to form larger fibrils within these tissues, suggesting that the tissue specific assembly of thick or thin collagen fibers may be partially dependent upon the altered expression ratios of collagen I and collagen V (Birk, 2001; Mienaltowski & Birk, 2014).

Further fibril assembly from nascent collagen protofibrils occurs in the tissue extracellular space through the lateral and linear assembly of further collagen fibrils mediated through binding interactions with proteins such as the small leucine rich proteoglycan (SLRP) family of proteins or additional collagen proteins (Mienaltowski & Birk, 2014). These proteins serve as adaptors whose binding domain diversity allows for expansion of collagen fibrils into larger order structures within a given tissue (Mienaltowski & Birk, 2014). Additionally, enzymatic and non-enzymatic crosslinking of larger collagen fibril structures can further alter collagen matrix architecture and mechanical properties.

1.2.2.3 Thrombospondins

Matricellular proteins are generally characterized as proteins which do not serve a direct structural role, like collagen which provides tensile strength or elastin which increases tissue elasticity, but rather are structurally distinct proteins that promote altered cell behavior, change

cellular migration patterns, and provide complimentary support for matrix organization – often during periods of tissue remodeling or following injury (Frangogiannis, 2012). The family of Thrombospondin proteins are one such class of matricellular proteins.

Thrombospondins can be divided into two subgroups based upon the oligomerization structure of protein, with group A thrombospondins being composed on trimeric protein architectures and group B thrombospondins composed of pentameric protein structures (Carlson, Lawler, & Mosher, 2008; Frangogiannis, 2012). The constitutive protein subunits of group A and group B thrombospondins also exhibit some compositional diversity. Both proteins contain EGF-like repeats, albeit in varying amounts, followed by seven TSP type 3 repeats and a C-terminal globular domain (Carlson et al., 2008; Frangogiannis, 2012). However, the N-terminal regions of the oligomeric subunits exhibit altered composition between group A and group B thrombospondins, with group A thrombospondins containing a pro-collagen homology binding domain and three properdin-like repeats not observed in group B proteins (Frangogiannis, 2012). The presence of these properdin-like repeats - also known as type 1 thrombospondin repeats - in group A thrombospondins is an important structural difference which confers differential function to group A thrombospondins, as these type 1 domain repeats have an important role in promoting the inhibition of angiogenesis and maintenance of cellular adhesion (Frangogiannis, 2012).

In vivo studies examining the impacts of thrombospondin signaling disruption on cardiac function have revealed several important roles of thrombospondin signaling in cardiac tissue (Frangogiannis, 2012). Thrombospondin-1 has been shown to induce TGF-β protein activation through type I repeat domain binding to latency-associated protein (LAP), inducing an altered TGF-β conformation capable of binding TGF-β receptors (Frangogiannis, 2012; Murphy-Ullrich, Schultz-Cherry, & Hook, 1992; Schultz-Cherry & Murphy-Ullrich, 1993). Additionally,

thrombospondin-1 and thrombospondin-2 are both strong inhibitors of angiogenesis (Good et al., 1990; Volpert et al., 1995). Thrombospondin-1 and -2 can both promote matrix protein maintenance through the inhibition of collagen degradation associated MMP2 and MMP9 (Krady et al., 2008; Rodriguez-Manzaneque et al., 2001). Taken together, these functions of group A thrombospondins can generally be characterized as supportive of matrix integrity through pleiotropic mechanisms such as TGF-β induced collagen fibril support or matrix metalloprotease inhibition.

While thrombospondins - particularly group A thrombospondins - have been shown to have important matrix support roles, their expression remains limited in healthy myocardium (Frangogiannis, 2012). Additionally, genetic ablation studies of group A thrombospondins in mice have demonstrated minimally altered cardiac function - suggesting that group A thrombospondins play a minimal role in homeostatic cardiac function (Frangogiannis, 2012; Isenberg et al., 2009; Malek & Olfert, 2009). Interestingly, group B thrombospondin-4 has been shown to both be highly expressed in cardiac tissue and play an important role in regulating the cardiovascular remodeling response to hypertension (Lawler et al., 1993; Palao et al., 2018). In a study examining the cardiac remodeling response to an angiotensin-infusion model of hypertension, genetic ablation of thrombospondin-4 induced significantly greater cardiomyocyte hypertrophy and perivascular collagen deposition as compared to wild type controls (Palao et al., 2018).

1.2.2.4 Tenascins

Tenascin matricellular proteins are a group of oligomeric glycoproteins with conserved structural motifs linked through an N-terminal oligomerization domain (Frangogiannis, 2012; Jones & Jones, 2000). While four tenascin paralogs have been identified in mammals, only two paralogs have been shown to have canonical matrikine function, tenascin-C and tenascin-X

(Frangogiannis, 2012). Tenascin-C and -X synthesis have been shown to be highly dependent upon local microenvironmental conditions (Tucker & Chiquet-Ehrismann, 2009). Tenascin-C is first expressed during embryogenesis at high levels in regions where cell migration is necessary for organogenesis, at epithelial-mesenchymal cell interfaces, and in connective tissue (Frangogiannis, 2012). Tenascin-C expression then sharply declines as organs mature and mammals reach adulthood, other than in connective tissue where expression remains abundant (Frangogiannis, 2012; Tucker & Chiquet-Ehrismann, 2009). Tenascin-C production in non-connective tissue is often a response to tissue damage and can be induced by a variety of growth factors, such as platelet-derived growth factor (PDGF), fibroblast growth factor 2 (FGF2), transforming growth factor beta (TGF-β), as well as by mechanical stress (Chiquet-Ehrismann et al., 1994; Frangogiannis, 2012).

Tenascin-C has a variety of impacts on cellular functionality. Similar to thrombospondin-1, tenascin-C can promote the de-adhesion of resident cells from extracellular matrix protein networks (Frangogiannis, 2012). Mechanistically, the promotion of cellular de-adhesion can partially be attributed to the disruption of matrix protein networks through the variety of binding interactions tenascin-C can have with other constitutive extracellular matrix proteins (Chiquet-Ehrismann, Kalla, Pearson, Beck, & Chiquet, 1988; Frangogiannis, 2012; Midwood & Schwarzbauer, 2002). Tenascin-C signaling has also been shown to play a role in the fibrotic remodeling response, most likely through TGF-β interactions (Carey, Taylor, Dean, & Bristow, 2010). Tenascin-C expression has also been shown to correlate with increased infiltration of inflammatory cells, most likely a result of induced expression following growth factor secretion which commonly occurs during tissue injury and inflammation inducing (Frangogiannis, 2012).

Tenascin-C expression in the adult heart is limited to the papillary muscle chordae tendinae and otherwise not expressed in healthy myocardium (Sato & Shimada, 2001). Additionally, genetic ablation of tenascin-C does not significantly impact cardiac function in healthy animals - suggesting minimal homeostatic function for tenascin-C in adult cardiac tissue (Nishioka et al., 2010). However, tenascin-C expression has been shown to be upregulated following cardiac tissue damage. Following myocardial infarction, tenascin-c expression has shown to be upregulated in border regions of the infarction where it is primarily produced by fibroblasts (Imanaka-Yoshida et al., 2001). Upregulation of tenascin-c in border zone regions, possibly a consequence of increased growth factor microenvironmental concentrations, is believed to play a role in facilitating fibroblast migration from border regions into remodeling myocardium, subsequently promoting further fibrotic remodeling and worsening diastolic dysfunction (Nishioka et al., 2010). Increased production of tenascin-c in border zone regions may also contribute to cardiomyocyte de-adhesion from the cardiac collagen matrix, contributing to further loss of cardiomyocytes and reduced contractile strength (Imanaka-Yoshida et al., 2001).

1.2.2.5 Secreted Protein Acidic and Rich in Cysteine (SPARC) or Osteonectin

SPARC is a multifunctional matricellular glycoprotein composed of three distinct regions (Brekken & Sage, 2000). The N-terminal region of the SPARC protein is comprised of a low affinity, high capacity Ca^{2+} binding domain (Frangogiannis, 2012). The central region contains a follistatin-like domain, a protease-like inhibitor region, and bioactive peptides which induce altered endothelial cell function (Frangogiannis, 2012). The C-terminal region contains an extracellular calcium binding domain, a collagen binding domain, and peptides which can inhibit endothelial cell proliferation (Kupprion, Motamed, & Sage, 1998; Sasaki, Hohenester, Gohring, & Timpl, 1998). SPARC is first expressed during embryogenesis in a variety of developing organs,

however adult SPARC homeostatic expression is typically limited to high turnover tissue sites – such as bone or gastrointestinal epithelium (Sage, Vernon, Decker, Funk, & Iruela-Arispe, 1989). Similar to other matricellular proteins, expression in adult tissue is largely upregulated following tissue injury (Reed & Sage, 1996). SPARC synthesis following tissue damage is believed to be induced by increased growth factor signaling, such as increased transforming growth factor family protein signaling (Frangogiannis, 2012).

Functionally, SPARC induces de-adhesion responses in resident cell populations similar to those discussed for other matricellular proteins (Frangogiannis, 2012). SPARC has also been shown to be an important regulator of fibroblast cell surface interaction with collagen I and collagen V peptides (Frangogiannis, 2012). SPARC also plays an important role in regulating the assembly of fibrillar collagen bundles within tissues. While SPARC null mice produce viable offspring, collagen assembly within various tissue has been observed to be significantly altered (Bradshaw et al., 2009; Bradshaw, Graves, Motamed, & Sage, 2003; Bradshaw, Puolakkainen, et al., 2003). SPARC null mice have generally been observed to exhibit less collagen content in various tissue sites, including in dermal and cardiac tissue, with fewer thick fibers formed in these tissue sites (Bradshaw et al., 2009; Bradshaw, Graves, et al., 2003; Bradshaw, Puolakkainen, et al., 2003). This suggests that while SPARC may not be a direct mediator of collagen fibril formation, it may be required for collagen fibril fusion (Bradshaw, 2009; Frangogiannis, 2012). In addition to regulating formation of thick collagen fibers in tissues, some observed dysregulation of basement membrane collagen deposition has been noted in SPARC null animals (Fitzgerald & Schwarzbauer, 1998; Gilmour et al., 1998; Yan, Clark, Wight, & Sage, 2002).

SPARC has also been shown to play an important role in regulating the fibrotic remodeling response to various experimentally induced tissue injuries, which would be expected given the

important role SPARC was observed to play in regulating matrix protein assembly (Frangogiannis, 2012). Loss of SPARC protein signaling has been associated with reduced fibrotic matrix deposition in a bleomycin-induced pulmonary fibrosis model as well as in an angiotensin-II infusion model of renal fibrosis (Socha, Manhiani, Said, Imig, & Motamed, 2007; Strandjord, Madtes, Weiss, & Sage, 1999). SPARC expression has also been shown to increase in a murine model of cardiac pressure overload following transverse aortic constriction (TAC) (Bradshaw et al., 2009). Additionally, SPARC null mice exhibited reduced collagen deposition and improved diastolic function following TAC relative to non-SPARC null controls (Bradshaw et al., 2009). Interestingly, bone marrow chimerism studies of pressure overload using wild type and SPARC null bone marrow have demonstrated that SPARC expression by infiltrating bone marrow-derived cells is essential for fibrotic matrix remodeling. Additionally, when SPARC expression was knocked out in bone marrow cell infiltrate, the total collagen volume fraction significantly decreased and the number of Iba1+ macrophages in cardiac tissue significantly decreased (Riley et al., 2021).

1.2.2.6 Osteopontin

Osteopontin is a phosphorylated, acidic glycoprotein produced by a variety of cell types - including osteoblasts, fibroblasts, epithelial cells, vascular smooth muscle cells, and various hematopoietic cell subsets. After osteopontin is synthesized, it is secreted into either bodily fluids where it functions as a cytokine or into the extracellular space where osteopontin binds matrix proteins and functions as a matrikine (Frangogiannis, 2012). Osteopontin contains two integrin binding motifs, one R-G-D (Arginine-Glycine-Asparagine) integrin binding domain commonly observed in many extracellular matrix binding proteins and a cryptic integrin binding domain which is accessible following osteopontin cleavage by thrombin (Barry, Ludbrook, Murrison, &

Horgan, 2000; Ito et al., 2009). In addition to thrombin cleavage, osteopontin can also be cleaved by various matrix metalloprotease enzymes, including MMP-2, -3, -7, -9, and -12, which has the possibility of exposing additional cryptic integrin binding domains following cleavage (Scatena, Liaw, & Giachelli, 2007).

Osteopontin can induce altered cellular behavior through integrin-mediated signal transduction or through CD44 receptor signaling pathways (Frangogiannis, 2012; Ito et al., 2009). Osteopontin has been shown to have a significant effect on promoting cell survival through the inhibition of apoptosis signaling pathways (K. X. Wang & Denhardt, 2008). Osteopontin has also been associated with the chemotaxis of various cell populations *in vitro* including monocytes, T-cells, endothelial cells, and smooth muscle cells (Frangogiannis, 2012). This chemotactic effect has also been observed *in vivo*, where injection of purified osteopontin was associated with macrophage accumulation in the dermis (Giachelli, Lombardi, Johnson, Murry, & Almeida, 1998). However, additional studies in other tissues have generated some conflicting results, suggesting the osteopontin-mediated chemotaxis may exhibit some tissue context dependance (Giachelli et al., 1998; Liaw et al., 1998; Ophascharoensuk et al., 1999). In addition to a chemotactic effect, osteopontin can play a significant role in altering the function of some immune cell subsets. This effect is particularly notable in macrophage subsets, where osteopontin is both produced in and acts upon these cell subsets to promote macrophage functional responses, particularly the promotion of type I, pro-inflammatory functional responses (Ashkar et al., 2000; Frangogiannis, 2012; O'Regan, Nau, Chupp, & Berman, 2000).

Osteopontin, similar to other matrikines, tends to be expressed at relatively low levels in healthy, adult myocardium but can undergo a large upregulation in expression following tissue injury or stress (Murry, Giachelli, Schwartz, & Vracko, 1994; K. Singh et al., 1999; M. Singh,

Foster, Dalal, & Singh, 2010; K. X. Wang & Denhardt, 2008). Osteopontin expression levels have been observed to acutely increase (1-2 days) following cryoinjury induced myocardial infarction, after which expression declines with increasing time – despite no observed significant decline in macrophage population size (Murry et al., 1994). These results suggest that osteopontin expression levels do not simply correlate with macrophage infiltration in infarcted myocardium, but instead osteopontin expression may be induced by or correlate with activation of specific cardiac resident macrophage subsets (Murry et al., 1994). Genetic disruption of monocyte chemoattractant protein (MCP-1), also known as C-C motif chemokine ligand 2 (CCL2), signaling resulted in an attenuation of osteopontin expression in infarcted myocardium disproportionate to the observed alterations in macrophage density (Dewald et al., 2005). MCP-1 signaling inhibition also reduced the secretion of pro-inflammatory factors, such as IL-1β or TNFα, following infarction (Dewald et al., 2005). Taken together, these results suggest that osteopontin expression following infarction is likely a result of the recruitment and activation of bone marrow-derived macrophages, which in turn upregulate an increased inflammatory response relative to other cardiac resident macrophage subsets (Dewald et al., 2005). Osteopontin also plays an important role in preventing deleterious left ventricular dilation or rupture following infarction through the promotion of left ventricular wall collagen deposition (Trueblood et al., 2001).

Osteopontin has also been shown to play an important role in regulating the fibrotic remodeling response to left ventricular pressure overload. Osteopontin expression has been shown to increase in spontaneous hypertensive rat models of heart failure (K. Singh et al., 1999). Increased angiotensin II signaling has also been associated with increased osteopontin expression levels and conversely treatment with angiotensin converting enzyme (ACE) inhibitors have been shown to attenuate osteopontin expression in remodeling cardiac tissue (Collins et al., 2004;

Matsui et al., 2004; K. Singh et al., 1999). Additionally, genetic ablation studies of cardiac fibrosis in osteopontin null mice demonstrated an attenuation of fibrotic matrix remodeling and reduced systemic hypertension with minimal to moderate noted impact on cardiomyocyte hypertrophy (Collins et al., 2004; Matsui et al., 2004). Mechanistically, the observed altered fibrotic remodeling regulation was hypothesized to be a result of decreased fibroblast matrix adhesion and not a result of increased TGF-β signaling, which was found to exhibit no significant difference in expression between wild type and osteopontin null mice (Collins et al., 2004). However, additional mechanistic pathways exist for osteopontin to exert pro-fibrotic remodeling effects on cardiac tissue in pressure overload models, including through the increased chemotactic recruitment and subsequent activation of bone marrow derived macrophages or through mitogen-activated protein kinase (MAPK) signaling induced cardiomyocyte hypertrophy (Matsui et al., 2004; Xie, Singh, & Singh, 2004)

1.2.2.7 Periostin

Periostin, first isolated from murine osteoblasts and identified as osteoblast-specific-factor-2, is an extracellular matrikine which functions in a similar manner to other discussed matrikines - namely by promoting altered cell adhesion, cell activation, or matrix organization (Kudo & Kii, 2018; Sugiura, Takamatsu, Kudo, & Amann, 1995). Periostin is a 90kDa protein consisting of a secretory domain followed by a cysteine-rich EMI domain, four fasciclin-like domains (FAS)-1 domains, and a carboxyl-terminal domain which can undergo significant post-translation splicing which is hypothesized to provide some function heterogeneity although specific matrix binding sequences have yet to be identified (Horiuchi et al., 1999; Kudo & Kii, 2018; Sugiura et al., 1995).

Periostin expression has been observed in the periosteum of bone as well as in other collagen rich tissue structures which are subject to higher mechanical stresses (Horiuchi et al.,

1999; Kruzynska-Frejtag, Machnicki, Rogers, Markwald, & Conway, 2001; Merle & Garnero, 2012; Yoshiba et al., 2007). In addition to osteoblast secretion, periostin expression has been noted in embryonic fibroblasts and pericardial cell populations during cardiovascular system development (Ieda et al., 2009; Snider et al., 2008). Periostin secretion can also be induced through growth factor or cytokine signaling cues - including through estradiol, TGF-β, BMP-2, IL-4, IL-13, and PDGF, and TNFα signaling pathways (Horiuchi et al., 1999; Inai, Norris, Hoffman, Markwald, & Sugi, 2008; G. Li et al., 2006; Mamalis, Markopoulou, Lagou, & Vrotsos, 2011; Rani, Barbe, Barr, & Litivn, 2010; Takayama et al., 2006). Additionally, angiotensin-II signaling has been noted to induce periostin production in fibroblasts through TGF-β1 and MAPK signaling pathways (L. Li et al., 2011).

Periostin has been shown to bind a variety of extracellular matrix proteins through which it can induce altered matrix remodeling and resident cell function. Periostin has been shown to directly bind fibronectin within the endoplasmic reticulum of fibroblasts and promotes further fibronectin secretion from these cells (Kii, Nishiyama, & Kudo, 2016; Kii et al., 2010; Norris et al., 2007). Periostin has also been shown to bind fibrillar collagen subtypes including collagen I and collagen V likely through binding interactions in the EMI domain (Maruhashi et al., 2010; Norris et al., 2007; Suzuki et al., 2004; Takayama et al., 2006). Given the role that fibronectin plays in collagen fibrillogenesis, periostin can also indirectly influence collagen fibril formation through binding interactions with fibronectin (Kudo & Kii, 2018; Norris et al., 2007).

Periostin FAS-1 domains have also been shown to bind a variety of extracellular matrix proteins or cytokines which can in turn alter matrix remodeling. Periostin has been shown to bind tenascin-C through FAS-1 domain interactions following carboxy-terminal domain cleavage post-translationally (Kii et al., 2010). Additionally, the four FAS-1 domains have been shown to interact

with bone morphogenic protein (BMP)-1, a collagen processing enzyme responsible for the cleavage of the carboxy-terminal pro-peptide sequences from pro-collagen (Vadon-Le Goff, Hulmes, & Moali, 2015). Given the ability of periostin to bind fibronectin, which is capable itself of binding collagen crosslinking enzyme lysyl oxidase, this ability to bind BMP-1 in FAS-1 domains presents a unique possible mechanism for the periostin-mediated promotion of collagen fibril maturation and strengthening in tissues where mechanical stress promotes increased periostin secretion (Gonzalez-Gonzalez & Alonso, 2018; Maruhashi et al., 2010). Periostin can also induce altered cell migratory behavior through integrin-binding and activation of the phosphatidyl-inositol-3-kinase (PI3K) signaling pathway (Norris, Moreno-Rodriguez, Hoffman, & Markwald, 2009).

Periostin also plays an important role in the development of non-cardiomyocyte cell lineages and valvular structures in the embryonic heart (Kruzynska-Frejtag et al., 2001; Snider et al., 2008). Periostin expression is first noted in the developing myocardium around embryonic day 10.5 in mice in endocardial cushions with a marked upregulation by embryonic day 12 (Kruzynska-Frejtag et al., 2001). During valvulogenesis, periostin is expressed by differentiating vascular smooth muscle cells and fibroblasts (Norris et al., 2007; Norris et al., 2004). The importance of periostin for promoting appropriate development of resident cardiac cell populations have been noted in several studies. Genetic ablation of periostin was noted to have a moderate embryonic lethality rate with notable excess cardiomyocyte progenitor cell differentiation in atrioventricular cushion regions (Norris et al., 2008). Additional valvulogenesis studies noted that periostin expression was important for proper collagen deposition and tissue maturation in cardiac valves, with periostin null mice often exhibiting insufficient fibrillar collagen deposition and encroachment of left ventricular cardiomyocytes into valvular structures (Norris et al., 2008;

Norris, Potts, et al., 2009). Periostin was also shown to play an important role in promoting the differentiation of cardiac fibroblasts from progenitor cell precursors (Norris, Potts, et al., 2009). Gene transcript array analysis of periostin null murine cardiac tissue revealed a significant alteration in the regulation of numerous genes associated with fibrotic matrix deposition and cellular adhesion, suggesting that loss of periostin signaling may reduce mesenchymal prescursor cell ability to differentiate into wild type cardiac fibroblast populations (Oka et al., 2007). Taken together, this data demonstrates the importance of periostin expression in the developing heart for proper differentiation of non-cardiomyocyte cell populations, proper tissue segmentation, and proper restriction of cell lineages within the appropriate regions of the developing myocardium (Frangogiannis, 2012).

Given the mechanosensitive nature of periostin production, fibroblast expression patterns, and notable interactions with collagen maturation associated enzymes; it is not surprising several studies have noted significant upregulation of periostin expression in pressure overload induced remodeling myocardium (Stansfield, Andersen, Tang, & Selzman, 2009; Teekakirikul et al., 2010; D. Wang et al., 2003). Additionally, studies of fibrotic remodeling in periostin null mice demonstrated significant reduction in the deposition of fibrotic matrix, preservation of cardiac function, and reduction of cardiomyocyte hypertrophy (Oka et al., 2007; Teekakirikul et al., 2010). Overexpression studies have also noted enhanced cardiomyocyte hypertrophy in periostin overexpressing animal model, with some variable impacts on cardiac function noted (Katsuragi et al., 2004; Litvin et al., 2006; Oka et al., 2007). Increased levels of periostin have also been observed in human myocardial tissue samples isolated from advanced heart failure patients (Stansfield et al., 2009). Interestingly, periostin levels were also shown to decline following

mechanical unloading of the left ventricular through implantation of a left ventricular assist device in human myocardial tissue (Stansfield et al., 2009).

1.2.2.8 CCN Protein Family

The CCN protein family, first named from the three constitutive members – cysteine-rich protein 61 (Cyr61, CCN1), connective tissue growth factor (Ctgf, CCN2), and nephroblastoma overexpressed protein (Nov, CCN3) – and later expanded to include three additional Wnt-inducible secreted CCN proteins (CCN4, CCN5, CCN6), is a group of matricellular proteins capable of inducing altered resident cell function and modulating growth factor signaling in tissue microenvironments (C. C. Chen & Lau, 2009; Leask & Abraham, 2006). CCN proteins share a fair amount of structural homology, with each protein generally consisting of an N-terminal secretory domain followed by an insulin-like growth factor binding protein domain, a von Willebrand factor type C repeat, a thrombospondin type I repeat, and a C-terminal domain which often contains a cysteine rich knot region (Bork, 1993; Frangogiannis, 2012). CCN protein production and secretion mechanisms have to date been best characterized for CCN2 (Frangogiannis, 2012). CCN2 production and secretion has been noted in a variety of cell types - including in endothelial cells, fibroblasts, smooth muscle cells, and osteoblasts - often following induction by TGF-β1 signaling pathway activation (Igarashi, Okochi, Bradham, & Grotendorst, 1993; Leask & Abraham, 2004; Parisi, Gazzerro, Rydziel, & Canalis, 2006; Rodriguez-Vita et al., 2005; Wunderlich, Senn, Todesco, Flammer, & Meyer, 2000). CCN2 production in fibroblast cell lines has also been noted following exposure to angiotensin-II (Iwanciw, Rehm, Porst, & Goppelt-Struebe, 2003). While additional studies examining the mechanisms underlying CCN family protein synthesis have suggested some similar mechanisms, such as induction through TGF-β

signaling, the mechanisms remain to be fully elucidated (Parisi et al., 2006; Riser et al., 2009; Sakamoto et al., 2004).

CCN proteins have been shown to exhibit a number of canonical matrikine associated alterations of cellular function and modulation of matrix organization. CCN1 and CCN2 have been shown to induce cytoskeletal reorganization and increased cellular adhesion in fibroblasts through integrin and heparin sulfate proteoglycan cell surface receptor signaling pathways (N. Chen, Chen, & Lau, 2000). CCN family proteins have also been shown to have some contradictory roles in regulating cellular activity and growth factor signaling. CCN1, CCN2, and CCN3 proteins have been shown to be associated with fibroblast and endothelial cell chemotaxis while CCN4 and CCN5 have been shown to have an inhibitory effect on cell migration (Babic, Kireeva, Kolesnikova, & Lau, 1998; Grzeszkiewicz, Kirschling, Chen, & Lau, 2001; Lake, Bialik, Walsh, & Castellot, 2003; C. G. Lin et al., 2003; Soon et al., 2003).Additionally, different CCN protein family members can modulate the signaling intensity of growth factor TGF-β. CCN2 has been shown to not only enhance TGF-β signaling in fibroblasts but also is necessary for transcription induction of a group of fibroblast genes associated with matrix remodeling downstream of TGF-β signaling pathways (Shi-wen et al., 2006). Conversely, recent data has demonstrated an anti-fibrotic effect of CCN5 signaling through an inhibition of TGF-β signaling pathways (Jeong et al., 2016). To better understand how CCN family proteins may exert these seemingly contradictory functions despite fairly large structural homology, one can examine the altered regulation of CCN protein domains in CCN2 and CCN5 (Diez et al., 2016). CCN2 directly binds TGF-β through the von Willebrand factor domain and promotes downstream TGF-β pathway activation through C-terminal domain cysteine knot domain interactions (Abreu, Ketpura, Reversade, & De Robertis, 2002). While CCN5 shares the von Willebrand factor domain homology with CCN2, CCN5 does

not share the cysteine knot in the C-terminal domain (Ball et al., 1998; Diez et al., 2016). Thus, CCN5 may act a negative regulator of fibrotic matrix deposition through the binding of TGF-β without subsequent downstream activation of TGF-β signaling pathways induced through the cysteine knot domain (Jeong et al., 2016). These results also demonstrate how the balance between CCN family proteins in a given microenvironment can either drive or inhibit the progression of fibrotic matrix remodeling in those tissue sites (Diez et al., 2016).

Contrary to previously discussed matrikine proteins, genetic ablation studies of CCN family proteins proved to be embryonically or perinatally fatal in many cases with animals whom survive to adulthood generally having some skeletal muscle or cardiovascular defects (Frangogiannis, 2012; Heath et al., 2008; Ivkovic et al., 2003; Mo et al., 2002). CCN1, CCN2, and CCN3 have been shown to be potent inducers of angiogenic processes (Babic, Chen, & Lau, 1999; Babic et al., 1998; C. G. Lin et al., 2003). When examining the cause of embryonic lethality in CCN1 and CCN2 null mice, a lack of neovascularization in the placenta or in developing growth plates is often the cause of death (Ivkovic et al., 2003; Mo et al., 2002). In addition to angiogenic defects, several cardiovascular developmental defects were noted in CCN null mutant mice. Significant atrioventricular septal defects were noted in CCN1 null mice due to significant apoptosis in cushion cell regions, suggesting that CCN1 functions as a pro-survival signal in these cushion cell populations (Mo & Lau, 2006). As CCN1 also functions as an inducer of MMP-2 production in cardiomyocytes, CCN1 null mice also may have experienced a reduced capacity for the requisite cardiac tissue remodeling necessary for cardiac tissue structure genesis (Mo & Lau, 2006).

CCN family proteins can also play a role in the remodeling response of cardiac tissue following injury. Mechanical stretch and pressure overload have both been shown to upregulate

cardiomyocyte CCN1 expression through angiotensin receptor 1 (AT1) signaling pathways (Hilfiker-Kleiner et al., 2004). CCN1 expression has also been shown to acutely increase in the first several hours following a myocardial infarction, although the significance of this upregulation in the production of CCN1 following infarction remains to be fully elucidated (Hilfiker-Kleiner et al., 2004). *In vitro* and *in vivo* experiments have demonstrated some protection of cardiomyocytes from oxidative stress induced damage in the presence of CCN1 as well as an attenuation of inflammation following CCN1 overexpression in a model of murine myocarditis (Rother et al., 2010; Yoshida et al., 2007). Taken together, the observed upregulation of CCN1 following infarction may be providing some cardioprotective effect, however further studies will be necessary to fully understand the impacts of CCN1 secretion following infarction.

As TGF-β signaling is an important mediator of the tissue remodeling following injury and CCN2 has been shown to be upregulated in response to TGF-β signaling, CCN2 upregulation is commonly observed in remodeling cardiac tissue both following infarction and pressure overload induced remodeling (Daniels, van Bilsen, Goldschmeding, van der Vusse, & van Nieuwenhoven, 2009). CCN2 expression has shown to be increased following myocardial infarction in cardiomyocytes and myofibroblasts in the border zone region, where tissue remodeling is occurring following infarction (Ahmed et al., 2004; Dean et al., 2005; Ohnishi et al., 1998). CCN2 has also been shown to co-localize with TGF-β and fibrillar collagen in areas of perivascular or interstitial fibrotic matrix remodeling in pressure overload models (Finckenberg et al., 2003). Interestingly, CCN2 overexpression studies in models of pressure overload have demonstrated less of a notable hypertrophic or fibrotic remodeling response, suggesting that CCN2 expression itself may be insufficient for fibrotic matrix remodeling and CCN2 instead functions as a potentiator of TGF-β signaling pathways (Frangogiannis, 2012; Panek et al., 2009; Yoon et al., 2010). Several

notable inhibitors of CCN2 secretion have also been identified which may play an important role in suppression of fibrotic matrix remodeling. Knockdown of microRNAs miRNA-133 and miRNA-30 was associated with an increased secretion of CCN2 in cultured fibroblast and cardiomyocyte cell populations (Duisters et al., 2009). Thus, regulation of microRNA expression coupled with the previously discussed balance between CCN2 and CCN5 expression within the tissue microenvironment may play an important role in determining the extent of fibrillar collagen deposition in remodeling cardiac tissue (Diez et al., 2016; Frangogiannis, 2012).

1.2.2.9 Galectins

Galectins are a family of globular proteins which can bind either carbohydrate sequences on glycosylated proteins, glycocalyx carbohydrates, or interact directly with protein binding partners independent of carbohydrate binding (Suthahar et al., 2018). Galectin-3 - first identified as Mac-2 antigen in a subpopulation of activated macrophages - exhibits complex distribution patterns on both a tissue and a cellular level, and has been shown to play a role in the pathogenic remodeling which occurs in numerous pathophysiologies - including fibrotic cardiovascular matrix remodeling (Henderson et al., 2006; Ho & Springer, 1982; Kolatsi-Joannou, Price, Winyard, & Long, 2011; Sundblad, Croci, & Rabinovich, 2011; Suthahar et al., 2018; Yu et al., 2013). Galectin-3 has also been shown to interact with both intracellular and extracellular protein and sugar moieties (Suthahar et al., 2018).

Functionally, Galectin-3 has been demonstrated to be an important modulator of both innate immune responses and fibroblast activation mediated through intracellular and extracellular Galectin-3 dependent mechanisms (Suthahar et al., 2018). Within the cardiovascular system, Galectin-3 was identified as a significant gene target for upregulation in the failing myocardium

(U. C. Sharma et al., 2004). Initially expressed by infiltrating macrophages which further secrete additional Galectin-3 into the cardiac microenvironment, Galectin-3 signaling promotes further innate immune cell extravasation, activation of fibroblast populations, and potentiates TGF-β signaling; all contributing to enhanced deposition of fibrillar collagen within the extracellular space (Henderson et al., 2008; Nabi, Shankar, & Dennis, 2015). Injection of Galectin-3 into the pericardial space of healthy animals was also shown to be a potent inducer of ventricular remodeling and dysfunction, with Galectin-3 injected pericardial regions generally exhibiting increased collagen I to collagen III ratios and increased inflammatory cell infiltrate (U. C. Sharma et al., 2004; Suthahar et al., 2018; Yu et al., 2013). Studies of the cardiac remodeling response to pressure overload in Galectin-3 knockdown animals also demonstrated a reduced fibrotic remodeling response in the Galectin-3 null mice with no significant difference in hypertrophy of cardiomyocytes noted (Gonzalez et al., 2016).

1.2.2.10 Syndecans

Syndecans are a group of transmembrane proteoglycans with heparin sulfate chains which are widely expressed in a variety of tissues (Frangogiannis, 2012; Woods, 2001). Syndecans are composed of three domains: an extracellular ectodomain which can be cleaved by matrix metalloproteases and released into the local microenvironment, a conserved transmembrane domain, and a short cytoplasmic domain (Fears & Woods, 2006; Miftode et al., 2019). Cleaved syndecan protein fragments have been shown to sequester growth factors and bind cell surface moieties to modulate cellular function (Miftode et al., 2019).

In the cardiovascular system, Syndecan-1 and Sydecan-4 have been demonstrated to have important effects on the remodeling response of injured myocardium. Syndecan-1 has been demonstrated to increase following myocardial infarction and helps prevent dilative remodeling

of the myocardium (Miftode et al., 2019; Ostrowski, Pedersen, Jensen, Mogelvang, & Johansson, 2013; Vanhoutte et al., 2007). Syndecan-1 was also found to be upregulated in cardiac tissue in an angiotensin-II infusion model of pressure overload (Schellings et al., 2010). Studies examining the effects of Sydecan-1 knockout in pressure overloaded ventricular tissue demonstrated that part of the pro-fibrotic effect of Syndecan-1 was due to the ability of Syndecan-1 to increase TGF-β and CCN2 protein secretion within the remodeling microenvironment (Schellings et al., 2010).

Conversely, Syndecan-4 has recently been demonstrated to induce an attenuation of cardiac fibrotic remodeling in a pressure overload model (Herum et al., 2020). In this model, a thrombin-mediated cleavage of osteopontin was associated with increased fibrillar collagen deposition in cardiac microenvironments following pressure overload (Herum et al., 2020). Syndecan-4 expression was also noted to increase during pressure overload-induced remodeling, with increased cleavage of the Syndecan-4 ectodomain noted as one progressed through later ventricular remodeling (Herum et al., 2020). When examining Syndecan-4 and osteopontin expression within cardiac tissue, an interaction of the heparin sulfate domains on Syndecan-4 and osteopontin was noted during the early time course of ventricular remodeling – suggesting that Syndecan-4 interactions with osteopontin through the heparin sulfate domain provides some anti-fibrotic effect at early time points by attenuating the ability of osteopontin to induce collagen fibrillogenesis (Herum et al., 2020).

1.2.2.11 Plasminogen Activation Inhibitor-1 (PAI-1)

Plasminogen activation inhibitor-1 (PAI-1) is a single chain glycoprotein which functions as a serine protease inhibitor of urokinase-type plasminogen activator (u-PA) and tissue-type plasminogen activator (t-PA) (Cesari, Pahor, & Incalzi, 2010). PAI-1 is produced by a variety of cell types including fibroblasts, liver cells, cardiomyocytes, endothelial cells, smooth muscle cells,

and macrophages (Cesari et al., 2010; Zorio et al., 2008). PAI-1 expression has been shown to be induced by a variety of factors including various cytokine signaling pathways, metabolic signaling pathways, and hormonal signaling cues (Cesari et al., 2010). PAI-1 expression has also been shown to correlate strongly with the stress response, often experiencing upregulation following periods of acute inflammatory insult, hypoxia, hypothermic stress, oxidative stress, or excess fatigue (Cesari et al., 2010; Pinsky et al., 1998; Uchida et al., 2004; Yamamoto & Loskutoff, 1996)

PAI-1 dysfunction *in vivo* is generally associated with pathological fibrin deposition and subsequent tissue damage (Cesari et al., 2010; Weisberg et al., 2005). PAI-1 expression has also been demonstrated to have a close interaction with the host inflammatory system, with notable increases in PAI-1 expression being observed following increases in TNFα or IL-6 secretion (Kruithof, Mestries, Gascon, & Ythier, 1997; van der Poll et al., 1991). Studies examining cardiac tissue development and homeostasis noted an age-associated robust fibrotic matrix remodeling in PAI-1 null mice, likely a result of excess u-PA signaling or spontaneous TGF-β activation (Frangogiannis, 2012; Moriwaki, Stempien-Otero, Kremen, Cozen, & Dichek, 2004). However, PAI-1 has additionally been shown to undergo transcriptional upregulation following increased angiotensin-II signaling (N. J. Brown, Agirbasli, Williams, Litchfield, & Vaughan, 1998; Skurk, Lee, & Hauner, 2001). Thus, further mechanistic studies may be necessary to tease out the relative contributions of impaired fibrinolytic activity *in vivo* to the development of pathophysiological cardiac matrix remodeling (Cesari et al., 2010).

1.2.2.12 Compositional Changes Which Occur in Cardiac Tissue With Increasing Age

Thus, one can see how not only cardiac tissue exhibits significant heterogeneity in matrix protein content but also how cardiac pathology can alter extracellular matrix protein content. This altered matrix regulation, particularly in the case of matricellular proteins associated with cell

mobility and TGF-β signaling potentiation, can then contribute to further cardiac microenvironmental remodeling and further attenuation of proper cardiac function. Given the previously discussed age-related cardiovascular disease incidence risk coupled with the minimal observed matricellular protein expression in healthy, adult cardiac tissue but increased expression in pathological cardiac tissue; it is important to understand the role that age-related cardiac microenvironmental compositional remodeling plays in promoting cardiovascular pathology development.

Cardiac tissue composition is highly variable across the mammalian lifespan. Liquid chromatography tandem mass spectrometry analysis of fetal, neonatal, and adult cardiac tissue exhibited significant alterations in cardiac extracellular matrix protein composition with increasing age - with fibronectin, periostin, emilin-1, and collagen IV decreasing with increasing age and collagen-I, collagen III, and laminin increasing with increasing age (Williams, Sullivan, & Black, 2015). These compositional changes have also been associated with different cardiac cell function when co-cultured *in vitro*, with fetal cardiac extracellular matrix promoting increased adhesion and expansion of neonatal cardiomyocytes relative to fetal or adult cardiac extracellular matrix (Williams, Quinn, Georgakoudi, & Black, 2014; Williams et al., 2015).

In addition to increasing in mass fraction with the transition from neonatal periods to adulthood, increased deposition of fibrillar collagen subtypes is commonly observed in highly aged cardiac tissue samples relative to control adult tissue samples (Horn & Trafford, 2016; Strait & Lakatta, 2012). It is important to note however that many of these age-related changes in collagen deposition have been characterized in animals models, as it can be difficult to non-invasively quantify collagen deposition in human cardiac tissue (Horn & Trafford, 2016). However, some data exists to suggest that the trend of increased extracellular collagen deposition in aged, non-

pathological cardiac tissue relative to young, healthy controls is observed in human cardiac aging as well. Both biopsy studies relying on histological quantification of positive collagen staining as well as quantification of extracellular volume by magnetic resonance imaging have demonstrated an increase in collagen deposition in aged human cardiac tissue (Gazoti Debessa, Mesiano Maifrino, & Rodrigues de Souza, 2001; C. Y. Liu et al., 2013; Mewton, Liu, Croisille, Bluemke, & Lima, 2011).

Fibrotic collagen deposition in cardiac tissue can generally be characterized as either reactive fibrosis, also known as diffuse fibrosis, or replacement fibrosis (Biernacka & Frangogiannis, 2011; Horn & Trafford, 2016; Silver et al., 1990). Reactive fibrosis, which is characterized by the expansion of existing collagen networks without significant cardiomyocyte loss, has been shown to increase in aged cardiac tissue both histologically as well as by cardiac magnetic resonance imaging (Horn & Trafford, 2016; Jellis, Martin, Narula, & Marwick, 2010; C. Y. Liu et al., 2013; Silver et al., 1990). Replacement fibrosis, which is characterized by deposition of new collagen to replace space left by necrotic cardiomyocytes, has been suggested to increase with increasing age as well (Horn & Trafford, 2016; J. Lin et al., 2008; Silver et al., 1990). Additionally, matrix deposition can also occur in regions around vasculature in cardiac tissue with increasing age, although any deleterious effects of this deposition seem not to exhibit a significant effect on overall cardiac output and, instead, the effects are likely largely paracrine (Horn & Trafford, 2016; van den Heuvel et al., 2000).

Fibrotic collagen deposition is also associated with several characterized alterations in resident cardiac cell function. Excess collagen deposition has been associated with increased left ventricular wall stress and contractile dysfunction (Capasso, Palackal, Olivetti, & Anversa, 1990; Horn & Trafford, 2016; J. Lin et al., 2008). Fibrotic matrix deposition can also impede proper

electrical conduction in cardiac tissue, potentially contributing to arrythmia development (Comtois & Nattel, 2011; Kawara et al., 2001). While these deleterious effects of fibrotic remodeling have been characterized in remodeling cardiac tissue, the relative contributions of interstitial and perivascular fibrotic matrix deposition individually on the observed decline in cardiac function remains to be fully elucidated (Horn & Trafford, 2016).

1.2.2.13 Functional Consequences of Altered Cardiac Tissue Composition

As increased collagen deposition in cardiac extracellular microenvironment begins, left ventricular wall stiffness begins to increase and the early ventricular filling rate declines (Schulman et al., 1992). Consequently, compensatory increases in late filling reliant upon increased atrial contraction become necessary to maintain cardiac output (North & Sinclair, 2012; Schulman et al., 1992). However, as cardiac sympathetic heart rate regulation and β-adrenergic receptor sensitivity decline, ejection fraction can again decline and induce compensatory cardiomyocyte hypertrophy (Lakatta & Levy, 2003b). Non-reversible cardiomyocyte hypertrophy - which occurs in the case of aging or following injury - can initially increase cardiac output, but is often considered a deleterious remodeling outcome which attenuates cardiac output in the long term (Levy et al., 1988).

1.2.3 Clinical Presentation of Cardiovascular Disease

While these age-related changes in cardiac tissue microenvironment and their respective impacts on cardiac function have been characterized, non-invasive recognition of the presentation of early age-related cardiac tissue remodeling remains difficult. Therefore, understanding the progression of change in common clinical parameters which occur with cardiac tissue remodeling

is important for identifying when pathological remodeling may be occuring in order to provide early intervention and improve patient outcomes. One common clinical imaging modality utilized in assessing patient cardiac function is echocardiography.

1.2.3.1 Echocardiographic Assessment of Cardiovascular Function

Echocardiographic assessment of healthy aged individuals will often demonstrate minimal reductions in ejection fraction or systolic function with increasing age (Daimon et al., 2008). However, aged individuals will often present with thickened left ventricular anterior and posterior walls, which is indicative of ventricular cardiomyocyte hypertrophy likely resultant of increased fibrotic matrix deposition or reduced contractile strength due to excess intracellular Ca^{2+} concentrations (Loffredo, Nikolova, Pancoast, & Lee, 2014). Additionally, as left ventricular wall stiffness increases, left ventricular filling dynamics are altered and increasingly reliant upon atrial contraction during late filling to maintain sufficient volume for cardiac output maintenance (North & Sinclair, 2012; Schulman et al., 1992). These changes in ventricular wall thickness and filling characteristics can be identified clinically using several ultrasound imaging modalities – including pulse wave mitral valve flow, B-mode, and doppler tissue imaging (Nagueh et al., 2016).

When studying flow across the mitral valve with pulse wave inflow imaging, mitral flow is typically characterized by biphasic flow with the first peak being indicative of the early ventricular filling (E) wave and the second peak being indicative of the late filling (A) wave (Xu & Daimon, 2016). In healthy individuals, early diastole causes a rapid reduction in left ventricular pressures and a rapid increase in pressure gradient between the left atrium and left ventricle, pushing the majority of blood volume into the left ventricle during early (E) filling (Xu & Daimon, 2016) (Figure 1). Since the majority of volume fills the ventricle during early diastole, less filling occurs during the late (A) diastolic period. Consequently, quantified ratios of the early (E) to late

(A) ventricular filling rates in healthy cardiac tissue are often greater than 1.0 (Xu & Daimon, 2016) (Figure 1).

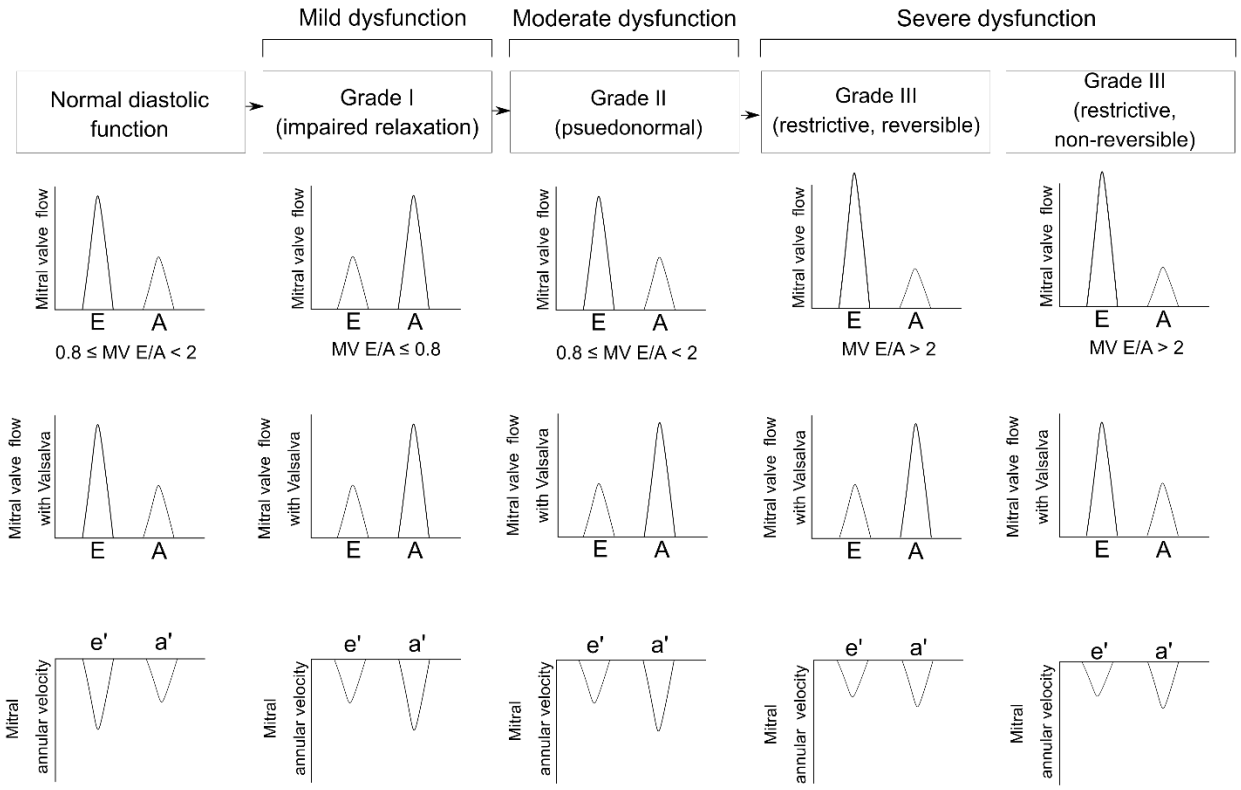

Figure 1 - Grades of left ventricular diastolic dysfunction and correlating echocardiography mitral valve flow and tissue annular velocity measurements. Normal flow across the mitral valve is characterized by mitral valve early wave (E) to late wave (A) filling rate ratios between 0.8 and 2. With grade I diastolic dysfunction, decreased ventricular compliance causes increased late wave ventricular filling. Consequently, the measured mitral valve E/A ratio are observed to decrease below 0.8. With moderate diastolic dysfunction (grade II), measured mitral valve E/A ratios are generally within normal ranges ($0.8 \leq MV < 2$). However, when measured with Valsalva, the mitral valve E/A ratios reflect those observed in grade I diastolic dysfunction (MV E/A<0.8). As diastolic dysfunction worsens (grade III) and left atrial pressure increases, mitral valve flow patterns are characterized by mitral valve E/A ratios greater than 2 as the increasingly large left atrial filling pressure surpasses the resistance to early flow caused by decreased ventricular compliance. Mitral valve tissue annular velocity also generally exhibits a decrease in magnitude with increasing diastolic dysfunction severity, as decreased tissue compliance reduces the early mitral valve tissue annular velocity.

As ventricular compliance decreases, mitral flow in early diastole is disrupted and early filling rates decline. To compensate for reduced early filling rates, increased ventricular filling occurs during late diastole due to atrial contraction, causing an increase in late filling rates (A) and a reduction in mitral E/A rates – often to values below 0.8 (Figure 1). This early stage of diastolic dysfunction is characterized as grade I diastolic dysfunction (Xu & Daimon, 2016). As grade I diastolic dysfunction progresses and left atrial pressures gradually increase, eventually atrial pressure gradients will exceed ventricular pressures again, and flow across the mitral valve will take on a "pseudo-normal" pattern of filling (Figure 1). "Pseudo-normal" filling is generally characterized by E/A rates within the range commonly observed in healthy individuals, despite underlying tissue pathology (Xu & Daimon, 2016). This further progression towards pseudo-normal filling patterns is characterized as grade II diastolic dysfunction. Differentiating grade II diastolic dysfunction from healthy filling patterns often relies upon doppler tissue imaging of the early mitral annulus velocity (e') which serves as an surrogate measure of ventricular relaxation rate (Nagueh et al., 2016). Since e' rates decrease linearly as diastolic dysfunction progresses, increasing ratios of early mitral filling rate to mitral annulus velocity can be utilized to identify grade II diastolic dysfunction (Nagueh et al., 2016) (Figure 2). Additionally, left atrial volume measurement can be utilized for left ventricular filling pressure inference (Xu & Daimon, 2016). Finally, Valsalva maneuver – which reduces ventricular preload due to patient breathing technique - can be utilized in conjunction with mitral valve flow imaging to discriminate normal from "pseudo-normal" filling patterns (Nagueh et al., 2016). In this case, the reduced ventricular preload caused by the modulation of patient breathing can remove the confounding effect that increased atrial filling pressures play in promoting "pseudo-normal" filling patterns in grade II diastolic dysfunctional cardiac tissue (Nagueh et al., 2016).

Further cardiac remodeling and functional decline can subsequently induce progression toward Grade III diastolic dysfunction. Grade III diastolic dysfunction is characterized by restrictive left ventricular filling patterns with mitral valve E/A ratios greater than 2.0 as further increased filling pressures cause further increased early filling rates (Nagueh et al., 2016; Xu & Daimon, 2016).

1.2.3.2 Echocardiographic Changes in Aged Individuals

Even in healthy individuals, cardiac tissue undergoes a decline in diastolic function with increasing age (Daimon et al., 2008; Daimon et al., 2011). Many individuals over 60 years of age exhibit at least grade I diastolic dysfunction, characterized by declining mitral valve early to late filling rate ratios and declining mitral annulus velocity associated with impaired left ventricular relaxation (Daimon et al., 2008; Daimon et al., 2011; Xu & Daimon, 2016). Left ventricular wall thickness and mass have also been observed to increase with increasing age, although the observed increase in mass often falls below clinically established cardiac hypertrophy thresholds (Daimon et al., 2008; Xu & Daimon, 2016).

1.3 Macrophage Ontogeny, Development, and Tissue Seeding

Macrophages are an innate immune cell subtype with important roles in maintaining tissue homeostasis as well as facilitating antigen presentation and inflammasome activation following tissue damage or infection. However, macrophages have also been implicated as mediators in the development and progression of a wide array of pathophysiologies. Thus, increased focus has been given to elucidating the mechanisms by which tissue resident macrophages develop from

embryologic and circulation-derived precursors, polarize, and change in disease pathogenesis in order to better identify therapeutic candidates to correct dysregulated inflammatory cell signaling (Ginhoux & Guilliams, 2016).

1.3.1 The Mononuclear Phagocyte System (MPS)

First described by Van Furth and colleagues in the 1970s, it was long believed that all tissue resident macrophage populations were continuously repopulated through blood monocyte extravasation from circulation and differentiation into macrophages - with blood monocytes being derived from a population of bone marrow-derived promonocytes (Ginhoux & Guilliams, 2016; van Furth et al., 1972). Additionally, while not identifiable at the time of publication, it was noted that there must exist some additional progenitor cell population contributing to the generation of new promonocytes within the bone marrow (Ginhoux & Guilliams, 2016; van Furth et al., 1972). The specific precursor cell hypothesized by Van Furth et. al. would not be discovered until over three decades later when adoptive transfer studies identified a population of macrophage DC precursor cells (MDPs) which were capable of recapitulating monocytes, dendritic cells, and certain resident macrophage subsets (Fogg et al., 2006). Subsequent efforts then focused on identifying the specific ontogenic origins of innate tissue resident cell subtypes.

During this period, bone marrow adoptive transfer studies in irradiated mice were beginning to suggest that not all tissue resident macrophage subsets were derived from circulating monocytic precursor cells as previously described in the MPS and subsequent *in vitro* or *in vivo* studies (Ginhoux & Guilliams, 2016; Merad et al., 2002). Langerhans cells, the resident macrophage population of the epidermis, were demonstrated to exhibit a resistance to high dose radiation with minimal repopulation by donor bone marrow-derived cells in adoptive transfer

studies (Merad et al., 2002). Rather, it was observed that the majority of Langerhans cell repopulation following radiation was from host-derived cell turnover within the local microenvironment (Merad et al., 2002). Subsequent studies identified similar self-proliferative ability of other previously thought to be monocyte derived tissue resident macrophage populations, including microglia and alveolar macrophages (Ajami, Bennett, Krieger, Tetzlaff, & Rossi, 2007; Ginhoux et al., 2010). Parabiosis studies, in which a young and aged mouse have their circulatory systems surgical connected, further extended the nuance of tissue macrophage seeding dynamics by identifying mixed developmental origin macrophage populations within a variety of organ systems (Ginhoux & Guilliams, 2016). With the identification of these different developmental origin macrophage populations, future work focused on identifying the distinct time course of macrophage tissue seeding during embryogenesis and with increasing age.

1.3.1.1 Embryonic Hematopoiesis

Macrophages are first noted in developing rodent embryos around embryonic day 10.5 (E10.5) in the brain rudiment and developing skin (Ginhoux & Guilliams, 2016). While fetal macrophages had been identified in previous studies and some suggestions had been made regarding their potential ability to contribute to adult tissue resident macrophage populations, it was not until lineage tracing experimental techniques became available that it was possible to definitely quantify the embryonic contribution to adult tissue resident macrophage populations (Alliot, Lecain, Grima, & Pessac, 1991; Ginhoux & Guilliams, 2016).

Primitive hematopoiesis - the first wave of identifiable hematopoiesis in the mammalian embryo - begins around E7.0 in the blood islands of the extraembryonic yolk sac, and gives rise to erythrocytes, macrophages, and megakaryocytes (Palis, Robertson, Kennedy, Wall, & Keller, 1999; Tober et al., 2007). A second wave of yolk sac hematopoiesis occurs then around E8.0-E8.5

with generation of erythro-myeloid progenitor (EMP) cell populations which exhibit broad erythroid and myeloid differentiation potential (Frame, McGrath, & Palis, 2013). These EMPs then migrate to the fetal liver following the establishment of the embryonic circulatory system, where they differentiate into additional hematopoietic cell lineages including fetal liver monocytes (Palis & Yoder, 2001). Concomitant with the initial period of erythromyeloid progenitor cell differentiation around embryonic day 8.0-8.5, another population of progenitor cells arises from the intraembryonic hemogenic endothelium and begin to differentiate into hematopoietic stem cells (Ginhoux & Guilliams, 2016). These hematopoietic stem cell progenitors will eventually colonize the fetal liver during embryogenesis, establish the onset of definitive hematopoiesis, and eventually migrate to bone marrow niches following birth (Ginhoux & Guilliams, 2016).

Additional lineage tracing studies expanded the embryonic hematopoietic paradigm further with the identification of an early wave of erythromyeloid progenitor cell differentiation which occurs at E7.5 and a late wave of erythromyeloid progenitor cell differentiation around E8.5 (Ginhoux & Guilliams, 2016; Hoeffel et al., 2015; Kierdorf et al., 2013). Yolk sac macrophages derived from the first wave of hematopoiesis are dependent upon colony stimulating factor-1 receptor (CSF-1R) gene transcription (Hoeffel et al., 2015). Consequently, genetic ablation or insertion of fluorescent protein coding regions downstream of *Csf1r* promoter regions under tamoxifen-inducible control can be utilized to study which resident macrophage populations are derived entirely from these early wave hematopoietic progenitors (Hoeffel et al., 2015). Runt-related transcription factor (*Runx1*) is a transcription factor important in both yolk sac macrophage development as well as in fetal monocyte differentiation (Hoeffel et al., 2015; Hoeffel et al., 2012). Thus, insertion of fluorescent protein coding regions downstream of the *Runx1* promoter under tamoxifen inducible control can be utilized to study yolk sac macrophage and fetal liver monocyte

tissue seeding with tamoxifen injections at E7.5 or E8.5, respectively (Hoeffel et al., 2012). Together these lineage tracing experimental systems coupled with subsequent imaging at various points of development can be used to determine which tissue resident macrophages are populated entirely by yolk sac progenitor-derived macrophages and which tissue resident macrophages are replaced by fetal liver monocyte-derived macrophages (Hoeffel et al., 2015; Hoeffel et al., 2012). It was noted that, while macrophages generated from early erythromyeloid progenitor cells initially seeded many developing tissue sites, these macrophages populations did not persist into adulthood; except for in the case of microglia populations, where a significant fraction of cells retained early erythromyeloid labeling (Hoeffel et al., 2015). These results suggest that early erythromyeloid progenitor derived macrophages only significantly contribute to the adult microglia cell population and that other tissue resident macrophage populations are progressively replaced during embryogenesis by more competitive late erythromyeloid progenitor derived or hematopoietic stem cell derived macrophage populations (Hoeffel et al., 2015) (Figure 2).

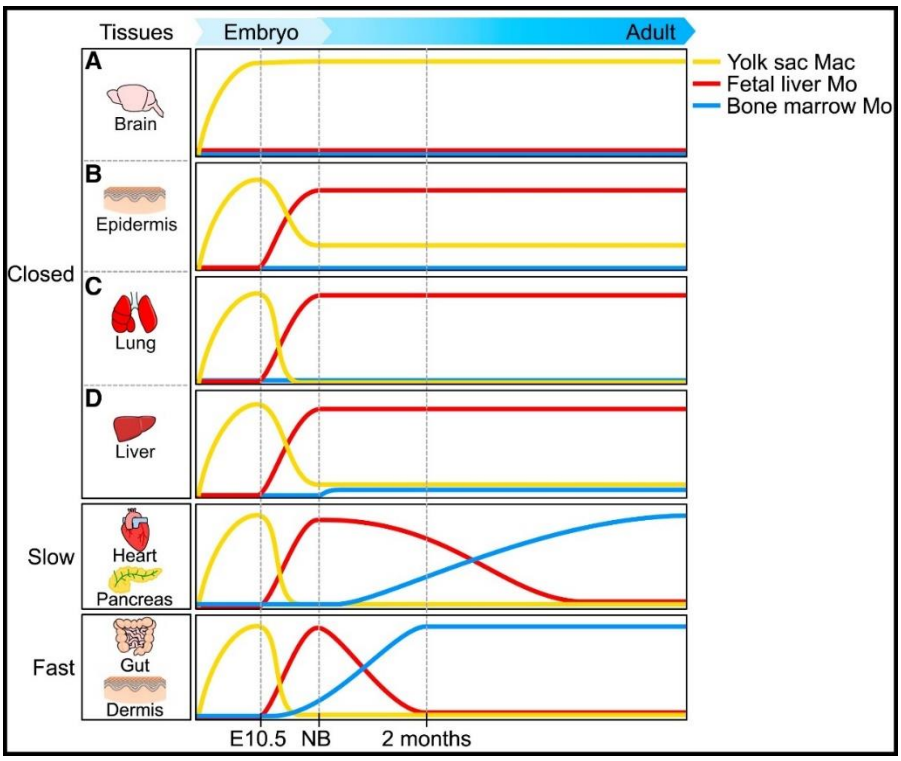

Figure 2 - Heterogenity of tissue resident macrophage ontogeny throughout development and in adulthood. Reproduced from (Ginhoux et. al., 2016). Here one can see the distinct waves of tissue resident macrophages which derive from unqiue precuror cells as well as the degree to which each macrophage subset persists into adulthood. For example, in **(A)** one can see the initial wave of yolk sac progenitor-derived macrophages colonizes the brain and self-proliferate within this microenvironment into adulthood with minimal colonization by fetal liver or bone marrow monocyte-derived macrophages. This would be an example of a "closed" tissue niche. In a similar manner, the epidermis **(B)**, lung **(C)**, and **(D)** liver are initially seeded by embryonic precurosor cell-derived macrophages and exhibit minimal post-natal colonization of bone marrow monocyte-derived macrophages into these tissue microenvironments; suggesting that these may also be "closed" tissue microenvironments. In tissue microenvironments which are not entirely closed off to bone marrow monocyte colonization, monocytes can either exhibit a slow colonization - such as that observed in the heart or pancreas - or a rapid colonization - such as that observed in the gut or dermis.

1.3.1.2 Fetal Liver Hematopoiesis

Based upon prior observations in Langerhans cell populations, it was hypothesized that the progressive loss of early erythromyeloid progenitor derived macrophages was likely due to competitive replacement by fetal liver derived macrophages (Hoeffel et al., 2015; Hoeffel et al., 2012). Using a *S100a4* tamoxifen-inducible lineage tracing model, it was observed that fetal liver monocyte-derived macrophages are the predominant source of fetal macrophages within the developing embryo and these macrophages are capable of self-proliferating within their respective tissue microenvironments into adulthood (Hoeffel et al., 2015). Additional flow cytometric characterization of fetal liver monocyte populations demonstrated some heterogeneity in Flt3 and Ly6C expression, similar to the continuum of monocytic precursors observed during bone marrow hematopoiesis (Hoeffel et al., 2015). Using additional tamoxifen inducible lineage tracing studies in *Runx1* promoter mice where tamoxifen was injected at E8.5 to label the late wave EMPs which migrate to the fetal liver, it was determined that the $Lin^{-}cKit^{+}Flt3^{-}CSF\text{-}1R^{+}Ly6C^{-}$ fetal liver myeloid progenitor populations were the main source of fetal liver monocytes; demonstrating the importance of late wave erythromyeloid progenitors for the establishment of fetal liver hematopoiesis and tissue seeding (Hoeffel et al., 2015). Additionally, it was noted that the other characterized fetal liver hematopoietic monocytic lineage diversity may be attributable to the progressive colonization of the fetal liver by hematopoietic stem cell precursors which gradually establish definitive hematopoiesis within the embryo (Hoeffel et al., 2015). It is also important to note that while the differences in tissue deposition dynamics between early and late wave erythromyeloid progenitors has been well characterized, it remains unclear if these cell populations are derived from unique progenitor cell populations or are a single cell population along a continuum of maturation states (Ginhoux & Guilliams, 2016). In the case of the later non-cell

intrinsic hypothesis, it was noted that this continuation of maturation states may be a consequence of the changing cell extrinsic microenvironmental stimuli between the extraembryonic yolk sac and fetal liver niches (Ginhoux & Guilliams, 2016).

However, some conflicting results have suggested alternate developmental sources for adult tissue resident macrophages. Since *Runx1* is transiently expressed in the developing embryo during early endothelial to hematopoietic cell transition, some doubt has been raised regarding the labeling efficacy of late wave erythromyeloid progenitor cell populations (Lacaud et al., 2002; Sheng, Ruedl, & Karjalainen, 2015). Alternative lineage tracing studies using stem cell factor c-Kit, which is expressed during all stages of hematopoiesis, have suggested that all adult tissue resident macrophage populations with the exception of microglia and some Langerhans cell populations are derived from hematopoietic stem cell precursor differentiation and tissue seeding (Sheng et al., 2015). However, given the common expression of c-Kit in both late wave erythromyeloid progenitors as well as early hematopoietic stem cell precursors, this labeling approach may fail to sufficiently differentiate between EMP or HSC-derived cells - which both begin arising in the developing embryo at E8.5 (Ginhoux & Guilliams, 2016).

1.3.2 Bone Marrow Hematopoiesis and the Perinatal Window

Bone marrow hematopoiesis is the primary source of hematopoietic cell generation in adult mammals, save for certain embryologically derived immune cell subsets - such as microglia, γδ T cells, or B-1 cells (Beaudin et al., 2016; Hoeffel & Ginhoux, 2018; Sawai et al., 2016). However, the long term regenerative capacity characteristic of mature hematopoietic stem cell populations does not fully develop until E17.5; suggesting that some perinatal hematopoiesis in the fetal liver and spleen may produce hematopoietic cells until hematopoietic stem cells have fully developed

and colonized the bone marrow niche (Hoeffel & Ginhoux, 2018). In a study examining circulating fetal monocyte levels in perinatal development periods, it was observed that despite an increasingly depleted population of EMPs, no detectable change in circulating fetal monocytes was observed (Hoeffel et al., 2015). This suggests that precursor hematopoietic stem cell populations may be capable of differentiating into fetal monocytes and other hematopoietic cell lineages during perinatal periods before mature hematopoietic stem cells colonize the developed bone marrow niche (Hoeffel et al., 2015; Hoeffel & Ginhoux, 2018).

It also appears that some additional important tissue colonization of fetal monocyte derived macrophages occurs during perinatal time frames. Lineage tracing of arterial macrophages demonstrated colonization of developing arterial tissue during multiple periods of embryogenesis including by fetal monocytes during perinatal periods (Ensan et al., 2016). Additionally, similar results have demonstrated a capacity for Kupffer cells, the resident liver macrophage population, and testis tissue resident macrophage seeding during perinatal periods (Mossadegh-Keller et al., 2017; Scott et al., 2016). Taken together, these results not only show that several important resident macrophage seeding events take place during perinatal periods before the establishment of the bone marrow hematopoietic niche, but also that colonization of a tissue by EMP or HSC-derived progenitors is partially dependent upon the openness of the tissue niche (Hoeffel & Ginhoux, 2018). For example, the ability of circulating cells to extravasate into neural tissue is reduced during the course of embryogenesis (Saili et al., 2017). Consequently, early wave erythromyeloid progenitor cell-derived macrophages (microglia) are the only population to seed this tissue as the niche is closed by the time any subsequent waves of hematopoietic cell generation begin (Hoeffel & Ginhoux, 2018). Alternatively, some tissue niches exhibit variable to complete openness to repopulation by circulation derived monocytes during perinatal and adult periods, with the degree

to which the resident macrophage compartment can be recapitulated by circulating monocytes exhibiting a tissue and animal age dependance (Hoeffel & Ginhoux, 2018).

Once hematopoietic stem cells have developed long term regenerative capacity, matured, and colonized the newly formed bone marrow niche, new macrophages are derived through a common macrophage-dendritic cell precursor (MDP) which differentiates into either a common dendritic cell precursor (DCP) or a common monocyte progenitor (cMoP) (Hoeffel & Ginhoux, 2018). Two subsets of monocytes, which can be discriminated by the level of surface marker Ly6C expression, can then differentiate from the cMoP in the bone marrow (Hoeffel & Ginhoux, 2018). While the exact function of these different subsets remain to be elucidated, some evidence has suggested an endothelial cell surveillance role for the $Ly6C^{lo}$ subset while the $Ly6C^{hi}$ subset has been implicated as more likely to extravasate into inflamed tissue sites (Carlin et al., 2013; Jakubzick, Randolph, & Henson, 2017). Following extravasation, these monocytes can undergo differentiation into either dendritic cells or macrophages, although the exact mechanisms by which the differentiation pathways is determined remains unclear (Jakubzick et al., 2017). However, some additional characterization of atypical monocyte populations as well as of monocytes persisting for extended periods in tissue niches have suggested additional complexity in monocyte heterogeneity (Hoeffel & Ginhoux, 2018; J. D. Lin et al., 2019).

1.3.3 Mechanisms of Altered Macrophage Phenotypic Regulation in Response to Diverse Microenvironmental Cues

After monocytes extravasate into a tissue niche, they differentiate into macrophages whose phenotype and function will be determined by the local tissue microenvironment (Hoeffel & Ginhoux, 2018; van de Laar et al., 2016). While the exact mechanisms by which specific tissue

niches alter macrophage genetic expression remain to be fully elucidated, several studies have been performed that have demonstrated a robust microenvironmental responsivity of naïve macrophage populations (van de Laar et al., 2016). In a study examining the ability of various monocyte and macrophage populations to repopulate an experimentally depleted alveolar macrophage niche, it was observed that - despite exhibiting significantly different initial gene expression profiles - yolk sac-derived macrophages, fetal liver monocytes, or bone marrow monocytes transplanted into an empty alveolar niche all took on a phenotype similar to that of control alveolar macrophages (van de Laar et al., 2016). Thus, given the numerous compositional and biomechanical changes which occur in both aging and pathologically remodeling tissue sites, understanding the mechanisms by which naïve macrophages integrate microenvironmental stimuli to acquire a tissue specific phenotype presents an interesting therapeutic target for treatment of a variety of pathophysiologies.

1.3.3.1 Macrophage Phenotype Can Be Better Understood as a Spectrum of Polarization States

In order to better understand how different gene expression patterns induce altered macrophage function within a given tissue site, a classification system of macrophage phenotype was developed to help segment functionally different macrophages within a given tissue. These phenotypes were initially derived from experimental treatment of naïve macrophage populations with either bacterial lipopolysaccharide (LPS) and Th1 cytokine interferon gamma (IFN-γ) or Th2 cytokine interleukin-4 (IL-4) (B. N. Brown, Haschak, Lopresti, & Stahl, 2017; Mills, Kincaid, Alt, Heilman, & Hill, 2000; P. J. Murray et al., 2014). Polarization states induced by treatment with LPS and IFN-γ - which were termed “M1” polarization states due to IFN-γ secretion being associated with type I immune responses - were found to be associated with pro-inflammatory

cytokine secretion, radical oxidant production, arginine metabolism through inducible nitric oxide synthase metabolic pathways, and monocyte chemoattractant secretion (B. N. Brown et al., 2017; Mills et al., 2000). Pro-inflammatory cytokines produced by M1 macrophage populations include tumor necrosis factor alpha (TNF-α), interleukin-1β (IL-1β), interleukin-6 (IL-6), interleukin-12 (IL-12) and are generally associated with activation of additional immune cell subsets - an expected feature of an immune response largely intended to clear pathogens or injury induced tissue damage (B. N. Brown et al., 2017). This functional enhancement of inflammation, which is characteristic of canonical M1 macrophages, can also be observed in the profile of chemoattractant cues secreted by these cells (B. N. Brown et al., 2017). M1 macrophage populations tend to secrete chemoattractant proteins such as C-C motif chemokine ligand 2 (CCL2/Mcp-1 (monocyte chemoattractant protein-1)) or CCL5, which function to recruit additional $Ly6C^{hi}$ monocytes that can subsequently differentiate into dendritic cells or macrophages to enhance the tissue immune response (B. N. Brown et al., 2017; Sica, Erreni, Allavena, & Porta, 2015).

Treatment with type II immune response associated IL-4 (termed "M2" polarization) was found to be associated with increased production of immunomodulatory cytokines such as IL-10, increased secretion of extracellular matrix modulatory enzymes, metabolism of arginine through arginase enzymatic pathways, and enhanced growth factor signaling (B. N. Brown et al., 2017; Mills et al., 2000). M2 macrophages tend to function in an immunomodulatory manner which can serve to help attenuate inflammation following M1 macrophage polarization and clearance of tissue damage or pathogens (B. N. Brown et al., 2017). The secretion of matrix modulatory enzymes - such as matrix metalloprotease-2 (MMP-2), matrix metalloprotease-9 (MMP-9), or tissue inhibitor of metalloprotease-1 (TIMP-1) – also suggests a functional role of M2 macrophage subsets with the tissue resolution response following the clearance of damage-associated or

pathogen-associated proteins from the local microenvironment (B. N. Brown et al., 2017). M2 macrophages have also been shown to enhance TGF-β signaling, which can further activate fibroblast populations and induce further matrix production and remodeling (B. N. Brown et al., 2017).

While these classification systems present interesting demonstrations of macrophage phenotypic plasticity, their value has been in their applicability to a variety of disease pathologies as well as in the mammalian host response to biomaterial implants *in vivo* (B. N. Brown et al., 2017). Chronic pro-inflammatory macrophage polarization has been characterized in numerous autoimmune pathophysiologies including inflammatory bowel disease, rheumatoid arthritis, diabetes, and systemic lupus erythematosus (Funes, Rios, Escobar-Vera, & Kalergis, 2018; Lumeng, Bodzin, & Saltiel, 2007; Triantafyllopoulou et al., 2010; Zhu et al., 2014). Macrophage polarization surrounding a biomaterial following implant has also been shown to correlate with the long term tissue remodeling response (B. N. Brown et al., 2017). In general, chronic macrophage polarization towards M1 phenotypes was noted to be associated with decreased biomaterial-tissue integration, increased fibrotic matrix deposition in the region proximal to the implant, and increased infiltration of additional immune and fibroblast cell populations to the local microenvironment (B. N. Brown et al., 2017; B. N. Brown, Ratner, Goodman, Amar, & Badylak, 2012).

Conversely, biomaterial implants which exhibited better functional integration within the implant site were found to be associated with timely shifts from M1 macrophage polarization to M2 macrophage polarization states. This phenotypic conversion, which will generally occur following the first few days of the initial inflammatory response, has been shown to be important for tissue remodeling and stabilization in the tissue-biomaterial interfacing regions.

Mechanistically, this can likely be attributed to the increased secretion of matrix modulatory enzymes, increased TGF-β signaling, and increased ornithine production through arginine metabolism - which together serve to stabilize the remodeling collagen at the biomaterial-tissue interface (B. N. Brown et al., 2017; B. N. Brown et al., 2012). Promoting phenotypic shifts in macrophage populations from M1 to M2 polarizations has also been demonstrated to correlate with improved disease state in several autoimmune disease pathology models (Funes et al., 2018). Increasing the relative ratio of M2 to M1 polarized macrophages by M2 macrophage transference has been shown to improve outcomes in murine colitis models (Haribhai et al., 2016; Zhu et al., 2014). Additionally, similar improvements in disease pathophysiology has been observed following M2 macrophage transference in murine models of systemic lupus and diabetes (Funes et al., 2018).

Several important considerations must be discussed when applying this system of macrophage classification to *in vivo* macrophage function. The first important consideration is that while macrophage polarization is defined as a spectrum of extreme pro- or anti-inflammatory phenotypic extremes, macrophage polarization is often not observed to completely replicate these characterized *in vitro* phenotypes *in vivo*, but rather macrophages often exhibit expression of both some M1-associated and M2-associated protein expression *in vivo* (B. N. Brown et al., 2017; Peter J. Murray, 2017). Additionally, it is important to note that macrophage polarization is not a constant in time (Peter J. Murray, 2017). Macrophage polarization is highly dynamic in response to changing microenvironmental conditions or extracellular cytokine concentrations (Peter J. Murray, 2017; P. J. Murray et al., 2014). Consequently, macrophages which extravasate and differentiate within a tissue microenvironment can often exhibit several unique phenotypes over the time course of pathogen or damage clearance and tissue repair. Thus, it is important to consider

that single timepoint characterization of macrophage polarization dynamics may not fully recapitulate the macrophage response to pathogen or tissue damage. Additionally, while macrophage polarization states can provide important referential insight regarding macrophage functionality within a given tissue microenvironment; phenotypic characterization of macrophage within a given tissue microenvironment does not always provide functional insight about a given tissue (Peter J. Murray, 2017).

1.3.3.2 Cytokine and Interleukin-mediated Mechanisms of Macrophage Polarization

As previously discussed, macrophage M1, pro-inflammatory and M2, anti-inflammatory polarization states were characterized based upon *in vitro* stimulation with cytokines or TLR agonist ligands to mimic the conditions present during a type I or type II immune response (Mills et al., 2000; Peter J. Murray, 2017; P. J. Murray et al., 2014). M1 macrophage polarization was characterized in response to treatment with type I immune response-associated t-cell cytokine interferon-γ (IFN-γ) and toll-like receptor agonist lipopolysaccharide (LPS). M2 polarization states were characterized in response to *in vitro* culture treatment with type II immune response-associated t-cell cytokine interleukin-4 (IL-4). In addition to these canonical polarization inducing stimuli, some addition polarization responses to various pro- or anti-inflammatory response-associated cytokines have been characterized. M1 macrophage polarization has been observed in response to inflammation-associated cytokine tumor necrosis factor alpha (TNF-α). Additionally, M2 macrophage polarization states have been observed in response to interleukin-13 (IL-13).

Macrophages cultured *in vitro* have also been shown to exhibit some altered morphologies in response to cytokine or pathogen-associated stimuli (Patel et al., 2012). It was observed that macrophages exhibited a significant change in morphology following treatment with bacterial LPS (Patel et al., 2012). This morphological change was characterized by an increase in cell area and

an increase in the number of filipodia observed on cultured macrophages (Patel et al., 2012). In addition to these altered morphological and polarization responses to canonical cytokine or pathogen ligand sensing, macrophages can also exhibit robust polarization following exposure to various microenvironmental stimuli.

1.3.3.3 Damage- and Pathogen-associated Molecular Pattern Receptor Mediated Mechanisms of Macrophage Polarization

Given the role that chronic M1 macrophage signaling has in promoting disease pathogenesis and poor biomaterial tissue integration, understanding the mechanisms by which macrophages integrate local microenvironmental stimuli to induce a polarization state can provide important therapeutic opportunities for diseases characterized by chronic pro-inflammatory macrophage activation. Additionally, understanding the mechanisms by which macrophage polarization is induced can help develop important principles which can be applied to biomaterial design and fabrication to promote enhanced functional tissue integration following implant.

Macrophages can sense local microenvironmental stimuli through a variety of surface receptor mediated pathways. Pattern-recognition receptors (PRRs) are a class of membrane bound receptor proteins which macrophages express that recognize damage- and pathogen-associated molecular patterns (DAMPs/PAMPs) (Akira, Uematsu, & Takeuchi, 2006; B. N. Brown et al., 2017). The Toll-like receptor (TLR) family is one such group of PRRs which are essential for a variety of immune cell-mediated processes.

The TLR family of PRRs, of which 12 constitutive TLR proteins have been characterized in mammals, is a family of transmembrane glycoproteins characterized by extracellular domains with leucine rich repeats and cytoplasmic domains exhibiting a structural homology similar to that of the interleukin-1β receptor (Akira et al., 2006; Bowie & O'Neill, 2000). TLR glycoproteins can

also be further subdivided based upon the type of pathogen associated ligand which the TLR binds. For example, TLR1, 2, and 6 bind pathogen-associated lipids while TLR7, 8, and 9 bind pathogen-associated nucleic acid sequences (Akira et al., 2006). However, not all TLR family glycoproteins can be grouped based solely on class of the ligands which they bind. TLR4 has been shown to bind a variety of ligands including fibronectin, heat shock proteins, or lipopolysaccharide (Akira et al., 2006). TLR family glycoprotein expression has been characterized in a variety of both immune and non-immune cell populations, including in macrophage, dendritic cell, fibroblast and endothelial cell populations (Akira et al., 2006). TLR expression is also not uniform but rather experiences dynamic upregulation during periods of infection, tissue damage, or organismal stress (Akira et al., 2006). Additionally, there exists some variability in TLR expression within cell populations, with certain TLR glycoproteins often being expressed on the cell surface (TLR1, 2, 4, and 6) while others have been noted to be primarily expressed intracellularly (TLR 3, 7, 8, and 9) (Akira et al., 2006).

TLR signal transduction begins with ligand binding, receptor dimerization, and recruitment of adaptor proteins to the cytoplasmic domain, such as myeloid differentiation factor (MyD88) - which can then lead to inflammasome formation, activation, and further pro-inflammatory cytokine secretion (Akira et al., 2006; B. N. Brown et al., 2017). Many other adaptor proteins in addition to MyD88 have been characterized within the mechanism of TLR signal transduction, and it has been hypothesized that some of the differential responsivity observed following TLR stimulation may be partially attributable to differential recruitment of adaptor proteins (Akira et al., 2006). Adaptor protein assembly can then alter the activity of NF-κB and MAP kinases, inducing increased pro-inflammatory gene expression and cytokine secretion (Akira et al., 2006).

In addition to TLR glycoproteins which are bound within the cell surface membrane or within the membranes of intracellular endosomal compartments, cytoplasmic pattern recognition receptors classified as either NOD-LRR proteins or CARD-helicase proteins and exhibit a specificity towards bacterial and viral components, respectively (Akira et al., 2006). NOD-LRR proteins are composed of several functional domains including leucine rich repeat domains, nucleotide oligomerization domains, and signal initiation domains, such as CARD or Pyrin domains (Akira et al., 2006). NOD-LRR proteins can induce inflammatory function in response to bacterial ligand binding through either direct NF-κB activation or Caspase-1 mediated pro-Il-1β cleavage (Akira et al., 2006).

CARD-helicase proteins are another group of cytoplasmic PRRs expressed within a variety of cell types which can induce TLR-independent Type I immune responses to viral cytosolic nucleic acids (Akira et al., 2006). Retinoic-acid-inducible protein 1 (RIG-1) and melanoma differentiation associated gene 5 (MDA5) are two such cytoplasmic double stranded DNA sensing receptors (Akira et al., 2006). While some evidence exists to suggest that viral replication mechanism and route of entry may play in role in dictating whether the viral replication triggers TLR3 or RIG-1/MDA5 activation, clear mechanisms of receptor activation following viral ligand binding remain to be elucidated. Additionally, further work will be necessary to determine if cell type has any impact on cytosolic viral replication sensing mechanisms (Akira et al., 2006).

1.3.3.4 Extracellular Matrix-mediated Mechanisms of Macrophage Polarization

In addition to receptors which bind pathogen-associated molecular patterns, macrophages also express receptors which are able to bind damage-associated molecular patterns (DAMPs) which function to induce phagocytosis and tissue remodeling responses in macrophage populations when tissue injury needs to be cleared and remodeled to restore function (B. N. Brown et al., 2017).

Numerous DAMPs are generated during tissue injury or during periods of stress, including heat shock proteins (HSPs), high mobility group box 1 protein (HMGB1), mitochondrial components, or extracellular matrix fragments (Pauwels, Trost, Beyaert, & Hoffmann, 2017). Cellular responses to this diverse array of ligands is often mediated through pattern recognition receptors, including some of the previously described TLR family signaling pathways (Pauwels et al., 2017). In addition to these damage-associated proteins released into the extracellular space following tissue injury, matrix degradation products - resultant of either tissue trauma or enzyme mediated matrix protein cleavage such as by MMP-2 or MMP-9 – can also be released into the extracellular microenvironment. These matrix fragments can in turn promote altered cellular adhesion, migration, and polarization dynamics in a given microenvironment (Boyd & Thomas, 2017).

While some characterization of the bioactivity of various matrix protein fragments has been performed, a complete characterization has proven difficult due to the vast number of fragments which can be generated following enzymatic cleavage as well as the large heterogeneity of matrix proteins present within any given tissue. However, some matrikine signaling mechanisms which have been elucidated in macrophages can help one understand how macrophage behavior may be altered in response to matrix protein fragment binding to various macrophage surface receptors (Boyd & Thomas, 2017).

One such matrix protein fragment which can influence innate immune cell behavior is a result of elastin protein cleavage by MMP-12 (Boyd & Thomas, 2017; Brassart et al., 2001; Senior et al., 1984). Following cleavage by MMP-12, an elastin peptide fragment with a six amino acid sequence VGVAPG is generated (Boyd & Thomas, 2017). This fragment has been shown to function as a chemoattractant for monocyte and fibroblast cell populations as well as to function as an inducer of increased matrix metalloprotease secretion in fibroblast and endothelial cell

populations (Boyd & Thomas, 2017; Brassart et al., 2001; Senior et al., 1984). This VGVAPG elastin fragment has also been implicated as an important mediator of the chronic macrophage accumulation in pulmonary tissue in murine models of emphysema (Hautamaki, Kobayashi, Senior, & Shapiro, 1997; Houghton et al., 2006).

Collagen peptide fragments have also been demonstrated to have bioactivity within innate immune cell populations. Collagen peptides containing a proline-glycine-proline (PGP) sequence has been shown to function as a chemoattractant, particularly for neutrophils (Pfister & Haddox, 1996). Believed to result following collagen protein cleavage by MMP-8 and MMP-9, collagen PGP peptides are believed to function mechanistically at least partially through a shared structural homology with other neutrophil chemoattractant cytokines, such as IL-8, CXCL1, or CXCL2 (Gaggar et al., 2008). These results demonstrating a robust PGP fragment mediated neutrophil efflux were also observed in human cystic fibrosis bronchoalveolar lavage samples (Gaggar et al., 2008). Additional murine models further demonstrated that MMP-8, MMP-9, and serine protease cleavage of collagen peptides generates PGP sequences *in vivo* and generation of these sequences is associated with neutrophil accumulation characteristic of cystic fibrosis pulmonary tissue microenvironments (Gaggar et al., 2008).

Collagen C-terminal pro-peptide cleavage fragments have also been suggested to potentially function as modulators of the fibroblast-mediated wound healing response (Lindsey et al., 2015). Collagen C-terminal pro-peptide fragments were found to have a cardioprotective effect following myocardial infarction through a promotion of reactive scarring and angiogenesis following infarction (Lindsey et al., 2015). Collagen C-terminal pro-peptides have also been suggested to have some chemoattractant functionality in endothelial cell populations; a

functionality which was hypothesized to partially contribute to the observed cardioprotective effects observed following myocardial infarction (Kisling et al., 2019; Lindsey et al., 2015).

Collagen IV degradation products have also been shown to possess various important matricellular functionality. Due to the three different α-chain trimers which constitute collagen IV, numerous peptide fragments could result following protein degradation. However, to date only six bioactive collagen IV-derived peptide fragments all derived from α-chain non-collagenous domains have been identified (Kisling et al., 2019). Arresten, an α1 chain matrikine, has been shown to exhibit antiangiogenic function (Ricard-Blum & Vallet, 2017). Canstatin, an α2 chain C-terminal pro-peptide cleavage product, has been shown to promote epithelial cell proliferation and function as a fibroblast chemoattractant (Kisling et al., 2019; Ricard-Blum & Vallet, 2017). Similarly, other collagen IV matrikines have been demonstrated to inhibit angiogenesis and alter fibroblast proliferation or migration (Kisling et al., 2019).

Additional matrix protein fragments have been demonstrated to possess innate immune cell bioactivity, however the mechanisms by which innate immune cells bind and induce altered gene expression are not fully clear. Hyaluronan protein degradation fragments have been demonstrated to alter immune cell function (Jiang, Liang, & Noble, 2011). Hyaluronan fragments can result following either hyaluronidase upregulation or as a consequence of increased radical oxidant concentrations within a tissue microenvironment (Jiang et al., 2011). Additionally, hyaluronan fragment signaling can be inhibited through extracellular superoxide dismutase secretion through direct superoxide dismutase hyaluronan fragment binding (Gao et al., 2008). Hyaluronan can also be enzymatically degraded into a variety of degradation products varying greatly in protein molecular weight (Jiang et al., 2011). Interestingly, there also appears to be some altered bioactivity between high and low molecular weight hyaluronan protein fragments. Low molecular

weight hyaluronan protein has been shown to increase pro-inflammatory cytokine production, chemokine secretion, secretion of matrix metalloproteases, and production of antifibrinolytic factors such as PAI-1 (Horton et al., 1998; Horton et al., 2000; Horton, Olman, & Noble, 1999; Horton, Shapiro, Bao, Lowenstein, & Noble, 1999; Jiang et al., 2011; McKee et al., 1997). This modulation of macrophage activity was also observed more prominently in infiltrating, bone marrow-derived macrophage populations than in resident macrophage subsets (Hodge-Dufour et al., 1997; Jiang et al., 2011). This altered macrophage function has been shown to be partially mediated through hyaluronan protein binding to either TLR family proteins or to CD44 surface receptors, providing some functional overlap in macrophage microenvironmental stimuli sensing mechanisms for PAMPS, DAMPS, or matrikines (Boyd & Thomas, 2017; Jiang et al., 2011).

1.3.3.5 The Impacts of Altered Tissue Biomechanics on Macrophage Polarization

As previously discussed, macrophage polarization dynamics in the weeks following biomaterial implant can have a significant impact on either promoting the functional integration of the biomaterial into the tissue microenvironment or promoting chronic inflammatory processes which inhibit biomaterial function and integration (B. N. Brown et al., 2017; McWhorter, Davis, & Liu, 2015). In general, beneficial immune responses following biomaterial implant are characterized by an initial pro-inflammatory macrophage polarization followed by a timely phenotypic conversion to more M2-like phenotypes (B. N. Brown et al., 2017). Thus, many biomaterial studies have sought to develop materials which are able to attenuate chronic inflammatory processes and promote timely conversion of macrophages to M2 polarization states (McWhorter et al., 2015).

These studies have elucidated several significant features of the macrophage response to differing culture substrate mechanics or topological features (McWhorter et al., 2015). When

examining the macrophage phenotypic response to material surface roughness, it was observed that macrophages exhibited increased pro-inflammatory cytokine secretion when cultured on materials with rough surfaces relative to smooth surface materials; an effect which was particularly pronounced when also cultured in the presence of pro-inflammatory polarizing cytokines (Refai, Textor, Brunette, & Waterfield, 2004). Interestingly, this response also seemed to exhibit some temporal dependence, with surface roughness-dependent effects being observable following 24 or 48 hours in culture but not at time points before 24 hours (Refai et al., 2004).

Material surface topology has also been shown to have some influence on the migratory behavior, phagocytic capacity, and pro-inflammatory cytokine secretion of cultured macrophages (McWhorter et al., 2015). Macrophages cultured on porous, electrospun poly(L-lactic) (PLA) scaffolds were shown to exhibit an attenuated inflammatory response relative to macrophages cultured on flat PLA sheets (Garg, Pullen, Oskeritzian, Ryan, & Bowlin, 2013). This macrophage phenotypic response was also supported by *in vivo* host response data demonstrating an increased fibrotic capsule formation following implant of polymer films while porous materials exhibited reduced fibrotic matrix deposition (Cao, McHugh, Chew, & Anderson, 2010). Additionally, the scaffold fiber diameter was found to have a significant impact on macrophage polarization, with thicker fibers generally promoting increased pro-inflammatory macrophage polarization relative to scaffolds composed of thinner diameter fibers (Garg et al., 2013; Sanders, Bale, & Neumann, 2002).

Macrophages have also demonstrated an altered migratory behavior and polarization response following culture on either 2-dimensional or 3-dimensional materials (McWhorter et al., 2015). It was observed that macrophage culture on 2-dimensional hydrogels promoted M1 macrophage polarization and pro-inflammatory cytokine secretion while macrophage culture on

3-dimensional, nanofibrous hydrogels attenuated M1 macrophage polarization (Bartneck et al., 2012). The 3-dimensional architecture of the culture microenvironment was also observed to have a significant impact on macrophage mechanism of migration (Van Goethem, Poincloux, Gauffre, Maridonneau-Parini, & Le Cabec, 2010). Macrophages can migrate in response to chemotactic or haptotactic gradients using either amoeboid or mesenchymal migratory mechanisms (Guiet et al., 2011; McWhorter et al., 2015). When cultured on dense collagenous matrices, it was observed that macrophage primarily used mesenchymal migration mechanisms (Guiet et al., 2011). Conversely, macrophage culture on less densely concentrated, more fibrillar collagen matrices was found to promote amoeboid migratory behavior (Guiet et al., 2011).

Macrophages have also been shown to exhibit altered phenotypic and functional responses to differing mechanical conditions (McWhorter et al., 2015). Macrophages have been shown to be responsive to both cyclic and static mechanical stretch (Ballotta, Driessen-Mol, Bouten, & Baaijens, 2014; Kurata et al., 2001; Pugin et al., 1998; Wehner et al., 2010). Cyclic stretch has been shown to upregulate the bone resorption functionality of osteoclasts, the resident macrophage of bone tissue microenvironments (Kurata et al., 2001). Cyclic stretch has also been shown to be associated with increased pro-inflammatory cytokine secretion in cultured macrophage populations, particularly when co-cultured in the presence of Th1 cytokines (Pugin et al., 1998). Cyclic stretch can also alter expression of matrix modulatory enzymes, such as MMP9 or TIMP1 (Pugin et al., 1998; Yang, Sakamoto, Xu, & Lee, 2000). Additionally, the degree of stretch to which cultured macrophages are subjected has been shown to induce biphasic macrophage polarization responses (Ballotta et al., 2014). In this model, it was observed that macrophage culture under moderate stretch conditions was associated with an increased ratio of M2/M1 macrophages (Ballotta et al., 2014). However, macrophage culture under high stretch conditions

resulted in reduced M2/M1 macrophage ratios (Ballotta et al., 2014). This biphasic polarization response suggests there may be an optimal range of tissue deformation for promoting alternative macrophage activation, and tissue stretch beyond this homeostatic range induces chronic inflammatory macrophage polarization (Ballotta et al., 2014; McWhorter et al., 2015).

In addition to this macrophage polarization response observed following differing cyclic or static stretch conditions, macrophages have also been shown to exhibit altered migratory behavior, phenotypic polarization, and functional capacity following culture in microenvironments of varying mechanical stiffness (Adlerz, Aranda-Espinoza, & Hayenga, 2016; Blakney, Swartzlander, & Bryant, 2012; McWhorter et al., 2015; Patel et al., 2012; Previtera & Sengupta, 2015; Sridharan, Cavanagh, Cameron, Kelly, & O'Brien, 2019). Macrophages have been observed to preferentially adhere to materials of increased mechanical stiffness (Irwin et al., 2008). Additionally, an increased secretion of pro-inflammatory cytokines was noted following macrophage culture in the presence of bacterial LPS on highly stiffened (~840kPa) substrates relative to less stiff (~130kPa) culture groups (Blakney et al., 2012). Subcutaneous implant of highly stiffened hydrogels was also found to be associated with an enhanced host response and increased fibrotic capsule formation relative to less stiff hydrogel implant (Blakney et al., 2012).

The stiffness of the material upon which macrophages were cultured was also demonstrated to have a significant impact on the migration velocity of cultured macrophages, with highly stiffened substrates reducing macrophage migratory velocity relative to culture groups of low or moderate stiffness (Sridharan et al., 2019). This reduction in migratory velocity in macrophages cultured on high stiffness substrates was observed to correlate with a large upregulation in intracellular adhesion molecule (ICAM-1) (Sridharan et al., 2019). Macrophage morphology was also noted to exhibit significant alterations between low stiffness and high stiffness culture groups,

with high stiffness macrophage culture generally being observed to promote more spread macrophage morphologies characterized by increased cellular adhesion areas (Sridharan et al., 2019). Mechanistically, these observed differences can be likely attributed to differing migratory mechanisms employed by macrophages cultured on either low stiffness or high stiffness substrates. In low stiffness substrate macrophage culture, macrophages were observed to exhibit amoeboid migratory behavior with limited podosome formation and reduced matrix metalloprotease expression (Sridharan et al., 2019). Conversely, high stiffness substrate macrophage culture was observed to promote podosome formation and increased matrix metalloprotease expression – two characteristic features of mesenchymal macrophage migratory behavior (Sridharan et al., 2019). This result demonstrates the ability of macrophages to not only alter their migratory behavior in response to varying matrix architecture, but also in response to varying microenvironmental mechanical properties (Sridharan et al., 2019; Van Goethem et al., 2010).

1.4 Cardiovascular Tissue Resident Macrophages

The cardiovascular tissue microenvironment undergoes significant compositional change both throughout development and perinatal periods as well as throughout adulthood and with increasing age. These compositional changes that occur in aged individuals, generally characterized by a robust accumulation of fibrillar collagen subtypes, alter tissue biomechanics and reduce the ability of the heart to function properly or without additional compensatory remodeling, such as cardiomyocyte hypertrophy. Given the role that the constitutive proteins of the cardiovascular system have in altering resident cell functionality as well as the pleiotropic mechanisms through which resident cardiac cell subsets can sense altered tissue biomechanics,

understanding the mechanisms by which the changing cardiac microenvironment promotes dysregulation of proper cardiac cell homeostatic function presents an interesting therapeutic intervention opportunity to attenuate the age-related risk of cardiovascular disease acquisition. Additionally, given the role that resident macrophage subsets have been shown to play in facilitating tissue development and maintaining homeostasis during adulthood in various mammalian organ systems, understanding the ontogeny and function of any cardiac resident macrophage subsets may provide previously unknown targets for pharmacological intervention to attenuate any macrophage-mediated component of cardiovascular disease.

1.4.1 Cardiac Tissue Resident Macrophage Ontogeny and Seeding of the Developing Cardiovascular Tissue Microenvironment

Macrophage seeding of the cardiovascular system begins during embryogenesis during the period of macrophage differentiation from multipotent erythromyeloid progenitor cells in the mammalian extraembryonic yolk sac (Epelman et al., 2014). Macrophage colonization of cardiac tissue is first visible at E9.5 in the developing murine embryo (Epelman et al., 2014). Lineage tracing studies have demonstrated this first wave of macrophages which colonize the developing cardiac tissue during this time are derived from a non-hematopoietic stem cell precursor, however it was unclear whether this was a result of macrophage differentiation from early or late wave erythromyeloid progenitor cells (Epelman et al., 2014). These macrophages were shown to exhibit some of the canonical surface marker expression patterns characteristic of yolk sac hematopoiesis-derived macrophage subsets, including high amounts of general macrophage marker F4/80 expression, low CD11b expression, and a robust expression of fractalkine receptor CX3CR1 (Epelman et al., 2014). The next wave of cardiac tissue colonization by macrophages occurs from

E12.5-E16.5 in the developing murine embryo and are primarily derived from fetal liver monocytes (Epelman et al., 2014). These macrophages tend to exhibit surface marker expression patterns characteristic of fetal monocytic origin, including high CD11b expression levels, low F4/80+ expression, and low CX3CR1 expression levels (Epelman et al., 2014). Additionally, it was shown that both of these macrophage populations which colonize the developing cardiac tissue are able to persist into adulthood within the cardiac tissue microenvironment through self-proliferation independent of any bone marrow-derived macrophage replacement (Epelman et al., 2014). However, it was also noted that in periods of stress or following resident macrophage depletion bone marrow monocyte extravasation and differentiation into cardiac resident macrophages has been observed (Epelman et al., 2014). Further lineage tracing studies within the developing cardiac tissue have provided additional indication that tissue resident macrophage seeding within a given organ is largely a function of tissue niche availability, the mechanisms by which hematopoietic cells are derived at that time, and the tissue microenvironment in which the hematopoiesis is occurring (Epelman et al., 2014).

1.4.2 Differences in Inflammasome Activation Between Developmentally Distinct Cardiac Resident Macrophage Populations

In addition to the unique temporal waves of cardiac tissue macrophage seeding during embryogenesis and throughout an organism's lifespan, tissue resident macrophages derived from unique hematopoietic cell progenitors exhibit differential gene expression patterns which suggest differing functional capacities for these various subsets. When comparing cardiac tissue resident macrophages derived from embryological progenitors to cardiac tissue resident macrophages derived from bone marrow monocytes, embryological progenitor derived macrophages tend to

exhibit an attenuated regulation of genes associated with inflammasome activation following TLR agonism and exhibit an upregulation of genes associated with antigen presentation and T-cell activation relative to bone marrow monocyte derived macrophages (Epelman et al., 2014). This suggests that bone marrow monocyte derived cardiac macrophage subsets are more likely to promote pro-inflammatory cytokine secretion and inflammasome activation following PAMP, DAMP, or matrikine stimulation of macrophage surface receptor proteins - such as those of the TLR family.

1.4.3 The Diverse Function of Various Developmentally Distinct Macrophage Populations

In addition to unique developmental origins, tissue resident cardiac macrophages exhibit unique patterns of gene expression which allow them to facilitate homeostatic cardiac function as well as coordinate various cellular responses during periods of cardiac stress or tissue remodeling (Epelman et al., 2014).

1.4.3.1 Cardiac Tissue Resident Macrophages Play an Important Role in Facilitating Electrical Conduction Between Cardiomyocytes

While cardiac resident macrophages had been observed in developing embryological cardiac tissue as well as within the left ventricle in adults, the distribution of these cells across other regions of the myocardium was unknown. Given the robust nature of CX3CR1 expression in cardiac resident macrophages, a study by Hulsman et. al. using CX3CR1-GFP transgenic mice was able to identify resident macrophages based on GFP expression and demonstrated a previously unrecognized heterogeneity in cardiac resident macrophage distribution (Hulsmans et al., 2017). In particular, a large population of spindle shaped macrophages expressing GFP were observed

within the AV bundle of murine cardiac tissue and often interspersed with HCN4-expressing cardiomyocytes (Hulsmans et al., 2017). When the relative density of macrophages per tissue region was analyzed, it was observed that the AV bundle exhibited a greater macrophage density than the LV free wall tissue regions (Hulsmans et al., 2017). Parabiosis studies of resident macrophage repopulation during periods of adult homeostatic cardiac function demonstrated a minimal repopulation by circulating monocyte-derived progenitor cells in both the AV bundle and the LV free wall, further demonstrating the tendency of cardiac resident macrophages to self-proliferate once resident in the cardiac tissue microenvironment rather than be constantly repopulated by bone marrow-derived monocyte differentiation, as observed in the gut for example (Hulsmans et al., 2017).

Characterization of connexin protein expression revealed an increased expression of connexin-43 protein in cardiac resident macrophage populations not only in the AV bundle but also in the RV or LV tissue microenvironment; an upregulation which was not observed in other tissue resident macrophages such as those derived from the peritoneum (Hulsmans et al., 2017). Connexin proteins facilitate intercellular communication and play an important role in connecting various cell populations which need to function in a concerted manner to properly transduce a given signal, such as in the case of cardiac electrical signal conduction. Interestingly, it was observed that cardiac macrophages in the AV bundle often exhibited several points of contact with AV bundle cardiomyocytes with connexin-43 proteins mediating intercellular communication between these cardiac resident cell types (Hulsmans et al., 2017).

In order to better understand the functional consequences of the observed connexin-43 mediated cardiomyocyte and cardiac resident macrophage intercellular communication, patch clamping *in vitro* co-culture studies of macrophage and cardiomyocyte populations was performed

(Hulsmans et al., 2017). A rhythmic depolarization was observed in approximately one quarter of cultured macrophages which was noted to be reminiscent of rhythmic depolarization dynamics in sinus rhythm cardiomyocyte electrical conduction (Hulsmans et al., 2017). Macrophages in which these depolarization dynamics were observed were also noted to exhibit greater connexin-mediated interaction with cultured cardiomyocytes and a reduced resting membrane potential relative to non-rhythmically depolarizing macrophages (Hulsmans et al., 2017). Functionally, cardiac macrophage connexin interactions with cardiomyocytes were demonstrated to increase cardiomyocyte cell resting membrane potential (Hulsmans et al., 2017). Additionally, pharmacological inhibition of connexin gap junction formation was shown to decrease cardiomyocyte resting membrane potential (Hulsmans et al., 2017). *In vivo* deletion of connexin-43 in macrophage populations also caused significantly delayed AV electrical signal conduction (Hulsmans et al., 2017). Furthermore, depletion of the total cardiac resident macrophage population was shown to induce AV block in mice (Hulsmans et al., 2017). These results taken together demonstrate the importance of cardiac resident macrophage populations in facilitating cardiomyocyte electrical signal conduction through a connexin-43 gap junction mediated increase in the resting membrane potential of cardiomyocyte cell membranes, in turn allowing for easier cell membrane depolarization and signal conduction. Additionally, these results demonstrate how loss of this homeostatically important macrophage population or reduced connexin-43 protein expression can induce electrical signal conduction faults and induce cardiac dysfunction.

1.4.3.2 Cardiac Tissue Resident Macrophage Subsets Facilitate Differing Cardiac Remodeling Responses With Varying Degrees of Functional Recovery Following Myocardial Infarction

In addition to the important homeostatic function resident macrophages have in facilitating proper cardiomyocyte membrane depolarization during AV node electrical signal conduction, resident macrophage populations have also been demonstrated to have an important role in regulating the cardiac tissue remodeling response following myocardial infarction. In addition to being important for any tissue remodeling response following infarction, ontogenically distinct cardiac resident macrophage populations have been shown to produce different remodeling responses following infarction, which in turn results in differing degrees of functional recovery (Lavine et al., 2014).

The importance of tissue resident macrophage populations for cardiac remodeling and functional recovery was first noted when studying the neonatal cardiovascular remodeling response to myocardial infarction. In mammalian neonates, apical resection of left ventricular tissue can be regenerated and function can be recovered if the apical resection is performed before the terminal cardiomyocyte division, which occurs several days postnatally (Porrello et al., 2011). Interestingly, in addition to displaying a reliance on the ability of non-terminally divided cardiomyocytes to proliferate following infarction during early postnatal time periods, neonatal cardiac tissue regeneration was also shown to have a partial reliance on tissue residence macrophage mediated angiogenesis promoted through macrophage secretion of vascular endothelial growth factor (VEGF) and other pro-angiogenic factors (Aurora et al., 2014; Lavine et al., 2014).

In adult mammals, cardiac tissue regeneration following myocardial infarction is not possible due to the limited number of mitotically capable cardiomyocytes within the adult myocardium relative to the large number of cardiomyocytes lost to either necrosis or apoptosis during the hypoxic period following coronary vessel occlusion. In cases where the coronary vessel occlusion is resolved and hypoxic cardiac tissue experiences reperfusion, some cardiac tissue function can be restored depending on the tissue remodeling response which occurs following the infarction. In addition to fibroblast cell populations, resident cardiac macrophages have been shown to play an important role in the regulation of this remodeling response (Dick et al., 2019; Lavine et al., 2014).

Active tissue remodeling in the post-infarction-reperfusion myocardium typically occurs in the border regions between the fibrillar collagen matrix, which forms in the hypoxic region where cardiomyocyte necrosis has occurred, and the healthy myocardium. While the dense collagen scar which forms in the region of cardiomyocyte death following infarction-reperfusion is essential for preventing left ventricular wall rupture due to the loss of cardiomyocyte mediated wall tension, further expansion of this fibrillar collagen matrix deposition into healthy myocardium in regions proximal to the collagen scar can determine the extent to which cardiac function is partially recovered or whether cardiac function will further decline towards heart failure. Interestingly, not only are macrophages essential mediators of this remodeling response, but macrophages derived from differing progenitor hematopoietic cell populations promote different remodeling responses within the myocardium (Dick et al., 2019; Lavine et al., 2014).

Congruent with the upregulation of inflammation associated genes in bone marrow monocyte-derived macrophage subsets, cardiac tissue remodeling responses following infarction that are primarily mediated by bone marrow monocyte-derived macrophages result in further

deposition of fibrillar collagen into healthy myocardium, excess fibroblast activation, chronic inflammatory signaling, and reduced cardiovascular system function (Dick et al., 2019; Epelman et al., 2014; Lavine et al., 2014). Conversely, when bone marrow-derived monocyte extravasation into cardiac tissue is blocked through pharmacological inhibition of the CCL2-CCR2 monocyte chemoattractant signaling pathway, self-renewing macrophage subsets promote timely attenuation of the inflammatory signaling, reduced border region collagen deposition, reduced cardiomyocyte hypertrophy, and improved recovery of function relative to bone marrow monocyte remodeled myocardium (Dick et al., 2019; Lavine et al., 2014).

1.4.3.3 Cardiac Resident Macrophages Function Within a Heart-brain-kidney Network of Resident Macrophage Signaling to Regulate the Cardiac Hypertrophic Remodeling Response to Pressure Overload

Transaortic constriction (TAC), which involves utilizing sutures or other banding materials to surgically reduce the diameter of the aorta, can be one model utilized to study left ventricular failure resultant of aortic stenosis and increased left ventricular pressures. Similar to post-infarction-reperfusion myocardial remodeling, cardiac tissue experiences a remodeling response following increased ventricular pressure intended to provide a compensatory response to maintain cardiac output despite increased systemic blood pressure. This compensatory response can then in turn determine the extent to which cardiac function is maintained or by which progressive increases in cardiac dysfunction occur.

Following TAC in mice, an expansion of Ly6C^{lo}F4/80+CD11b+ macrophages was observed in remodeling cardiac tissue (Fujiu et al., 2017). Depletion of this population of macrophages prior to TAC was found to be associated with a reduced compensatory cardiac remodeling response and subsequent increased animal mortality (Fujiu et al., 2017). It was also

observed that the expansion of this cardiac resident macrophage population is induced by increased secretion of colony-stimulating factor 2 (CSF2/GM-CFS) signaling within the myocardium (Fujiu et al., 2017). This increased CSF2 within the myocardium was found to result from increased expression of CSF2 by endothelial cells in the renal system following resident renal macrophage activation (Fujiu et al., 2017). Additionally, it was observed that renal sympathetic nerve ablation blunted the cardiac tissue compensatory response following TAC due to a reduced induction of CSF2 expression, suggesting that the sympathetic nervous system provides a link between the heart and the kidneys following TAC-induced left ventricular pressure overload (Fujiu et al., 2017).

1.4.4 The Aging Cardiovascular Microenvironment and Cardiac Tissue Resident Macrophage Phenotype and Function

Cardiac tissue resident macrophages exhibit unique temporal tissue seeding dynamics throughout embryology and into adulthood (Epelman et al., 2014; Molawi et al., 2014; Pinto et al., 2014). Additionally, cardiac resident macrophages have been shown to have numerous homeostatic and tissue remodeling functions important for the maintenance of cardiac tissue function (Epelman et al., 2014; Fujiu et al., 2017; Hulsmans et al., 2017; Lavine et al., 2014). Considering the importance that microenvironmental niche plays in inducing resident cardiac macrophage phenotype, the age-related risk of cardiovascular disease acquisition, and the numerous biochemical and biomechanical microenvironmental changes which occur in the aging cardiovascular system; understanding how these microenvironmental changes induce altered phenotype and function in cardiac resident macrophages may provide useful insights or novel

therapeutic targets for attenuating the macrophage-mediated component of the age-related CVD risk.

Some prior evidence has characterized a gradual decline in self-renewing macrophage populations in the murine cardiac tissue from postnatal time periods, when these macrophages comprise nearly the whole tissue resident macrophage population, to adulthood (30 weeks), when these macrophages have declined to approximately half of the total cardiac resident macrophage population (Molawi et al., 2014; Pinto et al., 2014). It was also observed that as the population of embryologically derived macrophages progressively declined, cardiac tissue increasingly was seeded with bone marrow monocyte-derived resident macrophage populations (Molawi et al., 2014; Pinto et al., 2014). This result reflects similar tissue macrophage deposition dynamics observed in other aging organ systems, namely - that tissue resident macrophage seeding is dependent upon niche availability and that macrophages which seed an empty niche will be derived through the dominant hematopoietic cell differentiation mechanism available during that period of development. In the case of the cardiovascular system, self-proliferation of embryologically derived subsets persists into adulthood to some extent, but as embryologically derived subsets enter either senescence or apoptosis, bone marrow-derived monocytes extravasate into cardiac tissue and differentiate into cardiac resident macrophages whose phenotype is partially reflective of developmental origin but largely reflective of the microenvironment stimuli at that time (Molawi et al., 2014; Pinto et al., 2014).

However, while cardiac tissue has been shown to exhibit some niche availability during adult time periods not observed in other tissues with large populations of embryologically derived resident macrophages - such as the brain or lungs - the mechanisms governing the age-related loss of embryologically derived subsets as well as the accumulation of bone marrow monocytes remain

to be elucidated. Additionally, while the preliminary aging studies examining how the cardiac resident macrophage compartment changes with increasing age have provided important characteristic insights, these studies only characterized the changes in cardiac tissue resident macrophage regulation over the first 30 weeks of the murine lifespan (Molawi et al., 2014; Pinto et al., 2014). Thus, further studies into how the relative population size, phenotype, and function of cardiac resident macrophages is altered at moderate (12 month) and highly (18 month+) aged mice will be necessary to fully understand the regulation of these cells at advanced age time points.

2.0 Development of an *In Vitro* Model to Study How Age-related Alterations in Cardiac Extracellular Matrix Composition and Biomechanics Impact Macrophage Phenotype and Function

2.1 Rationale Underlying *In Vitro* Model Development

2.1.1 Rationale

The cardiac tissue microenvironment undergoes numerous compositional alterations during development and into adulthood. These compositional alterations allow for the development of the complex set of structures necessary for cardiac tissue function as well as for the mechanical strengthening of cardiac tissue as systemic blood pressures increase postnatally. Generally, these alterations can be characterized by a reduced matricellular protein content and an increased concentration of fibrillar collagen proteins such as collagen I, III, or V (Williams et al., 2014; Williams et al., 2015). As these changes in cardiac matrix protein content occur, cardiac tissue biomechanics are altered as a consequence of the degree of fibrillar collagen deposition as well as the organization of the collagen matrix deposition within the heart.

Macrophage populations exhibit a robust sensitivity to the local tissue microenvironment (van de Laar et al., 2016). This sensitivity is mediated through a variety of surface receptor and integrin binding mediated mechanisms by which macrophages are able to integrate cytokine, matrikine, and DAMP or PAMP signaling cues to take on an appropriate phenotype and provide the needed functional response to restore tissue function. While many of the mechanisms by which macrophages integrate cytokine, growth factor, and DAMP/PAMP signaling cues have been

elucidated, both the phenotypic response as well as the mechanisms mediating that response for matrikine induced macrophage polarization require further study. Additionally, while some studies have provided preliminary insight into the mechanoresponsivity of macrophage populations, many of these results were derived from *in vitro* culture models where the majority of substrate stiffnesses examined were above the observed range of physiological cardiac tissue stiffness in young and aged individuals (Adlerz et al., 2016; Blakney et al., 2012; Engler et al., 2008; Sridharan et al., 2019). Thus, the present study sought to develop an *in vitro* model which could be utilized to assess the impacts of compositional alterations as well as biomechanical change on macrophage phenotype and function.

2.2 Methods for Development of the Experimental *In Vitro* Model and Evaluation of Macrophage Phenotypic and Functional Response to Varying Microenvironmental Conditions

2.2.1 Experimental Design and Overview of Experimental Groups

The composition of a given tissue is inherently linked with that tissue's biomechanical properties *in vivo*. For example, it can be difficult to assess the relative contributions of collagen deposition and increased tissue biomechanical stiffness as individual variables *in vivo* since increases in collagen deposition and the organization of that deposition will alter the biomechanics of that tissue. This makes it difficult to assess how much of the observed change in macrophage dynamics is resultant of increased matrikine signaling through DAMP or PAMP surface receptor pathways, through integrin mediated mechano-sensing of tissue biomechanics, or through some

combination of these mechanisms. While decoupling tissue composition and tissue biomechanics may prove difficult *in vivo*, utilization of appropriate *in vitro* models allows for better evaluation of the relative contributions of each of these variables in the induction of altered macrophage phenotype and function.

Since bone marrow derived macrophages comprise a substantial fraction of all adult cardiac resident macrophages and accumulation of this subset with age tends to be associated with poor tissue remodeling and functional outcomes, understanding how these cells respond to the changing cardiac microenvironment may help elucidate any macrophage mediated mechanisms of pathological cardiac tissue remodeling.

In order to understand the relative contributions of changing cardiac tissue composition and cardiac tissue biomechanics on bone marrow derived macrophage phenotype, an *in vitro* culture model was developed using poly-dimethly-siloxane (PDMS) hydrogels ranging in stiffness from 2kPA to 64kPA, encompassing the reported physiological range of cardiac tissue stiffness in young and aged individuals (Munch & Abdelilah-Seyfried, 2021). The PDMS hydrogels utilized for this model were functionalized to bind matrix proteins, which allowed for these hydrogels of varying stiffness to be coated with decellularized cardiac extracellular matrix derived from either young (2-4mo) or aged (18-24mo) murine donors. Cardiac tissue was decellularized prior to gel coating in order to provide an antigen-free material which could be utilized to better understand the macrophage response to cardiac matrix derived from young or aged mice. In addition to hydrogels of varying stiffness coated with either young or aged decellularized cardiac ECM, tissue culture plastic was coated with young or aged decellularized cardiac ECM was well to provide a highly stiffened control group, as the elastic modulus of tissue culture plastic (~>10MPa) is much greater than that observed in most tissues.

Following the generation of the various *in vitro* models of differing cardiac microenvironmental conditions, primary bone marrow was isolated from young (2-4mo) mice and cultured *in vitro* with macrophage differentiation media to promote macrophage differentiation from bone marrow isolates. Following culture and macrophage adherence, cells were accutased and re-plated at a uniform density on one of the experimental *in vitro* microenvironmental models. Cells were given 24 hours to adhere following replating, after which cells received either only macrophage differentiation media (M0), macrophage differentiation media supplemented with type I immune cytokine interferon-gamma (IFN-γ) and bacterial cell wall component lipopolysaccharide (LPS) to push cells towards an M1 phenotype (M1), or macrophage differentiation media supplemented with type II cytokine interleukin-4 (IL-4) to push cells towards M2 phenotypes (M2). Cells were treated with M0, M1, or M2 push for 24 hours after which time cell morphology, phenotype, and functional responses were evaluated to better understand the impacts of the various microenvironmental conditions on inducing altered macrophage phenotype and function at baseline as well as in pro- or anti-inflammatory signaling environments.

2.2.2 A Method to Remove Cellular Content From Young and Aged Cardiovascular Tissue

In order to remove cellular antigens from native cardiac tissue, a skeletal muscle decellularization protocol first described by Wolf et. al. was chosen as a protocol for tissue decellularization with several modifications added to help remove residual blood clots from cardiac tissue (Wolf, Daly, Reing, & Badylak, 2012). Cardiac tissue was isolated from both young (1-2month) and aged (20-24month) C57Bl/6 mice (Jackson, National Institutes of Aging). Any residual connective tissue or vasculature was removed from the samples and cardiac tissue was then washed three times in 1X PBS to remove clots from tissue. Cardiac tissue samples were then

minced and incubated in 1000 IU/mL Streptokinase (Sigma, St. Louis, MO) overnight at room temperature to break down any residual blood clots from tissue. Samples were then washed twice with 1X PBS. Samples were then shaken in a 2:1 (v/v) chloroform:methanol solution on an orbital shaker at 300RPM for 2 hours. Samples were then passed through a graded series of ethanol washes (100, 90, 70, 50, 0) for 30 minutes each with constant agitation at 300RPM. Cardiac samples were then incubated at 37C in 0.2% trypsin/0.2% EDTA for 2 hours. Samples then were washed twice with deionized water for 30 minutes at 300RPM followed by two 1X PBS washes for 30 minutes at 300RPM. Following wash, samples were shaken in 2% w/v sodium deoxycholate (Sigma, St. Louis, MO) for 5 hours at 300 RPM. Samples were then washed with deionized water for 30 minutes followed by 2X PBS for 30 minutes. Samples then were shaken in 2% sodium deoxycholate solution overnight for 14-16 hours at 300RPM, followed by agitation in 1% Triton X-100 for 1 hour at 300RPM. Samples were then washed in deionized water. Samples then were shaken in a 0.1% (w/v) peracetic acid/4 % (v/v) ethanol solution for 2 hours at 300RPM to sterilize decellularized tissue samples. Samples were finally washed twice in 1X PBS followed by two deionized water washes. Samples were then frozen in type I water and lyophilized. Lyophilized samples were then either split for scaffold characterization or for pepsin-digestion hydrogel coating.

2.2.3 Methods of Evaluating the Efficacy of Cardiac Tissue Decellularization

Following decellularization, it was necessary to confirm the removal of cell nuclear content prior to scaffold digestion and hydrogel coating in order to ensure the observed macrophage response to young or aged cardiac ECM is actually a result of altered ECM composition and not of any confounding macrophage responses to cellular antigens. There are several experimental

methodologies which allow for qualitative and quantitative evaluation of scaffold DNA content following decellularization. Qualitatively, sample staining with 4',6-diamidino-2-phenylindole (DAPI), which binds adenosine-thymine rich regions of DNA, was used to demonstrate the presence or absence of DNA fragments within a decellularized tissue sample. Quantitatively, a PicoGreen double stranded DNA (dsDNA) assay was performed on native and decellularized scaffolds to determine the total dsDNA content per scaffold sample. In an effectively decellularized tissue, qualitative DAPI nuclear staining and quantitative PicoGreen assay results should both demonstrate a significant removal of scaffold nuclear content following tissue decellularization.

2.2.3.1 DAPI Nuclear Staining

Native and decellularized cardiac samples were fixed in 10% neutral buffered formalin for 5 days, after which samples were submitted to the McGowan Institute for Regenerative Medicine Histology Core for paraffin block mounting and sample sectioning. Slides were deparaffinized and samples were stained with 4',6-diamidino-2-phenylindole (DAPI) nuclear stain for 1 minute at room temperature. Sections were washed 5 times with 1X PBS. Final wash was physically removed, and coverslips were mounted. Slides were stored at 4˚C until imaging. Images of DAPI stain in native and decellularized cardiac samples were acquired with a FLoid cell imaging station (Thermo Scientific) with acquisition settings of: blue laser intensity = 30%, optical zoom = 0%.

2.2.3.2 PicoGreen Double Stranded DNA Quantification Assay

Double stranded DNA content quantification for native and decellularized cardiac tissue samples was performed using a PicoGreen double stranded DNA quantification kit (Thermo, Waltham, MA). To quantify, first a dsDNA standard solution was prepared from a 2000ng/mL

stock and serially diluted in TE buffer. Isolated DNA samples were resuspended in 1mL of 1X TE buffer for 5 minutes at room temperature under gentle agitation. Samples were then serially diluted in 1X TE buffer. 100µL of each sample and standard was plated on a 96 well plate. 100µL of Quant-IT PicoGreen reagent was added to each standard of sample and the plate was incubated in the dark for 5 minutes at room temperature. Plate fluorescent emission was then measured using a Synergy HTX plate reader (BioTek, Winooski, VT) and an excitation wavelength of 480nm, an emission wavelength of 520nm, and a cutoff wavelength of 515nm. Sample dsDNA concentrations were calculated from the equation derived from the linear regression of dsDNA standard fluorescent emission against standard dsDNA concentration. The sample dilution whose emission value was most close to the center of the standard curve was used for calculating sample dsDNA concentration. The calculated dsDNA content was then multiplied by the sample dilution factor to provide an accurate quantification of sample dsDNA content.

2.2.4 Histological Methods of Evaluating Native Cardiac Tissue Composition

Native cardiac tissue samples were isolated, fixed in 10% neutral buffered formalin (NBF) for 5 days, after which samples were submitted to the McGowan Institute for Regenerative Medicine Histology Core to be paraffin embedded, sectioned, and mounted on slides for histologic staining. Prior to staining, slides were deparaffinized by washing in xylenes three times, washing through a graded series of alcohol washes, and a final wash in tap water. Tissue sections were then stained with either picrosirius red to visualize collagen or Alcian blue to visualize sulfated proteoglycans in cardiac tissue sections.

2.2.4.1 Picrosirius Red

Picrosirius red staining can be utilized to visualize collagen fibrils and cell nuclei in the isolated cardiac tissue samples. In order to accomplish this, deparaffinized sections were first stained with Wiegert's hematoxylin followed by a wash with tap water. Sections were then stained with picrosirius red, made up of direct red 80 in saturated picric acid (Sigma, St Louis, MO) for one hour to achieve near equilibrium staining, followed by washes in two changes of acidified water. Water was physically removed from slides and sections were dehydrated in three changes of 100% ethanol. Sections were then cleared in xylenes and mounted in permount mounting medium (Fisher, Hampton, NH). 4X and 20X brightfield images of stained sections were captured with a Nikon Eclipse 50i (Nikon, Melville, NY). 4X brightfield images were stitched together with Adobe Photoshop to make composite images of whole cardiac sections (Adobe, San Jose, CA). Semi-quantitative analysis of percent positive expression of picrosirius red per field of view was performed using NIH FIJI image analysis software (National Institutes of Health, Bethesda, MD).

2.2.4.2 Alcian Blue

Alcian blue staining can be utilized to visualize sulfated proteoglycans in cardiac tissue sections. In order to accomplish this, deparaffinized tissue sections were stained with Alcian blue for 30 minutes followed by a wash in tap water. Sections were then dehydrated through a graded series of ethanol washes with two final changes in absolute ethanol. Sections were then cleared in xylenes and mounted in a resinous mounting medium. 4X and 20X brightfield images of stained sections were captured with a Nikon Eclipse 50i (Nikon, Melville, NY).

2.2.5 Biochemical Assay Quantification of Collagen and Glycosaminoglycan Content

2.2.5.1 Papain Digest

Decellularized cardiac tissue extracellular matrix samples were lyophilized and massed prior to digestion. Papain digest solution was prepared by dissolving papain (Sigma, St. Louis, MO) at a concentration of 0.125mg/mL and L-cysteine (Sigma, St. Louis, MO) at a concentration of 0.10M in phosphate-buffered EDTA (PBE) buffer (0.1M Na_2HPO_4, 0.01M Na_2EDTA, pH 6.5). Samples were digested in 1mL of papain digest solution for 12-16 hours at 60˚C until samples were fully digested. Samples were then split for either hydroxyproline or glycosaminoglycan assay quantification following digestion.

2.2.5.2 Hydroxyproline Quantification Assay

To begin, a series of known concentration standards was generated by preparing a 500 μg/mL stock solution of hydroxyproline (Sigma, St. Louis, MO) in PBE buffer and serially diluting to generate standards for the assay. 50 μL of each sample or standard was then added to a 2 mL, screw-top microcentrifuge tube and 50 μL of 2M NaOH was added to each tube. Tops were secured on each tube. Samples and standard tubes were then incubated at 110˚C for at least 18 hours. Tubes were then centrifuged briefly. 10.5 μL of Type I water was added to each tube. 100 μL of 0.01M $CuSO_4$, 100 μL of 2.5M NaOH, and 100 μL of 6% H_2O_2 were then added sequentially to each tube, with care being taken to vortex tubes following each reagent addition. Tubes were incubated at room temperature following H_2O_2 addition until samples and standards turned blue or clear in color. Samples and standards were vortexed and then incubated at 80˚C for 5 minutes. Tubes were briefly centrifuged and subsequently placed into -80˚C freezer for 5 minutes to cool. 400 μL of 3N H_2SO_4 was added to each tube. Tubes were allowed to rest until cooled to room temperature. 200

μL of 5% dimethylaminobenzaldehyde (Sigma, St. Louis, MO) made up in propanol was added to each tube. Tubes were incubated at 70˚C for 15 minutes. Tubes were vortexed well. 200 μL of each prepared standard or sample solution was added in triplicate to a 96 well plate. The plate absorbance was read at 540nm with a Synergy HTX plate reader (BioTek, Winooski, VT). To determine experimental sample hydroxyproline content, hydroxyproline standard absorbance values were linearly regressed against the known standard concentrations to determine the equation which defines the relationship between sample absorbance and hydroxyproline content.

2.2.5.3 Glycosaminoglycan Quantification Assay

Glycosaminoglycan assay standards were generated by first preparing a 500 μg/mL stock of chondroitin-6-sulfate in PBE buffer and serially diluting. 50 μL of either glycosaminoglycan assay standard or sample was pipetted in triplicate into an empty 96 well plate. Dimethylmethylene blue solution was prepared by dissolving 1 mg of 1,9-dimethylmethylene blue zinc chloride double salt (Sigma, St. Louis, MO) in 0.313 mL of 100% ethanol, adding 0.148 g NaCl and 0.19 g of glycine, and diluting the solution up to 50 mL with Type I water. 250 μL of dimethylmethylene blue solution was added to each standard or sample well. Plate absorbance was then read at 575nm with a Synergy HTX plate reader (BioTek, Winooski, VT). To determine sample glycosaminoglycan content, the measured sample absorbance values were regressed against known standard concentrations to derive the quadratic equation which best defines the relationship between sample absorbance and concentration.

2.2.6 Coating of Poly-dimethyl-siloxane Hydrogels and Tissue Culture Plastic With Solubilized Young or Aged Decellularized Cardiac Extracellular Matrix

Decellularized cardiac tissue isolated from young or aged donor, C57Bl/6 mice was pepsin-digested for 48 hours at a concentration of 10mg/mL. cECM digests were then diluted to a concentration of 1mg/mL with 1X PBS, neutralized to 6 pH, and incubated with sterile poly-dimethyl siloxane (PDMS) hydrogels of either 2kPA (Advanced Biomatrix, San Diego, CA), 8kPA (Advanced Biomatrix, San Diego, CA), 16kPA (Advanced Biomatrix, San Diego, CA), 32kPA (Advanced Biomatrix, San Diego, CA), and 64kPA (Advanced Biomatrix, San Diego, CA) for 1 hour at room temperature. Following cECM incubation with PDMS hydrogels, the cECM digest was aspirated off of the hydrogels and the hydrogels were washed three times with 1X PBS. The final PBS wash was left on the hydrogel in order to maintain gel hydration prior to macrophage seeding.

2.2.7 Isolation of Bone Marrow From Young Mice for Macrophage Culture

The tibia and femur of young (1-2 month) C57Bl/6 mice (Jackson, Bar Harbor, ME) was isolated. Muscle and connective tissue was removed from the bone and bones were washed in fresh macrophage media - composed of Dubelco's modified eagle medium, 10% fetal bovine serum, 1% HEPES, 1% Pen/Strep, 2% non-essential amino acids, and 10% L929 fibroblast culture supernatant - to remove any residual tissue debris. Bones were then transferred to a sterile cell culture hood where the epiphysis of each tibia and femur was removed. Bones were then flushed with 10mL of macrophage media through the diaphysis of each bone to wash out and isolate bone marrow. Care was taken to ensure that all marrow was removed from each bone prior to discarding.

Additional macrophage media was washed through the diaphysis as necessary to fully isolated marrow. Bone marrow-culture media suspensions were then homogenized by pipetting up and down five times and suspensions were passed through a 100uM cell strainer to remove residual debris and break up cell aggregates. Filtered marrow suspensions were then centrifuged for 1500RPM for 5 minutes at room temperature. Following centrifugation, the culture media supernatant was decanted off and the cell pellet was resuspended in fresh macrophage culture media.

2.2.7.1 Macrophage Culture and Seeding of Coated Gel Substrates

Bone marrow isolates were resuspended at a concentration of $1x10^6$ cells/mL in macrophage L929 culture media, with approximately $1.5x10^7$ total cells plated per petri dish. After 7 days in culture, adherent cells were lifted from culture by incubating with accutase (Fisher, Waltham, MA) for 5 minutes. Cells in suspension were then counted and replated onto cECM coated PDMS hydrogels or tissue culture plastic substrates at a density of $1x10^6$ cells/mL. After 24 hours, cells received either no treatment, treatment with macrophage media supplemented with M1 polarizing cytokines lipopolysaccharide (LPS, 100ng/mL) and interferon gamma (IFN-γ, 20ng/mL), or treatment with M2 polarizing cytokine interleukin-4 (IL-4, 20ng/mL). Cells were incubated for an additional 24 hours following treatment, after which media supernatant was collected for media nitric oxide quantification and cells were either fixed for immunofluorescent staining and imaging or lysed for arginase activity assay.

2.2.8 Methods of Evaluating the Macrophage Phenotypic and Functional Response to Experimental Culture Conditions

There are numerous experimental methodologies which can probe macrophage phenotype and function. While macrophage polarization is complex and macrophages have often been noted to polarize toward more intermediate phenotypes within the M1-M2 polarization spectrum *in vivo,* evaluating the relative expression of various M1 and M2 associated genes and proteins can help us derived functional insights about these populations and contextualize macrophage polarization patterns. Quantitative real time polymerase chain reaction (qRT-PCR) and immunolabeling are two experimental tools available for the evaluation of M1 and M2 gene and protein expression patterns in cultured macrophages. In addition to altered gene and protein regulation in differentially polarized macrophage populations, morphological changes have been observed in macrophage populations following pro-inflammatory signaling (Patel et al., 2012). Thus, brightfield imaging and quantification of cell area and morphological features can be performed to infer cell polarization state as well. Finally, several important metabolic differences exist between differentially polarized macrophage subsets and can be utilized to both infer macrophage polarization state and evaluate macrophage functional response capacity. One such difference is the differential metabolism of arginine in M1 and M2 polarized macrophages (Rath, Muller, Kropf, Closs, & Munder, 2014). In M1 macrophages, arginine is metabolized through the inducible nitric oxide synthase (iNOS) protein pathway and generates radical oxidant nitric oxide and citrulline. Conversely, M2 macrophages metabolize arginine through arginase enzymatic pathways generating urea and ornithine. In both cases, the metabolic products of arginine metabolism provide important mechanisms of promoting appropriate M1 or M2 functional responses, such as pathogen cell death or increased matrix deposition, respectively. Thus, evaluation of the degree to

which these enzymatic products are produced can be utilized to infer macrophage phenotype as well as evaluate the competency of these respective pathways.

2.2.8.1 Greiss Reagent Nitric Oxide Assay

Standards were prepared from a 0.1M $NaNO_2$ stock solution serially diluted in macrophage media. 50µL of standard and sample media supernatant collected from *in vitro* cultures were plated in triplicate. 50µL of sulfanilamide (Sigma, St. Louis MO) was added to each well and plates were incubated in the dark for 10 minutes. 50µL of N-(1-Naphthyl)ethylenediamine (Sigma, St. Louis, MO) was added to each well and plates were incubated in the dark for 10 minutes. Following incubation, plates were transferred to a Synergy HTX plate reader (BioTek, Winooski, VT) and the absorbance at 540nm was measured for each standard and sample. Sample nitrite concentration was then calculated from the linear equation derived from the regression fit of serially diluted standard absorbance values.

2.2.8.2 Arginase Activity Assay

Cells were lysed in 50µL cell lysis buffer (0.1% Triton X-100/1% Halt Protease inhibitor (Thermo Scientific, Waltham, MA) in type I water) for 15 minutes at room temperature. 25µL of lysate was then pipetted into a new 96 well plate and 25µL of arginase activation solution (10mM $MnCl_2$ in 50mM Tris buffer, pH 7.5) was added to each sample. Samples were covered and incubated with activation solution for 10 minutes at 55˚C. Following incubation, 50µL of L-arginine (Sigma, St. Louis, MO) substrate solution was added to each sample. Samples were then incubated for 2 hours at 37˚C. Urea standards were made up at an initial concentration of 100mg/mL in cell lysis buffer and serially diluted to generate known concentration standards. To account for sample dilution which occurs during the experimental protocol, 75 µL of type I water

was added to each standard to normalize dilutions across groups. 20 μL of each standard and sample was pipetted into a new 96 well plate and 200 μL of urea detection solution was added to each well. Plates were incubated for 10 minutes at room temperature in the dark, after which plates were transferred to a Synergy HTX plate reader (BioTek, Winooski, VT) and plate absorbance was read at 430nM. Sample urea concentrations were then calculated using the equation derived from the linear regression of known concentration standard absorbance values.

2.2.8.3 Cell Fixation

Cells were fixed for 30 minutes in 2% paraformaldehyde (Fischer Scientific, Waltham, MA) at room temperature. After fixation with paraformaldehyde, fixed cells were washed in five changes of 1X PBS. The final change of 1X PBS was left on fixed samples and samples were stored at 4˚C prior to immunofluorescent staining.

2.2.8.4 Cell Brightfield Imaging and Morphological Feature Evaluation

Brightfield images of fixed cell samples were acquired at 20X magnification using a Zeiss Axio Observer microscope (ZEISS, Oberkochen, Germany). Cell area measurements were quantified using National Institutes of Health FIJI biological image analysis software package (National Institutes of Health, Bethesda, MD). The percentage of cells exhibiting filipodial extensions per field of view was also calculated for each image, with at least 75 cells counted per field of view.

2.2.8.5 Cellular Immunofluorescence and Imaging

1X PBS was removed from fixed samples and donkey blocking buffer (5% donkey serum (Fisher), 1% bovine serum albumin (Sigma), 0.1% tween-20 (Fisher), 0.1% Triton X-100(Fisher))

was added to each sample well for 1 hour at room temperature. Following block, samples were incubated with primary antibodies against either rabbit anti-NOS (ab3523, Abcam, Cambridge, UK) diluted 1:100 in donkey blocking buffer or goat anti-liver arginase (ab91279, Abcam, Cambridge, UK) diluted 1:50 in blocking buffer. Samples were incubated with primary antibody solution overnight for 14-16 hours in the dark at 4˚C. Following primary antibody incubation, samples were washed in 1X PBS three times. Cells incubated with rabbit anti-NOS antibody were then incubated with donkey anti-rabbit Alexa fluor 594 secondary antibody (ab150064, Abcam) diluted 1:200 in donkey blocking buffer for 1 hour in the dark at room temperature. Cells incubated with goat anti-liver arginase were incubated with donkey anti-goat Alexa fluor 594 (ab150136, Abcam) diluted 1:200 in donkey blocking buffer for 1 hour in the dark at room temperature. Following secondary antibody incubation, samples were washed three times with 1X PBS, after which samples were incubated with 4',6-diamidino-2-phenylindole (DAPI) nuclear stain for 1 minute in the dark at room temperature. Samples were washed five times with 1X PBS for 5 minutes per wash, with the final PBS wash being left on to preserve sample hydration. Images of sample immunofluorescence were acquired using a FLoid cell imaging station (Thermo Scientific) with acquisition settings of: blue laser intensity = 30%, red laser intensity = 50%, optical zoom = 0%.

2.2.8.6 Cellular RNA Isolation

Primary murine bone marrow derived macrophages were isolated and cultured in the experimental conditions as previously described. Cellular RNA was isolated using the Qiagen RNeasy Mini Kit (Qiagen, Hilden, Germany) following the protocol for cell monolayer RNA isolation. Briefly, cells were lysed by pipetting 600µL of Buffer RLT in each well and using a sterile cell scraper to disrupt the cell monolayer. 600µL of 70% ethanol was then pipetted into each

well and the lysate solution was mixed well by pipetting. 700µL of lysate was transferred to a RNeasy spin column placed within an empty 2mL collection tube and was centrifuged for 15 seconds at 8000g. Flow through in the collection tube was discarded and remaining sample lysate volume was transferred to the spin column and centrifuged at 8000g for 15 seconds. Flow through was discarded. 700µL of Buffer RW1 was then added to the spin column and samples were centrifuged for 15 seconds at 8000g. Flow through was again discarded. 500µL of Buffer RPE was added and samples were centrifuged for 15 seconds at 8000g. Flow through was discarded. 500µL of Buffer RPE was added again and columns were centrifuged for 2 minutes at 8000g to wash the column and to ensure any residual ethanol was removed. Flow through was discarded and the RNeasy spin column was placed in a new 1.5mL collection tube. 30µL of RNase-free water was added to each spin column and samples were centrifuged at 8000g for 1 minute to elute sample RNA. Eluate in collection tube was re-pipetted onto spin column and samples were centrifuged at 8000g for an additional minute to elute and residual RNA bound to spin columns. Sample RNA concentrations were determined using a NanoDrop Lite spectrophotometer (Thermo, Waltham, MA). Only samples with A260/80 ratios within 2.0 ± 0.10 were considered sufficiently purified for further qRT-PCR analysis.

2.2.8.7 cDNA Generation From RNA Isolates

Sample RNA isolates were homogenized by pipetting prior to cDNA synthesis. The total RNA used for the cDNA synthesis reaction was normalized to the least concentrated sample to normalize the amount of cDNA synthesized across samples. Samples which exhibited higher RNA concentrations were diluted with RNase-free water to normalize the concentration across samples prior to cDNA synthesis. 9µL of RNA or RNA diluted in RNase-free water was then transferred to a microcentrifuge tube. 1µL of 20X RT Enzyme Mix and 10µL of 2X RT Buffer Mix from the

Applied Biosystems High-Capacity RNA-to-cDNA kit (Applied Biosystems, Foster City, CA) was added to each tube. Sample tubes were then placed in a Veriti thermocycler (Applied Biosystems, Foster City, CA). The cDNA synthesis reaction was catalyzed by holding tubes at 37˚C for 60 minutes, followed by 95˚C for 5minutes, with a final rest and storage at 4˚C until ready for qRT-PCR analysis.

2.2.8.8 Quantitative RT-PCR for Macrophage Polarization Associated-genes

All preparation of samples and plates for qRT-PCR were performed on ice or at 4˚C. 1µL of sample cDNA was added to 8µL of RNase-free water, 10µL of TaqMan gene expression master mix (Applied Biosystems, Foster City, CA), and 1µL of TaqMan primer in a MicroAmp Optical 96-well reaction plate (Applied Biosystems). Plates were then sealed with MicroAmp Optical adhesive film (Applied Biosystems) and centrifuged at 300g for 4 minutes at 4˚C. The qRT-PCR reaction was catalyzed and Ct values were obtained using a QuantStudio 3 RT-PCR system (Applied Biosystems). Relative gene expression was determined using the double ΔC_t method (ddCT) of gene expression quantification. *Gapdh* was chosen as the housekeeping gene utilized for normalization in this experiment. Primers chosen for this experiment were selected due to previously reported upregulation following Th1/Th2 cytokine stimuli in macrophage populations: *Nos2* (Mm00440502_m1), *Il1b* (Mm00434228_m1), *Il6* (Mm00475988_m1), *Tnfa* (Mm00443258_m1), *Tgfb* (Mm01178820_m1), *Sod3* (Mm01213380_m1), *Arg* (Mm00475988_m1) (Themo Scientific).

2.2.8.9 Statistical Analysis

Collected result data was input into IBM SPSS 26 statistical analysis software package and data normality was assessed with a Kolmogorov-Smirnov test of normality. In cases where data

exhibited a normal distribution, a two-way ANOVA for dependent variables of substrate stiffness and cECM coating with post hoc Tukey testing was utilized to identify significant differences in experimental result data. In cases where data was observed to exhibit non-normal distributions, a non-parametric Kruskal-Wallis test with post hoc pairwise comparisons was used to identify significant differences in data distribution between experimental groups. The threshold for significance was defined to be $p<0.05$ for the described experiments.

2.3 *In Vitro* Model Results Demonstrate Significant Impacts on Macrophage Phenotype and Function Following Culture in Different Cardiac Microenvironmental Conditions

2.3.1 Cardiovascular Tissue Isolated From Advanced Age Individuals Exhibits Altered Composition Relative to Young Age Individuals

Several cardiac microenvironmental alterations which occur with increasing age were characterized histologically in young (1mo), moderately aged (12mo), and advanced age (23mo) cardiac tissue samples. Picrosirius red staining of cardiac samples demonstrated both a qualitative as well as a quantitative increase in collagen fiber deposition, with increasing age being associated with increases in both interstitial and perivascular collagen deposition (Figure 3A, B).

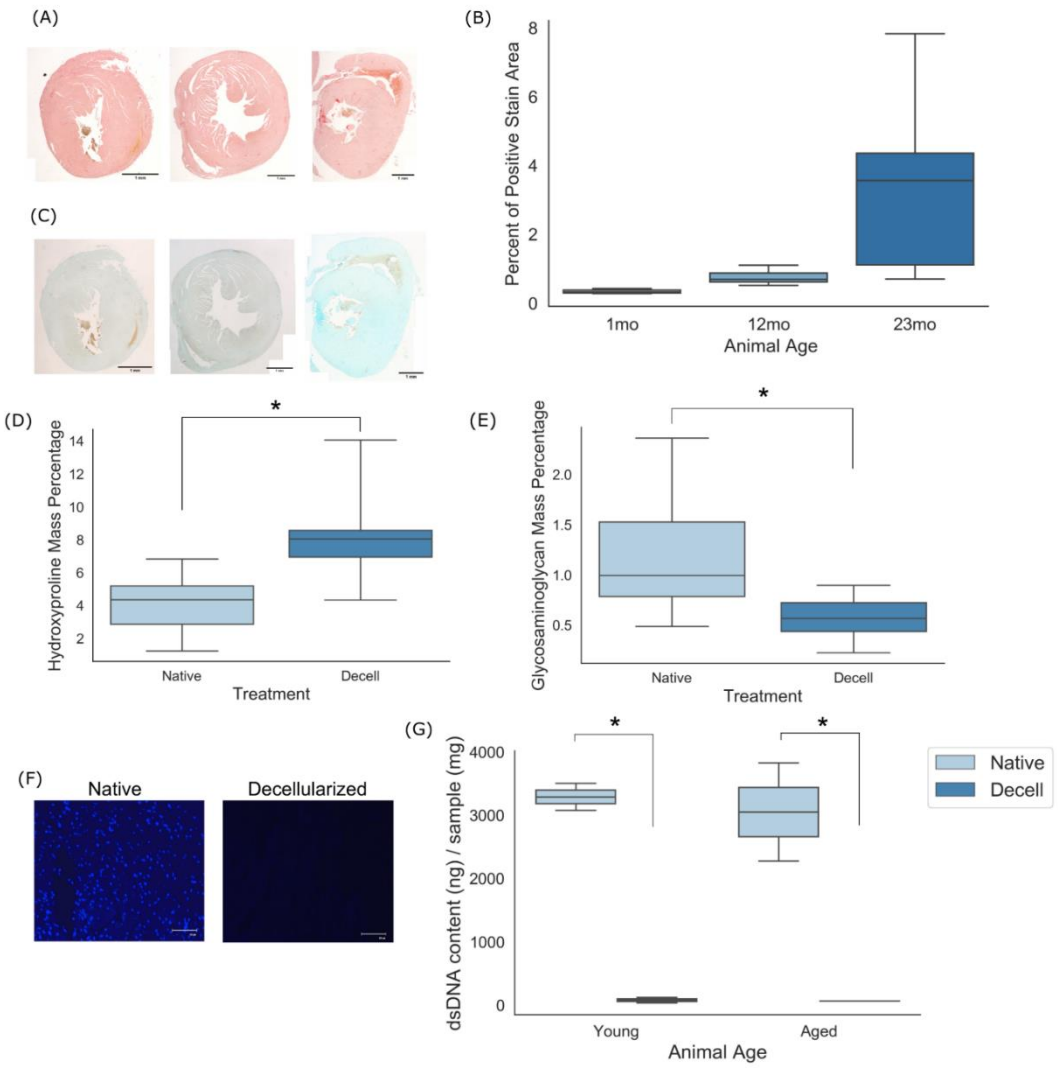

Figure 3 - Young and aged cardiac ECM can be decellularized. (A) Brightfield images of picrosirius red and **(C)** alcian blue stained cardiac tissue sections from mice aged 1 month, 12 months, or 23 months. **(B)** Quantification of percent positive area of collagen staining in brightfield picrosirius images. **(D)** Quantification of hydroxyproline and **(E)** glycosaminoglycan mass percentage in native and decellularized cardiac samples. **(F)** Images of DAPI nuclear staining for native and decellularized cardiac tissue. **(G)** PicoGreen assay double stranded DNA quantification results for native and decellularized cardiac tissue samples. Data presented as box and whisker plots. Lines indicate mean. N=4-5; *=$p<0.01$; Scale bars (A, C) = 1 mm; Scale bar (F) = 100 μm; Independent samples t-test used to assess significant trends in (D, E). One-way ANOVA with post-hoc Tukey's test used to assess significance in (G).

Staining of sulfated proteoglycans in young (1mo), moderately aged (12mo), or advanced age (23mo) cardiac tissue sections with Alcian blue demonstrated a qualitative increase in sulfated proteoglycan deposition with increasing age in cardiac tissue samples (Figure 3C).

2.3.2 Cardiac Tissue Isolated From Young and Advanced Age Murine Donors Can Be Decellularized

In order to assess the impacts of aged-related cardiac extracellular matrix compositional changes on naïve macrophage populations, it is first necessary to decellularize isolated tissue samples to remove cellular nuclear content and antigens from the tissue sample. As described prior, a skeletal muscle decellularization protocol first described by Wolf et. al. (Wolf et al., 2012) with additional blood clot dissociation steps was used to decellularize cardiac tissue samples isolated from young and aged murine donors. Successful decellularization of native tissue is characterized by retention of bioactive matrix proteins with a sufficient removal of cellular nuclear content and any other antigens from tissue samples - as these factors can induce confounding immune responses in macrophages (Keane, Londono, Turner, & Badylak, 2012).

The chosen protocol was found to have a significant impact on tissue sample nuclear content relative to age-matched control samples. Qualitative evaluation of sample nuclear content with 4'.6-diamidino-2-phenylindole (DAPI) nuclear staining demonstrated a substantial reduction in sample nuclear content following decellularization in young and aged samples (Figure 3F). PicoGreen double stranded DNA content quantification of native and decellularized samples demonstrated a significant decrease in mean double stranded DNA content following tissue decellularization for both young and aged tissue samples (Figure 3G). Taken together, these

quantitative and qualitative results indicate that the chosen decellularization protocol was sufficient for the removal of cellular nuclear content.

2.3.3 Macrophages Exhibit Altered Morphological Features When Cultured Upon Substrates of Varying Stiffness

In order to assess the contribution of biomechanics as a predictor of macrophage morphological features, naïve bone marrow-derived macrophages isolated from young (1-2 month) donor C57BL/6 mice were cultured on either the 8kPA PDMS gel, 32kPA PDMS gel, or tissue culture plastic substrates coated with decellularized cardiac extracellular matrix (cECM). Differing cell morphology was observed in response to increased culture substrates stiffness, with tissue culture plastic promoting more spread cellular morphologies (Figure 4A, white arrows), significantly greater cellular area measurements (Figure 4B), and a greater mean percentage of cells per field of view exhibiting filipodia (Figure 4C).

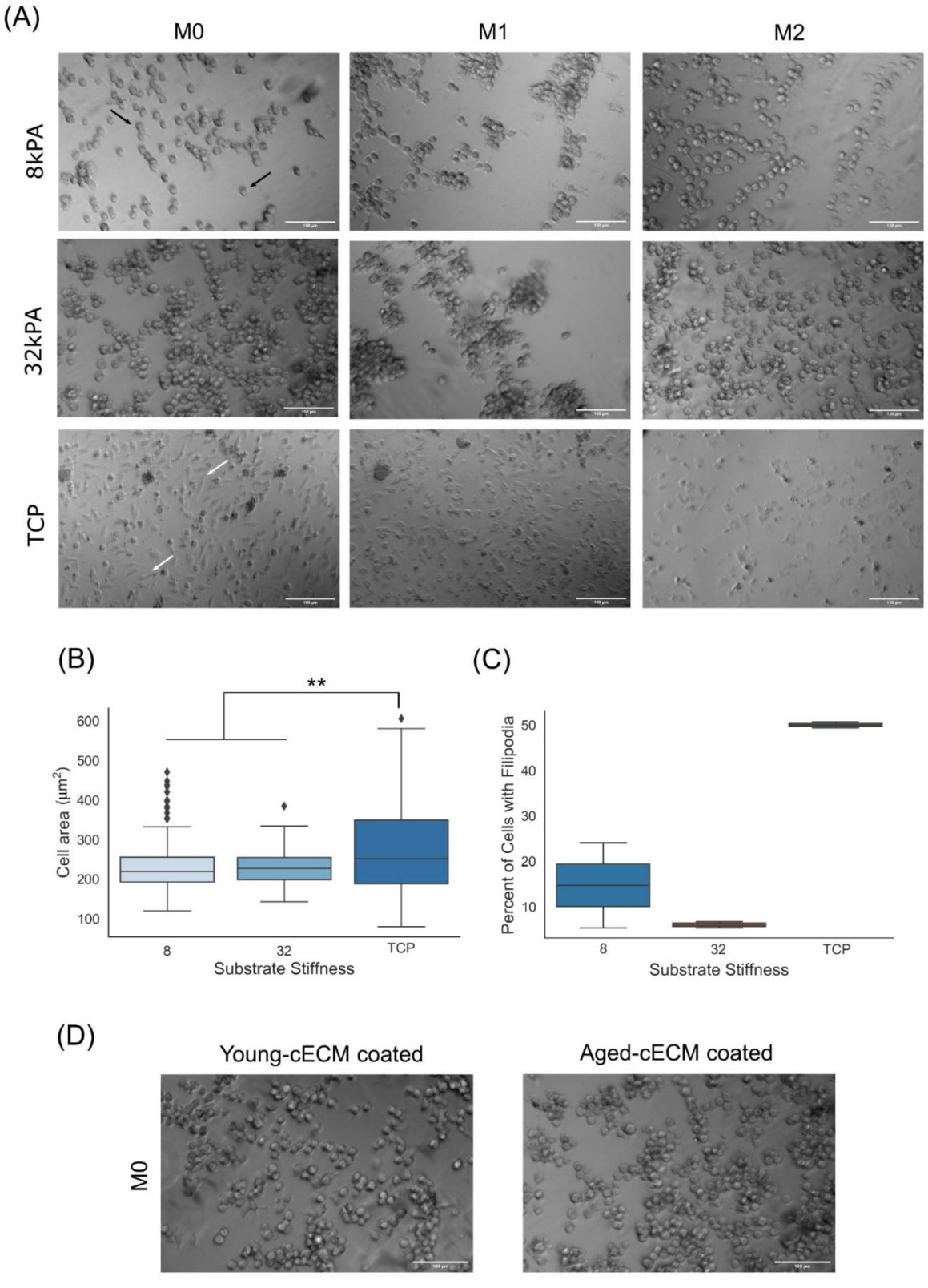
(A)
M0
M1
M2
8kPA
32kPA
TCP
(B)
**
Cell area (µm²)
600
500
400
300
200
100
8
32
TCP
Substrate Stiffness
(C)
Percent of Cells with Filipodia
50
40
30
20
10
8
32
TCP
Substrate Stiffness
(D)
Young-cECM coated
Aged-cECM coated
M0

Figure 4 - Increased substrate stiffness promotes altered macrophage morphologies. (A) Naïve bone marrow-derived macrophage culture on 8 kPA gel, 32 kPA gel, or tissue culture plastic (TCP). Macrophage culture on substrates of lower elastic modulus were observed to exhibit more round morphologies with few filipodia (black arrows, 8 kPA & 32 kPA gel groups). Conversely, macrophage culture on substrates of increased stiffness, such as tissue culture plastic, was found to be associated with spread cellular morphologies often with several filipodia (white arrows, TCP). **(B)** Cell area was found to be significantly increased for macrophages cultured on tissue culture plastic relative to cells cultured on either 8 kPA or 32 kPA gels. At least 70 cells were counted per field of view for 2-3 biological replicates. **(C)** Cells cultured on tissue culture plastic exhibited a greater percentage of cells with filipodia per field of view. At least 70 cells were counted per field of view for 2-3 biological replicates. **(D)** Naïve bone marrow-derived macrophages cultured on 32 kPA gel coated with decellularized cardiac extracellular matrix isolated from young (1-2 month) or advanced age (20-24 month) did not exhibit significantly altered morphologies. Note: brightfield 32kPA image reproduced here from (A) for qualitative comparison on coating in (D). TCP = tissue culture plastic. Scale bars = 100 μm. Data presented as box and whisker plots. Lines indicate mean. Black triangles signifiy any outlier data points. ANOVA with Tukey post-hoc analysis was used to identify any significant differences in data presented in (B). *$p<0.005$, **$p<0.001$.

In comparison, it was observed that less stiff gel substrate groups often promoted rounder cell morphologies (Figure 4A, black arrows), significantly decreased cellular area measurements (Figure 4B), and a decreased mean percentage of cells with filipodia per field of view (Figure 4C). To assess if the age of the donor mouse from which the cECM coating was derived affected macrophage morphology, macrophages were seeded onto 32kPA gels coated with decellularized cECM isolated from young or aged mice. It was noted that cell morphology did not appear substantially different between young or aged cECM coated gels, suggesting that substrate stiffness may be a greater determinant of macrophage morphological features than the age of the donor mouse from which the decellularized cECM was isolated (Figure 4D).

2.3.4 Macrophages Exhibit Altered Pro-inflammatory Macrophage Functionality When Cultured on Substrates of Varying Stiffness, Particularly in the Presence of Pro-inflammatory Cytokine Cues

In order to assess the ability of naïve macrophages to polarize to M1 phenotypes in response to Th1 cytokine signaling cues when cultured in conditions of varying stiffness and cECM coating, macrophages isolated from young (2-4 month) mice were seeded onto cECM-coated gels ranging in stiffness from 2kPA to 64kPA or onto tissue culture plastic and were subsequently polarized with canonical Th1 cytokine interferon gamma (IFN-γ) and lipopolysaccharide (LPS). Pro-inflammatory polarization and function was assessed through media nitrite quantification (Figure 5A, B) and immunolabeling for macrophage protein inducible nitric oxide synthase (iNOS) (Figure 5C).

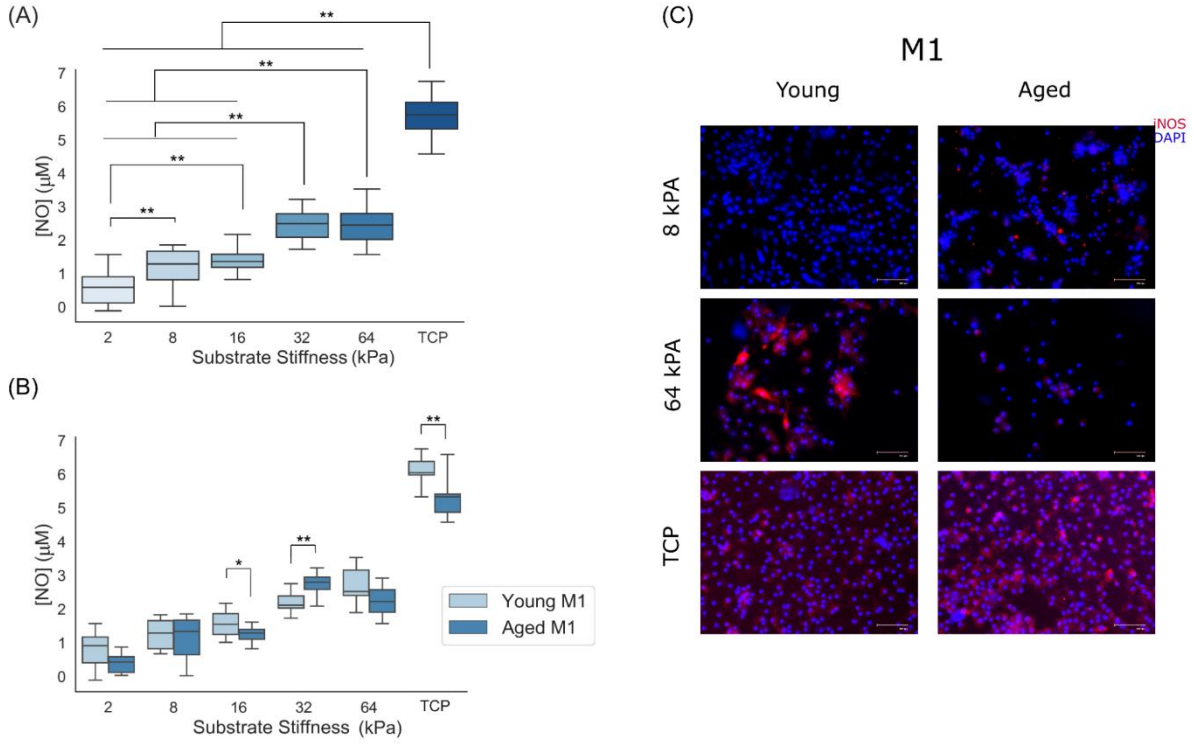

Figure 5 - Increased macrophage culture substrate stiffness enhances macrophage pro-inflammation-associated radical oxidant secretory response following M1 cytokine treatment. (A) Nitrite concentration in cell culture media supernatant from cells cultured on increasingly stiff substrates (n=32). **(B)** Nitrite concentration in cell culture media supernatant as a function of substrate stiffness and cardiac extracellular matrix coating (n=16). **(C)** Representative images of fixed macrophages immunolabeled with antibodies against inducible nitric oxide synthase (iNOS) and cell nuclei (DAPI) for macrophages cultured on 8 kPA gel, 64 kPA gel, and tissue culture plastic coated with cardiac extracellular matrix isolated from young or advanced age mice following pro-inflammatory stimuli treatment. TCP = tissue culture plastic. Scale bars = 100 μm. Data presented as box and whisker plots. Lines indicate mean. ANOVA with post-hoc Tukey testing was utilized to assess any significant trends in data distribution. *p<0.05, **p<0.001.

2.3.4.1 Greiss Reagent NO Assay Results

In order to assess the significance of the observed differences, a two-way ANOVA for the independent variables gel stiffness and cECM coating age and dependent variable nitrite supernatant concentration was performed. ANOVA results indicated a significant effect for both predictors gel stiffness ($p<0.001$, $n=32$) and cECM coating age ($p<0.001$, $n=92$) with a significant interaction between variables noted as well ($p<0.001$, $n=16$). Tukey post-hoc testing for multiple comparisons was used to assess significance between macrophage media nitrite concentrations between gels of different stiffnesses. A significant effect ($p<0.001$) was observed between all substrates of differing stiffness, save for between 8kPA and 16kPA ($p=0.348$, mean diff=.2141μM) and between 32kPA and 64kPA ($p=1.000$, mean diff=-0.0174μM) hydrogel culture substrates. In order to assess the significance of the interaction between gel stiffness and young or aged cECM coatings, independent samples t-tests were performed between equivalent stiffness gels coated with either young or aged decellularized cECM for each substrates stiffness tested. After correcting for multiple comparisons (Bonferroni correction – $p<0.05/6 = p<0.0083$), a significant difference in nitrite media concentration was found between cECM coating derived from young or aged mice for macrophages cultured on 16kPA ($p=0.006$, mean diff=0.3293μM), 32kPA ($p<0.001$, mean diff=-0.5547μM), and tissue culture plastic ($p<0.001$, mean diff=0.8927μM).

2.3.4.2 Macrophage iNOS Immunolabeling

Qualitative immunolabeling for inducible nitric oxide synthase (iNOS) in fixed macrophage cultures appeared to support the quantified trends observed following Griess reagent nitrite quantification. These results taken together with the quantified results suggest that expression of M1-associated protein inducible nitric oxide synthase and secretion of oxidant nitric

oxide in response to Th1 stimuli is dependent upon both the stiffness of the culture substrates as well as upon the age of the host from which the decellularized cECM coating was derived.

2.3.5 Macrophages Exhibit Altered Anti-inflammatory Macrophage Function When Cultured on Substrates of Varying Stiffness, Particularly in the Presence of Alternative Activation-associated Cytokines

In order to study the ability of naïve macrophages to polarize to M2 phenotypes in response to Th2 cytokine interleukin-4 (IL-4) when cultured in conditions varying in stiffness and cECM coating, macrophages isolated from young (2-4 month) mice were seeded onto cECM-coated gels ranging in stiffness from 2kPA to 64kPA or onto tissue culture plastic, and were subsequently polarized with IL-4. Alternative macrophage polarization was then assessed through quantification of M2 macrophage function and phenotype based on expression of arginase-1, which is upregulated in murine M2 macrophages (B. N. Brown et al., 2017; B. N. Brown et al., 2012). Arginase function was quantified through quantification of urea production, as urea is a downstream enzymatic product of arginase (Figure 6A, B). Arginase-1 protein expression was assessed by immunolabeling for arginase-1 (ARG) (Figure 6C).

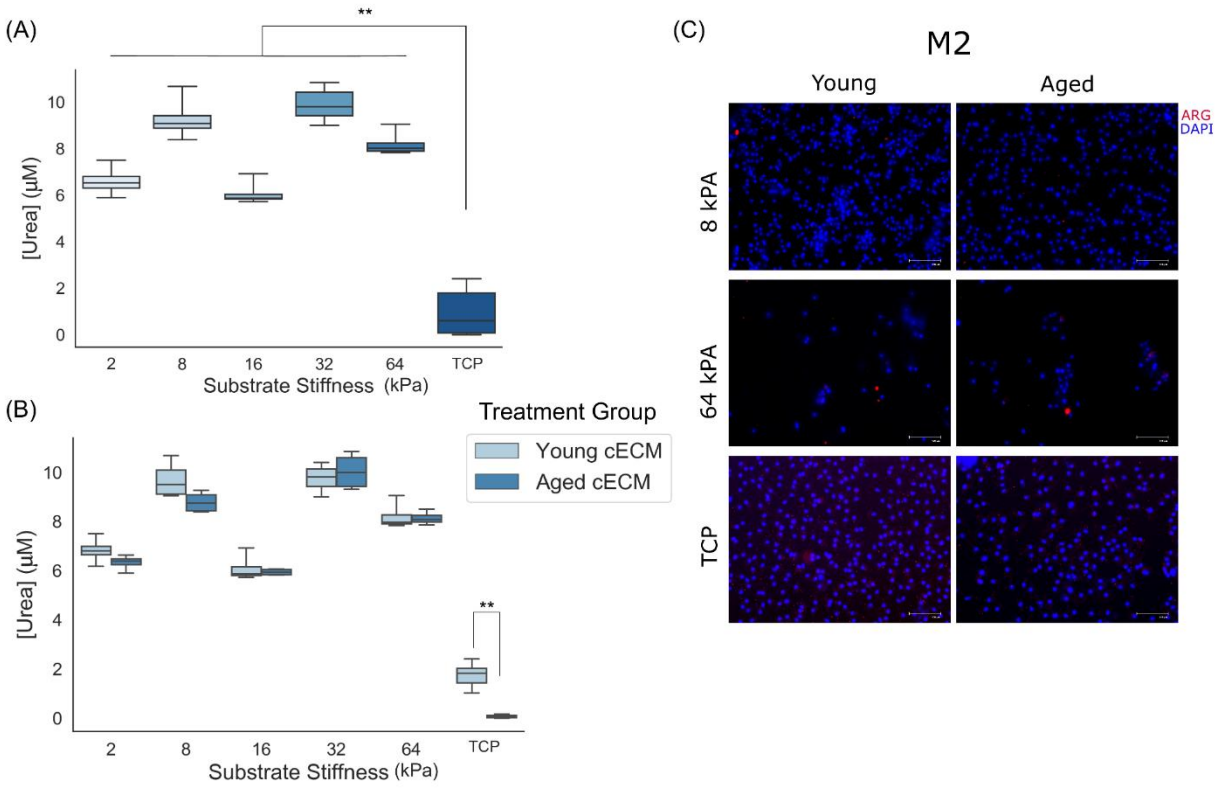

Figure 6 - Increased substrate stiffness attenuates alternative macrophage function following M2 cytokine treatment. (A) Urea concentration in cell lysates following arginase activity assay in experimental macrophage cultures (n=8-12). **(B)** Urea concentration in cell lysates following arginase activity assay as a function of both substrates stiffness and cECM coating donor age (n=4). **(C)** Representative images of Arginase-1 (ARG) and cell nuclei (DAPI) immunolabeling in IL-4 treated macrophages cultured on either 8 kPA, 64 kPA, or tissue culture plastic coated with cECM isolated from young or aged mice. Linear adjustments to image contrast were made to reduce background and improve staining visibility. Scale bar = 100μm. Data presented as box and whisker plots. Lines indicate mean. ANOVA with Tukey HSD post-hoc analysis was used to assess significance of data trends. *p<0.05, **p<0.001.

2.3.5.1 Macrophage Arginase Activity Assay

Urea concentration was found to exhibit variability between differentially stiffened gel cultures, which were all found to be greater than tissue culture plastic macrophage cultures. In order to assess the significance of the observed differences, a two-way ANOVA for variables gel stiffness and cECM coating age and dependent variable urea concentration was performed. ANOVA results indicated a significant effect for both predictors gel stiffness ($p<0.001$, $n=8-12$) and cECM donor age ($p=0.001$, $n=26$) with a significant interaction between variables noted as well ($p=0.001$, $n=4$). Tukey HSD post-hoc testing for multiple comparisons was used to assess significance between culture substrates of different stiffnesses. A significant effect ($p<0.001$) was observed between tissue culture plastic and all gel substrate groups. Additionally, significant differences were observed between all gel groups ($p<0.001$) except for between 2kPA and 16kPA ($p=0.237$, mean diff=0.5572μM) as well as between 8kPA and 32kPA ($p=0.105$, mean diff=-0.6590μM) gel substrates. In order to assess the significance of the interaction between gel stiffness and the cECM donor age, independent samples t-tests between equivalent stiffness gels coated with cECM derived from young or aged mice were performed for each substrate stiffness tested.

After correcting for multiple comparisons (Bonferroni correction – $p<0.05/6 = p<0.0083$), a significant effect was only observed between macrophages cultured on tissue culture plastic coated with cECM derived from either young or aged donor cardiac tissue ($p<0.001$, mean diff=1.670μM).

2.3.5.2 Macrophage Arginase Immunolabeling

Qualitative cellular immunolabeling evaluation of arginase-1 in fixed macrophage samples appeared variable between groups. These results together suggest that M2 polarization in response to canonical Th2 cytokine IL-4 appears to remain functional across culture groups of physiological

stiffness (2kPA to 64kPA), however a significant attenuation of function was noted at supraphysiological stiffnesses, such as in the case of naïve macrophage culture on tissue culture plastic.

2.3.6 The Impacts of Young and Aged Cardiac Extracellular Matrix Coating on Macrophage Phenotype and Function

In order to first assess how aging alters the regulation of inflammation associated gene transcripts in cardiac tissue, RNA was isolated from whole cardiac tissue homogenates isolated from either young (1 month), moderately aged (8 month) or advanced age (18-21 month) mice. Relative gene expression was quantified, normalized to housekeeping control gene *Gapdh* expression, and expressed as a fold change in expression using the described double ΔC_t analysis (Figure 7A). A general mean increase in expression of inflammation associated *Tnfa* and *Nos2* were observed with increasing age, with a significant effect noted in the case of the observed mean *Nos2* increase (Figure 7A). Additionally, a significant increase in the fold change of *Tgfb* expression was observed in cardiac RNA isolates derived from mice aged 18-21 months relative to RNA isolates derived from 1 month aged mice.

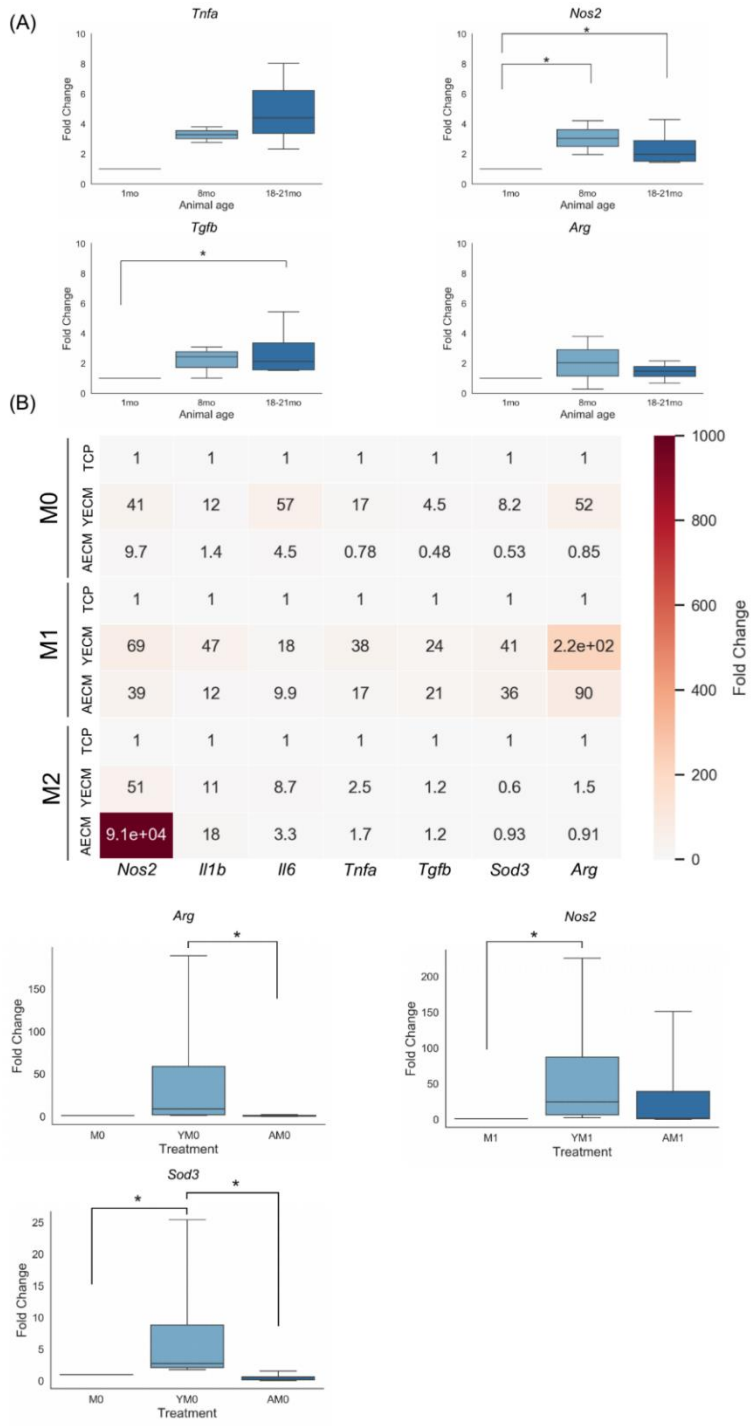

Figure 7 - Young cardiac ECM promotes alternative macrophage activation at baseline. (A) qRT-PCR results expressed as a fold change in expression of pro- (*Nos2, Tnfa*) and anti-inflammatory (*Tgfb, Arg*) genes in RNA isolated

from whole heart tissue homogenates isolated from young (1 month), moderately aged (8 months), or advanced age (18-21 month) C57/Bl6 mice (n=3-5). **(B)** Heatmap of qRT-PCR results for expression of pro- and anti-inflammatory gene expression in primary macrophages isolated from young (2-4 month) mice cultured on tissue culture plastic coated with decellularized cardiac extracellular matrix isolated from either young (Y, 2-4 month old) or advanced age (A, 18-21 month old) mice with either no supplemental cytokine treatment (M0, YM0, AM0), treatment with bone marrow culture media supplemented with interferon-γ (IFN-γ) and lipopolysaccharide (LPS) (M1, YM1, AM1), or treatment with bone marrow culture media supplemented with interleukin-4 (IL-4) (M2, YM2, AM2) (n=4). Significant differences in gene expression between experimental conditions highlighted in boxplots. A Kruskal-Wallis 1-way ANOVA with post-hoc pairwise comparisons was used to identify significant differences in gene expression patterns. *$p<0.05$.

In order to better understand how cardiac extracellular derived from young or advanced age mice may induce altered macrophage phenotype, macrophages were seeded onto tissue culture plastic coated with either young or aged cardiac ECM, followed by either no treatment (Y→M0, A→M0), treatment with Th1 immune response associated cytokine IFN-γ and bacterial product LPS (Y→M1, A→M1), or treatment with Th2 immune response associated cytokine IL-4 (Y→M2, A→M2). Differential gene expression was determined by normalizing to control gene expression in macrophages cultured on tissue culture plastic in either the M0, M1, or M2 macrophage conditions, in order to provide phenotype specific controls that aid in highlighting the ECM-induced differences in macrophage gene expression at baseline and following stimulation.

In general, cardiac ECM isolated from young mice was found to promote alternative activation associated gene signatures in culture macrophages, as evidenced by the observed significant mean increases in the expression of arginase (*Arg*) and superoxide dismutase 3 (*Sod3*) gene transcription in these experimental groups. This result suggests that young developmental

age cardiac ECM protein content promotes alternative macrophage polarization in the non-stimulated condition (Y→M0) (Figure 7B). Conversely, macrophages cultured on substrates coated with cardiac extracellular matrix derived from advanced age mice did not exhibit the mean increase in expression of alternative activation associated *Arg* or *Sod3* transcripts.

Macrophage culture on tissue culture plastic coated with cardiac ECM derived from young mice was also found to be associated with increased upregulation of M1-associated or M2-associated gene targets following M1 (IFN-γ and LPS) or M2 (IL-4) stimuli treatment, respectively (Figure 7B). Alternatively, RNA isolated from macrophages cultured on substrates coated with ECM isolated from aged animals often exhibited reduced or dysregulated expression of canonical M1 or M2 gene targets following M1 or M2 stimulation (Figure 7B). For example, macrophages cultured on tissue culture plastic coated with ECM derived from young animals exhibited greater expression of M1-associated *Nos2* or *Il1b* transcripts following M1 stimulation as well as greater expression of alternative activation associated *Arg* transcripts following M2 cytokine treatment (Figure 7B). However, culture with ECM derived from aged animals attenuated this expression of canonical M1 or M2 associated genes, and in some cases, even induced non-canonical gene expression following cytokine stimulation - such as in the case of the relatively large upregulation in M1-associated *Nos2* transcripts following treatment with IL-4 in the A→M2 macrophage experimental group (Figure 7B). Taken together, these results demonstrate an ability of cardiac extracellular matrix isolated from young animals to promote alternative macrophage activation at baseline as well as to support M1 or M2 phenotypic polarization following pro-inflammatory or anti-inflammatory stimulation, respectively. Conversely, macrophage culture with cardiac extracellular matrix derived from advanced age animals was found to not be associated with any

altered gene expression at baseline and a dysregulation of canonical M1 or M2-associated gene expression following stimulation.

2.4 In Vitro Model of Cardiac Microenvironmental Alterations Highlights the Significant Contributions of Both Biomechanical Change and Compositional Change in Promoting Altered Macrophage Phenotype and Function

Macrophage phenotypic plasticity is an essential feature of macrophage populations which allows these cells to perform a unique range of diverse functional responses within the local tissue microenvironment. However, this functional plasticity in macrophage polarization can also be deleterious. As tissue microenvironments change with increasing age or pathology-associated tissue remodeling, previously non-pathological macrophage polarization can be shifted to polarization states which promote pathological tissue remodeling rather than support tissue homeostasis. In these cases, understanding how changing macrophage phenotype contributes to pathological tissue remodeling as well as elucidating the mechanisms by which changing microenvironmental cues induce altered macrophage polarization can help identify point of therapeutic intervention to help attenuate pathologic tissue remodeling and disease progression.

Within the cardiovascular system, resident macrophage populations serve an important role in maintaining tissue homeostasis as well as in regulating the remodeling response following cardiac tissue damage (Fujiu et al., 2017; Hulsmans et al., 2017; Lavine et al., 2014). Given the importance of these cells in maintaining cardiac cell function and preventing adverse cardiac tissue remodeling following injury, understanding the mechanisms by which cardiac macrophages integrate cardiac microenvironmental cues to induce appropriate polarization and functional

responses as well as how changes in cardiac microenvironmental stimuli promote altered macrophage polarization states will further elucidate the role these cells play in promoting cardiac dysfunction.

Cardiac extracellular matrix exhibits significant changes in matrix protein composition and organization during the embryogenesis and physiological aging processes (Horn & Trafford, 2016; Williams et al., 2014; Williams et al., 2015). During embryogenesis and cardiac tissue maturation, cardiac matrix protein composition is heterogenous and characterized by developing tissue collagen fibril and elastin protein structures as well as by increased matricellular protein content (Williams et al., 2014; Williams et al., 2015). As cardiac tissue develops and matures during post-natal periods of development, matricellular protein content is reduced and increased fractions of extracellular matrix protein content is comprised of collagen proteins - particularly fibrillar collagen subtypes including collagens I, III, and V (Fan et al., 2012; Horn & Trafford, 2016; Williams et al., 2014; Williams et al., 2015). In addition to altered composition, cardiac extracellular matrix protein organization and assembly can be altered with the aging process (Biernacka & Frangogiannis, 2011; Eyre et al., 1984). Both extracellular matrix protein composition as well as matrix protein organization and incorporation into larger tissue level matrix structures are important determinants of tissue biomechanical properties (Phillip, Aifuwa, Walston, & Wirtz, 2015). Consequently, cardiac tissue biomechanical properties change throughout the cardiac tissue development, maturation, and aging processes.

Macrophage populations have demonstrated a polarization responsivity both to altered extracellular protein composition as well as to altered microenvironmental biomechanical properties (B. N. Brown et al., 2017; B. N. Brown et al., 2012; Patel et al., 2012; Sridharan et al., 2019; Wolf et al., 2012). However, these responses have largely been characterized using non-

cardiac specific extracellular matrix-derived biomaterials or under supraphysiological biomechanical conditions. Thus, the present study sought to leverage an *in vitro* model of differing cardiac microenvironmental conditions to better elucidate the macrophage polarization response to these varying microenvironmental stimuli and help further elucidate any macrophage-mediated role in the age-related risk of cardiovascular disease event incidence. Since cardiovascular microenvironmental composition and biomechanical properties are inherently linked *in vivo*, an *in vitro* model was first developed as a means to assess the relative contribution of each of these variables in inducing altered macrophage polarization.

2.4.1 Macrophage Culture on Substrates of Increased Stiffness is Associated With Increased Pro-inflammatory Functional Responses, Reduced Alternative Activation-associated Function, and Altered Cell Morphologies

The results of the *in vitro* model experiments demonstrated a significant impact of macrophage culture substrate stiffness both on macrophage morphology as well as on macrophage pro-inflammatory and anti-inflammatory function. When examining the impacts of substrates stiffness on macrophage morphology, culture substrates of lower elastic modulus were found to be associated with rounder macrophage morphologies exhibiting few to no filipodia. Conversely, macrophage culture on highly stiffened tissue culture plastic was observed to promote an altered macrophage morphology which was characterized by increased mean cell area and an increased number of macrophages with filipodia observed per field of view. Interestingly, this alteration in macrophage morphology from rounder morphologies to more spread morphologies exhibiting many filipodia has been previously observed following macrophage treatment with canonical M1 phenotype stimulant, LPS (Patel et al., 2012).

In addition to inducing macrophage morphological feature alterations reminiscent of those observed following M1 macrophage polarization, increased culture substrate stiffness was observed to have a significant impact on both pro- and anti-inflammatory macrophage functional responses. Macrophage culture on substrates of increased elastic modulus was found to both promote significantly greater pro-inflammatory functional responses following Th1 cytokine stimulation as well as significantly attenuate anti-inflammatory functional responses following Th2 cytokine stimulation. These results serve to further support previously characterized pro-inflammatory phenotypic biasing of macrophages cultured on highly stiffened substrates as well as provide an additional characterization of how differing substrate stiffness conditions promote altered macrophage functional responses across a physiologically relevant range of material stiffnesses (Adlerz et al., 2016; Blakney et al., 2012; Sridharan et al., 2019). However, it should also be noted that the difference in stiffness between the stiffest gel culture substrate and the highly stiffened tissue culture plastic control is relatively large compared to the difference in substrate stiffness between the most and least stiff gels. This relatively large jump in tissue culture plastic stiffness may account for some of the magnitude of difference in pro- and anti-inflammatory macrophage functional responses observed in tissue culture plastic culture groups relative to gel culture macrophages. Future studies may seek to incorporate additional controls or gel culture groups at supraphysiological stiffnesses to provide a more relevant highly stiffened control for comparison.

2.4.2 Macrophage Culture on Substrates Coated With Decellularized Cardiac Extracellular Matrix Isolated From Aged Murine Donors Were Observed to Exhibit Reduced Pro-inflammatory and Anti-inflammatory Functional Responses

In addition to macrophage culture substrate stiffness, the age of the donor animal from which the decellularized cardiac extracellular matrix coating was derived was found to have a significant impact on macrophage pro- and anti-inflammatory phenotype. Macrophage culture on substrates coated with decellularized cardiac extracellular matrix derived from aged animals was found to be associated with a significant reduction in both pro- and anti-inflammatory macrophage function. In the pro-inflammatory condition, culture with extracellular matrix coating derived from aged animals was associated with a 12% decrease in the observed media nitrite concentration, suggesting an attenuated responsivity to these pro-inflammatory signaling cues relative to macrophages cultured on substrates coated with cardiac extracellular matrix isolated from young murine donors. Anti-inflammatory function following co-culture with anti-inflammatory Th2 cytokines and cardiac extracellular matrix coatings derived from aged animals was found to be associated with an approximately 9.7% reduction in urea concentrations following arginase activity assay relative to macrophages cultured with cardiac extracellular matrix coatings derived from young animals.

2.4.3 Decellularized Cardiac Extracellular Matrix Derived From Young Mice Was Associated With Promoting Alternative Activation-associated Gene Expression Profiles at Baseline in Naïve Macrophage Populations

Altered macrophage phenotype following culture on substrates coated with cardiac extracellular matrix derived from either young or aged murine donors was also observed in the *in vitro* model qRT-PCR results. The first significant alteration in macrophage gene expression induced by decellularized cardiac extracellular matrix treatment was noted in macrophages cultured on tissue culture plastic coated with cardiac extracellular matrix derived from young animals, where a significant upregulation of anti-inflammatory associated *Arg* and *Sod3* transcripts was observed. This result suggests a partial ability of cardiac extracellular matrix coatings derived from young animals to promote alternative macrophage phenotypes at baseline, a result which reflects previously characterized induction of alternatively activated phenotypes in macrophages following exposure to extracellular matrix-based biomaterials derived from the small intestine of young animals (B. N. Brown et al., 2017; Sicari et al., 2012).

2.4.4 Macrophage Culture on Substrates Coated With Cardiac Extracellular Matrix Derived From Young Donors Support Canonical M1 or M2 Macrophage Polarization While Culture on Substrates Coated With Cardiac Extracellular Matrix Derived From Aged Donors Promote Dysregulated Macrophage Gene Transcription

Some differences in pro-inflammatory and anti-inflammatory gene expression were observed between culture groups following Th1 and Th2 cytokine push as well. In general, it was observed that macrophage culture on substrates coated with cardiac extracellular matrix derived

from young murine donors supported the expression of genes associated with the canonical M1 or M2 macrophage response following treatment with Th1 or Th2 cytokine signaling cues, respectively. Conversely, macrophage culture on substrates coated with cardiac extracellular matrix derived from aged murine donors attenuated the expression of canonical M1 or M2-associated gene transcripts and in some cases promoted non-canonical gene expression. For example, a large upregulation in M1 phenotype-associated *Nos2* transcripts was observed in macrophages cultured on substrates coated with cardiac extracellular matrix isolated from aged mice following Th2 cytokine treatment. However, it is also important to note that this non-canonical upregulation of pro-inflammatory factors following Th2 cytokine stimulation in macrophages cultured with cardiac extracellular matrix derived from aged mice was not observed for all gene targets assayed, such as in the case of *Il6* or *Tnfa*.

Taken together, these results suggest that cardiac extracellular matrix biomaterials isolated from young donor animals tend to promote alternative macrophage activation at baseline while also supporting gene expression of M1 or M2-associated genes in the presence of Th1 or Th2 cytokine signaling cues. Alternatively, macrophage culture on substrates coated with cardiac extracellular matrix materials derived from aged donor animals did not induce any altered phenotypes at baseline and promoted non-canonical gene expression following Th1 or Th2 cytokine stimulation.

2.4.5 *In Vitro* Study Limitations and Future Directions

It is important to acknowledge several limitations in the phenotypic comparisons presented for the described *in vitro* model. While gene expression and functional response characterization provide important insight regarding macrophage responsivity to differing microenvironmental

conditions, these experiments comprise only a fractional characterization of the myriad of possible changes in gene expression or function in macrophage populations. In order to better understand how alterations in these *in vitro* microenvironmental conditions alter macrophage phenotype, future studies may seek to isolate cultured macrophage RNA for sequencing or perform chromatin accessibility assays to provide a more comprehensive characterization of the microenvironmentally induced changes in macrophage gene expression.

It is also important to note that the described *in vitro* model, while providing an important means of evaluating the relative contributions of cardiac extracellular matrix composition and substrate biomechanics individually, does not fully recapitulate the complexity of the *in vivo* cardiac microenvironment or the numerous changes which can occur there throughout an organism's life. Cardiac macrophages comprise a relatively small fraction of total cardiovascular system cellularity. Cardiomyocytes, endothelial cells, fibroblasts, non-macrophage immune cell subtypes, and circulating progenitor cell populations play an important role in maintaining homeostatic cardiac tissue function. Additionally, prior studies have demonstrated the role that biochemical or biomechanical change in the cardiovascular system plays in promoting dysregulation of proper function in these cells. Therefore, the lack of inclusion of these cells in the described *in vitro* model limit the ability of the model to determine whether the observed macrophage responses to differing microenvironmental conditions promoted cardiac dysfunction directly through upregulated inflammatory responses or through induction of dysfunction in other constitutive cardiac cells mediated through altered macrophage secretome regulation. Future studies may seek to further develop the applicability of the described *in vitro* model by incorporating additional cardiac cell types in a co-culture model to better understand the direct and indirect mechanisms by which cardiac macrophages contribute to cardiac pathology development.

In a similar manner, future studies may also seek to incorporate additional, ontogenically distinct macrophage subsets into the described *in vitro* culture model to elucidate any macrophage subset specific differences in microenvironmental phenotypic response. While bone marrow-derived macrophage subset polarization dynamics are important to understand as attenuation of this population response has been shown to be associated with improved remodeling outcomes, elucidation of the yolk sac-derived or fetal liver-derived macrophage response to these varied microenvironmental conditions will also be important to understand the degree to which any macrophage subset intrinsic difference in polarization capacities exist. These studies may also help elucidate the degree to which macrophage ontogeny determines cell phenotype as compared to microenvironment induced phenotypic alterations.

Finally, it is important to note that while some characterization of the age-related changes in young and aged murine cardiac tissue matrix protein content was characterized in Figure 3, this histological characterization does not provide a complete quantification of the myriad of compositional changes or protein modifications which can occur with increasing age in cardiac tissue. Future studies may seek to use mass spectrometry or other analytic chemistry analysis to characterize the complete array of protein content changes and the extent of protein modification within the aging cardiac tissue microenvironment. Future studies may also extend the applicability of the described *in vitro* culture model by incorporating decellularized cardiac extracellular matrix constructs derived from pathological cardiac tissue microenvironments coupled with detailed protein content quantification to better model the pathologically remodeling or failing cardiac tissue microenvironment.

3.0 Development of an *In Vivo* Model to Better Understand How Age-related Alterations in the Cardiac Microenvironment Drive Altered Regulation of Cardiac Tissue Resident Macrophage Populations

3.1 Rationale

Cardiac tissue microenvironmental remodeling occurs throughout an organism's lifespan in response to a variety of physiological or injury-associated cues. One such physiological cue is the aging process, during which a variety of microenvironmental changes gradually occur over long temporal periods until eventually the cardiac tissue microenvironment is remodeled to a pathologic state and function is compromised to some extent. Studying the interactions of the remodeling cardiac microenvironment with the resident cardiac cell types has provided important mechanistic insights into the mechanisms by which cardiac microenvironmental alterations progressively compromise resident cell function, in turn providing important potential therapeutic targets for the attenuation of cardiac dysfunction. For example, when cardiomyocyte action potential duration was measured by patch clamping for cardiomyocytes cultured on hydrogels ranging in stiffness from 1-25kPa, it was observed that cardiomyocytes cultured on hydrogels resembling native myocardial stiffness exhibited the longest action potential duration while cardiomyocytes cultured on hydrogels with a stiffness greater than that of native myocardium exhibited reduced action potential duration (Boothe et al., 2016). Additional studies demonstrated that embryological cardiomyocytes cultured on substrates with an elasticity similar to that of native myocardium could be induced to beat, while culture on substrates with a scar-like elasticity inhibited cardiomyocyte beating (Engler et al., 2008). Supraphysiological cardiomyocyte strain

has also been shown to alter the secretome of cardiomyocytes, with increased cardiomyocyte strain associated with increased secretion of factors such as colony stimulating factor-1 (CSF-1) and platelet derived growth factor (PDGF) - which have both been shown to induce cardiac fibroblast proliferation (Herum, Choppe, Kumar, Engler, & McCulloch, 2017). In addition to the cardiomyocyte secretome mediated alteration of resident fibroblast function, fibroblasts have been shown to exhibit direct cell intrinsic mechanisms of mechanosensitivity.

Cardiac fibroblasts have been demonstrated to have a robust phenotypic response to altered substrate elasticity. When cultured on hyaluronic acid hydrogels of stiffness which mimic the native myocardium, cardiac fibroblasts exhibit minimal positive staining for myofibroblast activation marker αSMA and reduced vinculin staining, suggesting a reduced development of mature focal adhesion structures (Herum et al., 2017). αSMA gene expression also demonstrated a robust sensitivity to culture substrate stiffness, with fibroblasts cultured on 8kPA substrates exhibiting almost 300 fold upregulation of αSMA expression relative to fibroblasts cultured on 3kPA substrates (Herum et al., 2017). Additionally, fibroblast cyclic stretch on gel culture substrates of increased stiffness were shown to upregulate expression of genes associated with fibrillar collagen or fibronectin protein production (Herum et al., 2017). Finally, when hyaluronic acid culture substrates were experimentally stiffened to 30kPA to simulate pathological stiffening of cardiac tissue, a robust change in fibroblast morphology characterized by increased cell spread with a significant increased expression of αSMA was observed (Herum et al., 2017). Taken together, these results demonstrate the responsivity of fibroblast cell populations to physiological and pathological stiffening of the cardiac tissue niche.

While the experiments described for the *in vitro* macrophage culture model provided important insights into the manner in which cardiac microenvironmental alterations induce altered

macrophage phenotype or function, these *in vitro* models are often insufficient to fully recapitulate the complex intercellular and niche remodeling dynamics which occur during cardiac aging or pathology. In order to better contextualize the results of the *in vitro* experiments described above, an *in vivo* model of cardiac matrix remodeling was developed to determine the degree to which cardiac macrophage population size, phenotype, and function are dependent upon cardiac microenvironmental niche conditions. This model was additionally compared to the characterized cardiac tissue resident macrophage population in young and aged mice to determine the extent to which microenvironmental cardiac remodeling can explain the age-related CVD risk as well as identify potential macrophage mediated mechanisms of CVD development.

3.2 Methods for *In Vivo* Model Development, Evaluation of Cardiac Function in Experimental Mice, and Characterization of the Cardiac Tissue Microenvironment

3.2.1 Experimental Design and Overview of Experimental Groups

A modified murine model of cardiac dysfunction was chosen as an *in vivo* model for the evaluation of the impacts of cardiac microenvironmental remodeling on the cardiac tissue resident macrophage subsets. The non-modified murine model of diastolic cardiac dysfunction consists of implanting an osmotic minipump loaded with D-Aldosterone which delivers a constant rate of D-Aldosterone infusion over a 28-day period, replacing murine drinking water during this 28-day period of pump implant with 1% NaCl supplemented drinking water, and a surgical unilateral nephrectomy; the sum total of which induces cardiac diastolic dysfunction and cardiac failure (K. Tanaka et al., 2014; Valero-Munoz et al., 2016; Wilson, De Silva, Sato, Izumiya, & Sam, 2009).

However, given the importance of kidney macrophage populations in promoting the proliferation of certain cardiac macrophage subsets responsible for the cardiac compensatory tissue remodeling response, the experimental model chosen for these experiments did not include a unilateral nephrectomy and consisted only of D-Aldosterone loaded osmotic minipump implant and 1% NaCl drinking water administration over the period of pump implant (Fujiu et al., 2017). The osmotic minipump chosen for these experiments were selected to provide a constant infusion of D-Aldosterone at a rate of 0.25 μL per hour over a 28-day infusion period. This experimental intervention (denoted Ald+Salt in subsequent figures) was chosen, based upon studies in the literature, to induce cardiac remodeling reminiscent of that observed in aged cardiac microenvironments - including increased cardiomyocyte hypertrophy, increased deposition of fibrillar collagen subtypes in interstitial and perivascular tissue microenvironments, and impaired cardiac tissue relaxation (K. Tanaka et al., 2014; Valero-Munoz et al., 2016; Wilson et al., 2009).

In order to assess the degree to which the experimentally induced cardiac microenvironmental remodeling recapitulated the alterations in cardiac function observed in aged individuals, echocardiographic assessment of murine cardiac systolic and diastolic function coupled with tissue histologic analysis was performed for control and Ald+salt mice to characterize the cardiac remodeling response. Additionally, whole cardiac RNA isolates were collected and qRT-PCR analysis of differential gene expression for a variety of inflammation-associated, cardiac remodeling-associated, or stress-associated gene targets was performed to determine the degree to which the Ald+salt experimental intervention induced altered gene expression in cardiac tissue relative to age-matched controls. To quantify differences in regulation of the cardiac resident macrophage subsets in cardiac tissue following Ald+salt treatment, flow cytometric characterization of the cardiac tissue resident macrophage population size and phenotype for each

cardiac resident macrophage subset was profiled for cardiac single cell suspensions isolated from control and experimental cardiac tissue. In addition to flow cytometric quantification, immunolabeling of resident macrophage surface markers was used to confirm the observed flow cytometric results and identify any unique distribution patterns within cardiac tissue samples. Immunolabeling of extracellular matrix protein content was also performed to identify matrix remodeling features outside of fibrillar collagen remodeling which can be assessed through a variety of histological evaluation methodologies.

As previously discussed, the compensatory cardiac remodeling response following increased left ventricular afterload is important for the maintenance of cardiac output and systemic tissue perfusion. While this compensatory response initially serves as intended and preserves cardiac output, the long-term consequences of this remodeling ultimately lead to further cardiac tissue dysfunction and eventual heart failure. Given the importance of this remodeling response in determining the extent to which cardiac function is preserved or to which cardiac dysfunction is exacerbated, understanding the mechanisms by which cardiac collagen deposition and organization alter cardiac function as well as resident cell behavior may help identify potential targets for therapeutic intervention. In order to better understand the role collagen matrix stiffening and organization through lysyl oxidase (LOX) mediated collagen matrix crosslinking plays in this compensatory remodeling response, an additional experimental group was given daily injections with non-reversible inhibitor of LOX enzymatic activity, β-aminoproprionitrile (BAPN), for the five days prior to implant of D-Aldosterone loaded osmotic pumps coupled with 1% NaCl drinking water administration over the 28-day implant period (denoted as Ald+salt+BAPN in subsequent experiments). Following the conclusion of experimental intervention, murine cardiac function was evaluated with echocardiography to determine the extent to which murine systolic and diastolic

function is altered in Ald+salt animals where LOX-mediated collagen crosslinking has been inhibited. Cardiac tissue was then collected and histological, immunofluorescent, and flow cytometric characterization of the cardiac tissue microenvironment and tissue resident macrophage compartment was performed. These results serve as an important additional point of comparison to age-matched control and Ald+salt cardiac tissue and help to demonstrate any LOX-mediated mechanisms of tissue remodeling which alter cardiac tissue resident macrophage population size or phenotype.

3.2.2 D-Aldosterone and Beta-aminoproprionitrile (BAPN) Solution Preparation

D-Aldosterone solution was prepared for osmotic minipump loading by dissolving purified D-Aldosterone (Sigma, St. Louis, MO) into absolute ethanol at a concentration of 5μg/μL and then diluting the D-Aldosterone solution to 1μg/μL with sterile PBS. D-Aldosterone solution was sterile filtered following preparation and prior to osmotic minipump loading. Osmotic minipumps were loaded as described in the recommended loading procedure given by Alzet. β-aminopropionitrile (BAPN) solution was prepared by dissolving BAPN (Sigma, St. Louis, MO) at a dose of 100mg/kg in 100μL of sterile PBS.

3.2.3 Osmotic Minipump Loading and Implant Procedure

3.2.3.1 Loading of D-Aldosterone Solution Into Osmotic Pumps

Osmotic minipumps were loaded and prepared for implantation according to the manufacturer's recommended standard operating procedure. All procedures were performed under sterile conditions. Briefly, the empty pump was first weighed with the flow moderator. A 1mL

syringe was then used to take up D-Aldosterone drug solution and blunt tipped 27-gauge filling tip provided by the manufacturer was attached to the syringe. With the flow moderator removed, the empty pump was held upright, and the filling tube was inserted into the pump until the tube could go no further. The syringe plunger was slowly pressed to fill the pump while the pump was held in an upright position. Pumps were filled until some drug solution was noted around the pump insertion point, at which point the filling tube was removed and excess fluid was wiped from the pump. The flow moderator was then fully inserted into the loaded osmotic pump and any residual displaced drug solution was again cleaned from the pump surface. Filled pumps with inserted moderators were massed again to provide a rough estimate of pump fill volume, which approximately correlates with pump fill (D-Aldosterone solution density = ~1g/mL).

3.2.3.2 Surgical Procedure for Pump Implant in Mice

Mice were anesthetized using 1-2% isoflurane inhalation and hair around the implant site was removed with Nair. Murine skin was sterile prepped and scrubbed. Mice were then secured onto a surgical warming pad. The implant site was sterilized, and a small incision was made in the skin between the scapulae. A hemostat was then used to make a small pocket in the skin around the insertion site to insert the loaded minipumps. Loaded, sterile pumps were then inserted into the subcutaneous pocket with the flow moderator inserted first, so that the flow moderator was distal to the insertion site. Incisions were then closed using two to three 7mm wound clips (Alzet, Cupertino, CA) applied with the reflex wound clip applicator (Alzet, Cupertino, CA). Mice were transferred to a warming pad for monitoring following surgery, after which they were returned to their cages. Wound clips were removed with the wound clip remover (Alzet, Cupertino, CA) from incision site area following incision healing approximately 10-14 days following surgery.

3.2.4 Echocardiographic Assessment of Cardiac Function in Anesthetized Mice

The Ultrasonography Core Facility at the Vascular Medicine Institute at the University of Pittsburgh assisted with the acquisition and analysis of all echocardiographic images for this study. In order to acquire transthoracic echocardiographic images, anesthetization was induced with 3% isoflurane inhalation and murine hair was removed from the chest with Nair. Electrode gel was applied to murine limbs and mice were secured to the moveable stage with surgical tape. Ultrasound gel was applied to the murine chest and Visualsonics Vevo 3100 (Fujifilm, Tokyo, Japan) ultrasound transducer was contacted on the chest. Ultrasound images were then acquired by Ultrasonography Core trained sonographer. B-mode and pulse wave doppler images were acquired. All echocardiographic image evaluation was performed by a sonographer skilled in the evaluation of rodent cardiac function in Vevo lab software.

3.2.5 Fixation of Control, Ald+Salt, and Ald+Salt+BAPN Cardiac Tissue Samples

Cardiac tissue samples were isolated, washed once briefly with 1x HBSS to remove any residual clotted blood from the tissue samples, and then fixed for 5 days in 10% neutral buffered formalin at room temperature. After fixation for 5 days, samples were submitted to the McGowan Institute for Regenerative Medicine Histology Core facility for paraffin embedding, sample sectioning, and sample slide mounting for either subsequent histology or immunofluorescence analysis.

3.2.6 Histological Assessment of Cardiac Tissue

Paraffin embedded cardiac sections were deparaffinized by washing slides through three xylene changes followed by washing through a graded series of ethanol with a final tap water wash. Deparaffinized sections were then stained with either Masson's trichrome or picrosirius red to characterized histologically observable alterations in the cardiac tissue microenvironment.

3.2.6.1 Masson's Trichrome

Deparaffinized slides were placed in preheated Bouin's Solution for 15 minutes at 56˚C. Slides were then washed in running tap water until any residual yellow coloration was removed from the slides. Slides were then stained in Wiegert's Hematoxylin Solution for 5 minutes. Slides were then washed in running tap water for 5 minutes. Slides were placed in trichrome stain solution (Sigma) for 5 minutes. Slides were then placed in 0.5% acetic acid for 1 minute, after which slides were washed in tap water, dehydrated, and coverslips were mounted.

3.2.6.2 Picrosirius Red

Deparaffinized slides were placed in Wiegert's Hematoxylin Solution for 8 minutes and then washed in running tap water for 10 minutes. Slides were placed in picrosirius red staining solution made up of 0.5g Direct Red 80 (Sigma, St. Louis, MO) diluted in 500mL saturated picric acid for 1 hour at room temperature. Slides were washed in two changes of 0.5% acetic acid followed by slide dehydration and coverslip mounting.

3.2.6.3 Image Acquisition and Analytic Methods

20X magnification brightfield images of Masson trichrome and picrosirius red stained cardiac sections were acquired using a Nikon Eclipse microscope. Additionally, 20X scans of Masson's trichrome and picrosirius red stained cardiac tissue section were acquired using a Motic EasyScan slide scanner (Motic, British Columbia, Canada). Cardiomyocyte hypertrophy was quantified in 20X Masson's trichrome cardiac section scans using QuPath image analysis software package (Bankhead et al., 2017). Cardiomyocyte area was determined by direct measurement and area quantification of at least 100 cardiomyocytes within left ventricular tissue regions in at least four biological replicates per group. Perivascular fibrotic matrix deposition was quantified using QuPath biological image analysis software package by determining the positive expression area of collagen staining per total vessel area for all vessels identified in left ventricular tissue in 20X cardiac tissue scans (Bankhead et al., 2017). Polarized light images of picrosirius red staining were acquired using a Zeiss Observer (ZEISS, Oberkochen, Germany) microscope with a 20X objective. The relative composition of red or orange birefringent collagen fibers within polarized light images was quantified using QuPath analysis software (Bankhead et al., 2017).

3.2.7 Immunofluorescent Labeling of Fixed Tissue Sections

3.2.7.1 Antibody Selection Rationale

Immunofluorescent labeling experiments for the described *in vivo* model were intended to provide insight regarding any altered regulation of matricellular protein content within the cardiac microenvironment. To accomplish this, antibodies against Connective Tissue Growth Factor (CTGF/CCN2), Periostin, and Galectin-3 were used to label cardiac tissue sections from control, Ald+Salt, and Ald+Salt+BAPN cardiac tissue sections. Additionally, immunofluorescent labeling

of C-C motif chemokine receptor 2 (CCR2) and lymphatic vessel endothelial hyaluronan receptor 1 (LYVE1) in cardiac tissue sections was performed to provide additional characterization of any altered cardiac macrophage subset regulation. Finally, antibodies against alpha-smooth muscle actin (αSMA) were used to stain and quantify any differences in expression of this fibroblast activation-associated marker in control and experimental cardiac tissue sections.

3.2.7.2 Immunolabeling Protocol for Paraffin-embedded Control, Ald+Salt, and Ald+Salt+BAPN Cardiac Tissue Sections

Slides were deparaffinized and washed in tap water. Slide sections were then covered in 1X Proteinase K made up in TE buffer for 5 minutes at room temperature. Slides were then washed three times in 1X PBS. Slides were then placed in citric acid retrieval buffer for 20 minutes at 95-100˚C. Slides in citric acid retrieval buffer were then immediately placed on ice to cool for 20 minutes following antigen retrieval. Slides were then washed twice in deionized water followed by two washes in 1X PBS. A pap pen was then used to encircle cardiac tissue sections on the slides. Donkey serum blocking buffer was pipetted onto each tissue section. Sections were blocked in buffer for 2 hours at room temperature. Following block, primary antibodies were added to each encircled tissue section in the dilutions described below. Tissue sections were incubated with primary antibodies overnight at 4˚C. Care was taken to select sections to withhold primary antibody treatment from to serve as primary delete controls. Following primary antibody incubation, sections were washed five times in 1X PBS. Secondary antibody Donkey anti-rabbit 647 was then made up in donkey serum block buffer at a dilution of 1:250 and applied to cardiac tissue sections for 30 minutes at room temperature. Following incubation with secondary antibody, sections were washed five times with 1X PBS. Coverslips were then mounted using fluorogel with added DAPI nuclear stain. Slides were kept in the dark for 10 minutes while coverslip mount was

allowed to adhere, after which stained tissue sections were immediately imaged using a Zeiss Observer fluorescence microscope (ZEISS, Oberkochen, Germany). Primary antibodies and dilutions used for *in vivo* study staining as follows: rabbit anti-Connective Tissue Growth Factor (Abcam, ab6992, 1:200), rabbit anti-Galectin-3 (Abcam, ab76245, 1:250), rabbit anti-Periostin (Abcam, ab215199, 1:1000), rabbit anti-LYVE1 (Abcam, ab218535, 1:5000), rabbit anti-CCR2 (Abcam, ab273050, 1:250), and rabbit anti-αSMA (Abcam, ab5694, 1:100).

3.2.7.3 Imaging and Quantification of Immunolabeled Tissue Sections

Images of immunofluorescent labeled cardiac tissue sections were acquired using a Zeiss Axio Observer fluorescence microscope (ZEISS, Germany). Images were acquired with a 20X objective for monochrome DAPI and cy5 channel images. Quantification of differences in immunofluorescent labeling was performed using QuPath biological image analysis software (Bankhead et al., 2017). For matricellular protein immunolabeling experiments, the percent positive stain area for each marker was quantified using a QuPath pixel threshold classifier (Bankhead et al., 2017). For LYVE1, CCR2, and αSMA immunolabeled cardiac tissue sections, QuPath positive cell detection algorithm was utilized to first detect cells within cardiac tissue sections based upon DAPI nuclear staining and then quantify the number of those cells exhibiting mean Cy5 expression greater than the defined positive expression threshold (Bankhead et al., 2017).

3.2.8 Flow Cytometric Analysis of Cardiac Cell Populations

Flow cytometry can be utilized as a high throughput experimental methodology for the evaluation of differing cardiac resident macrophage compartment regulation. The first step of flow

cytometric cell characterization is the development of a single cell isolation protocol to generate a single cell suspension of cardiac cells, which can be subsequently stained with antibodies against markers of interest.

3.2.8.1 Tissue Digestion and Generation of a Cardiac Single Cell Suspension

Cardiac tissue samples from control, Ald+salt, or Ald+salt+BAPN were collected and washed once in 1x Hanks balanced salt solution (HBSS) (Sigma) to removed residual blood cell content. Cardiac tissue samples were then transferred to a digest buffer consisting of 1% Collagenase-I (Fisher) and 1% Collagenase-IV (Fisher) made up in FACS buffer (5% FBS/1% BSA made up in 1x HBSS). Cardiac tissue samples were then minced into small tissue pieces in the digest buffer. Digest buffer-cardiac tissue suspensions were then transferred to an incubator set at 37˚C under constant agitation. Samples were in the incubator for 30 minutes. After 30 minutes of incubation in Collagenase-I/-IV digest buffer, samples were vortexed and transferred to a sterile cell culture hood for removal of tissue debris from the cardiac single cell isolation and staining of cardiac cell isolates.

3.2.8.2 Staining of Cardiac Single Cell Suspension

Samples were filtered through a 100μM cell strainer and then centrifuged at 1000g for 5 minutes at 4˚C. Sample supernatant was decanted off and cells were resuspended in 100μL of FACS buffer. Samples were then diluted 10:1 with 1x red blood cell lysis buffer (Miltenyi Biotec, Auburn, CA) for 2 minutes. Samples were then centrifuged at 1000g for 5 minutes at 4˚C and supernatant was decanted off. Samples were washed once with FACS buffer and subsequently resuspended in 100 μL of FACS buffer. Cells were counted and split as appropriate to give unstained, viability, and stained samples for experimental procedures and analysis. Cells were then

treated with anti-CD16/32 antibody (Fisher) for 10 minutes at room temperature to prevent non-specific antibody binding within cell suspensions during staining. After blocking with anti-CD16/32, cells were centrifuged at 1000g for 5 minutes at 4˚C and supernatant was decanted off. Cells were washed once with FACS buffer and then resuspended in 100 µL of FACS buffer. Primary antibodies were added at optimized dilutions and samples were stained for 20 minutes in the dark at 4˚C. Samples were then washed with FACS buffer and resuspended in 200 µL of FACS. Single color compensation controls were stained by adding 1 µL of each primary antibody to one drop of UltraComp eBeads diluted in 50 µL of FACS buffer. Compensation beads were stained for 20 minutes in the dark at 4˚C similar to stained cell samples, after which beads were washed and resuspended in FACS buffer. Following completion of cell and bead staining and wash, samples were set aside in the dark at 4˚C while MACSQuant flow cytometer (Miltenyi Biotec) was calibrated and set up for experimental data acquisition. Once the experimental data collection procedure was set up, samples were removed from 4˚C, treated with 2 µL of propidium iodide (PI) to assess cell viability, and arranged in the Chill5 sample holder to be processed with the MACSQuant.

3.2.8.3 Quantification and Statistical Methods for Evaluating Flow Cytometry Data

The MACQuant cytometer was switched into acquisition mode and lasers were given 20 minutes to warm up prior to beginning the experiment. All data acquired with the MACSQuant flow cytometric platform was exported as a flow cytometry standard (FCS) file and analyzed using the Flowjo (BD, Franklin Lakes, NJ) flow cytometry analysis software. Sample compensation was performed using single color bead compensation samples to determine and correct for antibody spillover into neighboring detectors. The compensation matrix generated from quantification of single-color control tube spillover was then used to compensate and adjust sample staining values

to reduce the confounding effects of antibody fluorescence spillover. Unstained and viability only stained cell samples for each group were then used as negative controls to determine background autofluorescence within the cell samples and provide insight into appropriate cell gate placement. Using these control samples to set gates, a gating scheme was developed to characterize the size and phenotype of each cardiac resident macrophage subset. In general, the gating strategy for these experiments first involved a debris-exclusion and a doublet-exclusion step performed based upon measured FSC and SSC detector voltages. Then, viable cells were identified in stained suspensions by selecting for the cell population exhibiting negative PI expression - as PI tags dead cells in suspension by diffusion through porous cell membranes common in apoptotic or necrotic cells.

Viable cell fractions were then further separated based upon expression of general pan-leukocyte marker, CD45. CD45 positive, viable cells were selected for further analysis. F4/80 and CD11b expression was then characterized. Macrophage lineage marker expression was then characterized within any identified cardiac macrophage populations in order to identify the population size of each macrophage fraction as well as identify any unique surface marker expression patterns within the isolated immune cell populations. Given the previously published results of lineage tracing studies which identified TIMD4 (t-cell immunoglobulin and mucin domain containing 4), LYVE1 (lymphatic vessel endothelial hyaluronan receptor 1), and CD163 (high affinity scavenger receptor for hemoglobin-haptoglobin complex) as markers of embryologically-derived macrophage subsets; these markers were used to identify differential regulation of macrophages derived from embryological precursors (Dick et al., 2019; Epelman et al., 2014). Additionally, CX3CR1 (C-X3-C motif chemokine receptor/fractalkine receptor) was used as a marker of general cardiac residence and CCR2 was used as a marker of bone marrow

monocyte-derived macrophage populations (Dick et al., 2019; Epelman et al., 2014). Finally, expression of macrophage M1-associated phenotypic marker CD86 and macrophage M2-associated phenotypic marker CD206 was characterized within each subset to provide some preliminary insight into any altered phenotypic regulation of these resident macrophages following experimental intervention.

3.2.9 Isolation of RNA From Cardiac Tissue Samples for qRT-PCR

3.2.9.1 RNA Isolation Protocol

Cardiac tissue sections were placed in RNAlater following isolation and stored at -80˚C until ready for RNA isolation from tissue samples. Once ready, tissue samples were removed from RNAlater and placed into 600µL of Buffer RLT. Tissue and buffer suspensions were then transferred to a 2mL microcentrifuge tube and homogenized using a Bead Ruptor Elite (Omni International, Kennesaw, GA) bead homogenizer. Tissue homogenate tubes were then centrifuged at full speed for 3 minutes. Tissue homogenate was pipetted out of bead microcentrifuge tube and into a new microcentrifuge tube with care taken to avoid pipetting any tissue debris from the tube. 600µL of 70% ethanol was then pipetted into sample tube and the lysate solution was mixed well by pipetting. 700µL of lysate was transferred to a RNeasy spin column placed within an empty 2mL collection tube and was centrifuged for 15 seconds at 8000g. Flow through in the collection tube was discarded and remaining sample lysate volume was transferred to the spin column and centrifuged at 8000g for 15 seconds. Flow through was discarded. 700µL of Buffer RW1 was then added to the spin column and sample were centrifuged for 15 seconds at 8000g. Flow through was discarded. 500µL of Buffer RPE was added and samples were centrifuged for 15 seconds at 8000g. Flow through was discarded. 500µL of Buffer RPE was added again and columns were centrifuged

for 2 minutes at 8000g to wash the column and to ensure any residual ethanol is removed. Flow through was discarded and the RNeasy spin column was placed in a new 1.5mL collection tube. 30μL of RNase-free water was added to each spin column and samples were centrifuged at 8000g for 1 minute to elute sample RNA. Eluate in collection tube was re-pipetted onto spin column and samples were centrifuged at 8000g for an additional minute to elute any residual RNA bound to spin columns. Sample RNA concentrations were determined using a NanoDrop Lite spectrophotometer (Thermo, Waltham, MA). Only samples with A260/80 ratios within 2.0 ± 0.10 were considered sufficiently purified for further qRT-PCR analysis.

3.2.9.2 Primer Selection Rationale

Whole cardiac RNA qRT-PCR studies were intended to provide additional insight into any altered regulation of inflammation-associated, matrix-remodeling associated, or stress-associated gene expression between control and Ald+salt experimental groups. Double Δ C_t analysis of *Col1a1, Mmp2, Mmp9,* and *Timp1* fold change in gene expression will help evaluate the change in collagen-1 RNA transcript levels as well as the change in expression of metalloproteases MMP-2, MMP-9, and metalloprotease inhibitor TIMP-1. *Tgfb* (TGF-β) expression will also be quantified for control and Ald+salt cardiac tissue, since TGF-β has a myriad of roles within remodeling tissue microenvironments. With aging, the cardiac microenvironment generally experiences an increased deposition of fibrillar collagen subtypes - with collagen-1 comprising the majority of produced collagen proteins (Williams et al., 2014; Williams et al., 2015). Aging also promotes an altered balance in the regulation of metalloprotease-to-metalloprotease inhibitor gene transcription, with an increased expression of metalloprotease inhibitors attenuating MMP-mediated matrix degradation being observed with increasing age (Horn et al., 2012). Selection of the described primers should help elucidate the degree to which the experimental model is able to recapitulate

these observed age-related changes in the cardiac microenvironmental transcriptional landscape. Additionally, quantification of TGF-β transcripts will help contextualize any observed αSMA immunolabeling in cardiac tissue sections as well as help elucidate the degree to which matrix remodeling may be occurring in the local microenvironment.

In order to assess any change in inflammation-associated gene regulation following Ald+salt experimental treatment, double ΔC_t analysis of the fold change in expression of *Il1b, Il6, Nos2,* and *Tnfa* will be performed to quantify any change in expression of inflammasome activation associated gene targets. The selected primers here also reflect some of the primer choice used for the *in vitro* evaluation of macrophage microenvironmental response to provide some common reference points between experimental models. In addition to these inflammation-associated genes, double ΔC_t analysis of the fold change in expression of monocyte chemoattractant protein-1/C-C motif chemokine ligand 2 (*Ccl2*) RNA transcript levels will be performed to assess the degree to which Ald+salt experimental treatment alters the expression of monocyte chemoattractant protein gene transcription. These results can be used in conjunction with the flow cytometric characterization described above to assess the degree to which the described experimental treatment induced the monocyte extravasation and differentiation into cardiac resident macrophages.

Finally, double ΔC_t analysis of the fold change in expression of stress response associated genes can help one infer the state of cellular or oxidative stress within cardiac tissue microenvironments. Quantification of the change in transcription levels of x-box binding protein-1 (*Xbp1*) - a protein which is an important component of the unfolded protein and endoplasmic reticulum stress response - between control and Ald+salt will also be performed to better understand how the experimental treatment altered misfolded protein and endoplasmic reticular

stress-related signaling pathways. Double ΔC_t analysis of fold change in superoxide dismutase 3 (*Sod3*) expression can also be used to infer mesenchymal cell stress as well as infer about changes in concentration of oxidative species within the cardiac microenvironment. Superoxide dismutase is an enzyme responsible for catalyzing the conversion of the radical oxidative species superoxide into hydrogen peroxide, which can subsequently be further converted into water and oxygen; functionally clearing a NAPDH-oxidase (NOX) enzyme generated radical oxidative species which is highly cytotoxic (Lambeth, 2004). Taken together, quantification of the change in expression of these gene targets can together be used to infer some information regarding the cardiac cellular stress pathways regulation following experimental intervention.

3.2.9.3 Quantification and Statistical Methods for Evaluation of qRT-PCR Data

All preparation of samples and plates for qRT-PCR were performed on ice or at 4˚C. 1μL of sample cDNA was added to 8μL of RNase-free water, 10μL of TaqMan gene expression master mix (Applied Biosystems, Foster City, CA), and 1μL of TaqMan primer in a MicroAmp Optical 96-well reaction plate (Applied Biosystems). Plates were then sealed with MicroAmp Optical adhesive film (Applied Biosystems) and centrifuged at 300g for 4 minutes at 4˚C. The qRT-PCR reaction was catalyzed and C_t values were obtained using a QuantStudio 3 RT-PCR system (Applied Biosystems). Relative gene expression was determined using the double ΔC_t method (ddCT) of gene expression quantification. *Gapdh* was chosen as the housekeeping gene utilized for normalization in this experiment. Primers chosen for this experiment were selected due to previously reported upregulation following Th1/Th2 cytokine stimuli in macrophage populations or due to their role in the microenvironmental tissue remodeling response: *Nos2* (Mm00440502_m1), *Il1b* (Mm00434228_m1), *Il6* (Mm00475988_m1), *Tnfa* (Mm00443258_m1), *Tgfb* (Mm01178820_m1), *Sod3* (Mm01213380_m1), *Xbp1*

(Mm00457357_m1), *Mmp2* (Mm00439498_m1), *Mmp9* (Mm00442991_m1), *Timp1* (Mm00441818_m1), *Col1a1* (Mm00801666_g1), *Ccl2* (Mm00441242_m1) (Themo Scientific).

3.2.9.4 Statistical Analysis

Data was analyzed with IBM SPSS 26 (IBM, Armonk, NY) statistical analysis package. Data was first assessed for normality using a Kolmogorov-Smirnov test. Normally distributed data was analyzed with a one-way ANOVA with post hoc Tukey test to identify any significant differences in data distribution. Non-normally distributed data was analyzed with a Kruskal-Wallis test with pairwise post hoc comparisons performed to identify any significant differences in experimental data distribution. The threshold for statistical significance was selected to be $p<0.05$.

3.3 Results

3.3.1 Echocardiographic Assessment of Cardiovascular Function Demonstrated a Significant Alteration in Cardiac Function Following Experimental Treatment

Following the conclusion of the 28-day period of constant osmotic minipump infusion of D-Aldosterone coupled with 1% NaCl drinking water treatment, mice were anesthetized, and cardiac function was evaluated using echocardiography (Figure 8, Table 1).

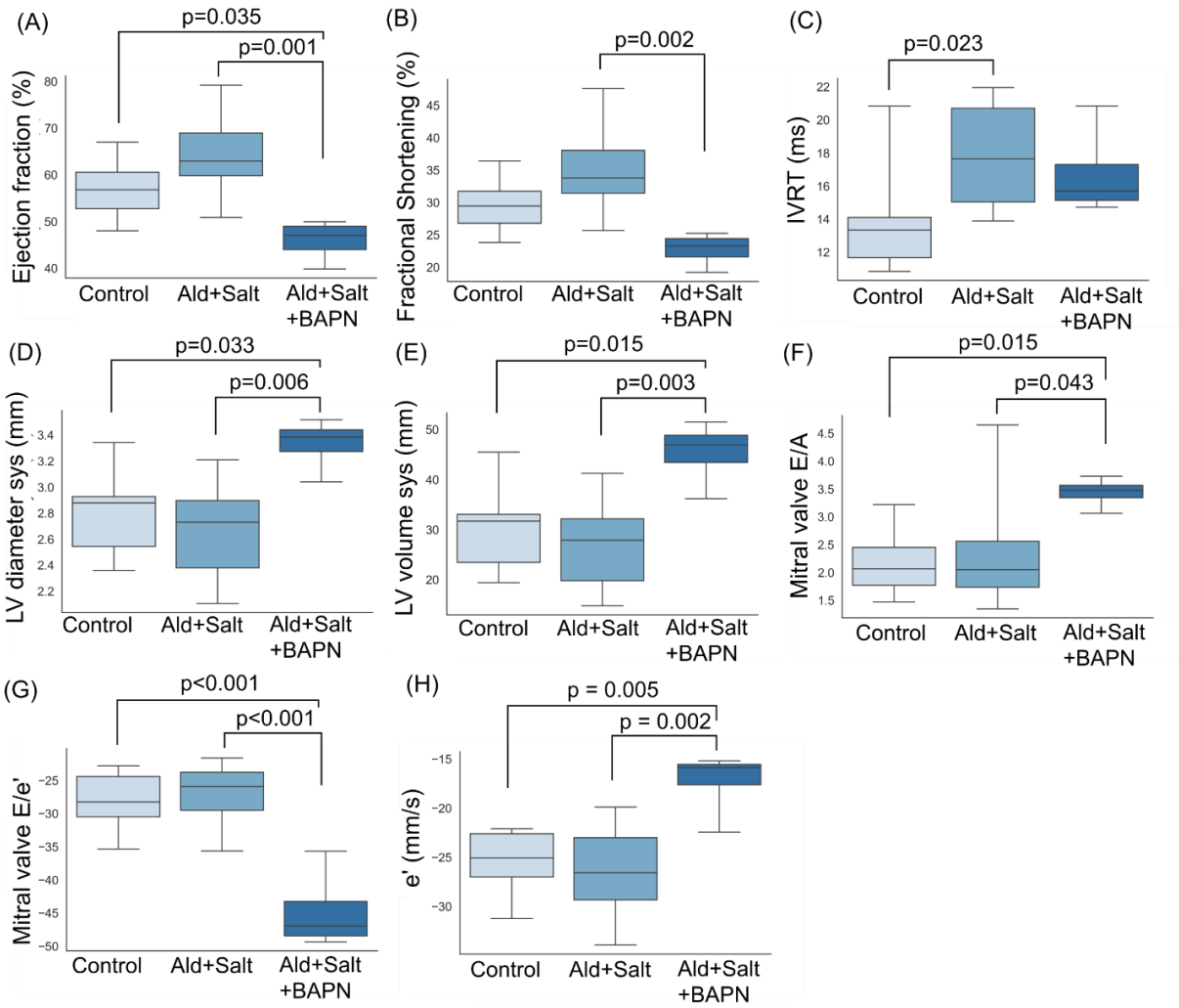

Figure 8 – Chronic D-Aldosterone infusion coupled with 1% NaCl drinking water supplementation treatment is associated with significantly incresaed mean isovolumic relaxation times relative to controls. Inhibition of collagen crosslinking through BAPN administration prior to D-Aldosterone+1% NaCl drinking water treatment was associated with altered cardiac function relative to control and Ald+salt groups. (A) Calculated mean ejection fraction, **(B)** fractional shortening percentage, **(C)** isovolumic relaxation time, **(D)** measured left ventricular systolic diameter, **(E)** measured left ventricular volume, **(F)** mitral valve early (E) to late (A) filling rate ratio (MV E/A), **(G)** mitral valve early filling rate (E) to early mitral valve tissue annular velocity (E') ratio (MV E/E'), **(H)** mitral valve tissue early annular velocity (E') for control (n=10), D-Aldosterone+1% NaCl drinking water (Ald+Salt) treated mice (n=10), and Ald+Salt treated mice which received BAPN pre-treatment

(BAPN+Ald+Salt) (n=4). Data presented as box and whisker plots. Lines indicate mean. Data normality was assessed with Kolmogorov-Smirnov (K-S) test. Significant differences in normally distributed data were identified with a one-way ANOVA with post-hoc Tukey test. Non-normally distributed data was analyzed with Kruskal-Wallis independent samples test with post-hoc pairwise comparisons.

The results of this echocardiographic assessment of cardiac function in control mice, mice which received D-Aldosterone minipump implant coupled with 1% NaCl drinking water with no BAPN pre-treatment (Ald+salt), and mice which received a D-Aldosterone minipump implant coupled with 1% NaCl drinking water with daily BAPN injections for the five days preceding pump implant (Ald+salt+BAPN) identified several significant alterations in cardiac geometry and function as a result of experimental intervention (Table 1, significant p-values noted in bold).

Table 1 - Parameter values derived from echocardiographic assessment of murine cardiac function

Measure	Control (0)	Ald+salt (1)	Ald+salt+BAPN (2)	p-value	Post hoc p-value (0 vs 1)	Post hoc p-value (0 vs 2)
Mitral valve E wave (mm/s)	708 ± 66	699 ± 61	760 ± 34	p = 0.241		
Mitral valve A wave (mm/s)	347 ± 65	341 ± 129	222 ± 19	p = 0.086		
Mitral valve E/A	2.1 ± 0.5	2.3 ± 1.0	3.4 ± 0.3	**p = 0.018**	p = 0.804	**p = 0.015**
e' (mm/s)	-25.5 ± 3.3	-26.4 ± 4.5	-17.3 ± 3.4	**p = 0.002**	p = 0.877	**p = 0.005**
a' (mm/s)	-20.5 ± 7.6	-19.1 ± 5.0	-12.4 ± 3.5	p = 0.095		
Mitral valve E/e'	-28.2 ± 4.2	-27.1 ± 4.4	-44.8 ± 6.2	**p < 0.001**	p = 0.870	**p < 0.001**
e'/a'	1.355 ± 0.362	1.415 ± 0.180	1.425 ± 0.117	p = 0.851		
a'/e'	0.809 ± 0.304	0.718 ± 0.096	0.705 ± 0.058	p = 0.988		
Aortic ejection time (ms)	50 ± 3	53 ± 3	54 ± 2	**p = 0.046**	p = 0.067	p = 0.128

Table 1 (continued).						
Isovolumic contraction time (ms)	12 ± 3	14 ± 4	16 ± 3	p = 0.131		
Isovolumic relaxation time (ms)	14 ± 3	18 ± 3	17 ± 3	**p = 0.027**	**p = 0.023**	p = 0.273
Left ventricular myocardial performance index (LV MPI)	0.514 ± 0.080	0.596 ± 0.091	0.601 ± 0.050	p = 0.068		
Heart Rate (BPM)	464 ± 43	423 ± 53	406 ± 12	p = 0.059		
Systolic diameter (mm)	2.8 ± 0.3	2.7 ± 0.4	3.3 ± 0.2	**p = 0.008**	p = 0.572	**p = 0.033**
Diastolic diameter (mm)	4.0 ± 0.3	4.1 ± 0.2	4.3 ± 0.2	p = 0.150		
Systolic volume (μL)	30 ± 8	27 ± 15	45 ± 7	**p = 0.004**	p = 0.608	**p = 0.015**
Diastolic volume (μL)	70 ± 13	73 ± 10	84 ± 10	p = 0.150		
Stroke volume (μL)	39 ± 7	46 ± 6	39 ± 6	p = 0.051		

Table 1 (continued).						
Ejection fraction (%)	57 ± 6	64 ± 8	46 ± 5	**p = 0.001**	p = 0.086	**p = 0.035**
Fractional shortening (%)	30 ± 4	35 ± 6	23 ± 3	**p = 0.002**	p = 0.076	p = 0.074
Cardiac output (mL/min)	18.1 ± 2.5	19.6 ± 3.7	15.7 ± 3.0	p = 0.132		
Left ventricular mass (mg)	130 ± 25	145 ± 37	150 ± 30	p = 0.515		
Corrected left ventricular mass (mg)	104 ± 20	116 ± 30	120 ± 24	p = 0.515		
Left ventricular anterior wall - systole (mm)	1.2 ± 0.1	1.3 ± 0.2	1.1 ± 0.2	p = 0.219		
Left ventricular anterior wall – diastole (mm)	0.9 ± 0.1	1.0 ± 0.2	0.9 ± 0.2	p = 0.625		
Left ventricular posterior wall – systole (mm)	1.1 ± 0.1	1.3 ± 0.3	1.0 ± 0.1	p = 0.052		

Table 1 (continued).						
Left ventricular posterior wall - diastole (mm)	0.8 ± 0.1	0.9 ± 0.3	0.8 ± 0.04	p = 0.712		
Left ventricular posterior wall - diastole (mm)	0.8 ± 0.1	0.9 ± 0.3	0.8 ± 0.04	p = 0.712		
Left Atrial A-P (mm)	2.3 ± 0.3	2.0 ± 0.4	2.0 ± 0.4	p = 0.175		
Global longitudinal stain (GLS) (%)	-16.4 ± 2.2	-18.6 ± 4.0	-16.6 ± 5.3	p = 0.359		
Circumferential strain (%)	-19.3 ± 3.0	-21.4 ± 4.2	-17.2 ± 3.4	p = 0.143		
Radial strain (%)	27.5 ± 4.0	26.7 ± 7.2	26.5 ± 9.7	p = 0.946		
Global circumferential strain (GCS) (%)	-19.7 ± 2.7	-21.9 ± 3.9	-17.5 ± 3.2	p = 0.097		

3.3.1.1 D-Aldosterone Infusion Coupled With 1% NaCl Drinking Water Impaired Ventricular Relaxation

In order to better characterize cardiac tissue function between control and mice which received treatment with osmotic minipump infusion of D-Aldosterone coupled with 1% NaCl drinking water for 28 days, echocardiographic assessment of mitral valve flow and mitral valve tissue annular velocity was analyzed to partially infer the functional consequences of cardiac tissue remodeling (Table 1, Figure 8). No significant change in early (E) or late (A) wave fill rates between control and Ald+salt experimental groups was observed, although a slight decrease in both early and late filling rates were observed in Ald+salt mice relative to controls (Table 1). When comparing the early to late filling rate (MV E/A) for control and Ald+salt mice, a slight, non-significant increase in MV E/A ratios was observed in Ald+salt mice relative to controls (Table 1).

In addition to MV early and late filling rate measurements, the annular tissue velocity of the mitral valve during early and late diastole can be measured to infer more information about the left ventricular cardiac tissue stiffness as well as better contextualize the observed MV E and A filling waves. When comparing control and Ald+salt early (e') and late (a') mitral valve annular tissue velocities, it was observed that Ald+salt experimental treatment induced a slight mean increase in e' and a slight mean decrease in a' tissue velocities (Table 1).

Finally, one can quantify the isovolumic contraction time, isovolumic relaxation time, and aortic ejection time to infer some additional information about cardiac systolic and diastolic function between control and Ald+salt groups (Table 1, Figure 8). A non-significant mean increase in isovolumic contraction time and a significant increase in mean isovolumic relaxation time was observed in Ald+salt mice as compared to controls (Table 1, Figure 8C). Additionally, a mean

increase in the aortic ejection time was noted following Ald+salt treatment (Table 1). These results suggest that the left ventricular remodeling induced by Ald+Salt treatment did not significantly alter the early and late wave filling dynamics but did induce some impaired left ventricular relaxation (Figure 8C).

3.3.1.2 BAPN Administration Prior to D-Aldosterone Pump Implant Attenuates Some of the Observed D-Aldosterone+Salt Induced Cardiac Remodeling, but Worsens Cardiac Systolic and Diastolic Function

The cardiac compensatory remodeling response occurs to preserve cardiac output in response to a variety of stimuli or changing physiological conditions. In order to understand the functional consequences of disruption of lysyl oxidase mediated crosslinking of collagen fibrils, BAPN was used to inhibit lysyl oxidase function prior to D-Aldosterone osmotic pump implant and 1% NaCl drinking water administration. Cardiac function was then evaluated using echocardiography to determine what if any functional consequences presented in the *in vivo* model (Table 1, Figure 8).

When comparing the observed left ventricular posterior and anterior wall measurements in the Ald+salt and Ald+salt+BAPN groups, BAPN administration prior to pump implant was found to cause a slight mean reduction in the measured posterior and anterior wall dimensions both in systole and diastole as compared to Ald+salt ventricular wall measurements (Table 1). When comparing these measurements to control left ventricular posterior and anterior wall measurements, it was observed that BAPN administration prior to pump implant either slightly reduced or caused no change in the mean left ventricular wall dimensions (Table 1). While BAPN administration was found to preserve left ventricular posterior and anterior wall dimensions, Ald+salt+BAPN treatment was also found to be associated with significantly altered left

ventricular chamber dimensions and volumes (Table 1, Figure 8D-E). BAPN administration prior to D-Aldosterone minipump implant was found to induce a significant mean increase in systolic left ventricular chamber size (Figure 8D) as well as in systolic left ventricular chamber volume (Figure 8E) relative to both control and Ald+salt groups. In addition to the observed significant left ventricular chamber dilation in systole, a non-significant increase in Ald+salt+BAPN group mean diastolic left ventricular chamber diameter and diastolic left ventricular volume was observed relative to control and Ald+salt mice (Table 1).

In addition to the deleterious dilative cardiac remodeling suggested by the increased mean systolic and diastolic left ventricular chamber measurements, a significant reduction in cardiac ejection fraction was observed in mice which received BAPN administration prior to D-Aldosterone minipump implant relative to both control and Ald+salt mice (Figure 8A). BAPN administration was also observed to have several significant impacts on mitral valve flow and tissue annular velocity measurements, suggesting some dysregulated diastolic cardiac function (Figure 8F-H). BAPN administration was found to increase mean mitral valve E filling rates and decrease mean A wave filling rates, in turn inducing a mean increase in the derived MV E/A ratio for Ald+salt+BAPN mice relative to control and Ald+salt animals (Table 1, Figure 8F). In addition to the altered MV E and A filling rates, a significant reduction in magnitude of the early wave tissue annular velocity (e') was observed in the Ald+salt+BAPN group relative to both control and Ald+salt groups (Figure 8H). Consequent this significant reduction in MV e', Ald+salt+BAPN mice also exhibited a significant increase in MV E/e' ratios relative to control and Ald+salt mice (Figure 8G). Finally, while not observed to significantly differ from control values, Ald+salt+BAPN mice were observed to generally exhibit increased mean isovolumic contraction times, increased mean isovolumic relaxation times, and increased mean aortic ejection times

(Table 1). Taken together, these results demonstrate how while BAPN administration can reduce some of the observed left ventricular anterior and posterior wall hypertrophic remodeling response following Ald+salt treatment, disruption of lysyl oxidase-mediated compensatory remodeling can cause dysregulation of cardiac systolic and diastolic function relative to both control and Ald+Salt mice (Figure 8, Table 1).

3.3.2 Histological Evaluation of Cardiac Tissue Morphology

While echocardiography is an important, non-invasive clinical tool for the diagnosis of dysregulated cardiac systolic or diastolic function, echocardiographic imaging can only provide limited information regarding the remodeling cardiac microenvironment. In order to provide a more complete characterization of the remodeling response induced by experimental intervention, control, Ald+salt, and Ald+salt+BAPN cardiac tissue sections were stained with Masson's trichrome or picrosirius red (Figure 9).

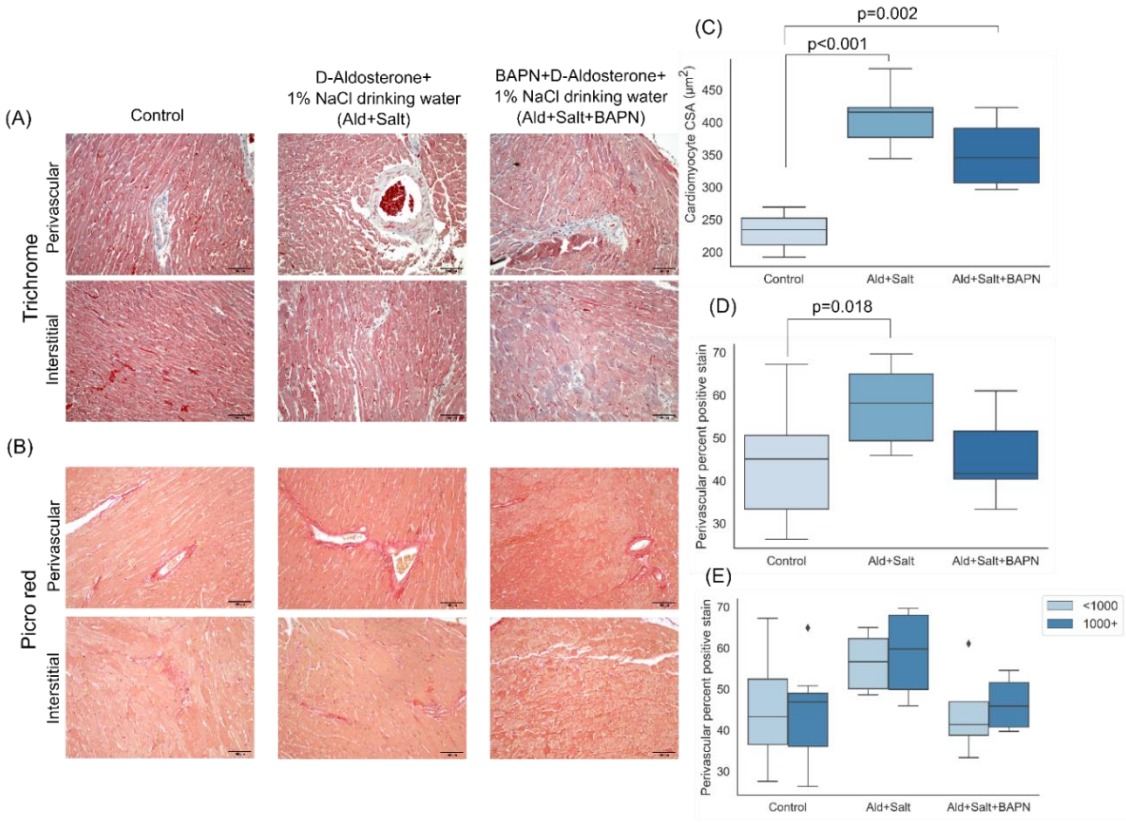

Figure 9 - Masson's trichrome and picrosirius red staining of control, Ald+Salt, and Ald+Salt+BAPN cardiac tissue sections demonstrated significantly altered perivascular collagen deposition and cardiomyocyte hypertrophy. (A) 20x images of Masson's trichrome and, **(B)** picrosirius red stained cardiac sections with representative images of perivascular and interstitial collagen deposition noted in ventricular regions for control, Ald+Salt, and Ald+Salt+BAPN experimental groups. Scale bars = 100μm. **(C)** Quantification of measured cardiomyocyte areas from 20x masson's trichrome stained cardiac tissue sections for control (n=7), Ald+Salt (n=6), and Ald+Salt+BAPN (n=4) groups. **(D)** Quantification of percent positive collagen staining in perivascular tissue regions for control (n=7), Ald+Salt (n=6), and Ald+Salt+BAPN (n=4) cardiac sections. **(E)** Perivascular collagen positive stain area separated by vessel area. (C, D) data presented as box and whisker plots. Lines indicate mean. Black triangles signify outliers. Data normality was assessed with Kolmogorov-Smirnov test. A one-way ANOVA with post-hoc Tukey testing in (C) and two-way ANOVA for treatment group and vessel size with post-hoc Tukey testing in (D).

3.3.2.1 Masson's Trichrome Staining Demonstrates Ald+Salt Induces Increased Perivascular Collagen Deposition and Cardiomyocyte Hypertrophy Relative to Age-matched Controls

Masson's trichrome histological staining - where collagen is stained blue, cell nuclei are stained purple, and the cell cytoplasm is stained red - can be utilized to both identify differences in perivascular and interstitial collagen deposition as well as quantify differences in mean cardiomyocyte area between control and Ald+salt cardiac tissue sections (Figure 9A, C-D). Qualitatively, an increased deposition of collagen denoted by increased aniline blue staining was noted both in perivascular tissue regions as well as within interstitial tissue regions of the left ventricle in Ald+salt cardiac sections relative to control tissue sections (Figure 9A). Quantification of the percent of the perivascular area comprised of positively stained collagen in control and Ald+salt cardiac tissue sections also demonstrated a significant mean increase in perivascular collagen deposition in Ald+salt sections relative to control sections (Figure 9D). Of note, a non-significant but notable mean increase in the percent positive perivascular stain area was observed in larger vessels quantified within cardiac tissue sections for both groups (Figure 9E). In addition to identifying differences in collagen deposition between sections by qualitative and semi-quantitative evaluation of aniline blue staining characteristics, Masson's trichrome stained sections can be utilized for the quantification of cardiomyocyte area (Figure 9C). Quantification of cardiomyocyte short-axis cross sectional area in control and Ald+Salt cardiac tissue sections demonstrated that Ald+salt treatment induced a significant mean increase in cardiomyocyte area (Figure 9C). This result suggests that Ald+Salt experimental treatment induced cardiomyocyte hypertrophy relative to age-matched controls.

3.3.2.2 Ald+Salt Cardiac Tissue Sections Exhibit an Increased Fraction of Thick or Disorganized Collagen Fibrils Relative to Control Sections

Picrosirius red histological staining can assist with the qualitative evaluation of collagen deposition characteristics as well as the elucidation of collagen fibril thickness in control and Ald+salt cardiac tissue sections (Figure 9B). Collagen deposition in brightfield images of picrosirius red stained cardiac tissue sections was observed to qualitatively increase in both perivascular as well as in interstitial ventricular tissue regions in Ald+Salt cardiac tissue sections relative to controls (Figure 9B). In addition to brightfield images, polarized light images of picrosirius red stained sections were captured to infer differences in collagen fibril thickness or organization between control and Ald+salt cardiac sections (Figure 10).

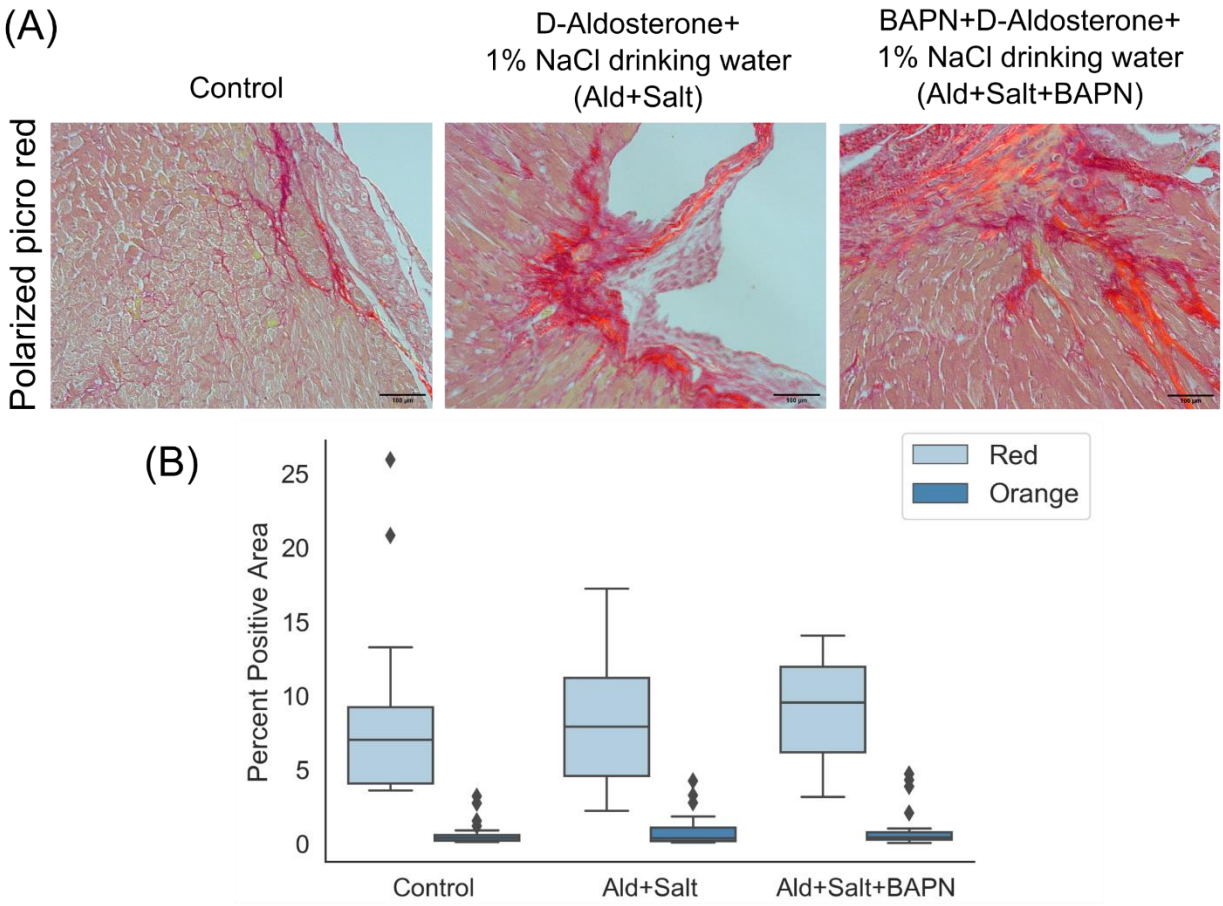

Figure 10 - Polarized light imaging of picrosirius red stained cardiac sections demonstrated an altered deposition of thick collagen fibers between control and experimental group mice. (A) Polarized light images of picrosirius red stained cardiac tissue sections for control, Ald+Salt, and Ald+Salt+BAPN experimental group mice acquired in ventricular tissue proximal to aortic outflow track. **(B)** Quantification of the percent of positive expression of birefringent red or orange collagen fibers in control, Ald+Salt, and Ald+Salt+BAPN cardiac tissue sections. Data presented as box and whisker plots. Lines indicate mean. Black triangle represent data point outliers. Image magnification = 20x. 5-10 images acquired in 3-4 biological replicates. (A) Scale bars = 100μm.

In polarized light imaging of collagen fibrils, thicker more mature collagen fibers show up in red and orange, while thinner less mature collagen fibrils show up in green. Qualitatively, one can see a general increase in the red and orange collagen fibril content in the Ald+salt cardiac sections relative to control (Figure 10A). Quantification of the percent positive area of red and orange collagen fibers in 20x images of control and Ald+salt cardiac sections also demonstrated a mean increase in the percent of red and orange birefringent collagen fibers in Ald+salt cardiac sections (Figure 10B). This increase in red and orange birefringent collagen fibers in Ald+Salt cardiac sections suggest not only an increased collagen deposition within Ald+salt cardiac tissue, but also an increased maturation of collagen fibrils within that extracellular microenvironment.

3.3.2.3 BAPN Reduces Perivascular Collagen Deposition and Cardiomyocyte Hypertrophy

BAPN injection prior to D-Aldosterone minipump implant and 1% NaCl drinking water administration was found to have several significant impacts on the histologically characterized cardiac tissue remodeling response (Figures 9, 10). Masson's trichrome and picrosirius red images of Ald+Salt+BAPN cardiac tissue sections were generally characterized by an increase in perivascular and interstitial collagen staining relative to control sections (Figure 9A, B). When compared to Ald+Salt cardiac tissue sections, qualitative differences were less apparent - although Ald+Salt+BAPN sections did appear to exhibit some increased interstitial collagen deposition (Figure 9A, B). Quantification of perivascular percent positive collagen staining indicated BAPN treatment did not significantly alter perivascular collagen deposition relative to either control or Ald+Salt groups (Figure 9C). However, the quantified mean value in the Ald+Salt+BAPN group was observed to decrease from mean Ald+Salt percentages, and instead was found to more closely reflect control values (Figure 9D). Quantification of red and orange birefringent collagen fiber content in polarized light imaged picrosirius red stained sections demonstrated a mean increase in

the red and orange fibril content in Ald+salt+BAPN cardiac sections relative to both control and Ald+salt sections (Figure 10B). Taken together, these results indicate Ald+salt+BAPN induced increased deposition and maturation of collagen fibrils within the cardiac microenvironment, although this effect was not pronounced within the perivascular regions.

Cardiomyocyte cross sectional area was also quantified from Masson's trichrome stained sections for Ald+Salt+BAPN cardiac tissue (Figure 9A, C). It was observed that BAPN treatment attenuated the cardiomyocyte hypertrophic remodeling response observed in Ald+Salt cardiac sections (Figure 9C). However, it was also noted that mean Ald+Salt+BAPN cardiomyocyte areas were significantly greater than measured control areas, suggesting BAPN treatment did not wholistically block the cardiac hypertrophic remodeling response to Ald+Salt treatment (Figure 9C). These results indicate that BAPN treatment induces a distinct cardiac microenvironmental remodeling response to Ald+Salt treatment characterized by reduced cardiomyocyte hypertrophy but increased collagen deposition.

3.3.3 Immunofluorescent Labeling of Matricellular Proteins in Cardiac Sections Demonstrate Increased Mean Labeling Following Experimental Intervention

In addition to increased fibrillar collagen deposition, altered regulation of matricellular proteins associated with mediating extracellular matrix assembly or promoting altered cell migratory behavior have been observed to increase in expression in both the pressure overloaded myocardium as well as in advanced age cardiac microenvironments. In order to better understand how experimental intervention may have promoted the altered secretion of matricellular proteins within the cardiac microenvironment, immunofluorescent labeling of Connective Tissue Growth

Factor (CTGF/CCN2), Galectin-3, and Periostin was performed, and images were acquired with Zeiss fluorescent microscope (Figure 11).

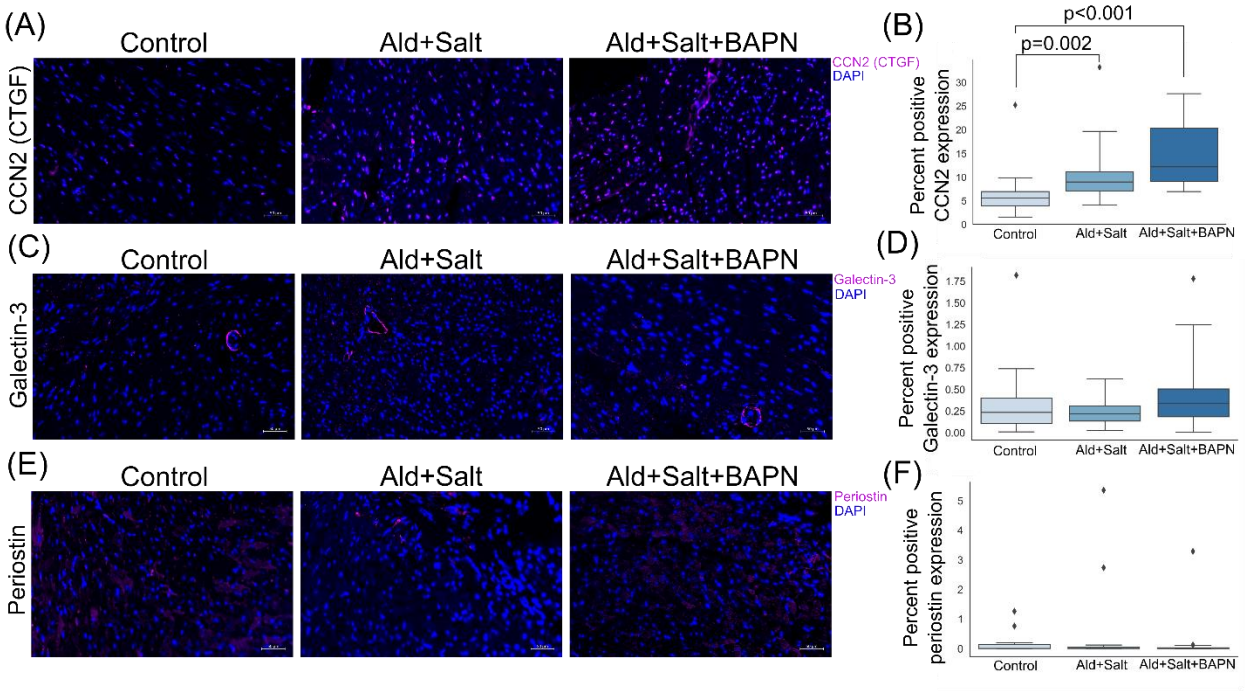

Figure 11 - Immunofluorescent labeling of Connective Tissue Growth Factor (CTGF/CCN2), Galectin-3, and Periostin in control, Ald+Salt, and Ald+Salt+BAPN cardiac tissue sections. (A) 20x magnification images of CCN2, **(C)** galectin-3, and **(E)** periostin immunolabeling in control, Ald+Salt, and Ald+Salt+BAPN cardiac tissue sections. **(B)** Quantification of positive CCN2 (CTGF), **(D)** galectin-3, and **(F)** periostin expression area in labeled cardiac tissue sections. (A, C, E) Scale bars = 50μm. Linear adjustments to image brightness and contrast were made uniformly to help improve labeling visibility. (B, D, F) data presented as box and whisker plots. Line s indicate mean. Black triangles signify outliers. 5-10 sections imaged in at least 3 biological replicates. Data normality was determined using a Kolmogorov-Smirnov test. Significant differences in normally distributed data were identified with a one-way ANOVA with post-hoc Tukey test. Significant differences in non-normally distributed data were assessed with a Kruskal-Wallis independent samples test with post-hoc pairwise comparisons.

Imaging results of Connective Tissue Growth Factor (CTGF/CCN2) immunofluorescent labeling demonstrated a qualitative increase in expression following Ald+Salt treatment relative to age-matched control cardiac tissue (Figure 11A). When examining the impacts of lysyl oxidase inhibition on CTGF expression, a further increase in qualitative expression was observed relative to both control and Ald+Salt cardiac tissue sections (Figure 11A). Quantification of positive CTGF expression area per field of view in immunolabeled cardiac sections supported the qualitative trend observed in Figure 11A, with significant increases in mean CTGF expression noted between Ald+Salt and control cardiac sections as well as between Ald+Salt+BAPN and control cardiac sections (Figure 11B).

Immunofluorescence results of Galectin-3 labeling did not demonstrate any substantial qualitative differences in labeling noted between control and Ald+Salt conditions (Figure 11C). Additionally, inhibition of lysyl oxidase function through BAPN treatment prior to experimental intervention was not noted to induce any substantial alterations in Galectin-3 expression (Figure 11C). Quantification of positive Galectin-3 expression area per field of view demonstrated a slight reduction in mean expression of Galectin-3 following Ald+Salt treatment relative to age-matched controls (Figure 11D). Inhibition of lysyl oxidase function through BAPN administration was found to be associated with no significant differences in Galectin-3 expression relative to controls (Figure 11D). Expression of Galectin-3 was noted to exhibit the greatest mean expression in Ald+Salt+BAPN cardiac tissue sections, however the magnitude of this difference was noted to be minor.

Periostin immunolabeling demonstrated no significant qualitative differences in deposition between Ald+Salt and control cardiac tissue sections (Figure 11E). Additionally, BAPN treatment was not observed to be associated with any altered deposition of periostin (Figure 11E).

Quantification of periostin positive expression area per field of view supported the minimal periostin labeling observed in experimental and control cardiac tissue sections (Figure 11F). It was noted that areas of positive periostin expression in cardiac tissue sections tend to be more restricted than expression of other matricellular proteins - with several areas of higher periostin expression noted, but the majority of cardiac tissue area exhibiting minimal to no positive expression (Figure 11E, F).

3.3.4 Flow Cytometry Can Be Used to Characterize Changes in the Cardiac Resident Macrophage Compartment in the Aging Heart

Flow cytometric staining of cardiac single cell isolates derived from young, moderately aged, or advanced age mice was performed to evaluate differences in the regulation of cardiac resident macrophage subsets induced by the physiological aging process (Figure 12). As previous studies have focused on the repopulation dynamics within the first 30 weeks of the murine lifespan, timepoints for this study were selected to try to provide additional insight on the period from 52 weeks to 2 years of age (Molawi et al., 2014; Pinto et al., 2014). The gating strategy for the flow cytometric characterization of cells isolated from cardiac tissue samples was based upon first performing a debris-, doublet-, and non-viable cell exclusion (Figure 12A). CD45+ cells were then selected from the viable cell fraction and expression of general macrophage surface markers F4/80 and CD11b was evaluated. Cells which were positive for both F4/80 and CD11b were identified as cardiac macrophages and selected for further analysis of lineage-associated surface marker expression. CD45+CD11b+F4/80+ cell fraction expression of TIMD4, a marker associated with embryonic hematopoiesis, and CCR2, a marker associated with bone marrow monocyte-derived macrophage differentiation, was performed to identify cardiac macrophage subsets isolated from

cardiac tissue samples (Figure 12A, B). Finally, expression of CX3CR1, a surface marker associated with cardiac residence in macrophages, was evaluated for the identified cardiac macrophage subsets as well as for the CD45+ cell fraction.

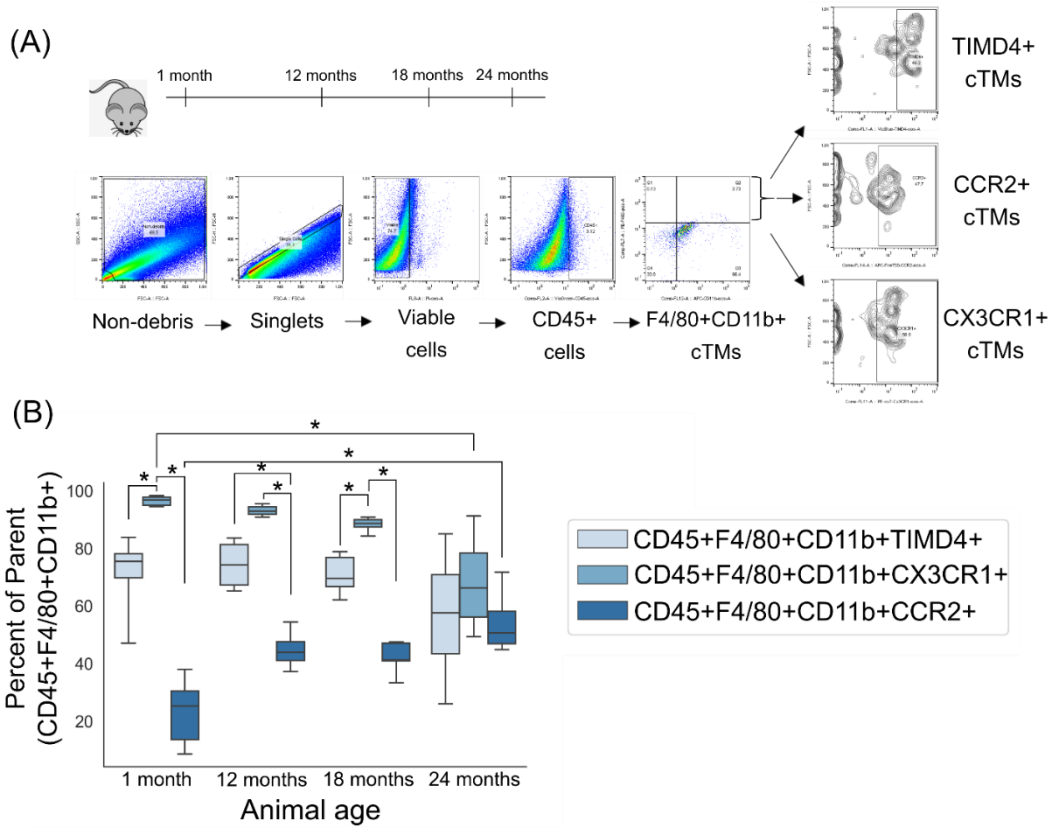

Figure 12 - Flow cytometric characterization of the cardiac macrophage compartment in young and advanced age murine cardiac tissue. (A) Overview of experimental timepoints and gating strategy. Briefly, debris and non-single cells were gated out of stained single cell suspension. Next, viable cells which exhibit negative PI expression were selected. CD45+ (pan-leukocyte) cells were then selected, and from that population, F4/80+CD11b+ cells were selected for further analysis. Within this F4/80+CD11b+ population, expression of embryological hematopiesis associated marker TIMD4, resident cardiac macrophage marker CX3CR1, and bone marrow monocyte marker CCR2 was then quantified. **(B)** Quantification of cardiac macrophage subset surface marker expression within the CD45+F4/80+CD11b+ cardiac macrophage cell fraction at different young and aged timepoints (n=4-7). Data presented as box and whisker plots. Lines indicate mean. Data normality was assessed with Kolmogorov-Smirnov test. Due to normal data distribution, an ANOVA with post hoc Tukey test was performed to identify significant differences in distribution between subsets at single age timepoints and in subsets at different age timepoints. *$p<0.05$

3.3.4.1 TIMD4+ Macrophage Subsets Comprise a Reduced Fraction of the Total Cardiac Resident Macrophage Pool With Increasing Age

Characterization of the cardiac resident macrophage (CD45+CD11b+F4/80+) viable cell fraction in young (1 month), moderately aged (12 month), and advanced age (18, 24 month) demonstrated a non-significant mean decrease in the percentage of TIMD4+ macrophages with increasing age (Figure 10B). As TIMD4 expression has been previously correlated with embryonic precursor-derived macrophage populations, this reduction in expression suggests that aging is associated with a reduction in embryonic precursor-derived macrophages population size (Dick et al., 2019).

3.3.4.2 CCR2+ Macrophage Subsets Comprise an Increased Fraction of All CD45+F4/80+CD11b+ Cardiac Macrophages With Increasing Age

Converse to the observed decrease in expression of embryological hematopoiesis marker TIMD4 expression with increasing age, characterization of CD45+CD11b+F4/80+ cardiac macrophage expression of bone marrow hematopoiesis associated marker CCR2 demonstrated a significant increase in mean expression with increasing age (Figure 12B). CCR2+ expression within CD45+CD11b+F4/80+ macrophages approximately doubled between 1 month and 24 months of age, suggesting that the previously characterized accumulation of CCR2+ macrophages in the first 30 weeks of aging can be extended to further aged time points as well.

Additionally, it was observed that TIMD4+ macrophages often comprise a significantly greater mean fraction of the CD45+CD11b+F4/80+ macrophage population than CCR2+ macrophages, such as in the case of 1 month or 12 month old macrophage populations (Figure 12B). However, at 24 months of age, no significant difference in TIMD4+ and CCR2+ macrophage

subset size was noted, suggesting that the observed significant fractionation of these subsets is lost in the highly aged cardiac microenvironment (Figure 12B).

3.3.5 Flow Cytometry Can Be Used to Characterize the Changes in the Cardiac Resident Macrophage Compartment Following Ald+Salt or Ald+Salt+BAPN Induced Cardiac Microenvironmental Remodeling and Evaluate the Degree to Which the Observed Changes Recapitulate Those Observed With Aging

In order to better understand how the characterized changes in cardiac function and microenvironment for the described *in vivo* model alter the regulation of the cardiac resident macrophages, flow cytometric characterization of isolated cardiac single cell suspensions from control mice, mice which received D-Aldosterone minipump implant coupled with 1% NaCl drinking water, and mice which received BAPN injections for five days preceding Ald+salt treatment was performed (Figure 13).

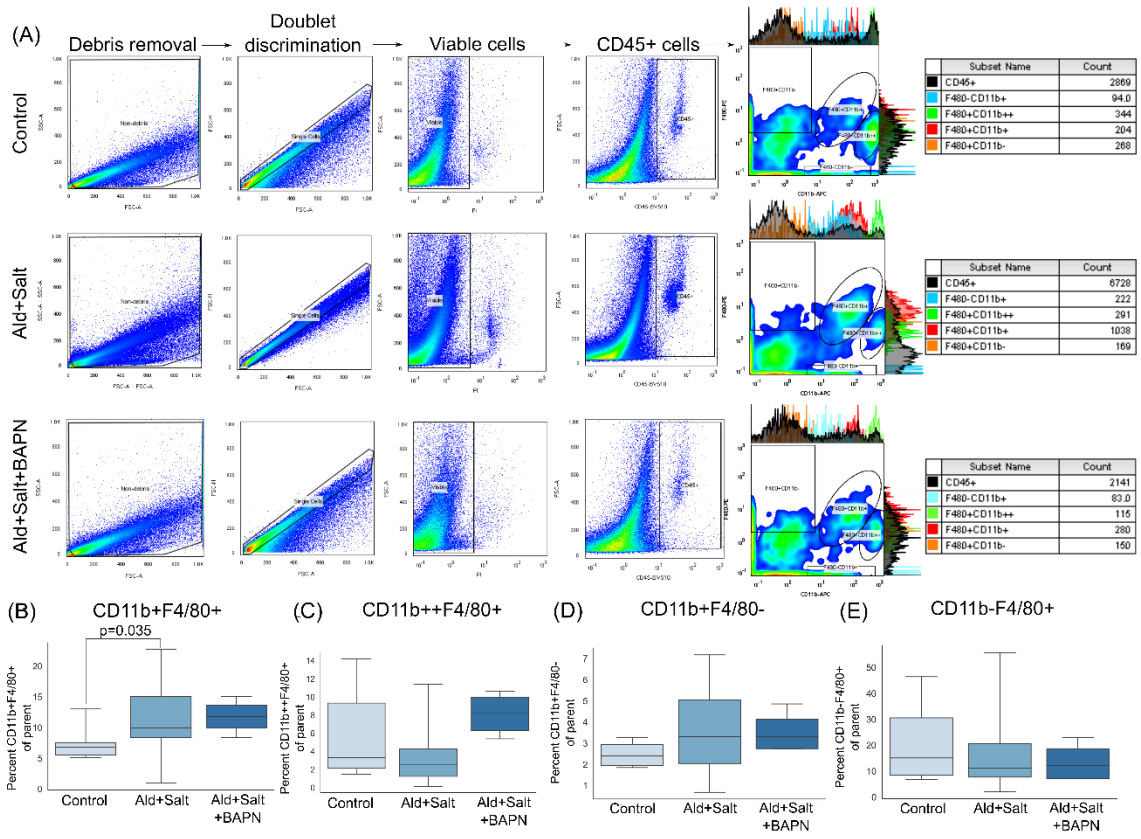

Figure 13 - Ald+Salt promotes altered patterns of F4/80 and CD11b expression in cardiac immune cell populations. (A) Representative graphs and gating strategy overview for characterization of cardiac resident macrophages in control, Ald+Salt, and Ald+Salt+BAPN cardiac cell isolates. **(B)** Quantification of the fraction of CD45+ cells which were found to be CD11b+F4/80+, **(C)** CD11b++F4/80+, **(D)** CD11b+F4/80-, and **(E)** CD11b-F4/80+ in control (n=10), Ald+Salt (n=15), and Ald+Salt+BAPN (n=4) cardiac cell isolates. Data presented as box and whisker plots. Lines indicate mean. Data normality was assessed with Kolmogorov-Smirnov test. Significant differences in normally distributed data were identified with a one-way ANOVA with post hoc Tukey test.

In order to first remove debris and non-viable cells from the characterization, a debris and doublet discrimination gate were applied to identify single cells for characterization (Figure 13A). Cells which exhibited negative expression of cell viability marker propidium iodide (PI), which is taken up in apoptotic or necrotic cells, were selected for to ensure analysis of viable cells (Figure 13A). Viable, single cell expression of pan-leukocyte surface marker CD45 was evaluated and cells positive for CD45 were selected (Figure 13A). F4/80 and CD11b expression patterns were then evaluated to identify any differential regulation of the cardiac resident macrophages following experimentally induced cardiac tissue remodeling (Figure 13A).

When examining distribution patterns of F4/80 and CD11b expression in CD45+ cardiac cell isolates, four cell populations were observed (Figure 13A). The first population was found to exhibit moderate to high F4/80 expression with minimal to no CD11b expression (F4/80+CD11b-). The second population was observed to exhibit moderate levels of CD11b expression with no detectable F4/80 expression (F4/80-CD11b+). The final two observed populations were characterized to both exhibit positive expression of F4/80 and CD11b (Figure 13A). These two double positive populations were found to exhibit some differential expression of CD11b, with the first (F4/80+CD11b+) generally exhibiting a reduced level of CD11b expression relative to the second double positive subset (F4/80+CD11b++).

In order to better identify how experimental intervention-induced cardiac microenvironmental remodeling altered the regulation of resident macrophage subsets, each subsets' percent composition of the total CD45+ cell fraction was characterized for control, Ald+salt, and Ald+salt+BAPN cardiac tissue (Figure 13B-E). A significant increase in the mean fraction of F4/80+CD11b+ cells within the total viable, CD45+ cell fraction was observed following D-Aldosterone minipump implant coupled with 1% NaCl drinking water administration

(Figure 13B). In addition, a non-significant mean increase in the percent of F4/80-CD11b+ cells was observed in the Ald+salt treatment group (Figure 13D). Conversely, Ald+salt treatment was found to be associated with a non-significant decline in the mean percentage of F4/80+CD11b- (Figure 13E) and F4/80+CD11b++ positive cells (Figure 13C) within the CD45+ viable cell fraction.

BAPN-mediated inhibition of collagen crosslinking in the cardiac matrix remodeling response to Ald+salt treatment was observed to not be associated with any significant changes relative to either control or Ald+salt treatment groups, although the mean fractional composition of macrophage subsets was observed to more closely reflected that of Ald+salt cardiac cell isolates than of control cell isolates (Figure 13B). However, a large mean increase relative to both control and Ald+salt was observed in the F4/80+CD11b++ cell fraction of Ald+salt+BAPN cardiac cells (Figure 13B).

3.3.5.1 Expression Patterns of Cardiac Resident Macrophage Markers TIMD4, CX3CR1, and CCR2 in Cardiac Macrophage Populations

In order to understand if the experimentally induced cardiac remodeling promoted altered regulation of individual cardiac macrophage subsets, flow cytometry was used to characterize TIMD4, CX3CR1, and CCR2 surface marker expression patterns in F4/80+CD11b+ cardiac macrophage populations (Figure 14).

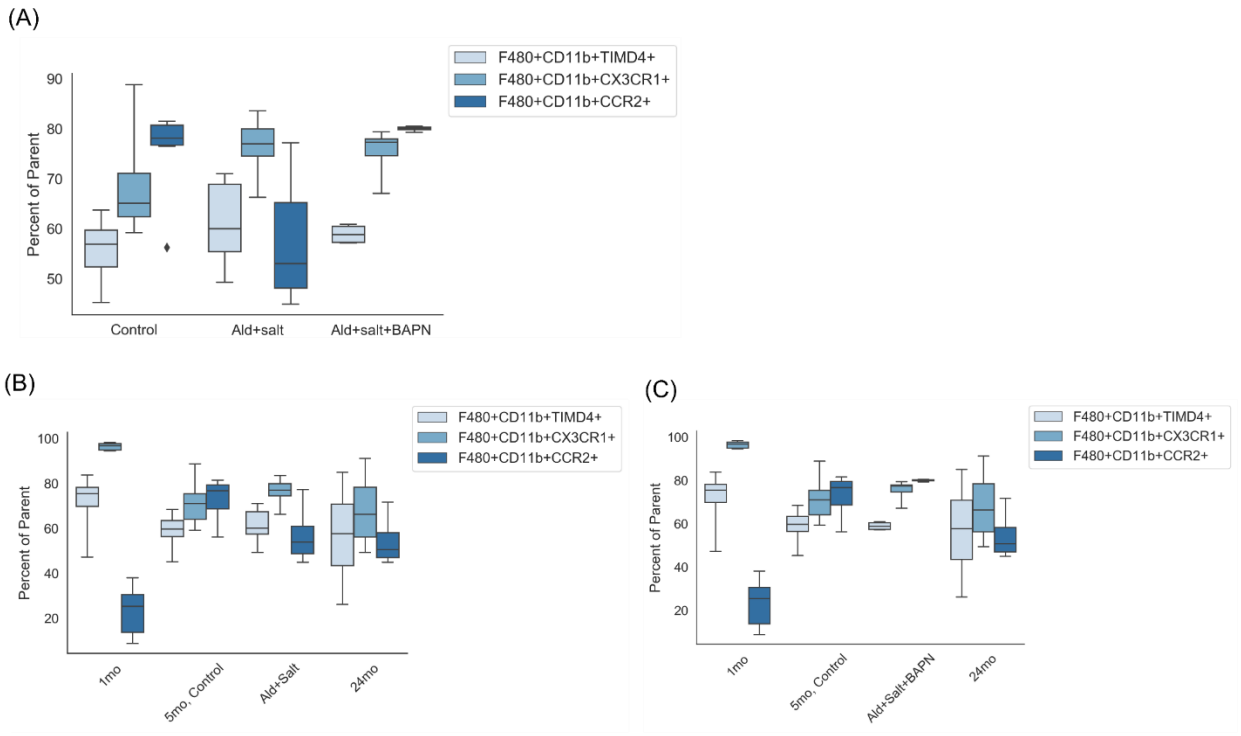

Figure 14 - Flow cytometry can be used to compare the regulation of the cardiac resident macrophages following experimental intervention and in young or advanced age control cardiac cell isolates. (A) Quantification of TIMD4, CX3CR1, and CCR2 expression in F4/80+CD11b+ macrophages from control (n=10), Ald+Salt (n=15), and Ald+Salt+BAPN (n=4) cardiac cell isolates **(B)** Comparison of TIMD4, CX3CR1, and CCR2 expression patterns in Ald+Salt and, **(C)** Ald+Salt+BAPN cardiac cell isolates and control cardiac cell isolates isolated from 1 month, 5 month, or 24 month old mice. Data presented as box and whisker plots. Lines indicate mean. Black triangle represent outlier data points.

Control cardiac cell isolates from 5-month aged mice were found to largely be composed of macrophages positive for CCR2 and CX3CR1, with moderate TIMD4 expression noted in these cell isolates (Figure 14A). Following Ald+Salt treatment, several alterations in surface marker

expression patterns were noted. The expression of CCR2 in F4/80+CD11b+ macrophages was found to decline from approximately 80% expression in control cardiac cell isolates to approximately 55% in Ald+Salt cardiac cell isolates (Figure 14A). CX3CR1 expression conversely was observed to increase in cardiac cell isolates following Ald+Salt experimental intervention (Figure 14A). When examining Ald+Salt+BAPN cardiac cell isolate surface marker expression, it was observed that the expression patterns of TIMD4, CX3CR1, and CCR2 expression largely reflected that which was observed in control cardiac cell isolates (Figure 14A).

In order to better contextualize how these characterized changes in surface marker expression in control, Ald+Salt, and Ald+Salt+BAPN cardiac cell isolates compare with the profiled changes in physiologically aged tissue, surface marker expression in 1 month and 24 month aged cardiac cell isolates profiled in Figure 9 were compared with either 5mo, control and Ald+Salt or with 5mo, control and Ald+Salt+BAPN surface marker expression (Figure 14B, C). It was observed that Ald+Salt cardiac cell isolate surface marker expression patterns most closely reflected those characterized in highly aged, 24 month cardiac cell isolates (Figure 14B). Alternatively, Ald+Salt+BAPN cardiac cell isolate TIMD4, CX3CR1, and CCR2 expression patterns were not observed to reflect those observed in 24 month cell isolates, but rather most closely resembled those characterized in control, 5month cardiac cell isolates (Figure 14C).

Taken together, these results demonstrate that D-Aldosterone minipump implant coupled with chronic 1% NaCl drinking water administration promoted an altered regulation of the cardiac macrophage compartment which was characterized by a significant mean increase in F4/80+CD11b+ macrophages which exhibited surface marker expression patterns closely resembling those observed in aged cardiac macrophage cell isolates.

3.3.5.2 CD163 and LYVE1 Can Also Be Utilized to Discriminate Between Functionally Distinct Macrophage Subsets

In order to better understand how the Ald+Salt experimental treatment altered the regulation of the cardiac resident macrophage compartment, additional flow cytometric characterization of CD163 (high affinity scavenger receptor for the hemoglobin-haptoglobin complex), lymphatic vessel endothelial hyaluronan receptor 1 (LYVE1), CX3CR1, and CCR2 surface marker expression was performed for F4/80+CD11b+ cardiac macrophage cell isolates (Figure 15).

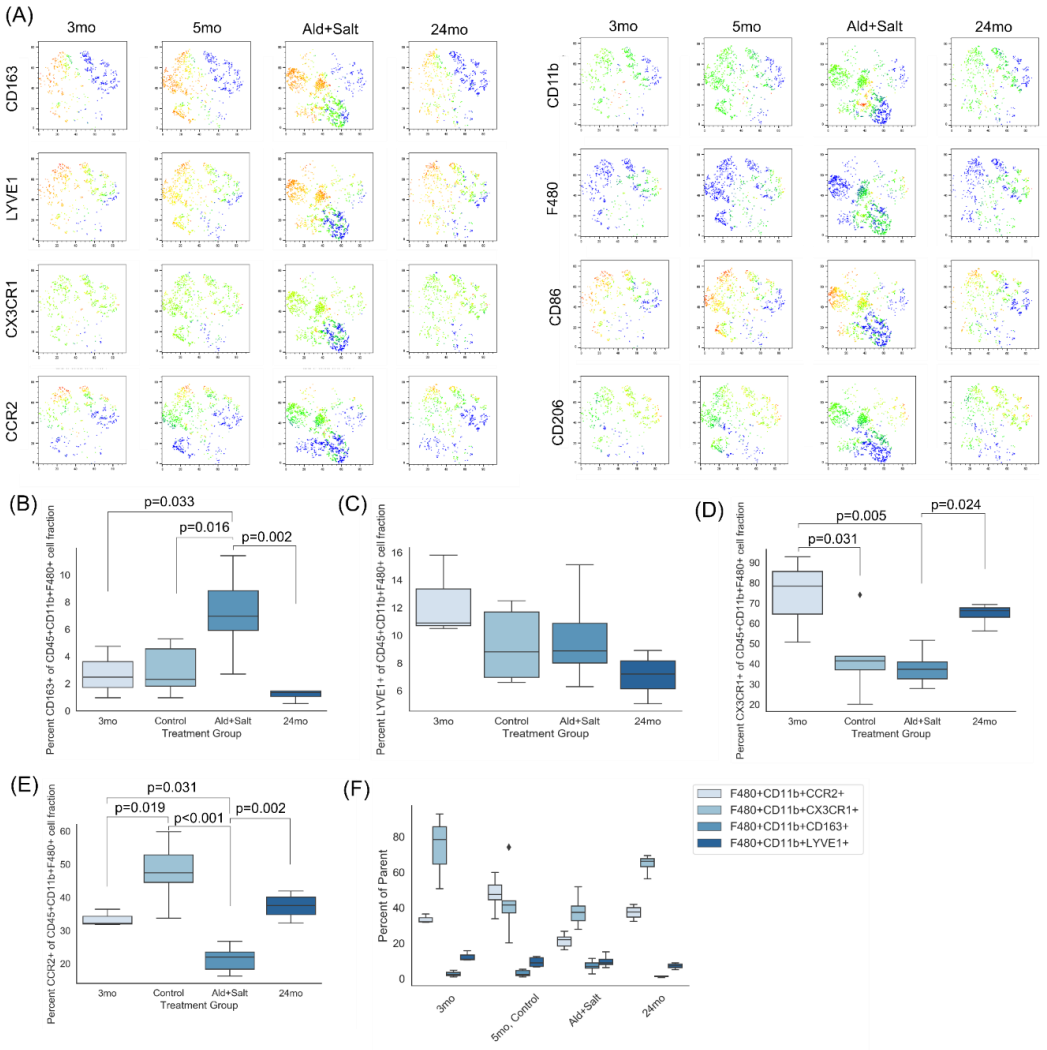

Figure 15 - CD163 and LYVE1 can be used to identify differential regulation of embryologically derived macrophage subsets in control and Ald+Salt cardiac cell isolates. (A) Representative plots of marker expression following tSNE analysis of CD45+ cells. **(B)** Quantification of CD163, **(C)** LYVE1, **(D)** CX3CR1, and **(E)** CCR2 expression in cardiac cell isolates from control mice aged 3 months (n=3), 5 months (n=5), or 24 months (n=4) as well as in Ald+Salt (n=8) mice. **(F)** Relative surface marker expression in the cardiac macrophage compartment in 3 month, 5 month, and 24 month control and in Ald+Salt mice. Note: data here is alternate presentation of data in (B-E). (B-F) Data presented as box and whisker plots. Lines indicate mean. Black triangles signify outliers. Significant trends were identified with a one-way ANOVA with post-hoc Tukey test.

In order to qualitatively assess differences in surface marker expression patterns within the CD45+ cell fraction isolated from 3 month control, 5 month control, 5 month Ald+Salt, or 24 month cardiac cell isolates, non-biased tSNE clustering was performed on CD45+ viable cells (Figure 15A). The first qualitative difference noted between tSNE plots generated for 5 month control and 5 month Ald+Salt cardiac cell isolates is the presence of additional F4/80+CD11b+ cell populations in Ald+Salt CD45+ cell fractions, a similar result to that quantified in Figure 9B (Figure 15A). Additionally, an increased expression of pro-inflammatory phenotype-associated CD86 was noted in several clusters within the tSNE plots for cardiac cell isolates from Ald+Salt cardiac tissue relative to controls (Figure 15A).

In order to quantify differences in cardiac resident macrophage population regulation between control and Ald+Salt cardiac cell isolates, a gating strategy similar to that described in Figure(s) 10/11 was utilized to isolate single, viable, CD45+ cells from a cardiac cell suspension for characterization. F4/80+CD11b+ macrophages were then selected from the CD45+ cell fraction and the expression of embryologically-derived macrophage associated surface markers CD163 and LYVE1 was quantified (Figure 15B, C). A significant mean increase in CD163+ macrophages was noted in Ald+Salt cell isolates relative to both age-matched as well as to young (3 month) and advanced age (24 month) controls (Figure 15B). Additionally, a significant reduction in CCR2+ macrophages was noted within CD45+F4/80+CD11b+ cell fractions in Ald+Salt cardiac cell isolates relative to age-matched controls (Figure 15F). Interestingly, a similar reduction in CCR2 expression within CD45+F4/80+CD11b+ cells was observed in the previous flow cardiac cell characterization in Figure 14 (Figure 14, Figure 15E). No significant difference in CX3CR1 of LYVE1 expression was noted in CD45+F4/80+CD11b+ cell fractions in age-matched control and Ald+Salt cardiac cell isolates however (Figure 15C, D).

3.3.5.3 Alterations in Pro-inflammatory (M1)-associated CD86 and Alternative Activation (M2)-associated CD206 Expression Patterns in LYVE1+ and CX3CR1+ Resident Cardiac Macrophage Subsets With Increasing Age

In addition to characterizing the differences in cardiac macrophage subset population size regulation resultant of experimentally induced cardiac microenvironmental remodeling, a characterization of the expression of pro-inflammatory (M1) phenotype-associated marker CD86 and alternatively activation (M2) phenotype-associated marker CD206 was performed to infer how microenvironmental remodeling may alter macrophage subset phenotype (Figure 16).

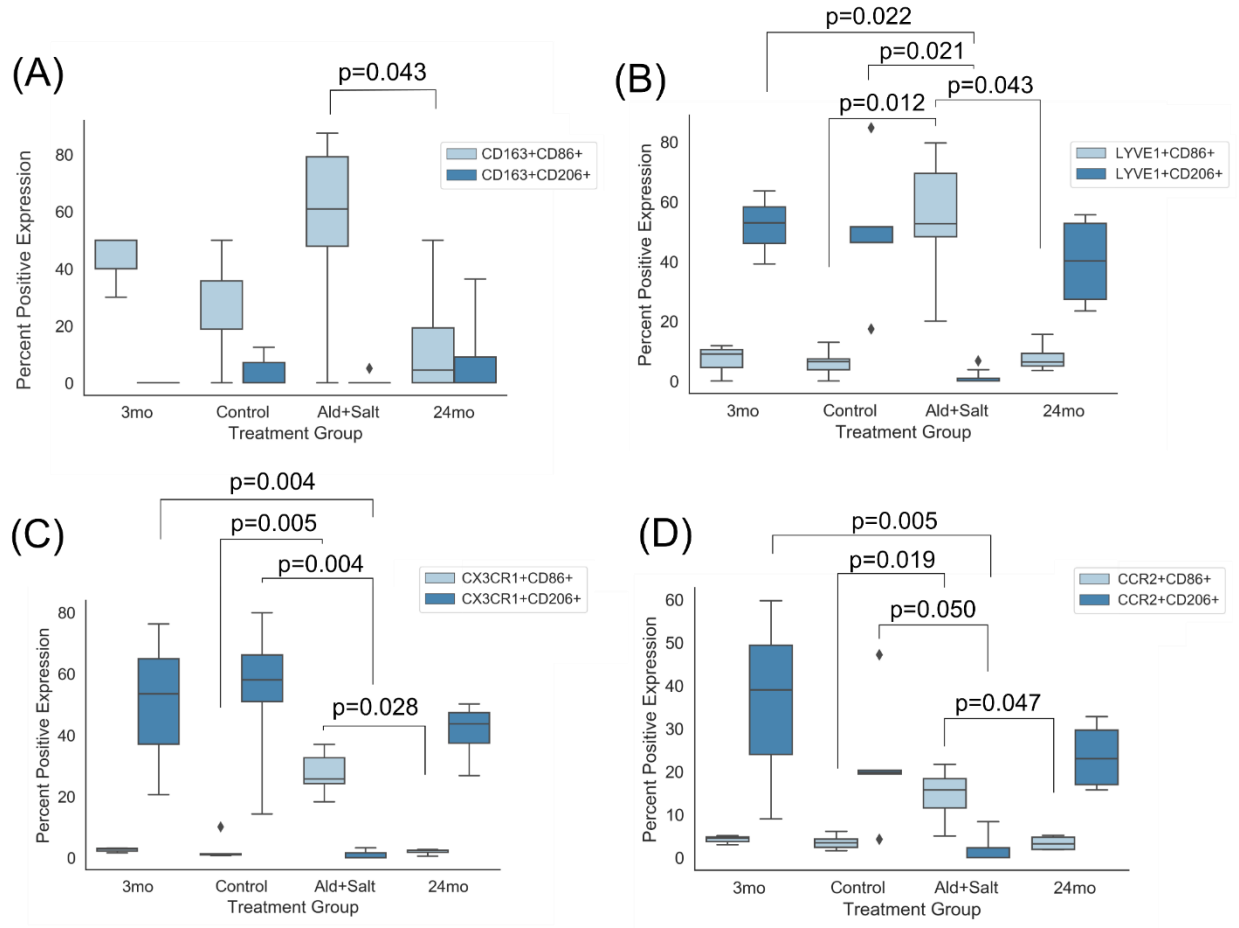

Figure 16 - Flow cytometry can be used to characterize the differences in expression of pro-inflammatory associated CD86 and anti-inflammatory associated CD206 expression in characterized cardiac macrophage subsets. (A) Expression of CD86 and CD206 in CD163+, **(B)** LYVE1+, **(C)** CX3CR1+, and **(D)** CCR2+ macrophage subsets in 3 month (n=3), 5 month (n=5), and 24 month (n=4) cardiac cell isolates as well as in Ald+Salt (n=8) cardiac cell isolates. Data presented as box and whisker plots. Lines indicate mean. Black triangles represent data point outliers. Data normality was assessed with Kolmogorov-Smirnov test. Significant trends in normally distributed data were identified with one-way ANOVA with post-hoc Tukey test. Significant trends in non-normally distributed data were identified with Kruskal-Wallis non-parametric test with post hoc pairwise comparisons.

LYVE1+ and CX3CR1+ macrophage subsets were found to exhibit a more pronounced expression of M2 phenotype associated CD206 and a reduced expression of M1-associated CD86 in control cell isolates (Figure 16B, C). Additionally, some age-related differences in the relative expression of CD86 and CD206 were noted within these subsets. 3 month and 5 month CX3CR1+ and LYVE1+ control cell isolates generally exhibit around 50% of macrophages exhibiting CD206 expression and only 5-10% of macrophages exhibiting CD86 expression (Figure 16B, C). However, both 24-month LYVE1+ and CX3CR1+ macrophages exhibit reduced CD206+ expression coupled with either sustained or slightly increased CD86 expression; suggesting that aged cardiac microenvironments promote increased M1:M2 macrophage ratios resultant of decreased M2 macrophage polarization (Figure 16B, C).

3.3.5.4 Alterations in Pro-inflammatory (M1)-associated CD86 and Alternative Activation (M2)-associated CD206 Expression in CCR2+ Resident Cardiac Macrophage Subsets With Increasing Age

Characterization of CD86 and CD206 expression in CCR2+ macrophages demonstrated a similar trend to that observed in LYVE1+ and CX3CR1+ control macrophages with several important notes (Figure 16D). First, the general magnitude of the difference in CD206 and CD86 noted in CCR2+ macrophages was generally decreased across age time points in control cell isolates (Figure 16D). Additionally, while the decrease in alternative activation associated CD206 expression was only noted in advanced age (24 month) in LYVE1+ and CX3CR1+ macrophages, a decrease in CD206 expression can be noted earlier in CCR2+ macrophages - with 5 month control isolates exhibiting reduced CD206 expression relative to 3 month controls (Figure 16B-D).

3.3.5.5 Alterations in Pro-inflammatory (M1)-associated CD86 and Alternative Activation (M2)-associated CD206 Expression in Cardiac Macrophage Subsets Following Ald+Salt Experimental Treatment

Aldosterone minipump implant coupled with chronic 1% NaCl drinking water treatment was found to be associated with several significant alterations in CD86 and CD206 expression in characterized cardiac resident macrophage subsets (Figure 16). Ald+Salt treatment was found to be associated with a general mean increase in pro-inflammatory (M1) phenotype associated CD86 expression in all characterized macrophage subsets (Figure 16A-D). Additionally, significant mean increases in CD86 expression were noted in LYVE1+ and CCR2+ macrophages relative to age-matched LYVE1+ and CCR2+ control macrophages (Figure 16B, D). Several significant decreases in CD206 expression were noted in cardiac resident macrophage subsets from Ald+Salt cardiac cell isolates (Figure 16). Significant mean decreases in CD206 expression were observed in LYVE1+, CX3CR1+, and CCR2+ cardiac macrophages isolated from Ald+Salt cardiac tissue as compared to LYVE1+, CX3CR1+, or CCR2+ macrophages isolated from age-matched control cardiac tissue (Figure 16B-D). Taken together, these results suggest that Ald+salt induced alterations in the cardiac microenvironment promote increase ratios of M1:M2 macrophages through both an increase in M1 polarization as well as through a decrease in alternative macrophage activation.

3.3.6 Immunolabeling of CCR2, LYVE1, and αSMA in Cardiac Tissue Sections Exhibit Significant Differences in Expression Following Experimental Intervention

In addition to flow cytometric characterization of LYVE1 and CCR2 expression patterns within cardiac resident cell populations, immunofluorescent labeling of cardiac sections from

control, Ald+Salt, and Ald+Salt+BAPN cardiac tissue sections was performed to better determine how experimental intervention induced cardiac matrix remodeling may have promoted altered expression of LYVE1 or CCR2 (Figure 17).

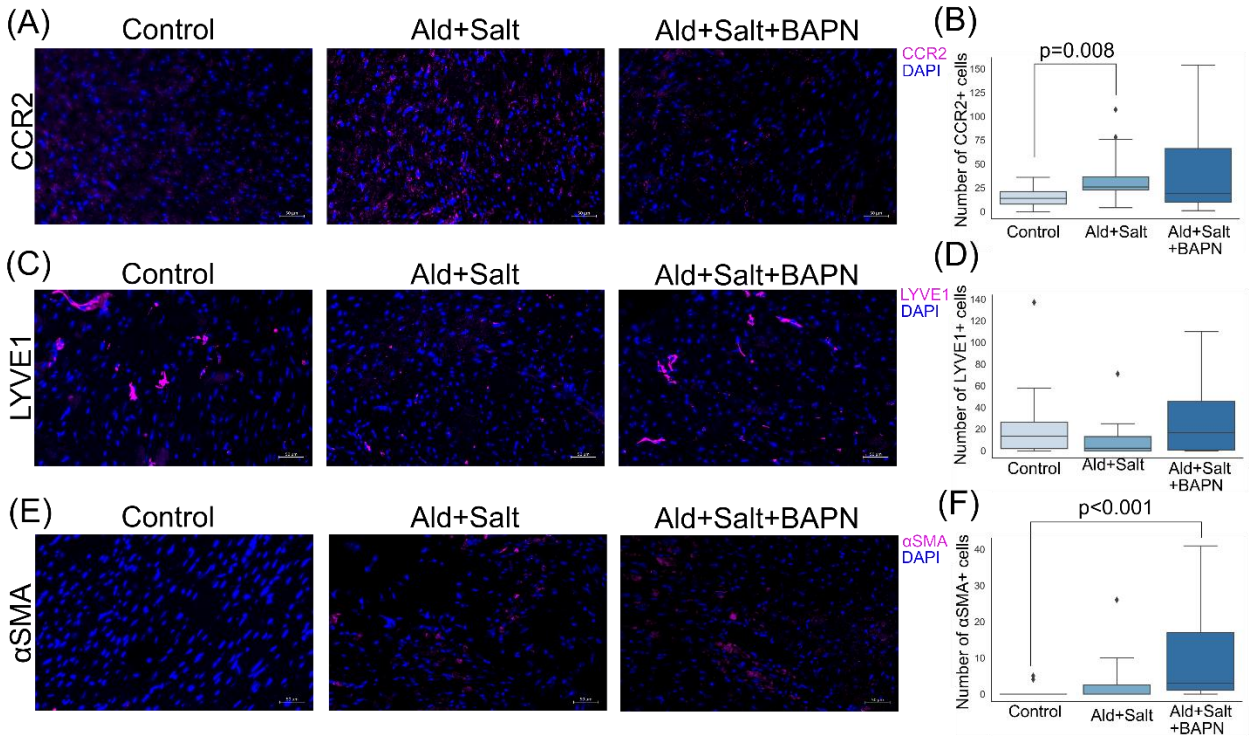

Figure 17 – Immunolabeling of CCR2, LYVE1, and αSMA in control, Ald+Salt, and Ald+Salt+BAPN cardiac tissue sections demonstrate differences in expression following experimental intervention. (A) 20x magnification of C-C chemokine receptor type 2 (CCR2), **(C)** lymphatic vessel endothelium hyaluronan receptor 1 (LYVE1), and **(E)** alpha smooth muscle actin (αSMA) immunolabeling in control, Ald+Salt, and Ald+Salt+BAPN cardiac tissue sections. **(B)** Quantification of the number of cells per 20x field of view exhibiting positive CCR2, **(D)** LYVE1, and **(F)** αSMA expression. (A, C, E) scale bars = 50μm. Linear adjustments to image brightness and contrast to reduce background and improve staining visibility made uniformly across images. (B, D, F) Data presented as box and whisker plots. Lines indicate mean. Black triangle represent outlier data points. 5-10 20x sections imaged in at least 3 biological replicates. Data normality was assessed with Kolmogorov-Smirnov test. Significant trends in normally distributed data were identified with a one-way ANOVA with post-hoc Tukey test. Significant trends in non-normally distributed data were identified with Kruskal-Wallis non-parametric test with pairwise comparison post-hoc.

CCR2 immunolabeled images demonstrated an increase in the number of CCR2+ cells in Ald+Salt cardiac tissue sections relative to age-matched controls (Figure 17A). Inhibition of lysyl oxidase function through BAPN administration prior to Ald+Salt experimental treatment was observed to be associated with a qualitative decline in CCR2 expression relative to Ald+Salt cardiac tissue sections (Figure 17A). Quantification of the number of cells exhibiting positive levels of CCR2 expression per field of view in control, Ald+Salt, and Ald+Salt+BAPN cardiac tissue sections supported the observed qualitative trends in CCR2 expression (Figure 17B). A significant increase in the number of cells exhibiting positive CCR2 expression was noted between Ald+Salt and age-matched control cardiac tissue sections (Figure 17B). Additionally, a non-significant decrease in the mean number of CCR2+ cells was observed in mice treated with BAPN prior to Ald+Salt experimental treatment, with the number of CCR2+ cells noted to reflect those observed in control cardiac sections (Figure 17B).

Qualitative results of lymphatic vessel endothelial hyaluronan receptor 1 (LYVE1) immunolabeling demonstrated a decrease in LYVE1 expression in Ald+Salt cardiac tissue sections relative to controls (Figure 17C). Inhibition of lysyl oxidase function with BAPN treatment was observed to be associated with a qualitative increase in LYVE1 expression in cardiac tissue sections relative to Ald+Salt cardiac tissue sections (Figure 17C). When compared to control sections, no substantial qualitative difference in LYVE1 expression was noted between control and Ald+Salt+BAPN cardiac tissue sections (Figure 17C). Quantification of the number of cells exhibiting positive LYVE1 expression per field of view demonstrated a non-significant decline in the number of LYVE1+ cells in Ald+Salt cardiac tissue sections relative to controls (Figure 17D). BAPN treatment was found to be associated with an attenuation of the reduction in LYVE1+ cell numbers following Ald+Salt treatment (Figure 17D). Additionally, BAPN

treatment was found to promote a non-significant increase in LYVE1+ cell number relative to controls (Figure 17D).

Qualitative analysis of alpha-smooth muscle actin (αSMA) immunolabeling demonstrated an increase in αSMA expression in Ald+Salt cardiac tissue sections relative to controls (Figure 17E). BAPN-mediated inhibition of lysyl oxidase function was not noted to be associated with any substantial alteration in αSMA expression (Figure 17E). Quantification of the number of cells exhibiting positive αSMA expression per field of view suggested Ald+Salt experimental treatment was associate with an increased number of αSMA+ cells, although this difference was not noted to be significant (Figure 17F). However, a significant increase in the number of αSMA+ cells was noted between Ald+Salt+BAPN and control cardiac tissue sections (Figure 17F).

3.3.7 Evaluation of Differential Expression of Pro- and Anti-inflammatory Associated Genes in Experimental Cardiac RNA Isolates

In order to better understand if the difference in regulation of cardiac resident macrophage subsets following Ald+salt treatment could induce detectable alterations in gene expression in whole cardiac RNA isolates, qRT-PCR analysis was performed for a variety of inflammation, fibrosis, and stress-response associated gene transcripts (Figure 18).

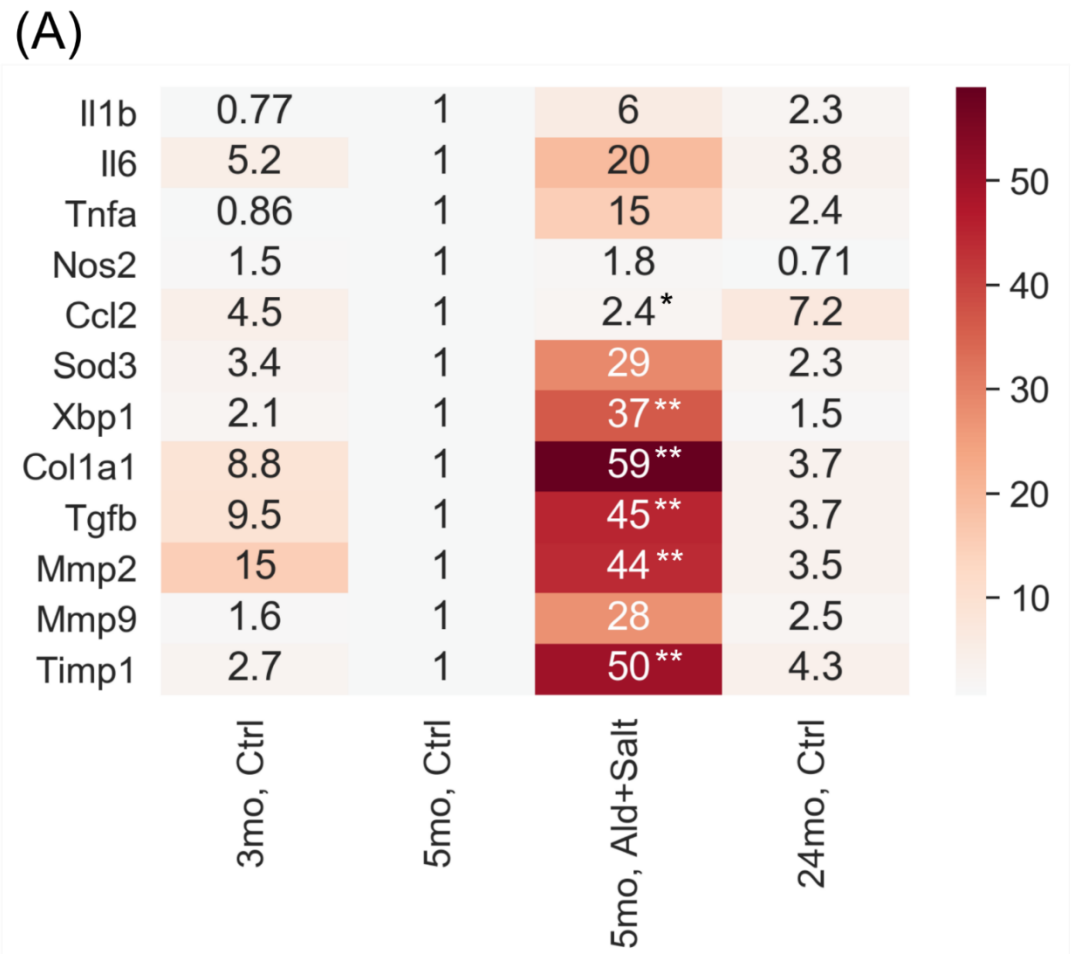

Figure 18 - qRT-PCR analysis of 3-month control, 5-month control, 5-month Ald+Salt, and 24-month control whole cardiac RNA isolates demonstrates an increase in pro-inflammatory, pro-fibrotic, and stress-associated gene expression in Ald+Salt RNA isolates relative to controls. (A) Fold change in expression of genes associated with inflammatory (*Il1b, Il6, Tnfa, Nos2, Ccl2*), fibrotic (*Col1a1, Tgfb, Mmp2, Mmp8, Timp1*), and stress (*Sod3, Xbp1*) responses in 3mo control, 5mo control, Ald+Salt, and 24mo control whole cardiac RNA isolates. Fold change expression quantified with double Δ Ct method normalized with housekeeping gene *Gapdh*. Data normality was assessed with Kolmogorov-Smirnov test. Significant differences in expression between 5mo control and 5mo Ald+Salt cardiac RNA isolates were identified with either independent samples t-test in normally distrubted data or Mann-Whitney U-test in non-normally distriubted data. *=$p<0.05$, **=$p<0.001$

3.3.7.1 Ald+Salt Cardiac RNA Isolates Exhibited a Mean Increase in Expression of Inflammation-associated Gene Transcripts Relative to Age-matched Control RNA Isolates

In order to determine how Aldosterone minipump implant coupled with 1% NaCl drinking water treatment may have altered the regulation of inflammation-associated gene transcription relative to age-matched controls, qRT-PCR with subsequent double Δ C_t analysis of the fold change in gene expression normalized to housekeeping *Gapdh* controls for interleukin-1β (*Il1b*), interleukin-6 (*Il6*), tumor necrosis factor-α (*Tnfa*), and C-C motif chemoattractant ligand 2(*Ccl2*) was performed (Figure 18). Ald+Salt treatment was found to be associated with a general, non-significant mean increase in inflammasome activation associated *Il1b* and *Tnfa* gene transcripts as well as a mean increase in *Il6* transcripts (Figure 18). This result demonstrates that Ald+Salt experimental treatment promoted increased, yet variable expression of pro-inflammatory and inflammasome activation-associated gene transcripts - potentially resultant of the altered cardiac resident macrophage polarization response characterized in Figure 16A-D. Additionally, a significant mean increase in *Ccl2* expression was observed in Ald+Salt RNA isolates relative to age-matched controls (Figure 18). This significant increase in *Ccl2* transcripts observed in Ald+Salt cardiac RNA isolates is interesting given the characterized reduction in CCR2+ cardiac macrophages within the F4/80+CD11b+ cell fraction analyzed in Figures 14 and 15. Given the role that CCL2 (monocyte chemoattractant protein-1) plays as a chemoattractant for CCR2+ monocytes, this significant increase coupled with the observed decrease in CCR2+ cardiac macrophages may suggest either a reduction in the ability of monocytes to extravasate into remodeling Ald+Salt cardiac tissue microenvironments or a loss of CCR2+ expression following monocyte extravasation and differentiation.

3.3.7.2 Ald+Salt Cardiac RNA Isolates Exhibited a Mean Increase in Expression of Fibrosis- and Extracellular Matrix Protein-associated Gene Transcripts Relative to Age-matched Controls

In addition to the characterized alterations in inflammation associated gene transcript expression, qRT-PCR with subsequent double ΔC_t analysis of the fold change in gene expression normalized to housekeeping *Gapdh* controls was performed for genes associated with the matrix remodeling response, including transcripts for collagen 1a1 (*Col1a1*), transforming growth factor-β (*Tgfb*), matrix metalloprotease-2 (*Mmp2*), matrix metalloprotease-9 (*Mmp9*), and tissue inhibitor of metalloprotease-1 (*Timp1*) (Figure 18). The first significant difference noted between 5 month control RNA isolates and those derived from Ald+Salt cardiac tissue was a significant upregulation in the expression of transcripts for collagen 1a1 protein, a constitutive subunit of fibrillar collagen oligomers (Figure 18). A significant upregulation in expression of TGF-β (*Tgfb*), an important growth factor which induces a myriad of altered cell behaviors that support the fibrotic matrix remodeling response, was also observed in Ald+Salt RNA isolates relative to control isolates (Figure 18). As TGF-β plays an important role in inducing the fibroblast to myofibroblast phenotypic conversion which is associated with increased fibrotic matrix protein production, the observed significant increases in *Col1a1* and *Tgfb* transcripts observed in Ald+Salt cardiac RNA isolates suggest that Ald+Salt treatment not only induced the increased collagen protein deposition characterized histologically in Figure 11 but also induced transcription of genes associated with further fibrotic matrix deposition and increased TGF-β signaling.

Expression of matrix metalloprotease-2 (*Mmp2*), matrix metalloprotease-9 (*Mmp9*), and tissue inhibitor of metalloprotease-1 (*Timp1*) was also quantified to determine how Ald+Salt treatment altered the regulation of these enzymes essential for the regulation of extracellular matrix

protein turnover (Figure 18). A significant mean increase in expression of *Mmp2* and *Timp1* transcripts was observed in Ald+Salt RNA isolates compared to control isolates (Figure 18). Additionally, a non-significant mean increase was noted in *Mmp9* expression in Ald+Salt RNA isolates relative to control isolates (Figure 18). In order to better understand how the upregulation of matrix turnover associated transcripts observed in Ald+Salt RNA isolates impacted the tissue remodeling response, the relative ratio of expression of metalloprotease to inhibitor of metalloprotease proteins was compared. Generally, an increased expression of matrix metalloprotease proteins relative to inhibitor of metalloprotease proteins is observed in younger individuals and is associated with physiological matrix turnover (Horn et al., 2012). Similarly, in young (3 month) RNA isolates analyzed with qRT-PCR, a positive expression ratio of metalloprotease to inhibitor of metalloprotease ratios were observed (Figure 18). However, in aged individuals as matrix turnover declines and increased fibrotic matrix deposition increases, expression ratios of metalloprotease to inhibitor of metalloprotease have been observed to decline. This decline in metalloprotease to inhibitor of metalloprotease ratio can be observed in the characterized 24 month cardiac RNA isolate gene expression data as well, where *Timp1* transcripts were observed to exhibit greater mean expression than both *Mmp2* and *Mmp9* transcripts (Figure 18). When comparing the expression ratio of metalloprotease to inhibitor of metalloprotease transcripts in Ald+Salt cardiac RNA isolates, it was observed that Ald+Salt treatment generally reduced the ratio of metalloprotease to inhibitor of metalloprotease transcripts (Figure 18). This increased expression of metalloprotease inhibitor protein relative to metalloprotease enzyme both resembles the change observed in advanced age cardiac RNA isolates (24 months) and suggests that these microenvironments are promoting a transcriptional balance of these factors which favors matrix protein deposition and maintenance (Figure 18).

3.3.7.3 Ald+Salt Cardiac RNA Isolates Exhibited a Mean Increase in Stress-associated Gene Transcripts Relative to Age-matched Control RNA Isolates

Numerous mechanisms exist by which alterations in local microenvironmental inflammatory stimuli induce alterations in resident cell metabolism and stress response associated gene regulation. In order to better understand how these redox and stress response associated gene transcripts are regulated with physiological aging as well as following Ald+Salt treatment, qRT-PCR with subsequent double ΔC_t analysis of the fold change in gene expression normalized to housekeeping *Gapdh* controls was performed for redox associated nitric oxide synthase-2 (*Nos2*) and superoxide dismutase-3 (*Sod3*) transcripts as well as for stress response associated x-box binding protein-1 (*Xbp1*) transcripts (Figure 18). Nitric oxide synthase 2 is a protein generally upregulated in canonical type I immune responses which also provides a link between macrophage metabolic state and polarization state. Macrophages exposed to pro-M1 signaling cues tend to exhibit altered arginine metabolism characterized by nitric oxide synthase-mediated breakdown of arginine with subsequent radical nitrogenous species generation. In Ald+Salt cardiac RNA isolates, a slight, non-significant upregulation in mean *Nos2* gene transcript expression was noted relative to age-matched controls (Figure 18). Additionally, Ald+Salt cardiac RNA isolates generally exhibited the greatest mean expression of *Nos2* transcripts as compared to all control isolates, although it is worth noting that the magnitude of differential expression was not largely different from control expression levels (Figure 18).

A non-significant upregulation of mean *Sod3* transcript expression was noted in Ald+Salt cardiac RNA isolates relative to age-matched control RNA isolates as well (Figure 18). Superoxide dismutase 3 is a protein secreted into the extracellular space which is responsible for reducing radical oxidative species present within the tissue microenvironment. Given the increased mean

expression of pro-inflammatory gene transcripts characterized in Ald+Salt cardiac RNA isolates, it is interesting to note that the increased expression of the protein responsible for reducing radical oxidants relative to the radical producing, M1-associated *Nos2*. This may suggest radical oxidant secretion into the extracellular space in Ald+Salt cardiac microenvironments is mediated through another pathway outside of the nitric oxide synthase-mediated pathway. This result may also be consequent of intermediary macrophage polarization states in which macrophage secrete factors associated with both M1 and M2 phenotypes.

In addition to redox state associated gene transcript expression, the expression of endoplasmic stress response associated gene x-box binding protein-1 (*Xbp1*) was evaluated in young control (3 month), age-matched control (5 month), Ald+Salt (5 month), and advanced age control (24 month) cardiac RNA isolates (Figure 18). Increased *Xbp1* expression is generally associated with increased activation of the unfold protein response within the cell endoplasmic reticulum. This response provides not only an important cellular mechanism for promoting the degradation of misfolded proteins under homeostatic conditions but also a surrogate measure for inference regarding endoplasmic reticular stress, as increased intracellular oxidant concentrations or metabolic alterations in stressed cells can increase protein misfolding. Ald+Salt cardiac RNA isolates were found to exhibit a significant upregulation in *Xbp1* transcript expression relative to age-matched controls, suggesting that Ald+Salt treatment promoted increased endoplasmic stress (Figure 18).

3.3.8 Correlation of Cardiac Immune Population Dynamics to Cardiac Functional Parameter Measures

Non-invasive clinical assessment of cardiac function typically relies upon physiological parameter measurements coupled with imaging modalities such as echocardiography or magnetic resonance imaging to infer details regarding the function of the cardiovascular system. Recent studies have improved upon the diagnostic ability of clinical imaging modalities by combining cardiac imaging with histological and biochemical analysis of cardiac matrix protein content to generate models where non-invasive clinical imaging can be used to infer more information regarding the state of the cardiac microenvironment (Pinkert, Hortensius, Ogle, & Eliceiri, 2018). Since the described *in vivo* model evaluated cardiac function with echocardiography prior to cardiac tissue isolation and subsequent flow characterization, it is possible to correlate cardiac functional parameter measurements with the characterized differences in cardiac macrophage subset regulation (Figure 19).

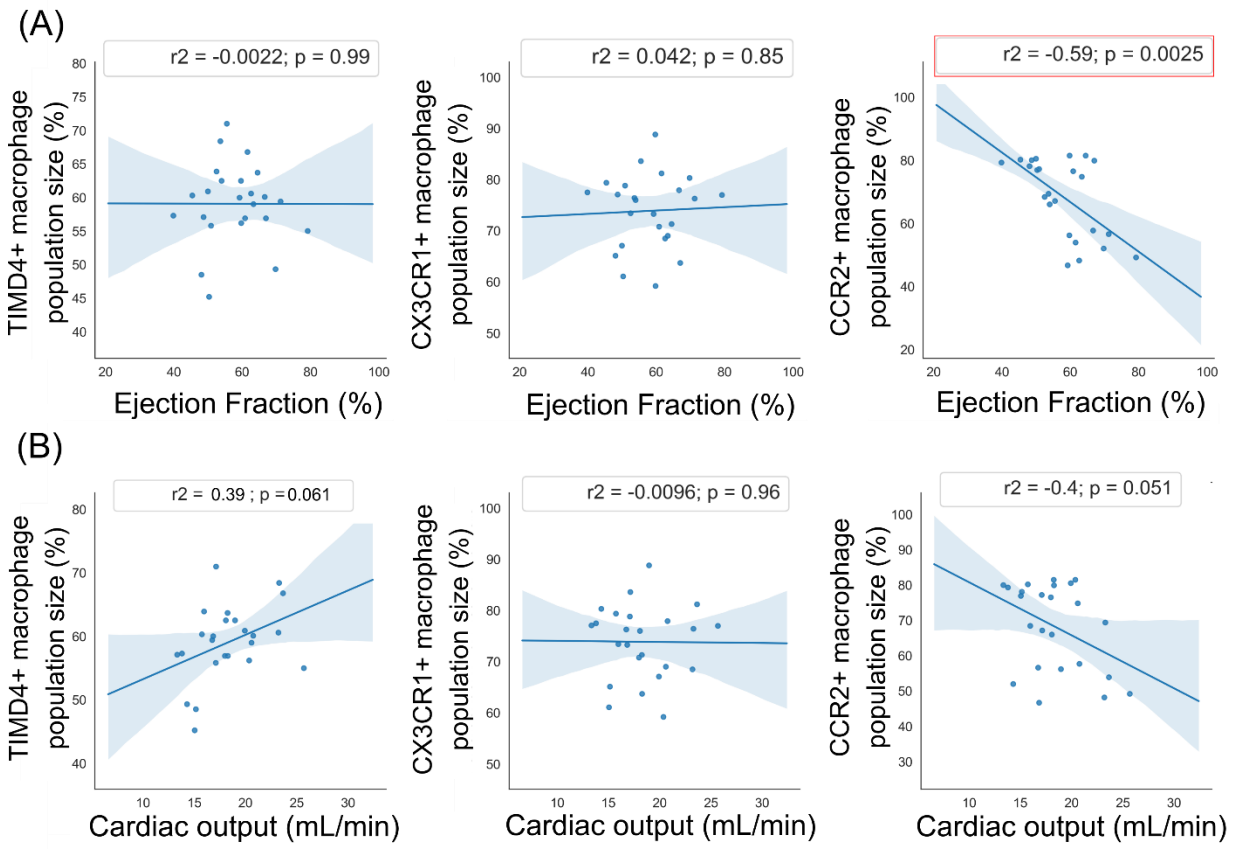

Figure 19 – Increased fractions of CCR2+ macrophages correlate with decreased ejection fractions. (A) Regression of measured murine ejection fraction and **(B)** cardiac output against TIMD4, CX3CR1, and CCR2 macrophage population percentage of the total resident macrophage compartment as determined by flow cytometry. Linear regression coefficient of determination and p-values reported for each regression. Linear fit is represented by dark blue line with model confidence interval depicted in light blue overlay. Individual points represented as points overlaid on plot. Significant correlations highlighted in red boxes.

3.3.8.1 An Increase in CCR2 Expression in F4/80+CD11b+ Cardiac Macrophage Populations Correlates With Reduced Cardiac Ejection Fraction and Cardiac Output

In order to better understand how differential regulation of cardiac resident macrophage subsets correlates with altered cardiac function parameters, echocardiographic functional parameters were regressed against previously characterized cardiac F4/80+CD11b+ macrophage TIMD4, CX3CR1, and CCR2 subset size measurements (Figure 19). A significant correlation was noted between increasing CCR2+ macrophage subset size and both decreasing ejection fraction and decreasing cardiac output (Figure 19A, B). Additionally, while no significant correlation was noted between ejection fraction and CX3CR1+ or TIMD4+ macrophage subset size, a significant positive correlation between TIMD4+ macrophage subset fraction and cardiac output was observed (Figure 15B).

3.3.8.2 Increased CX3CR1+ Macrophage Fractions Positively Correlate With Increased Isovolumic Relaxation Time

Given the significant increase in mean isovolumic relaxation time (IVRT) observed following Ald+Salt treatment, individual IVRT measurements were regressed against macrophage subset fraction measurements to infer how increased IVRT may correlate with changing cardiac macrophage subset regulation (Figure 20A, Figure 15D).

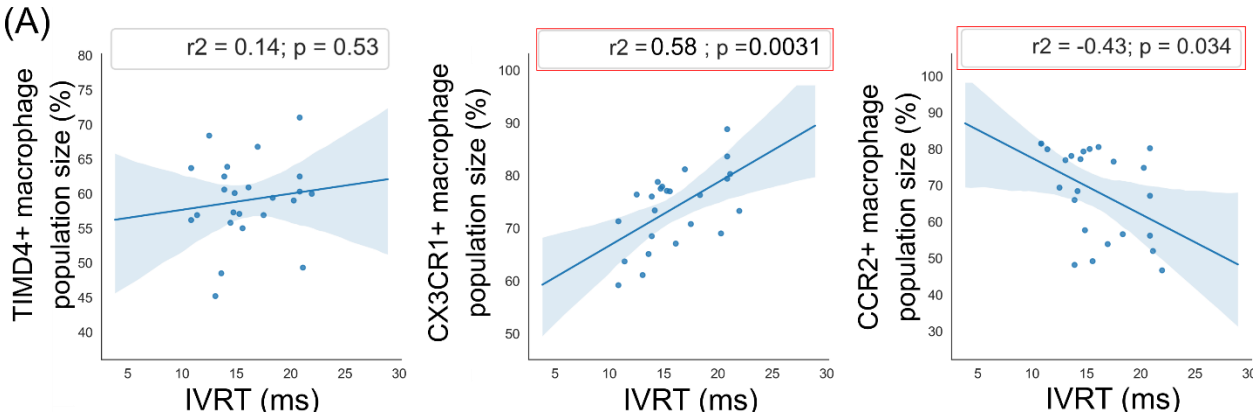

Figure 20 - CX3CR1+ and CCR2+ macrophage population fractions correlate with altered left ventricular isovolumic relaxation times. (A) Regression of measured IVRT against TIMD4, CX3CR1, and CCR2 macrophage population percentage of the total resident macrophage compartment as determined by flow cytometry. Linear regression coefficient of determination and p-values reported for each regression. Linear fit is represented by dark blue line with model confidence interval depicted in light blue overlay. Individual points represented as points overlaid on plot. Significant correlations highlighted in red boxes.

A significant positive correlation was observed between increased CX3CR1+ macrophage fractions and increased mean measured isovolumic relaxation times (Figure 20A). Additionally, a significant negative correlation was noted between increase CCR2+ macrophage subset size and increased mean IVRTs (Figure 20A).

3.3.8.3 CCR2+ Macrophage Fraction Size Correlates With Mitral Valve E/e' and Mitral Valve E/A Ratios

In order to better understand how the characterized significant alterations in mitral valve early to late filling rate (MV E/A) as well as how mitral valve early filling rate to early tissue

annular velocity (MV E/e') ratios correlate with cardiac macrophage subset regulation, measured MV E/A ratios and MV E/e' ratios were regressed against characterized macrophage TIMD4, CX3CR1, and CCR2 subset fraction sizes (Figure 21A, B).

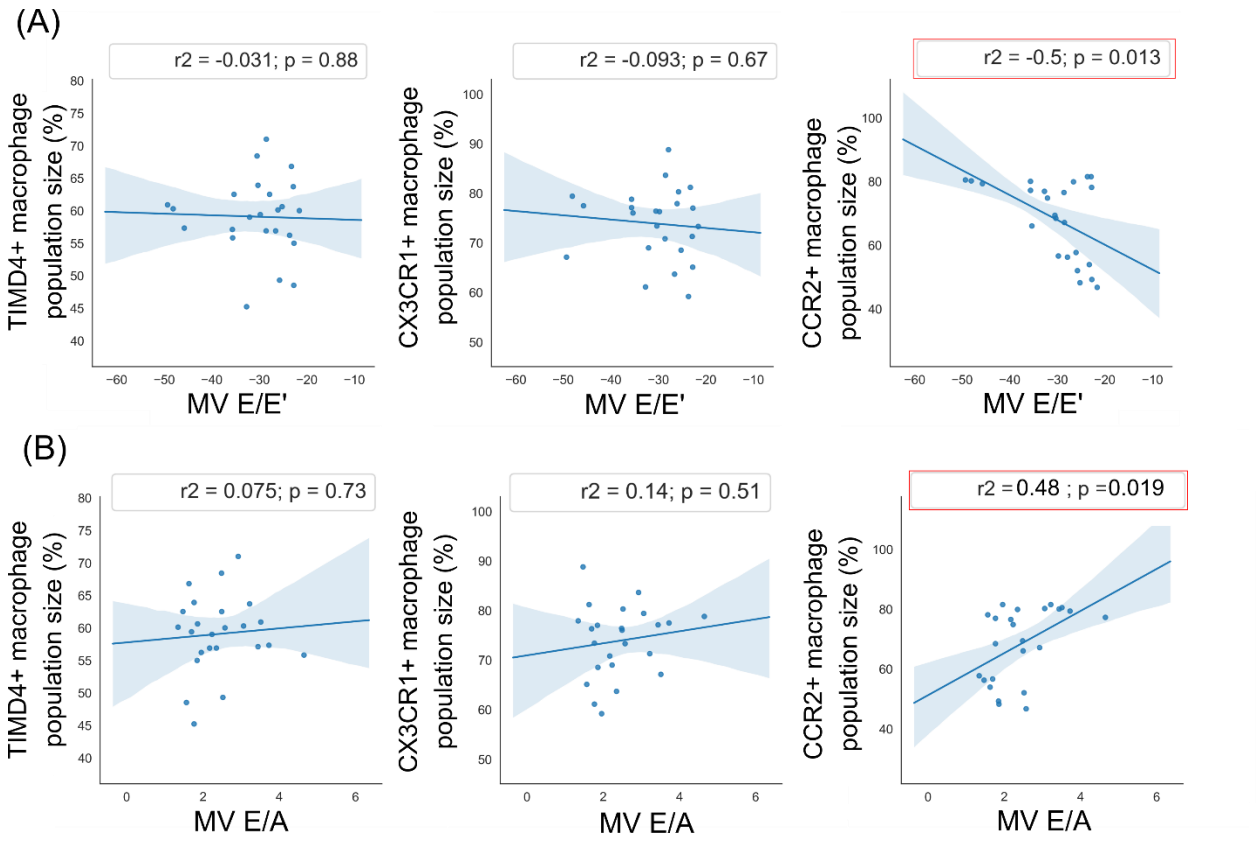

Figure 21 - Increased CCR2+ macrophage population fractions correlate with reduced MV E/e' ratios and increased MV E/A ratios. (A) Regression of measured MV E/e' ratio and **(B)** MV E/A ratio against TIMD4, CX3CR1, and CCR2 macrophage population percentage of the total resident macrophage compartment as determined by flow cytometry. Linear regression coefficient of determination and p-values reported for each regression. Linear fit is represented by dark blue line with model confidence interval depicted in light blue overlay. Individual points represented as points overlaid on plot. Significant correlations highlighted in red boxes.

A significant positive correlation was observed between increased CCR2+ macrophage subset size and decreased MV E/e' ratios (Figure 21A). CCR2+ macrophage fraction size was also observed to exhibit a significant positive correlation with MV E/A ratios, with increasing CCR2+ macrophage fractions associated with increased MV E/A ratios (Figure 21B).

3.3.8.4 CX3CR1+ Macrophage Population Size Positively Correlates With Increased Mean Aortic Ejection Times

Aortic ejection time (AET) measurements were correlated with flow characterization derived macrophage subset size measurements to determine if the experimentally induced significant differences in AET correlated with any altered cardiac macrophage subset regulation. While no significant relationship was noted between TIMD4+ and CCR2+ macrophage subsets, a significant associated was observed following the regression of CX3CR1+ macrophage fraction size with aortic ejection time (Figure 22A).

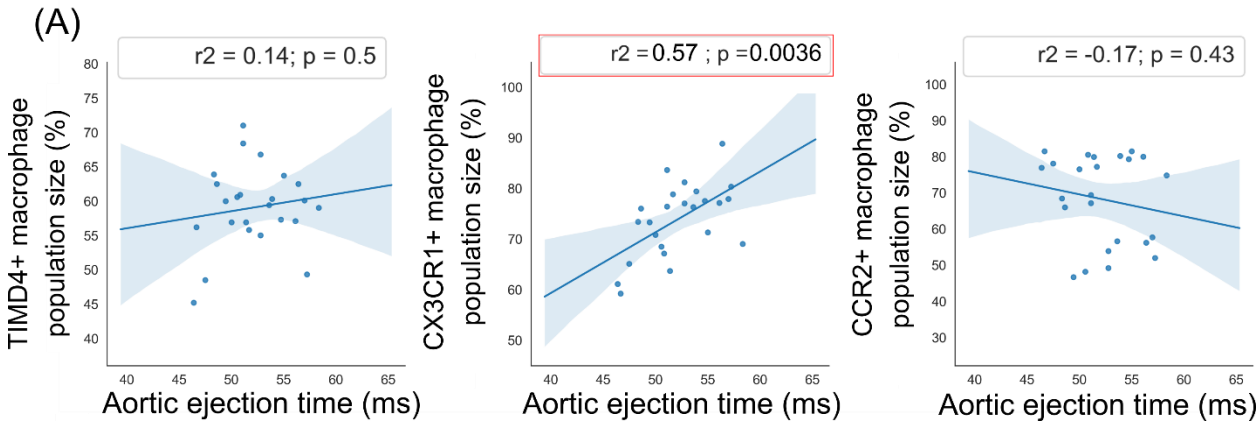

Figure 22 - Increased CX3CR1+ macrophage population fractions correlate with increased AET. (A) Regression of measured AET against TIMD4, CX3CR1, and CCR2 macrophage population percentage of the total resident macrophage compartment as determined by flow cytometry. Linear regression coefficient of determination and p-values reported for each regression. Linear fit is represented by dark blue line with model confidence interval depicted in light blue overlay. Individual points represented as points overlaid on plot. Significant correlations highlighted in red boxes.

It was observed that increased mean aortic ejection time was associated with increased mean CX3CR1+ macrophage subset size within the F4/80+CD11b+ cardiac macrophage population.

3.3.8.5 Increased CCR2+ Macrophage Fractions Positively Correlate With Decreased Cardiac Tissue Elasticity

Global circumferential strain (GCS) and global longitudinal strain (GLS) are two measurements of cardiac tissue deformation which can be acquired with speckle-tracing echocardiography to infer details about cardiac tissue elasticity. In order to better understand how differences in observed cardiac deformation correlate with differential macrophage subset regulation, GCS and GLS values were regressed against flow characterized macrophage TIMD4, CX3CR1, and CCR2 macrophage subset size (Figure 23A, B).

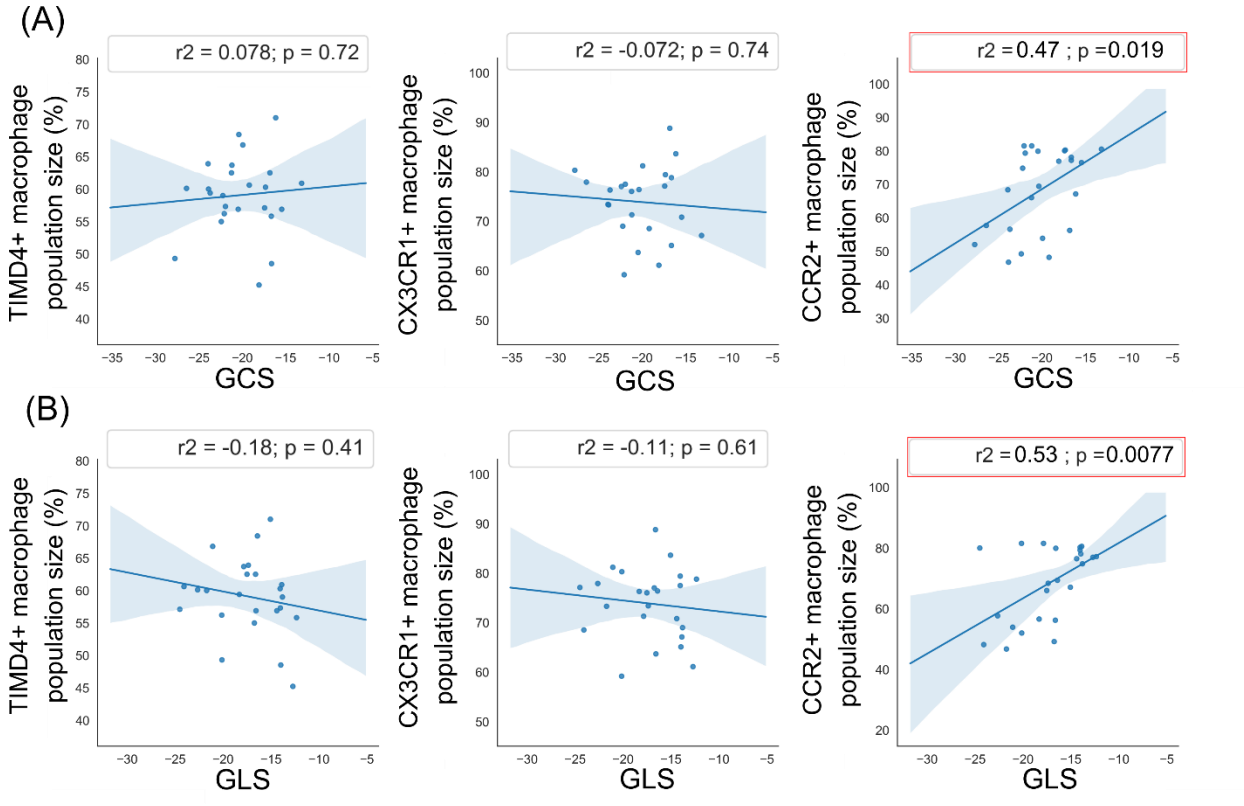

Figure 23 - Increased CCR2+ macrophage population fractions correlate with reduced ventricular GCS and GLS. (A) Regression of measured left ventricle GCS and **(B)** GLS against the TIMD4, CX3CR1, and CCR2 macrophage population percentage of the total resident macrophage compartment as determined by flow cytometry. Linear regression coefficient of determination and p-values reported for each regression. Linear fit is represented by dark blue line with model confidence interval depicted in light blue overlay. Individual points represented as points overlaid on plot. Significant correlations highlighted in red boxes.

While no significant association between TIMD4+ or CX3CR1+ macrophage subset size and cardiac deformation was observed, a significant correlation between both CCR2+ macrophage subset fraction and GCS as well as CCR2+ macrophage subset size and GLS was observed (Figure

23A, B). As GCS and GLS represent deformation measurements which become increasingly negative with increased cardiac tissue deformation, moving left to right along the x-axis in Figure 23A and Figure 23B represent reduced cardiac tissue deformation in the circumferential and longitudinal directions, respectively. It was observed that CCR2+ macrophage fraction size positively correlates with reduced circumferential and longitudinal cardiac tissue deformation, suggesting that increases in CCR2+ cardiac macrophages correlate with reduced cardiac tissue elasticity (Figure 23A, B).

3.4 Ald+Salt Model of Cardiac Microenvironmental Remodeling Demonstrates a Significantly Altered Regulation of Cardiac Macrophage Subsets Relative to Controls

While the described *in vitro* model of cardiac microenvironmental change provided a platform for decoupling the relative contributions of both altered cardiac extracellular matrix composition and biomechanics, the described model only reproduced a fraction of the complexity of the *in vivo* cardiac microenvironmental remodeling response. Therefore, the described *in vivo* model was developed to characterize the cardiac macrophage subset population size and phenotypic response to changing cardiac microenvironments, with a focus on comparing the ability of the described model to recapitulate the hallmark changes commonly observed in the aged cardiovascular microenvironment.

With increasing age, the cardiac microenvironment undergoes compositional remodeling resultant of changing physiological tissue oxygen needs or altered tissue biomechanical properties. In order to sustain or increase cardiac output and maintain sufficient systemic tissue perfusion, cardiomyocytes within the left ventricle hypertrophy to increase cardiac contractile strength - in

turn maintaining or improving cardiac output. While this hypertrophic response may not be associated with reduced cardiac function when induced by exercise, non-exercise induced cardiomyocyte hypertrophy is generally associated with a progressive decline in cardiac function (Boyle et al., 2011).

In addition to a noted increase in cardiomyocyte hypertrophy, increasing age is also associated with changes in matrix protein content which occur as resident cardiac cell behavior is altered in response to changing microenvironmental cues. Increases in left ventricular wall pressures can promote fibroblast to myofibroblast phenotypic conversion and increased secretion of fibrillar collagen proteins into the extracellular space (Biernacka & Frangogiannis, 2011; Fan et al., 2012). Additionally, increasing age has been shown to be associated with an altered secretion of matrix proteins into the cardiac extracellular space, including some increased matricellular protein expression (Frangogiannis, 2012). Matricellular proteins generally exhibit upregulation around areas of cardiac tissue damage or active remodeling. Thus, these expression patterns are likely a result of the important role matricellular proteins play both in mediating the interaction between different matrix proteins as well as in promoting altered cell migratory behavior.

In addition to matrix protein compositional remodeling, aged cardiac microenvironments can also exhibit an increased degree of enzymatic and non-enzymatic crosslinking of matrix proteins relative to cardiac microenvironments in young individuals (Horn & Trafford, 2016). Non-enzymatically, matrix proteins can be crosslinking through the interactions of glycosylated amino acid residues. These glycosylated protein crosslinks - collectively referred to as advanced glycation end products (AGEs) - are commonly observed in hyperglycemic microenvironments, and are generally long-term protein crosslinks (Hartog et al., 2007). In addition to non-enzymatic crosslinking mechanisms, many enzymes are capable of modifying matrix protein amino acid

residues in a manner which induces matrix protein crosslinking. One such protein which is important in the collagen fibril enzymatic crosslinking response is lysyl oxidase, which mediates collagen fibril crosslinking through free amine oxidation on accessible lysine residues in collagen peptides (Heck, Faccio, Richter, & Thony-Meyer, 2013).

Taken together, these mechanisms of cardiac tissue remodeling provide the cardiovascular system with the ability to maintain cardiac output in response to changing systemic oxygen consumption demands or physiological state. In addition to the direct structural support role cardiac matrix remodeling plays in maintaining cardiac output, cardiac microenvironmental remodeling also alters resident cell function in a manner which further promotes cardiac output maintenance. However, as in the case of non-exercise induced cardiomyocyte hypertrophy, many of these alterations in cell function provide support in the short term, but ultimately contribute to the long-term dysregulation of cardiac function. While the results of the *in vitro* experiments described above suggest that the characterized age-related changes in cardiac microenvironment which occur with increasing age would reduce homeostatic function and increase pro-inflammatory phenotypic regulation; a full characterization of the impacts of age-related cardiac microenvironmental modeling on cardiac resident macrophages remains to be performed. Additionally, characterization of these dynamics in a physiological aging model alone would fail to decouple the impacts of cell intrinsic aging processes from microenvironmental induced alterations in cell function. Thus, an additional *in vivo* model was developed, cardiac function was evaluated, and the resident macrophage compartment was characterized to help decouple cell intrinsic mechanisms of reduced function from microenvironmental induced dysfunction.

3.4.1 D-Aldosterone Minipump Implantation Coupled With 1% NaCl Drinking Water Administration Induces Cardiac Microenvironmental Remodeling Characterized by Increased Cardiomyocyte Hypertrophy and Increased Perivascular Fibrosis

Two hallmark remodeling responses observed in aged cardiac tissue microenvironments are cardiomyocyte hypertrophy and increased perivascular fibrotic matrix deposition (Biernacka & Frangogiannis, 2011; Gerstenblith et al., 1977; K. Sharma & Kass, 2014; Silver et al., 1990). When comparing quantified mean cardiomyocyte areas and perivascular collagen deposition in Masson's trichrome stained cardiac tissue sections from 5-month age control mice or 5-month aged mice implanted with a D-Aldosterone loaded minipump and given 1% NaCl drinking water for the duration of minipump implant (Ald+Salt), a significant increase in cardiomyocyte hypertrophy and perivascular collagen deposition was observed in trichrome stained Ald+Salt cardiac sections. This remodeling response characterization was also supported qualitatively by brightfield Masson's trichrome and picrosirius red stained cardiac section images. Quantification of collagen birefringence with polarized light imaging of picrosirius red stained sections also suggested that an increased composition of thick collagen fibers in Ald+Salt cardiac sections relative to age-matched controls. These results, taken together, suggest that the designed experimental *in vivo* model successfully induced cardiac microenvironmental remodeling features similar to those observed in advanced developmental age cardiac microenvironments - including reproduction of hallmark cardiomyocyte hypertrophy, perivascular fibrotic collagen matrix deposition, and an increased number of thick collagen fibers present within the tissue microenvironment.

3.4.1.1 D-Aldosterone Minipump Implantation Coupled With 1% NaCl Drinking Water Administration Induced Cardiac Microenvironmental Remodeling Was Associated With Increased Mean Isovolumic Relaxation Times and Increased Mean Left Ventricular Wall Dimensions As Measured by Echocardiography

While cardiac imaging modalities are increasingly capable of non-invasively quantifying extracellular matrix remodeling in cardiac tissue, the resolution with which these changes can be quantified to as well as the degree to which these changes correlate with altered cardiac function requires additional study (Pinkert et al., 2018). Thus, the present study sought to couple echocardiographic assessment of murine cardiac function with the described microenvironmental characterization to better understand how matrix protein deposition correlates with altered cardiac functional parameter measurements. Generally, as left ventricular tissue remodels with increasing age and tissue elasticity decreases, several alterations in cardiac functional parameters can be characterized with echocardiography (Chang et al., 2014; Daimon et al., 2008; Gerstenblith et al., 1977; Levy et al., 1988; Nagueh et al., 2016; Xu & Daimon, 2016). Ventricular hypertrophy can be partially evaluated with echocardiography through the measurement of left ventricular posterior and anterior wall dimensions in systole and diastole. Additionally, mitral value doppler flow imaging can provide insight regarding cardiac diastolic function and inference regarding tissue elasticity. With increasing age, mitral valve early to late filling rate ratios (MV E/A) generally decline as impaired tissue relaxation following systole attenuates the rate of early left ventricular filling rate (E) and late filling rate (A) filling during atrial contraction is increasingly responsible for maintaining systolic volume within the left ventricle. In addition to the characterized MV E/A ratio alterations, age-related diastolic dysfunction can also alter the ratio of mitral valve early filling rates (E) to mitral valve early annular tissue velocity (e') ratio (MV E/e'). Generally, this

alteration will be characterized by a reduction in the measured mitral valve early annular tissue velocity (e') as ventricular elasticity decreases, subsequently increasing the measured MV E/e' ratio.

A significant increase in both mean isovolumic relaxation time (IVRT) and mean aortic ejection time (AET) was observed in Ald+Salt treatment group mice relative to age-matched controls. Additionally, non-significant increases in mean left ventricular anterior and posterior wall dimensions were characterized in Ald+salt murine cardiac tissue relative to controls. Taken together, these results support the quantified cardiomyocyte hypertrophy measured in Ald+salt Masson's trichrome cardiac sections as well as demonstrate the promotion of some impairment of ventricular relaxation in Ald+salt treatment group mice. However, mitral valve flow imaging results did not fully recapitulate the entirety of changes which have been characterized with echocardiography in aged populations. In particular, Ald+salt treatment was not found to reduce measured MV E/A ratios or to decrease MV E/e' ratios relative to age-matched controls. Given the characterized increase in cardiomyocyte hypertrophy and perivascular collagen deposition in Ald+Salt cardiac tissue, the observed increased mean IVRT without observed mitral valve flow imaging parameter measurements may be due to the compensatory remodeling response partially normalizing parameter measurements relative to controls. Alternatively, these results may suggest that the time course over which the cardiac remodeling was experimentally induced was not sufficient to fully induce all previously characterized echocardiography parameter measurement changes. Future studies may seek to develop a model which couples a longer D-Aldosterone minipump infusion and 1% NaCl drinking water treatment duration with repeat echocardiographic imaging over that period to determine if the time course of cardiac remodeling is associated with the manner in which echocardiography parameter changes present.

3.4.1.2 D-Aldosterone Minipump Implantation Coupled With 1% NaCl Drinking Water Administration Induced Cardiac Microenvironment Remodeling Promotes CX3CR1+ Macrophage Subset Expansion

D-Aldosterone minipump implant coupled with 1% NaCl drinking water treatment was found to be associated with significant changes to the cardiac microenvironment relative to age-matched controls. When the macrophage compartment within the CD45+ viable cell fraction isolated from Ald+salt cardiac tissue was characterized with flow cytometry, a significant increase in both the size of the F4/80+CD11b+ macrophage population within the CD45+ viable cell population as well as in CX3CR1 expression in F4/80+CD11b+ macrophages was observed. Additionally, when examining the relative composition of each resident macrophage subset in Ald+Salt cardiac cell isolates, it was observed that surface marker expression patterns most closely resembled the patterns of expression observed in highly aged (24mo) control cardiac tissue cell isolates.

Several interesting observations stem from the characterized macrophage compartment regulation in both control and Ald+Salt cardiac cell isolates. In previous studies examining the age-related regulation of the cardiac macrophage population from post-natal to 30 weeks of age time points, a reduction of CX3CR1+ macrophages and an increase in mean CCR2+ expression was observed in cardiac macrophages (Molawi et al., 2014; Pinto et al., 2014). A similar result can be observed by comparing 1-month control and 5-month control cardiac cell isolates characterized in this study, where cardiac macrophages initially exhibit more robust CX3CR1 and TIMD4 expression, which is then replaced by CCR2 expression with increasing time. However, characterization of the regulation of the cardiac macrophage subset surface marker expression in moderately aged (12 month) and advanced age (18-24 month) control cardiac cell isolates suggests

that CCR2 expression increases in macrophage populations may not occur indefinitely. Instead, some equilibrium in subset size regulation was observed from moderate to advance age in control cell isolates with minor decreases in CCR2 expression and slight increases in CX3CR1 expression noted from 5 month to 24 months of age. However, it is not clear if this increase in CX3CR1 expression at moderate and advanced age time points relative to 5-month controls is due to proliferation of resident macrophages seeded during development or phenotypic change coupled with loss of CCR2 expression in monocyte-derived macrophages.

This characterized expansion in CX3CR1+ macrophages observed at moderate or advanced age is also interesting when considered within the time course of observed cardiac matrix remodeling in mice. In Figure 3, a slight mean qualitative and quantitative increase in collagen deposition can be noted by 12 months of age and is further increased by 24 months of age in murine cardiac tissue. In a similar manner, *in vivo* Ald+salt treatment induced both increased mean collagen deposition as well as promoted the expansion of CX3CR1+ macrophages. While not definitive proof of the fibrotic remodeling response promoted CX3CR1 macrophage subset expansion, the parallels in expansion of this subset around the period of increased collagen deposition in physiologically aged control tissue as well as in Ald+Salt treatment remodeled cardiac tissue is interesting and necessitates further study. Future studies may seek to isolate CX3CR1+ macrophages from cardiac tissue with flow cytometry for culture in the described *in vitro* model to better understand the role this macrophage subsets plays in conjunction with cardiac fibroblast populations in promoting the cardiac fibrotic remodeling response.

3.4.1.3 Exploring the Relationship Between CX3CR1+ Macrophage Populations and Fibrotic Disease Progression

While not evaluated in a cardiovascular disease specific context, there is some evidence derived from other organs to suggest not only a role for CX3CR1+ macrophages in fibrotic or chronic inflammatory disease progression, but also a potential for pharmacological inhibition of CX3CL1-CX3CR1 signaling to attenuate this disease progression (Mizutani et al., 2021; Y. Tanaka et al., 2020). Rheumatoid arthritis, a chronic autoimmune condition which causes joint deterioration, had been shown to exhibit some age-related increase in disease incidence (Crowson et al., 2011). Interestingly, murine models of rheumatoid arthritis pathology progression suggest an essential role for CX3CR1+ immune cells - including CX3CR1+ macrophage populations - in promoting chronic inflammatory cell activation within joint synovial microenvironments; resulting in the subsequent degradation of these environments due to chronic MMP enzyme secretion and osteoclast mediated bone resorption induced by these CX3CR1+ immune cells (Brennan & McInnes, 2008; Nanki et al., 2004; Y. Tanaka et al., 2020). Pharmacological inhibition of CX3CL1-CX3CR1 signaling was also shown to improve arthritis disease severity scores in rheumatoid mice and attenuate synovial tissue degradation (Hoshino-Negishi et al., 2019; Y. Tanaka et al., 2020). Further studies in murine models of rheumatoid arthritis performed in humanized TNFα mice which do not express CCR2 confirmed the role that non-classical monocyte extravasation and subsequent differentiation into macrophages within synovial tissue microenvironments plays in the progression of rheumatoid arthritis (Puchner et al., 2018; Y. Tanaka et al., 2020). Studies examining CX3CL1 serum concentrations in human rheumatoid arthritis patients have also identified a significant positive correlation between circulating CX3CL1 concentrations and arthritis disease severity (Odai et al., 2009).

CX3CL1-CX3CR1 signaling has also been implicated in the pathogenesis of pulmonary fibrosis through the selective recruitment of alternatively activated, CX3CR1+ macrophages into the pulmonary microenvironment (Ishida et al., 2017). In a murine model of pulmonary fibrosis induced by intratracheal bleomycin injection which causes injuries similar to those observed in human idiopathic pulmonary fibrosis, genetic ablation of CX3CR1 was found to be associated with reduced pulmonary fibrocyte accumulation, reduced TGF-β expression, and reduced pulmonary collagen deposition relative to wild type mice (Ishida et al., 2017). Additionally, pharmacological inhibition of CX3CL1 signaling was recently demonstrated to attenuate pulmonary interstitial fibrotic matrix deposition in an SKG murine model (Mizutani et al., 2021).

CX3CR1+ macrophage and monocyte cell populations have also been demonstrated to play a role in atherosclerotic disease progression (Ensan et al., 2016; J. D. Lin et al., 2019; H. Liu & Jiang, 2011). Arterial macrophages first arise during embryological development and exhibit robust CX3CR1 expression (Ensan et al., 2016). The next wave of arterial tissue macrophage colonization occurs immediately post-birth and relies primarily on CX3CR1+ bone marrow monocyte extravasation and differentiation into macrophages within the arterial tissue microenvironment (Ensan et al., 2016). RNA-sequencing of CX3CR1+ progenitor cell-derived arterial macrophages has identified a significant heterogeneity in gene expression within this cell population, including both M1- and M2-like macrophage populations within the larger CX3CR1+ progenitor-derived macrophage population (J. D. Lin et al., 2019). It was also found that differing CX3CR1+ progenitor-derived macrophage subsets uniquely correlated with either atherosclerotic plaque progression or regression (J. D. Lin et al., 2019). Additionally, some phenotypic heterogeneity was observed within both the progression- and regression-associated CX3CR1+ macrophage subsets, with characterized macrophages exhibiting features of both type I and type

II immune response-induced gene expression (J. D. Lin et al., 2019). This suggests that the prior characterized association of M1 macrophage phenotype with atherosclerotic disease progression and M2 macrophage phenotype with disease regression may be too simplistic, and that plaque progression or regression depends more upon certain CX3CR1+ macrophage subpopulations rather than certain macrophage phenotypes (Cochain et al., 2018; J. D. Lin et al., 2019).

These results demonstrate a capacity for CX3CR1+ macrophage subpopulations within the heart to play a role in the observed increased collagen deposition which occurs within the remodeling cardiac microenvironment either with increasing age or following Ald+Salt experimental intervention (Figure 1, Figure 9). These results also suggest that CX3CL1-CX3CR1 signaling pathway inhibition may have potential to attenuate pathological cardiovascular fibrotic matrix deposition (Ishida et al., 2017; Mizutani et al., 2021). Finally, these results highlight the importance of acquiring measures of organ function in addition to macrophage phenotypic quantification, as macrophage M1 or M2 polarization may correlate with both disease progression and regression (J. D. Lin et al., 2019).

3.4.1.4 D-Aldosterone Minipump Implantation Coupled With 1% NaCl Drinking Water Administration Induced Cardiac Microenvironment Remodeling Promotes a Phenotypic Shift in All Characterized Resident Subsets Characterized by Increased CD86 Expression and Reduced CD206 Expression

With increasing age, a general increase in the transcription of inflammation associated genes and secretion of pro-inflammatory cytokines, such as TNF-α or IL-6, can be observed both within systemic circulation as well as within various tissue microenvironments. This general increase in pro-inflammatory cytokine secretion coupled with increasingly chronic inflammatory cell activation observed in aged individuals, coined ‘inflamm-aging’, can be partially attributable

for the age-related risk of pathology development such as in the case of rheumatoid arthritis. In cardiac tissue, increased pro-inflammatory immune cell signaling has been shown to be associated with deleterious tissue remodeling and reduced function following cardiac tissue injury (Lavine et al., 2014; Shirazi, Bissett, Romeo, & Mehta, 2017).

A significant increase in pro-inflammatory CD86 expression coupled with a significant decrease in alternative activation-associated CD206 expression was observed in all macrophage subsets characterized in Ald+Salt cardiac cell isolates, suggesting that the altered cardiac microenvironmental conditions promoted increased M1-like phenotypes in macrophage subsets. This phenotypic biasing is similar to that observed in the *in vitro* model characterization, where it was observed that increased culture substrate stiffness promoted increased M1 phenotype-associated function and reduced M2-associated functional capacity. However, it is important to note that while this phenotype inference by M1 or M2-associated surface marker expression characterization is useful for inferring macrophage phenotype and function; macrophage polarization tends to exhibit more intermediary phenotypes *in vivo* and often exhibit expression of both M1 and M2 associated surface markers (Cochain et al., 2018; Dick et al., 2019). Consequently, phenotype and functional inference based upon flow characterization of CD86 and CD206 alone may be insufficient to fully capture the gene expression pattern complexity within cardiac resident macrophage subsets. Future studies may seek to utilize additional characterization methodologies such as RNA sequencing of flow separated resident macrophage subsets to more completely quantify the experimentally induced alterations in macrophage gene expression and more accurately infer the functional consequences of that regulation.

Additionally, it is important to note the partial confounding effect that macrophage phenotypic biasing induced by aldosterone-mediated macrophage mineralocorticoid receptor

activation plays in the flow cytometry characterized macrophage phenotypes (Fraccarollo et al., 2019; Usher et al., 2010). However, the observed phenotypic biasing of all characterized resident macrophage subsets in Ald+Salt experimental groups further supports prior evidence suggesting the potential efficacy of cardiac macrophage mineralocorticoid receptor block on attenuating deleterious fibrotic matrix deposition following cardiac tissue injury (Fraccarollo et al., 2019).

3.4.1.5 qRT-PCR Characterization of Gene Regulation in Remodeling Cardiac Tissue Supports the Characterized Histological Remodeling Response and the Characterized Phenotypic Shift in Macrophage Populations

In addition to flow characterization-based inference regrading macrophage phenotype regulation in Ald+salt cardiac tissue microenvironments, qRT-PCR quantification of differential gene expression patterns in pro-inflammatory gene expression in whole cardiac RNA isolates from Ald+Salt and 5 month control cardiac tissue help provide inference regarding the inflammatory state of the cardiac tissue microenvironment following remodeling. Consistent with the altered macrophage phenotype observed in Ald+Salt cell isolates, Ald+Salt cardiac RNA isolates exhibited an increased transcription of inflammation associated genes, including *Il1β*, *Il6*, and *Tnfa*. In many cases, this increased transcription of pro-inflammatory genes not only mirrored the characterized increase observed in advanced age control cardiac RNA isolates but often exceeded advanced age RNA isolates in expression levels of pro-inflammatory genes.

In addition to supporting the observed phenotypic shift in resident macrophage populations following Ald+Salt treatment, qRT-PCR analysis of Ald+Salt RNA isolates demonstrated a significantly increased expression of matrix protein as well as matrix modulatory protein gene expression. Ald+salt treatment was found to both increase expression of fibrillar collagen subunit protein *Col1a1* as well as promote *Mmp2*:*Timp1* expression ratios reminiscent of those observed

in RNA isolates derived from advanced age cardiac tissue. Coupled with the characterized increase in perivascular collagen deposition and well as the increased presence if thick collagen fibers in Ald+Salt cardiac tissue sections, the observed increased in fibrillar collagen protein subunit gene expression demonstrates a significant induction and sustained deposition of fibrillar collagen within the Ald+Salt remodeling myocardium. Additionally, the characterized alteration in the relative expression of *Mmp2* transcripts to *Timp1* transcripts suggests that Ald+Salt and advanced age cardiac microenvironments exhibit increased inhibition of collagen protein degradation by MMP-mediated mechanisms.

A significant increase in *Ccl2* transcripts was also observed in Ald+Salt cardiac RNA isolates when compared to age-matched controls. CCL2 functions as a primary monocyte chemoattractant protein responsible for promoting extravasation of bone marrow-monocytes from circulation. This significant upregulation in monocyte chemoattractant protein expression is interesting given the decrease in CCR2 expression noted within the cardiac macrophage populations when characterized by flow, but the increase in CCR2 expression observed when evaluated by immunolabeling quantification. This result may suggest that initial cardiac remodeling promotes CX3CR1 macrophage expansion initially, but with increasing treatment duration time – increasing CCR2 macrophage differentiation from monocyte progenitors may occur. This result may also suggest that Ald+Salt induced remodeling is promoting monocyte extravasation into cardiac tissue with a subsequent loss of CCR2 expression following macrophage differentiation. Given the increase in CCR2+ immunolabeling coupled with reduced CD45+F4/80+CD11b+CCR2+ cell population fraction, CCR2+ monocyte accumulation without subsequent macrophage differentiation may also be occurring in Ald+Salt remodeling cardiac microenvironments. Future studies which incorporate either longer Ald+Salt treatment durations

or additional lineage tracing methodologies may be able to better elucidate the temporal dynamics related to cardiac macrophage compartment regulation in response to Ald+Salt induced remodeling.

3.4.2 Inhibition of Collagen Crosslinking Through Non-reversible Lysyl Oxidase Inhibition With BAPN Was Associated With Significant Alterations in Both the Observed Remodeling and Tissue Resident Macrophage Regulation Responses

Compensatory cardiac matrix remodeling relies not only upon increased matrix deposition within the extracellular space but also on various mechanisms of matrix protein crosslinking to confer sufficient tensile strength and prevent left ventricular wall rupture during periods of increased physiological pressures. Lysyl oxidase is one such enzyme responsible for collagen lysine residue modification and subsequent collagen fibril crosslinking. While some evidence has suggested that lysyl oxidase inhibition may attenuate cardiomyocyte hypertrophy as well as perivascular collagen deposition following ventricular pressures overload, the impacts of altering the cardiac microenvironmental remodeling response to pressures overload through inhibition of matrix crosslinking on the cardiac macrophage subsets resident to that microenvironment was unclear.

3.4.2.1 While Lysyl Oxidase Inhibition Attenuated the Cardiac Compensatory Remodeling Response, Measurement of Cardiac Functional Parameters With Echocardiography Suggested Increased Cardiac Tissue Dysfunction

Quantification of perivascular collagen deposition in mice which were treated with lysyl oxidase inhibitor BAPN prior to D-Aldosterone minipump implant coupled with 1% NaCl

drinking water treatment (Ald+Salt+BAPN) demonstrated no significant mean difference from either control or Ald+Salt in mean positive percent expression of collagen. However, it was noted that the mean quantified collagen positivity percentage in perivascular regions of cardiac tissue sections was greater than control values but less than that quantified in Ald+Salt cardiac sections, suggesting some inhibition of collagen deposition in perivascular regions in BAPN treated animals relative to non-BAPN Ald+Salt mice. This result reflects similarly observed inhibition of perivascular collagen deposition when lysyl oxidase functionality is attenuated in the pressure overloaded ventricle (Martinez-Martinez et al., 2016).

Additionally, a decrease in mean cardiomyocyte area was observed in BAPN treated animals relative to Ald+Salt mice given no BAPN treatment. When compared to control cardiomyocyte measurements, the quantified mean Ald+Salt+BAPN murine cardiomyocyte area was observed to significantly increase. Taken together, these results demonstrate how Ald+Salt treatment induced varying degrees of cardiomyocyte hypertrophy relative to age-matched controls, with the hypertrophic response relying partially on lysyl oxidase functionality within the remodeling myocardium.

Considered independently, these two results would suggest an attenuation of what is often considered deleterious left ventricular pressure induced remodeling. However, assessment of cardiac function with echocardiography suggested BAPN-mediated inhibition of lysyl oxidase activity worsened cardiac function relative to both Ald+Salt and control mice. BAPN treated mice exhibited significant declines in ejection fraction and fractional shortening. BAPN treatment was also associated with a significant observed increase in mean left ventricular systolic diameter and volume. When examining the alterations in mitral flow doppler resultant of BAPN-mediated lysyl oxidase inhibition, both significantly increased mean mitral valve early to late wave filling rate

ratios (MV E/A) as well as significantly decreased mitral valve early filling rate to early tissue annular velocity ratios (MV E/e').

Taken together, these alterations observed in cardiac functional parameter measurements in BAPN treated mice suggest that inhibition of the lysyl oxidase mediated compensatory remodeling response to left ventricular pressure overload attenuates histologically characterized deleterious microenvironmental remodeling but worsens systolic and diastolic cardiac function. As hyperaldosteronism and chronic NaCl administration promotes increased systemic pressures, the cardiac compensatory remodeling response is induced to maintain cardiac output. Thus, while lysyl oxidase inhibition may improve histological metrics often associated with deleterious fibrotic matrix remodeling, without this compensatory remodeling response providing important short-term protection against pressure induced dilative cardiomyopathy cardiac dysfunction may occur closer to the onset of altered physiological stimulus.

3.4.2.2 Inhibition of Cardiac Compensatory Remodeling Was Observed to Not Significantly Alter Cardiac Macrophage Compartment Regulation From That Observed in Control Cardiac Microenvironments

In addition to altered matrix remodeling characteristics resultant of BAPN treatment observed in Ald+Salt+BAPN cardiac histological analysis, an altered regulation of the resident macrophage compartment in Ald+Salt+BAPN cardiac cell isolates was observed. Macrophage subset distribution in Ald+Salt+BAPN cardiac cell isolates was found to largely resemble the subset distribution characterized in age-matched control cell isolates. This may suggest several things regarding the macrophage subsets regulation dynamics in compensatory remodeling cardiac tissue. In Ald+Salt cardiac cell isolates, a general upregulation of CX3CR1+ macrophage subsets was observed while a slight decrease in CCR2+ subsets within the F4/80+CD11b+ macrophage

fraction was observed. In addition, a significant upregulation in monocyte chemoattractant protein-1/CCL2 gene transcripts was observed in Ald+Salt cardiac RNA isolates. In Ald+Salt+BAPN cardiac cell isolates, a large upregulation of CCR2+ macrophages within the F4/80+CD11b+ macrophage population was observed. This may suggest that the initial compensatory remodeling response is largely reliant upon either local proliferation of CX3CR1+ cardiac macrophages or monocyte recruitment with subsequent differentiation into CX3CR1+ macrophages, while the later stages of pressure overload induced cardiac microenvironmental remodeling promote increasing CCR2+ macrophage subsets.

However, the observed preservation or further accumulation of CCR2+ macrophages within the cardiac resident macrophage compartment in Ald+Salt+BAPN cardiac tissue may also be resultant of dilative remodeling-associated alterations in the function of other cardiac resident cell populations. Additionally, the question of macrophage subset ontogeny for CX3CR1+ macrophages persist within this model, and further elucidation regarding the respective contributions of embryonic macrophage self-proliferation as compared to monocytic differentiation into CX3CR1+ macrophages within the myocardium will help demonstrate the role microenvironment plays in promoting macrophage phenotype as compared to cell ontogeny.

3.4.3 A Discussion of the Cardiac Macrophage Population Dynamics Which Correlate With Changes in Cardiac Echocardiographic Functional Parameters

In order to better understand if the hypothesized macrophage subset regulation dynamics proposed to occur in myocardium following advanced age-associated cardiac matrix remodeling correlate with measured alterations in cardiac tissue function, echocardiographic parameter measurements were regressed against the characterized cardiac resident macrophage

compartments. The first correlation of note identified was the relationship between murine cardiac output and either the size of the TIMD4+ macrophage subset or the size of the CCR2+ macrophage subset. TIMD4+ macrophages, which are often derived from embryological macrophage precursor cells and exhibit alternative activation-like phenotypes, were observed to positively correlate with cardiac output. Conversely, a significant negative association was noted between the CCR2+ macrophage population size and measured cardiac output. These results further support the role of embryologically derived macrophage subsets in promoting the maintenance of homeostatic maintenance, while accumulation of bone marrow monocyte derived CCR2+ macrophages is associated with cardiac output attenuation.

CCR2+ macrophage subset fraction size was also observed to correlate with measured global circumferential strain (GCS) and global longitudinal strain (GLS) rates. While no significant differences in GCS or GLS was observed between experimental treatment groups, a significant positive associated was found between increased CCR2+ macrophage size and reduced cardiac circumferential or longitudinal deformation. This positive association between increased CCR2+ macrophage population fraction and decreased cardiac deformation (here denoted by increases in GCS or GLS which are negative vector quantities measured from the left ventricular chamber wall outward) suggest that as cardiac tissue stiffens and is less able to deform, CCR2+ macrophages comprise an increasingly large fraction of the resident macrophage population.

While the size of the CCR2+ macrophage fraction was observed to correlate with several echocardiographic parameter measurement changes generally indicative of increasing cardiac dysfunction, a significant negative association between CCR2+ macrophage subset size and measured isovolumic relaxation times was observed. Increased isovolumic relaxation times are commonly observed in patients exhibiting grade II diastolic dysfunction and often correlate with

increased fibrotic matrix deposition in the cardiac extracellular space. Instead, a significant positive association between the CX3CR1+ cardiac macrophage population size and increased mean isovolumic relaxation times was observed. This may suggest either a differential regulation of macrophage subsets based upon diastolic cardiac dysfunction disease state progression, where earlier grade diastolic dysfunction is characterized by a proliferation of CX3CR1+ macrophage subsets while later grade diastolic dysfunction is characterized by CCR2+ macrophage accumulation, or a differential regulation of subset surface marker expression patterns induced by differing microenvironmental cues.

The temporal progression of subset regulation with changing diastolic dysfunction disease grade presents an interesting hypothesis given the characterized alternatively activation-associated phenotypic bias of this macrophage subset. Alternatively activated (M2) macrophages are generally associated with a matrix modulatory functionality and increased secretion of matrix modulatory function associated growth factors, such as that of TGF-β (B. N. Brown et al., 2017). The observed upregulation of CX3CR1+ subsets in early diastolic dysfunction may be important for support of the compensatory remodeling response to pressure overload. This potential role of CX3CR1+ macrophage subsets in regulating the fibrotic matrix remodeling response has also been observed in murine models of pulmonary fibrosis and atherosclerosis, providing further evidence of a potential role for this macrophage subset in the early cardiac remodeling response (Cochain et al., 2018; Ishida et al., 2017).

However, as function increasingly declines, increased fractions of resident macrophages are derived from more pro-inflammatory biased bone marrow monocyte populations, and promotion of alternative activation-associated phenotypes is attenuated. This hypothesis is partially supported by the characterized significant increase in *Ccl2* gene expression in Ald+Salt

cardiac RNA isolates relative to age-matched controls, which might represent an early stage of CCR2+ monocyte recruitment to increasingly stiff cardiac tissue (Figure 18). However, an increase in CCR2+ cell immunolabeling was also observed in Ald+Salt cardiac sections relative to age-matched controls, suggesting that monocytes are being recruited to cardiac tissue but are either losing CCR2 expression following differentiation or are remaining CCR2+ monocytes within the cardiac tissue microenvironment (Figure 17). This hypothesized accumulation of non-differentiating monocytes has recently been identified in atherosclerotic arterial tissue, where a population of self-proliferating monocytes was found during RNA sequencing of inflamed arterial tissue (J. D. Lin et al., 2019). Further experiments which utilize lineage tracing or RNA sequencing experimental methodologies may better elucidate whether these characterized dynamics in subset expansion relative to progressively declining cardiac diastolic function are resultant of altered proliferation dynamics of macrophages derived from unique precursor cells or from the microenvironment induced alteration of cell surface marker expression.

3.4.4 Interactions of Cardiac Resident Macrophages With the Cardiac Extracellular Microenvironment

Microenvironmental stimuli – including those derived from pathogens, tissue damage, stress, biomechanics, or altered resident cell secretome – are essential determinants of macrophage phenotype (van de Laar et al., 2016). Thus, understanding the interactions between remodeling cardiac microenvironments and cardiac resident macrophages will be essential for understanding the macrophage-mediated component of cardiac dysfunction. Prior studies on the macrophage-mediated cardiac remodeling response to injury have focused on selective recruitment of certain cardiac resident macrophage subsets with subsequent characterization of the cardiac tissue

microenvironment following selective macrophage subset enrichment (Dick et al., 2019; Lavine et al., 2014). These studies have not only demonstrated the importance of CX3CR1+ cardiac macrophage subsets in promoting beneficial cardiac tissue remodeling following infarction, but also the potential for CCL2-CCR2 signaling pathway inhibition in improving cardiac tissue remodeling by preventing CCR2+ monocyte extravasation (Dick et al., 2019; Lavine et al., 2014). These studies provide strong evidence of the role that cardiac resident macrophages play in regulating the tissue microenvironmental remodeling response.

However, it is also important to consider how differing cardiac tissue microenvironments may select for different macrophage subset recruitment or proliferation. The present study approaches this question by examining how experimental manipulation of cardiac microenvironmental remodeling can promote the expansion of different cardiac macrophage subsets. In this model, Ald+Salt induced cardiac remodeling was found to induce a cardiac compensatory remodeling response which was accompanied by a reduction in CCR2+ cardiac macrophages and an expansion of CX3CR1+ macrophages. This resulted in some increased mean isovolumic relaxation times in Ald+Salt animals, but cardiac function was found to be largely maintained relative to controls. However, when lysyl oxidase function was disrupted with BAPN treatment, the cardiac compensatory remodeling response was also disrupted; and Ald+Salt+BAPN animals were observed to exhibit increased systolic and diastolic cardiac dysfunction relative to both control and Ald+Salt mice. This increased dysfunction also correlated with a different pattern of cardiac resident macrophage subset regulation, with CCR2+ macrophages being the largest observed macrophage subset within the cardiac resident macrophage population in Ald+Salt+BAPN cardiac cell isolates.

This characterized regulation provides an interesting parallel with prior work demonstrating the cardioprotective tissue remodeling responses following CX3CR1+ resident macrophage expansion in post-myocardial infarction cardiac remodeling (Dick et al., 2019; Lavine et al., 2014). Additionally, the results of this study characterized an expansion of CCR2+ macrophages in Ald+Salt+BAPN cardiac microenvironments, where lysyl oxidase inhibition disrupted compensatory remodeling and induced increased systolic and diastolic dysfunction. A significant negative relationship between the size of the CCR2+ macrophage population and the measured murine ejection fraction was also identified. This relationship between CCR2+ macrophage population size and ejection fraction reflects some of the previously reported results of post-myocardial infarction tissue remodeling studies, where CCR2+ macrophage subset expansion was associated with infarct scar spreading and attenuated cardiac function (Dick et al., 2019; Lavine et al., 2014). These results help highlight both the importance of cardiac resident macrophage-extracellular microenvironment interactions in the cardiac tissue remodeling response to stress or damage as well as how manipulation of these interactions can promote altered cardiac tissue remodeling responses – which can then in turn either improve or further attenuate cardiac function (Dick et al., 2019; Lavine et al., 2014)

4.0 Conclusions

4.1 Summary of Results

4.1.1 An *In Vitro* Model to Assess the Impacts of Cardiac Microenvironmental Change on Macrophage Phenotype and Function

The goal of the described *in vitro* model was to develop a culture system which could be utilized to assess the macrophage response to differing cardiac-specific microenvironmental conditions and to compare the macrophage response to *in vitro* microenvironments similar to young cardiac microenvironments or to advanced age cardiac microenvironments. To accomplish this, a culture model utilizing poly-dimethyl-siloxane hydrogels of varying relevant physiological stiffness coated with decellularized cardiac extracellular matrix isolated from either young developmental age or advanced developmental age murine donors was developed and macrophages were seeded onto the various culture substrates. Both culture substrate stiffness as well as the developmental age of the donor from which the extracellular matrix coating was derived were determined to have a significant impact on macrophage phenotype and function. Additionally, culture substrates stiffness was found to significantly alter seeded macrophage morphology. Increased culture substrate stiffness was found to promote macrophage morphologies previously associated with pro-inflammatory stimulated macrophage populations, increased functional M1 macrophage responses following Th1 cytokine treatment, and a significant attenuation of anti-inflammatory macrophage function following Th2 cytokine stimulation. Conversely, macrophage culture on substrates with elastic moduli closer to that observed in young

cardiac tissue promoted reduced pro-inflammatory phenotype-associated morphologies in cultured macrophages as well as reduced pro-inflammatory functional responses relative to macrophages cultured on substrates with elasticity similar to advanced age myocardium.

When examining the role that decellularized cardiac extracellular matrix coating played in altering the observed macrophage phenotypic and functional responses, a general attenuation of both pro- and anti-inflammatory macrophage functional capacity following pro-inflammatory (IFN-γ + LPS) or anti-inflammatory (IL-4) stimuli was observed in cultured macrophages. This general attenuation of macrophage pro- or anti-inflammatory functional capacity was also supported by qRT-PCR analysis of gene expression patterns in cultured macrophage RNA isolates; where macrophage culture with decellularized cardiac extracellular matrix isolated from advanced age cardiac tissue was observed to be associated with reduced expression of canonical M1- or M2-associated genes following pro- (IFN-γ + LPS) or anti-inflammatory (IL-4) stimuli, respectively. Additionally, qRT-PCR analysis of macrophage culture with decellularized cardiac extracellular matrix from advanced age individuals was noted to be associated with some non-canonical regulation of the macrophage phenotype associated genes, including the noted large increase in macrophage *Nos2* expression following M2 stimuli (IL-4) treatment in macrophages cultured with decellularized extracellular matrix from advanced age individuals.

These results suggest several important features about the macrophage response in aged individuals. These results suggest that aged microenvironments promote dysregulation of canonical M1 and M2 polarization responses following pro- or anti-inflammatory stimuli, respectively. These results also suggests that the timely attenuation of M1 macrophage polarization with a conversion toward M2 phenotypes, which is an essential feature of functional biomaterial-tissue integration or tissue repair responses following damage, may be impaired in advanced age

individuals. The lack of baseline alternative activation observed in macrophages cultured with cECM isolated from aged individuals also suggests a reduced ability to promote constructive remodeling in aged microenvironments. Additionally, as the tissue microenvironment remodels with increasing age and experiences an increase in stiffness, the results of the described *in vitro* study suggest that macrophage pro-inflammatory functional responses to M1 stimuli will increase in intensity while alternatively activated function will be reduced. However, it is also important to note that the interaction of matrix composition and biomechanics is more complex *in vivo*, and the macrophage response to these changing matrix conditions may not fully be recapitulated *in vitro* without inclusion of additional cell populations or signaling cues.

4.1.2 An *In Vivo* Model to Determine the Role of Age-related Changes in Cardiac Matrix Remodeling in Promoting Altered Regulation of the Cardiac Tissue Resident Macrophage Compartment

The goal of the described *in vivo* model was to assess the role of microenvironmental change as a mechanism underlying the characterized age-related changes in cardiac resident macrophage subset regulation. To accomplish this, a model of chronic osmotic minipump infusion of D-Aldosterone coupled with 1% NaCl drinking water supplementation was developed to recapitulate the age-related cardiac microenvironmental remodeling features in a developmentally young age murine cardiac microenvironment. Significant murine cardiomyocyte hypertrophy, significant increases in perivascular collagen deposition, and an observed increase in the presence of thick collagen fibrils was observed following experimental treatment. Coupled with the observed increase in left ventricular wall dimension measurements and increased mean isovolumic relaxation times quantified with echocardiography, these results suggest that the experimental

intervention was successful in inducing the desired advanced age-associated cardiac microenvironmental remodeling features which in turn induced several cardiac functional alterations often observed in advanced age individuals exhibiting diastolic dysfunction.

When examining the impacts of aldosterone infusion and salty drinking water mediated cardiac microenvironmental remodeling on the regulation of cardiac resident macrophage subsets, it was observed that aldosterone infusion coupled with 1% NaCl drinking water treatment induced an altered regulation of the cardiac tissue resident macrophage compartment relative to age-matched controls. When comparing this regulation to the macrophage subset regulation characterized in control cardiac cell isolates derived from mice aged 1 month, 5 months, or 24 months, the relative composition of macrophage subsets observed in D-aldosterone+1%NaCl drinking water cardiac cell isolates most closely reflected the composition observed in cardiac cell isolates from 24-month cardiac tissue. These results suggest that the described *in vivo* model was successful in demonstrating the role that age-related cardiac microenvironmental remodeling plays in promoting an altered regulation of the cardiac resident macrophage compartment.

This altered macrophage compartment regulation was also noted to be accompanied by increased expression of pro-inflammatory, stress-associated, or matrix remodeling associated gene transcripts relative to age-matched controls. This observed mean increase in pro-inflammatory gene transcript expression in Ald+Salt cardiac RNA isolates reflects the characterized mean increases in inflammation-associated gene expression characterized in advanced age cardiac RNA isolates. Additionally, *in vitro* and *in vivo* qRT-PCR analysis of *Tgfb* expression in young and advanced age cardiac RNA isolates demonstrated a mean increase in *Tgfb* expression with increasing age; an increase which was also observed in Ald+Salt cardiac RNA isolates relative to age-matched controls.

4.2 Clinical Relevancy of Results

Cardiovascular disease is a heterogenous class of pathologies often characterized by dysfunction in several resident cardiac cell subsets, which in turn attenuates cardiac tissue function. While cardiovascular disease therapeutic efficacy has improved, limited therapies exist for advanced stage cardiac organ dysfunction and often patients are reliant upon donor cardiac tissue availability for treatment. In addition to issues in treatment availability imposed by limited donor tissue, an increase in aged population demographic size in the United States necessitates understanding the mechanisms underlying cardiovascular disease pathology – particularly the age-associated risk for development of this pathology.

Cardiac tissue resident macrophages have been recently identified as important mediators of both homeostatic cardiac function as well as cardiac tissue remodeling following tissue damage (Epelman et al., 2014; Fujiu et al., 2017; Hulsmans et al., 2017; Lavine et al., 2014). Heterogeneity in macrophage cell origin was also noted within the cardiac resident macrophage pool, with some significant impacts on macrophage phenotype and function being correlated with cell developmental origin (Epelman et al., 2014). The resident macrophage population heterogeneity was also noted to not be static, exhibiting some alterations in subset population size with increasing age (Molawi et al., 2014; Pinto et al., 2014). However, the mechanisms underlying this shift in subset regulation required further study. Thus, the present study sought to better characterize the changes in macrophage phenotype and function induced by cardiac microenvironmental remodeling to provide further insight into any mechanistic role that altered cardiac resident macrophage phenotype and function has in promoting cardiac pathology development.

4.2.1 Understanding the Microenvironmental-mediated Mechanisms of Macrophage Subset Phenotypic and Functional Regulation Can Help Develop Strategies to Promote Constructive Tissue Remodeling and Improve Tissue Function Following Cardiac Injury

Many cardiac tissue pathologies are characterized by a dysregulation of tissue microenvironmental function following prolonged periods of altered physiological stresses or tissue damage. This damage or stress attenuates the ability of cardiac tissue to maintain sufficient cardiac output without tissue microenvironmental remodeling. For example, following myocardial infarction-related injury to cardiac tissue, left ventricular tissue undergoes rapid deposition of fibrillar collagen scar tissue in the region of cardiomyocyte necrosis to prevent left ventricular wall rupture. Following initial collagen scar deposition, further cardiac tissue remodeling occurs in the border zones between the deposited scar tissue and the healthy myocardium in the subsequent days following infarction. While the initial collagen scar tissue deposition serves an important function in preventing left ventricular wall rupture following cardiomyocyte necrosis, border zone remodeling can attenuate cardiac tissue function over time and eventually necessitate the need for organ transplant due to cardiac failure.

A similar example can be observed in the case of heart failure with preserved ejection fraction (HFpEF) cardiac tissue remodeling. Initially, cardiac tissue remodeling occurs as a response to prolonged changes in physiological state, such as prolonged elevations in systemic blood pressure. This initially compensatory remodeling response - here characterized by increased cardiomyocyte hypertrophy, increased deposition of fibrillar collagen within the cardiac microenvironment, and upregulated secretion of matrix-remodeling associated matricellular proteins in the extracellular space – serves an important function in maintaining cardiac output.

However, with increasing time, prolonged cardiac tissue remodeling increasingly attenuates resident cardiac cell function and contributes to diastolic dysfunction. In both the case of post-myocardial infarction border zone remodeling as well as HFpEF-associated remodeling, the initial cardiac remodeling response serves an important function of preserving cardiac output but chronic activation of these tissue remodeling pathways following the initial remodeling response can lead to systolic or diastolic cardiac dysfunction.

4.2.2 Different Cardiac Resident Macrophage Subsets Promote Different Patterns of Matrix Protein Deposition and Cardiac Functional Recovery Following Myocardial Infarction

The interactions of cardiac resident macrophage and fibroblast cell populations following myocardial infarction are important determinants of the border region myocardial remodeling response (Jugdutt, 2003). Within the cardiac macrophage compartment, preferential expansion of macrophage populations which derive from embryonic precursors has been shown to be associated with attenuated border region remodeling, reduced systemic pro-inflammatory cytokine secretion, and improved cardiac function following myocardial infarction (Dick et al., 2019; Lavine et al., 2014). Conversely, embryonic precursor-derived cardiac macrophage depletion with subsequent extravasation and colonization of the empty cardiac tissue niche by CCR2+, bone marrow monocyte-derived resident macrophages has been shown to be associated with increased ischemic scar area resultant of chronic fibrotic border region remodeling, increased pro-inflammatory cytokine secretion, and increased rates of systolic heart failure development (Dick et al., 2019; Lavine et al., 2014).

The results of the described *in vitro* and *in vivo* models can help further develop this understanding of the macrophage mediated component of the cardiac tissue remodeling response following myocardial infarction to better identify targets for therapeutic intervention. First, the characterized changes in cardiac resident macrophage population subset size in advanced developmental age cardiac tissue suggest that aged individuals may be more likely to exhibit deleterious remodeling responses following ischemic cardiac tissue injury due to the decline in LYVE1+/TIMD4+ resident macrophages and the subsequent increase in CCR2+ monocyte-derived macrophages. Correlation studies performed for the described *in vivo* model identified a significant negative correlation of CCR2+ monocyte-derived macrophage subset fraction size and cardiac systolic function. Additionally, a significant positive association of TIMD4+ macrophage subset size and cardiac systolic function was noted. Taken together, these results suggest that either timely attenuation of CCR2+ macrophage accumulation in cardiac tissue or promotion of phenotypes more closely reflective of those observed in embryologic precursor-derived macrophages following myocardial infarction may serve as potential therapeutic targets to limit adverse remodeling following ischemic injury.

In the case of promoting embryonic precursor-derived phenotypes in monocyte-derived macrophage populations, further study regarding the relative contributions of precursor cell identity and microenvironmental stimuli as contributors of macrophage phenotype throughout an organism's lifespan will be necessary. While some evidence suggests embryonic derived macrophage precursors self-maintain within tissue niches and monocytes are not able to fully recapitulate these cells once lost, it is unclear if this is a consequence of the unique identity of the precursors cells from which these macrophages derive or a consequence of the differing tissue niches each precursor resides in during the different stages of hematopoiesis (Dick et al., 2019;

Epelman et al., 2014; Ginhoux & Guilliams, 2016; Hoeffel & Ginhoux, 2018). Thus, it will be necessary to further elucidate the differences in gene expression and regulation between primitive hematopoiesis erythro-myeloid progenitors and definitive hematopoiesis stem cell progenitors to better understand if re-inducing embryonic-like gene expression in monocyte derived macrophages can be accomplished in advanced age individuals.

In addition to cell intrinsic mechanistic study of gene regulation between unique developmental origin macrophage subsets, further examination of the macrophage phenotypic and functional response to varying microenvironmental stimuli will help to identify the role that microenvironment plays in macrophage proliferation and phenotype induction for each resident macrophage subset. The described *in vitro* model has demonstrated feasibility in evaluating macrophage morphological, phenotypic, and functional responses to varying cardiac specific microenvironmental stimuli. Derivation and culture of erythro-myeloid progenitor derived macrophage populations within the described *in vitro* model would help further identify mechanisms by which microenvironment may alter the proliferation and function of yolk sac progenitor-derived macrophage populations. Additionally, these studies may help elucidate the optimal microenvironmental conditions for expansion and promotion of constructive remodeling associated phenotypes in yolk sac progenitor-derived cardiac macrophages; providing further therapeutic guidance for optimal cardiac microenvironmental conditions for macrophage-mediated constructive matrix remodeling.

4.2.3 The Results of the *In Vivo* Model Suggest Inhibition of Lysyl Oxidase-mediated Crosslinking May Attenuate Ald+Salt Induced Alterations in Cardiac Resident

Macrophage Subset Regulation, but the Efficacy of This Intervention During Acute Periods of Physiological Stress May Limit Therapeutic Applicability

When comparing cardiac resident macrophage subset regulation following implant of D-Aldosterone loaded minipump coupled with 1% NaCl drinking water administration either with or without BAPN-mediated lysyl oxidase inhibition, it was generally noted that BAPN administration promoted cardiac macrophage subset regulation most closely reflective of that observed in control cardiac macrophage populations. However, a noted decrease in cardiac tissue systolic function was observed in the mice given BAPN prior to experimental treatment. These results suggest that while pharmacological alteration of the cardiac matrix remodeling response can be utilized to alter regulation of cardiac resident macrophages, inhibition of compensatory remodeling - if not accompanied with pharmacological management of hemodynamics - can ultimately worsen cardiac function. This attenuation of cardiac function was noted to likely develop due to dilated cardiomyopathy-related cardiac tissue remodeling resultant of increased physiological blood pressure coupled with a reduced compensatory crosslinking capacity.

4.2.4 The Relationship Between Observed Clinical Cardiac Remodeling Response Following Left Ventricular Assist Device (LVAD) Implant and the Characterized Experimental Relationship Between Cardiac Microenvironment and Resident Macrophage Subset Regulation

Left ventricular assist devices serve as important clinical cardiovascular support tools for advanced stage heart failure patients who require either bridge-to-transplant, bridge-to-recovery, or destination therapy support. Early studies on patient cardiac function following LVAD implant

suggested LVAD support was associated with reduced left ventricular volumes and leftward shifts in measured left ventricular pressure-volume (P-V) loops relative to pre-LVAD implant (Burkhoff, Topkara, Sayer, & Uriel, 2021; Levin, Oz, Catanese, Rose, & Burkhoff, 1996; Madigan et al., 2001). Further characterization of LVAD support associated change in cardiomyocyte function following device implant demonstrated an increase in cardiomyocyte contractility, rearrangement of cytoskeletal proteins to more closely reflect non-pathological cytoskeletal arrangements, alteration of cardiomyocyte metabolism, and increased cardiomyocyte proliferation (Burkhoff et al., 2021; Dipla, Mattiello, Jeevanandam, Houser, & Margulies, 1998; Gupte et al., 2014; Wohlschlaeger et al., 2010; Zafeiridis, Jeevanandam, Houser, & Margulies, 1998). Within the noncardiomyocyte cell fraction, LVAD device implant was found to be associated with endothelial cell activation with improvements in cardiac micro- and macro-vasculature noted (Ambardekar et al., 2018; Drakos et al., 2010). LVAD support was also noted to alter regulation of cardiac macrophage populations following device implant, with LVAD support generally being noted to attenuate some pro-inflammatory cytokine secretion and promote CCR2+ macrophage extravasation (Bajpai et al., 2018; Burkhoff et al., 2021).

LVAD treatment was also noted to be associated with some altered regulation of extracellular matrix protein deposition, with increased collagen fibril content and increased extent of collagen crosslinking noted in post-LVAD treatment cardiac tissue (Bruggink et al., 2006; Klotz et al., 2005; Y. Y. Li et al., 2001). This either maintenance or increase in collagen deposition following LVAD treatment was noted to likely result from a reduced expression of matrix metalloprotease enzymes as well as increased tissue inhibitor of metalloprotease enzyme expression (Burkhoff et al., 2021; Y. Y. Li et al., 2001). The degree to which this characterized myocardial fibrotic matrix deposition correlates with the degree to which myocardial performance

is recovered following the start of LVAD support remains unclear, although some evidence has suggested that the degree of cardiac tissue fibrosis at the time of LVAD implant correlates with patient outcomes (Bruckner et al., 2004; Burkhoff et al., 2021; Oriyanhan et al., 2007; Redfern et al., 2000).

The observed relationship between cardiac tissue microenvironment and macrophage phenotype and function evaluated in the described *in vitro* and *in vivo* models can provide some additional insight regarding the impacts of LVAD support on the cardiac tissue resident macrophage compartment. First, the observed decrease in pro-inflammatory macrophage responses following culture on substrates of reduced stiffness in the presence of pro-inflammatory stimuli may account for the characterized reduction of pro-inflammatory cardiac tissue gene expression following LVAD-mediated ventricular unloading (Burkhoff et al., 2021; Torre-Amione et al., 1999). Additionally, evaluation of the naïve macrophage response to advanced developmental age cardiac extracellular matrix coating *in vitro* suggest that aged cardiac microenvironments attenuate the baseline anti-inflammatory phenotypes observed in young cardiac extracellular matrix culture groups and also attenuate canonical gene responsivity to M1 or M2-associated signaling cues. Taken together, these anti-inflammatory and phenotype supporting effects of cardiac matrix derived from young individuals may partially explain the improved recovery rate of young individuals relative to aged individuals following LVAD therapy (Burkhoff et al., 2021).

In vivo model results also suggest a potential role for LVAD support-mediated cardiac microenvironmental remodeling in promoting the observed altered resident macrophage subset regulation. For example, a significant difference in macrophage subset regulation was noted when matrix crosslinking through lysyl oxidase enzymatic pathways was inhibited by BAPN treatment

when compared to Ald+Salt cardiac isolates not given BAPN treatment. When characterizing this regulation, it was noted that this altered subset composition most closely reflected that previously characterized in control, 5 month cardiac cell isolates; suggesting inhibition of matrix protein crosslinking attenuated Ald+Salt treatment-associated changes in resident macrophage subset composition.

In a similar manner, a difference in resident macrophage subset accumulation within cardiac tissue microenvironments was observed following mechanical ventricular unloading with LVAD support (Bajpai et al., 2018; Burkhoff et al., 2021). Taken together, these results demonstrate how as the cardiac microenvironment undergoes biochemical and mechanical alterations with pathology or therapeutic intervention the resident macrophage compartment experiences altered subset regulation. Interestingly, some of the hallmarks of LVAD support-mediated microenvironmental remodeling were noted in the Ald+Salt+BAPN condition, including decreased cardiomyocyte hypertrophy and increased collagen deposition. These common microenvironmental alterations were also noted to correlate with increased CCR2+ macrophage fraction size, although a divergent functional response consequent of this CCR2+ macrophage accumulation was noted between LVAD studies and the described *in vivo* model (Bajpai et al., 2018; Burkhoff et al., 2021). This divergent functional response can likely be attributed to additional differences between microenvironmental conditions resultant of organismal physiological state, as LVAD supported patients often receive additional pharmacological support to provide optimal hemodynamic support while Ald+salt and Ald+salt+BAPN animals did not receive any pharmacological blood pressure suppression or support. However, these observed characterization results together provide evidence of a microenvironment mediated regulation of the cardiac resident macrophage compartment. Additionally, prior studies demonstrating the

beneficial cardiac functional outcomes following myocardial infarction when specific cardiac resident macrophage subset expansion is promoted, suggesting that unloading pathological myocardium in a manner which promotes expansion of beneficial remodeling associated macrophage subsets may provide a therapeutic strategy for improving recovery rates in heart failure patients following LVAD implant.

4.3 Implications of Study Results for Biomaterial Design and Fabrication

Biomaterials are an important component of many currently utilized clinical therapeutics which serve to support patients suffering from a myriad of cardiovascular pathologies. In general, biomaterial selection for an implantable device depends upon the requisite mechanical properties needed for device function, the duration of the implant, and the antigenicity of the material. For long term implantable cardiovascular therapeutics, materials which exhibit robust physical strength with minimal cellular antigenicity are generally selected to minimize the host response to the implanted material. The host response to implanted cardiac biomaterials can generally be characterized by an activation of the innate immune system with a subsequent fibroblast mediated deposition of fibrillar collagen matrix at the device-tissue interface. In cases where this host response does occur, device function may be compromised due to fibrotic matrix encapsulation of the material. One example of matrix encapsulation-based device failure can be observed in pacemaker devices, in which fibrotic matrix encapsulation of device lead materials can impede proper electrical signal transduction.

Increasingly, biomimetic and cardiovascular tissue derived biomaterial therapeutics have been developed or incorporated into existing therapeutics to improve the treatment

biocompatibility and host immune response. However, limited allogenic human cardiac tissue sources for therapeutic treatment generation exist and are often limited to non-transplant viable cardiac tissue. Consequently, xenogeneic or allogeneic non-transplant viable cardiac tissue must be utilized for the generation of these therapeutics. Thus, understanding how altered cardiac tissue composition promotes altered macrophage phenotype may help identify best practices for extracellular matrix material sourcing and decellularization for biomaterial-based therapeutic development.

In the described *in vitro* model, several significant features which may have important implications for the cardiovascular biomaterial therapeutic field were identified. The first significant feature noted was the promotion of alternative activation phenotype associated gene expression at baseline in young ECM treated macrophages. Additionally, young cardiac extracellular matrix treatment was observed to support the upregulation of genes associated with the canonical M1 or M2 phenotypic response following Th1 or Th2 cytokine treatment, respectively. These results taken together indicate that cardiac extracellular matrix biomaterial therapeutics derived from young developmental age cardiac tissue may assist with functional integration of biomaterials within the cardiac tissue microenvironment through promotion of alternative activation associated phenotypes in resident macrophage populations. As timely immune response resolution following biomaterial implant has been shown to be associated with better biomaterial functional integration, one can see how materials or coatings which are able to help promote this phenotypic shift in resident macrophage populations may in turn experience better tissue integration and sustained functionality within that microenvironment (B. N. Brown et al., 2017).

In addition, the observed increase in pro-inflammatory macrophage response with accompanying attenuation of alternative activation associated macrophage function in response to culture upon substrates of increased stiffnesses suggest that biomaterial therapeutics which can mimic the mechanics of young myocardium may promote more constructive macrophage phenotypes and assist in attenuating any chronic pro-inflammatory macrophage polarization. While this consideration is only applicable to materials which do not require supraphysiological mechanical properties for function, these observed macrophage responses will be applicable for the increasing number of regenerative therapeutics which rely on polymeric or extracellular matrix derived hydrogels for growth factor or cell delivery to injured myocardium.

Bibliography

Abreu, J. G., Ketpura, N. I., Reversade, B., & De Robertis, E. M. (2002). Connective-tissue growth factor (CTGF) modulates cell signalling by BMP and TGF-beta. *Nat Cell Biol, 4*(8), 599-604. doi:10.1038/ncb826

Adlerz, K. M., Aranda-Espinoza, H., & Hayenga, H. N. (2016). Substrate elasticity regulates the behavior of human monocyte-derived macrophages. *Eur Biophys J, 45*(4), 301-309. doi:10.1007/s00249-015-1096-8

Ahmed, M. S., Oie, E., Vinge, L. E., Yndestad, A., Oystein Andersen, G., Andersson, Y., . . . Attramadal, H. (2004). Connective tissue growth factor--a novel mediator of angiotensin II-stimulated cardiac fibroblast activation in heart failure in rats. *J Mol Cell Cardiol, 36*(3), 393-404. doi:10.1016/j.yjmcc.2003.12.004

Ajami, B., Bennett, J. L., Krieger, C., Tetzlaff, W., & Rossi, F. M. (2007). Local self-renewal can sustain CNS microglia maintenance and function throughout adult life. *Nat Neurosci, 10*(12), 1538-1543. doi:10.1038/nn2014

Akira, S., Uematsu, S., & Takeuchi, O. (2006). Pathogen recognition and innate immunity. *Cell, 124*(4), 783-801. doi:10.1016/j.cell.2006.02.015

Alliot, F., Lecain, E., Grima, B., & Pessac, B. (1991). Microglial progenitors with a high proliferative potential in the embryonic and adult mouse brain. *Proc Natl Acad Sci U S A, 88*(4), 1541-1545. doi:10.1073/pnas.88.4.1541

Ambardekar, A. V., Weiser-Evans, M. C. M., Li, M., Purohit, S. N., Aftab, M., Reece, T. B., & Moulton, K. S. (2018). Coronary Artery Remodeling and Fibrosis With Continuous-Flow Left Ventricular Assist Device Support. *Circ Heart Fail, 11*(5), e004491. doi:10.1161/CIRCHEARTFAILURE.117.004491

Ashkar, S., Weber, G. F., Panoutsakopoulou, V., Sanchirico, M. E., Jansson, M., Zawaideh, S., . . . Cantor, H. (2000). Eta-1 (osteopontin): an early component of type-1 (cell-mediated) immunity. *Science, 287*(5454), 860-864. doi:10.1126/science.287.5454.860

Aurora, A. B., Porrello, E. R., Tan, W., Mahmoud, A. I., Hill, J. A., Bassel-Duby, R., . . . Olson, E. N. (2014). Macrophages are required for neonatal heart regeneration. *J Clin Invest, 124*(3), 1382-1392. doi:10.1172/jci72181

Babic, A. M., Chen, C. C., & Lau, L. F. (1999). Fisp12/mouse connective tissue growth factor mediates endothelial cell adhesion and migration through integrin alphavbeta3, promotes endothelial cell survival, and induces angiogenesis in vivo. *Mol Cell Biol, 19*(4), 2958-2966. doi:10.1128/MCB.19.4.2958

Babic, A. M., Kireeva, M. L., Kolesnikova, T. V., & Lau, L. F. (1998). CYR61, a product of a growth factor-inducible immediate early gene, promotes angiogenesis and tumor growth. *Proc Natl Acad Sci U S A, 95*(11), 6355-6360. doi:10.1073/pnas.95.11.6355

Baicu, C. F., Zhang, Y., Van Laer, A. O., Renaud, L., Zile, M. R., & Bradshaw, A. D. (2012). Effects of the absence of procollagen C-endopeptidase enhancer-2 on myocardial collagen accumulation in chronic pressure overload. *Am J Physiol Heart Circ Physiol, 303*(2), H234-240. doi:10.1152/ajpheart.00227.2012

Bajpai, G., Schneider, C., Wong, N., Bredemeyer, A., Hulsmans, M., Nahrendorf, M., . . . Lavine, K. J. (2018). The human heart contains distinct macrophage subsets with divergent origins and functions. *Nat Med, 24*(8), 1234-1245. doi:10.1038/s41591-018-0059-x

Ball, D. K., Surveyor, G. A., Diehl, J. R., Steffen, C. L., Uzumcu, M., Mirando, M. A., & Brigstock, D. R. (1998). Characterization of 16- to 20-kilodalton (kDa) connective tissue growth factors (CTGFs) and demonstration of proteolytic activity for 38-kDa CTGF in pig uterine luminal flushings. *Biol Reprod, 59*(4), 828-835. doi:10.1095/biolreprod59.4.828

Ballotta, V., Driessen-Mol, A., Bouten, C. V., & Baaijens, F. P. (2014). Strain-dependent modulation of macrophage polarization within scaffolds. *Biomaterials, 35*(18), 4919-4928. doi:10.1016/j.biomaterials.2014.03.002

Bankhead, P., Loughrey, M. B., Fernandez, J. A., Dombrowski, Y., McArt, D. G., Dunne, P. D., . . . Hamilton, P. W. (2017). QuPath: Open source software for digital pathology image analysis. *Sci Rep, 7*(1), 16878. doi:10.1038/s41598-017-17204-5

Barry, S. T., Ludbrook, S. B., Murrison, E., & Horgan, C. M. (2000). A regulated interaction between alpha5beta1 integrin and osteopontin. *Biochem Biophys Res Commun, 267*(3), 764-769. doi:10.1006/bbrc.1999.2032

Bartneck, M., Heffels, K. H., Pan, Y., Bovi, M., Zwadlo-Klarwasser, G., & Groll, J. (2012). Inducing healing-like human primary macrophage phenotypes by 3D hydrogel coated nanofibres. *Biomaterials, 33*(16), 4136-4146. doi:10.1016/j.biomaterials.2012.02.050

Barzilai, N., Huffman, D. M., Muzumdar, R. H., & Bartke, A. (2012). The critical role of metabolic pathways in aging. *Diabetes, 61*(6), 1315-1322. doi:10.2337/db11-1300

Beaudin, A. E., Boyer, S. W., Perez-Cunningham, J., Hernandez, G. E., Derderian, S. C., Jujjavarapu, C., . . . Forsberg, E. C. (2016). A Transient Developmental Hematopoietic Stem Cell Gives Rise to Innate-like B and T Cells. *Cell Stem Cell, 19*(6), 768-783. doi:10.1016/j.stem.2016.08.013

Biernacka, A., & Frangogiannis, N. G. (2011). Aging and Cardiac Fibrosis. *Aging Dis, 2*(2), 158-173.

Birk, D. E. (2001). Type V collagen: heterotypic type I/V collagen interactions in the regulation of fibril assembly. *Micron, 32*(3), 223-237. doi:10.1016/s0968-4328(00)00043-3

Blackburn, E. H., Greider, C. W., & Szostak, J. W. (2006). Telomeres and telomerase: the path from maize, Tetrahymena and yeast to human cancer and aging. *Nat Med, 12*(10), 1133-1138. doi:10.1038/nm1006-1133

Blakney, A. K., Swartzlander, M. D., & Bryant, S. J. (2012). The effects of substrate stiffness on the in vitro activation of macrophages and in vivo host response to poly(ethylene glycol)-based hydrogels. *J Biomed Mater Res A, 100*(6), 1375-1386. doi:10.1002/jbm.a.34104

Blasco, M. A. (2007). Telomere length, stem cells and aging. *Nature Chemical Biology, 3*(10), 640-649. doi:10.1038/nchembio.2007.38

Boothe, S. D., Myers, J. D., Pok, S., Sun, J., Xi, Y., Nieto, R. M., . . . Jacot, J. G. (2016). The Effect of Substrate Stiffness on Cardiomyocyte Action Potentials. *Cell Biochem Biophys, 74*(4), 527-535. doi:10.1007/s12013-016-0758-1

Bork, P. (1993). The modular architecture of a new family of growth regulators related to connective tissue growth factor. *FEBS Lett, 327*(2), 125-130. doi:10.1016/0014-5793(93)80155-n

Bornstein, P. (2009). Matricellular proteins: an overview. *J Cell Commun Signal, 3*(3-4), 163-165. doi:10.1007/s12079-009-0069-z

Bowie, A., & O'Neill, L. A. (2000). The interleukin-1 receptor/Toll-like receptor superfamily: signal generators for pro-inflammatory interleukins and microbial products. *J Leukoc Biol, 67*(4), 508-514. doi:10.1002/jlb.67.4.508

Boyd, D. F., & Thomas, P. G. (2017). Towards integrating extracellular matrix and immunological pathways. *Cytokine, 98*, 79-86. doi:10.1016/j.cyto.2017.03.004

Boyle, A. J., Shih, H., Hwang, J., Ye, J., Lee, B., Zhang, Y., . . . Lee, R. (2011). Cardiomyopathy of aging in the mammalian heart is characterized by myocardial hypertrophy, fibrosis and a predisposition towards cardiomyocyte apoptosis and autophagy. *Exp Gerontol, 46*(7), 549-559. doi:10.1016/j.exger.2011.02.010

Bradshaw, A. D. (2009). The role of SPARC in extracellular matrix assembly. *J Cell Commun Signal, 3*(3-4), 239-246. doi:10.1007/s12079-009-0062-6

Bradshaw, A. D., Baicu, C. F., Rentz, T. J., Van Laer, A. O., Boggs, J., Lacy, J. M., & Zile, M. R. (2009). Pressure overload-induced alterations in fibrillar collagen content and myocardial diastolic function: role of secreted protein acidic and rich in cysteine (SPARC) in post-synthetic procollagen processing. *Circulation, 119*(2), 269-280. doi:10.1161/CIRCULATIONAHA.108.773424

Bradshaw, A. D., Graves, D. C., Motamed, K., & Sage, E. H. (2003). SPARC-null mice exhibit increased adiposity without significant differences in overall body weight. *Proc Natl Acad Sci U S A, 100*(10), 6045-6050. doi:10.1073/pnas.1030790100

Bradshaw, A. D., Puolakkainen, P., Dasgupta, J., Davidson, J. M., Wight, T. N., & Helene Sage, E. (2003). SPARC-null mice display abnormalities in the dermis characterized by decreased collagen fibril diameter and reduced tensile strength. *J Invest Dermatol, 120*(6), 949-955. doi:10.1046/j.1523-1747.2003.12241.x

Brassart, B., Fuchs, P., Huet, E., Alix, A. J., Wallach, J., Tamburro, A. M., . . . Debelle, L. (2001). Conformational dependence of collagenase (matrix metalloproteinase-1) up-regulation by elastin peptides in cultured fibroblasts. *J Biol Chem, 276*(7), 5222-5227. doi:10.1074/jbc.M003642200

Brekken, R. A., & Sage, E. H. (2000). SPARC, a matricellular protein: at the crossroads of cell-matrix. *Matrix Biol, 19*(7), 569-580. doi:10.1016/s0945-053x(00)00105-0

Brennan, F. M., & McInnes, I. B. (2008). Evidence that cytokines play a role in rheumatoid arthritis. *J Clin Invest, 118*(11), 3537-3545. doi:10.1172/JCI36389

Brown, B. N., Haschak, M. J., Lopresti, S. T., & Stahl, E. C. (2017). Effects of age-related shifts in cellular function and local microenvironment upon the innate immune response to implants. *Semin Immunol, 29*, 24-32. doi:10.1016/j.smim.2017.05.001

Brown, B. N., Ratner, B. D., Goodman, S. B., Amar, S., & Badylak, S. F. (2012). Macrophage polarization: an opportunity for improved outcomes in biomaterials and regenerative medicine. *Biomaterials, 33*(15), 3792-3802. doi:10.1016/j.biomaterials.2012.02.034

Brown, N. J., Agirbasli, M. A., Williams, G. H., Litchfield, W. R., & Vaughan, D. E. (1998). Effect of activation and inhibition of the renin-angiotensin system on plasma PAI-1. *Hypertension, 32*(6), 965-971. doi:10.1161/01.hyp.32.6.965

Bruckner, B. A., Razeghi, P., Stetson, S., Thompson, L., Lafuente, J., Entman, M., . . . Youker, K. (2004). Degree of cardiac fibrosis and hypertrophy at time of implantation predicts myocardial improvement during left ventricular assist device support. *J Heart Lung Transplant, 23*(1), 36-42. doi:10.1016/s1053-2498(03)00103-7

Bruggink, A. H., van Oosterhout, M. F., de Jonge, N., Ivangh, B., van Kuik, J., Voorbij, R. H., . . . de Weger, R. A. (2006). Reverse remodeling of the myocardial extracellular matrix after prolonged left ventricular assist device support follows a biphasic pattern. *J Heart Lung Transplant, 25*(9), 1091-1098. doi:10.1016/j.healun.2006.05.011

Burkhoff, D., Topkara, V. K., Sayer, G., & Uriel, N. (2021). Reverse Remodeling With Left Ventricular Assist Devices. *Circ Res, 128*(10), 1594-1612. doi:10.1161/CIRCRESAHA.121.318160

Calderwood, S. K., Murshid, A., & Prince, T. (2009). The shock of aging: molecular chaperones and the heat shock response in longevity and aging--a mini-review. *Gerontology, 55*(5), 550-558. doi:10.1159/000225957

Campisi, J., & d'Adda di Fagagna, F. (2007). Cellular senescence: when bad things happen to good cells. *Nat Rev Mol Cell Biol, 8*(9), 729-740. doi:10.1038/nrm2233

Cao, H., McHugh, K., Chew, S. Y., & Anderson, J. M. (2010). The topographical effect of electrospun nanofibrous scaffolds on the in vivo and in vitro foreign body reaction. *J Biomed Mater Res A, 93*(3), 1151-1159. doi:10.1002/jbm.a.32609

Capasso, J. M., Palackal, T., Olivetti, G., & Anversa, P. (1990). Severe myocardial dysfunction induced by ventricular remodeling in aging rat hearts. *Am J Physiol, 259*(4 Pt 2), H1086-1096. doi:10.1152/ajpheart.1990.259.4.H1086

Carey, W. A., Taylor, G. D., Dean, W. B., & Bristow, J. D. (2010). Tenascin-C deficiency attenuates TGF-ss-mediated fibrosis following murine lung injury. *Am J Physiol Lung Cell Mol Physiol, 299*(6), L785-793. doi:10.1152/ajplung.00385.2009

Carlin, L. M., Stamatiades, E. G., Auffray, C., Hanna, R. N., Glover, L., Vizcay-Barrena, G., . . . Geissmann, F. (2013). Nr4a1-dependent Ly6C(low) monocytes monitor endothelial cells and orchestrate their disposal. *Cell, 153*(2), 362-375. doi:10.1016/j.cell.2013.03.010

Carlson, C. B., Lawler, J., & Mosher, D. F. (2008). Structures of thrombospondins. *Cell Mol Life Sci, 65*(5), 672-686. doi:10.1007/s00018-007-7484-1

Caulfield, J. B., Norton, P., & Weaver, R. D. (1992). Cardiac dilatation associated with collagen alterations. *Mol Cell Biochem, 118*(2), 171-179. doi:10.1007/BF00299396

Cerletti, M., Jang, Y. C., Finley, L. W., Haigis, M. C., & Wagers, A. J. (2012). Short-term calorie restriction enhances skeletal muscle stem cell function. *Cell Stem Cell, 10*(5), 515-519. doi:10.1016/j.stem.2012.04.002

Cesari, M., Pahor, M., & Incalzi, R. A. (2010). Plasminogen activator inhibitor-1 (PAI-1): a key factor linking fibrinolysis and age-related subclinical and clinical conditions. *Cardiovasc Ther, 28*(5), e72-91. doi:10.1111/j.1755-5922.2010.00171.x

Chang, W. T., Chen, J. S., Hung, Y. K., Tsai, W. C., Juang, J. N., & Liu, P. Y. (2014). Characterization of aging-associated cardiac diastolic dysfunction. *PLoS One, 9*(5), e97455. doi:10.1371/journal.pone.0097455

Chen, C., Li, R., Ross, R. S., & Manso, A. M. (2016). Integrins and integrin-related proteins in cardiac fibrosis. *J Mol Cell Cardiol, 93*, 162-174. doi:10.1016/j.yjmcc.2015.11.010

Chen, C. C., & Lau, L. F. (2009). Functions and mechanisms of action of CCN matricellular proteins. *Int J Biochem Cell Biol, 41*(4), 771-783. doi:10.1016/j.biocel.2008.07.025

Chen, N., Chen, C. C., & Lau, L. F. (2000). Adhesion of human skin fibroblasts to Cyr61 is mediated through integrin alpha 6beta 1 and cell surface heparan sulfate proteoglycans. *J Biol Chem, 275*(32), 24953-24961. doi:10.1074/jbc.M003040200

Chiquet-Ehrismann, R., Kalla, P., Pearson, C. A., Beck, K., & Chiquet, M. (1988). Tenascin interferes with fibronectin action. *Cell, 53*(3), 383-390. doi:10.1016/0092-8674(88)90158-4

Chiquet-Ehrismann, R., Tannheimer, M., Koch, M., Brunner, A., Spring, J., Martin, D., . . . Chiquet, M. (1994). Tenascin-C expression by fibroblasts is elevated in stressed collagen gels. *J Cell Biol, 127*(6 Pt 2), 2093-2101. doi:10.1083/jcb.127.6.2093

Cochain, C., Vafadarnejad, E., Arampatzi, P., Pelisek, J., Winkels, H., Ley, K., . . . Zernecke, A. (2018). Single-Cell RNA-Seq Reveals the Transcriptional Landscape and Heterogeneity of Aortic Macrophages in Murine Atherosclerosis. *Circ Res, 122*(12), 1661-1674. doi:10.1161/CIRCRESAHA.117.312509

Collins, A. R., Schnee, J., Wang, W., Kim, S., Fishbein, M. C., Bruemmer, D., . . . Hsueh, W. A. (2004). Osteopontin modulates angiotensin II-induced fibrosis in the intact murine heart. *J Am Coll Cardiol, 43*(9), 1698-1705. doi:10.1016/j.jacc.2003.11.058

Comtois, P., & Nattel, S. (2011). Interactions between cardiac fibrosis spatial pattern and ionic remodeling on electrical wave propagation. *Annu Int Conf IEEE Eng Med Biol Soc, 2011*, 4669-4672. doi:10.1109/IEMBS.2011.6091156

Conboy, I. M., & Rando, T. A. (2012). Heterochronic parabiosis for the study of the effects of aging on stem cells and their niches. *Cell Cycle, 11*(12), 2260-2267. doi:10.4161/cc.20437

Crowson, C. S., Matteson, E. L., Myasoedova, E., Michet, C. J., Ernste, F. C., Warrington, K. J., . . . Gabriel, S. E. (2011). The lifetime risk of adult-onset rheumatoid arthritis and other inflammatory autoimmune rheumatic diseases. *Arthritis Rheum, 63*(3), 633-639. doi:10.1002/art.30155

D'Agostino, R. B., Sr., Pencina, M. J., Massaro, J. M., & Coady, S. (2013). Cardiovascular Disease Risk Assessment: Insights from Framingham. *Glob Heart, 8*(1), 11-23. doi:10.1016/j.gheart.2013.01.001

Daimon, M., Watanabe, H., Abe, Y., Hirata, K., Hozumi, T., Ishii, K., . . . Investigators, J. S. (2008). Normal values of echocardiographic parameters in relation to age in a healthy Japanese population: the JAMP study. *Circ J, 72*(11), 1859-1866. doi:10.1253/circj.cj-08-0171

Daimon, M., Watanabe, H., Abe, Y., Hirata, K., Hozumi, T., Ishii, K., . . . Japanese Normal Values for Echocardiographic Measurements Project Study, I. (2011). Gender differences in age-related changes in left and right ventricular geometries and functions. Echocardiography of a healthy subject group. *Circ J, 75*(12), 2840-2846. doi:10.1253/circj.cj-11-0364

Daniels, A., van Bilsen, M., Goldschmeding, R., van der Vusse, G. J., & van Nieuwenhoven, F. A. (2009). Connective tissue growth factor and cardiac fibrosis. *Acta Physiol (Oxf), 195*(3), 321-338. doi:10.1111/j.1748-1716.2008.01936.x

Dawber, T. R., & Kannel, W. B. (1958). An epidemiologic study of heart disease: the Framingham study. *Nutr Rev, 16*(1), 1-4. doi:10.1111/j.1753-4887.1958.tb00605.x

Dawber, T. R., Meadors, G. F., & Moore, F. E., Jr. (1951). Epidemiological approaches to heart disease: the Framingham Study. *Am J Public Health Nations Health, 41*(3), 279-281.

Dean, R. G., Balding, L. C., Candido, R., Burns, W. C., Cao, Z., Twigg, S. M., & Burrell, L. M. (2005). Connective tissue growth factor and cardiac fibrosis after myocardial infarction. *J Histochem Cytochem, 53*(10), 1245-1256. doi:10.1369/jhc.4A6560.2005

Dechat, T., Pfleghaar, K., Sengupta, K., Shimi, T., Shumaker, D. K., Solimando, L., & Goldman, R. D. (2008). Nuclear lamins: major factors in the structural organization and function of the nucleus and chromatin. *Genes Dev, 22*(7), 832-853. doi:10.1101/gad.1652708

Dewald, O., Zymek, P., Winkelmann, K., Koerting, A., Ren, G., Abou-Khamis, T., . . . Frangogiannis, N. G. (2005). CCL2/Monocyte Chemoattractant Protein-1 regulates inflammatory responses critical to healing myocardial infarcts. *Circ Res, 96*(8), 881-889. doi:10.1161/01.RES.0000163017.13772.3a

Dick, S. A., Macklin, J. A., Nejat, S., Momen, A., Clemente-Casares, X., Althagafi, M. G., . . . Epelman, S. (2019). Self-renewing resident cardiac macrophages limit adverse remodeling following myocardial infarction. *Nat Immunol, 20*(1), 29-39. doi:10.1038/s41590-018-0272-2

Diez, J., Gonzalez, A., & Ravassa, S. (2016). Understanding the Role of CCN Matricellular Proteins in Myocardial Fibrosis. *J Am Coll Cardiol, 67*(13), 1569-1571. doi:10.1016/j.jacc.2016.01.029

Dipla, K., Mattiello, J. A., Jeevanandam, V., Houser, S. R., & Margulies, K. B. (1998). Myocyte recovery after mechanical circulatory support in humans with end-stage heart failure. *Circulation, 97*(23), 2316-2322. doi:10.1161/01.cir.97.23.2316

Drakos, S. G., Kfoury, A. G., Hammond, E. H., Reid, B. B., Revelo, M. P., Rasmusson, B. Y., . . . Li, D. Y. (2010). Impact of mechanical unloading on microvasculature and associated central remodeling features of the failing human heart. *J Am Coll Cardiol, 56*(5), 382-391. doi:10.1016/j.jacc.2010.04.019

Duisters, R. F., Tijsen, A. J., Schroen, B., Leenders, J. J., Lentink, V., van der Made, I., . . . Creemers, E. E. (2009). miR-133 and miR-30 regulate connective tissue growth factor: implications for a role of microRNAs in myocardial matrix remodeling. *Circ Res, 104*(2), 170-178, 176p following 178. doi:10.1161/CIRCRESAHA.108.182535

Engler, A. J., Carag-Krieger, C., Johnson, C. P., Raab, M., Tang, H. Y., Speicher, D. W., . . . Discher, D. E. (2008). Embryonic cardiomyocytes beat best on a matrix with heart-like elasticity: scar-like rigidity inhibits beating. *J Cell Sci, 121*(Pt 22), 3794-3802. doi:10.1242/jcs.029678

Ensan, S., Li, A., Besla, R., Degousee, N., Cosme, J., Roufaiel, M., . . . Robbins, C. S. (2016). Self-renewing resident arterial macrophages arise from embryonic CX3CR1(+) precursors and circulating monocytes immediately after birth. *Nat Immunol, 17*(2), 159-168. doi:10.1038/ni.3343

Epelman, S., Lavine, K. J., Beaudin, A. E., Sojka, D. K., Carrero, J. A., Calderon, B., . . . Mann, D. L. (2014). Embryonic and adult-derived resident cardiac macrophages are maintained

through distinct mechanisms at steady state and during inflammation. *Immunity, 40*(1), 91-104. doi:10.1016/j.immuni.2013.11.019

Eyre, D. R., Paz, M. A., & Gallop, P. M. (1984). Cross-linking in collagen and elastin. *Annu Rev Biochem, 53*, 717-748. doi:10.1146/annurev.bi.53.070184.003441

Fan, D., Takawale, A., Lee, J., & Kassiri, Z. (2012). Cardiac fibroblasts, fibrosis and extracellular matrix remodeling in heart disease. *Fibrogenesis Tissue Repair, 5*(1), 15. doi:10.1186/1755-1536-5-15

Fears, C. Y., & Woods, A. (2006). The role of syndecans in disease and wound healing. *Matrix Biol, 25*(7), 443-456. doi:10.1016/j.matbio.2006.07.003

Finckenberg, P., Inkinen, K., Ahonen, J., Merasto, S., Louhelainen, M., Vapaatalo, H., . . . Mervaala, E. (2003). Angiotensin II induces connective tissue growth factor gene expression via calcineurin-dependent pathways. *Am J Pathol, 163*(1), 355-366. doi:10.1016/S0002-9440(10)63659-0

Fitzgerald, M. C., & Schwarzbauer, J. E. (1998). Importance of the basement membrane protein SPARC for viability and fertility in Caenorhabditis elegans. *Curr Biol, 8*(23), 1285-1288. doi:10.1016/s0960-9822(07)00540-4

Fogg, D. K., Sibon, C., Miled, C., Jung, S., Aucouturier, P., Littman, D. R., . . . Geissmann, F. (2006). A clonogenic bone marrow progenitor specific for macrophages and dendritic cells. *Science, 311*(5757), 83-87. doi:10.1126/science.1117729

Fraccarollo, D., Thomas, S., Scholz, C. J., Hilfiker-Kleiner, D., Galuppo, P., & Bauersachs, J. (2019). Macrophage Mineralocorticoid Receptor Is a Pleiotropic Modulator of Myocardial Infarct Healing. *Hypertension, 73*(1), 102-111. doi:10.1161/HYPERTENSIONAHA.118.12162

Frame, J. M., McGrath, K. E., & Palis, J. (2013). Erythro-myeloid progenitors: "definitive" hematopoiesis in the conceptus prior to the emergence of hematopoietic stem cells. *Blood Cells Mol Dis, 51*(4), 220-225. doi:10.1016/j.bcmd.2013.09.006

Frangogiannis, N. G. (2012). Matricellular proteins in cardiac adaptation and disease. *Physiol Rev, 92*(2), 635-688. doi:10.1152/physrev.00008.2011

Fujiu, K., Shibata, M., Nakayama, Y., Ogata, F., Matsumoto, S., Noshita, K., . . . Manabe, I. (2017). A heart-brain-kidney network controls adaptation to cardiac stress through tissue macrophage activation. *Nat Med, 23*(5), 611-622. doi:10.1038/nm.4326

Funes, S. C., Rios, M., Escobar-Vera, J., & Kalergis, A. M. (2018). Implications of macrophage polarization in autoimmunity. *Immunology, 154*(2), 186-195. doi:10.1111/imm.12910

Gaggar, A., Jackson, P. L., Noerager, B. D., O'Reilly, P. J., McQuaid, D. B., Rowe, S. M., . . . Blalock, J. E. (2008). A novel proteolytic cascade generates an extracellular matrix-derived

chemoattractant in chronic neutrophilic inflammation. *J Immunol, 180*(8), 5662-5669. doi:10.4049/jimmunol.180.8.5662

Gao, F., Koenitzer, J. R., Tobolewski, J. M., Jiang, D., Liang, J., Noble, P. W., & Oury, T. D. (2008). Extracellular superoxide dismutase inhibits inflammation by preventing oxidative fragmentation of hyaluronan. *J Biol Chem, 283*(10), 6058-6066. doi:10.1074/jbc.M709273200

Garg, K., Pullen, N. A., Oskeritzian, C. A., Ryan, J. J., & Bowlin, G. L. (2013). Macrophage functional polarization (M1/M2) in response to varying fiber and pore dimensions of electrospun scaffolds. *Biomaterials, 34*(18), 4439-4451. doi:10.1016/j.biomaterials.2013.02.065

Garinis, G. A., van der Horst, G. T., Vijg, J., & Hoeijmakers, J. H. (2008). DNA damage and ageing: new-age ideas for an age-old problem. *Nat Cell Biol, 10*(11), 1241-1247. doi:10.1038/ncb1108-1241

Gazoti Debessa, C. R., Mesiano Maifrino, L. B., & Rodrigues de Souza, R. (2001). Age related changes of the collagen network of the human heart. *Mech Ageing Dev, 122*(10), 1049-1058. doi:10.1016/s0047-6374(01)00238-x

Gerstenblith, G., Frederiksen, J., Yin, F. C., Fortuin, N. J., Lakatta, E. G., & Weisfeldt, M. L. (1977). Echocardiographic assessment of a normal adult aging population. *Circulation, 56*(2), 273-278.

Giachelli, C. M., Lombardi, D., Johnson, R. J., Murry, C. E., & Almeida, M. (1998). Evidence for a role of osteopontin in macrophage infiltration in response to pathological stimuli in vivo. *Am J Pathol, 152*(2), 353-358.

Gilmour, D. T., Lyon, G. J., Carlton, M. B., Sanes, J. R., Cunningham, J. M., Anderson, J. R., . . . Colledge, W. H. (1998). Mice deficient for the secreted glycoprotein SPARC/osteonectin/BM40 develop normally but show severe age-onset cataract formation and disruption of the lens. *EMBO J, 17*(7), 1860-1870. doi:10.1093/emboj/17.7.1860

Ginhoux, F., Greter, M., Leboeuf, M., Nandi, S., See, P., Gokhan, S., . . . Merad, M. (2010). Fate mapping analysis reveals that adult microglia derive from primitive macrophages. *Science, 330*(6005), 841-845. doi:10.1126/science.1194637

Ginhoux, F., & Guilliams, M. (2016). Tissue-Resident Macrophage Ontogeny and Homeostasis. *Immunity, 44*(3), 439-449. doi:10.1016/j.immuni.2016.02.024

Gonzalez-Gonzalez, L., & Alonso, J. (2018). Periostin: A Matricellular Protein With Multiple Functions in Cancer Development and Progression. *Front Oncol, 8*, 225. doi:10.3389/fonc.2018.00225

Gonzalez, G. E., Rhaleb, N. E., D'Ambrosio, M. A., Nakagawa, P., Liao, T. D., Peterson, E. L., . . . Carretero, O. A. (2016). Cardiac-deleterious role of galectin-3 in chronic angiotensin II-

induced hypertension. *Am J Physiol Heart Circ Physiol, 311*(5), H1287-H1296. doi:10.1152/ajpheart.00096.2016

Good, D. J., Polverini, P. J., Rastinejad, F., Le Beau, M. M., Lemons, R. S., Frazier, W. A., & Bouck, N. P. (1990). A tumor suppressor-dependent inhibitor of angiogenesis is immunologically and functionally indistinguishable from a fragment of thrombospondin. *Proc Natl Acad Sci U S A, 87*(17), 6624-6628. doi:10.1073/pnas.87.17.6624

Green, D. R., Galluzzi, L., & Kroemer, G. (2011). Mitochondria and the autophagy-inflammation-cell death axis in organismal aging. *Science, 333*(6046), 1109-1112. doi:10.1126/science.1201940

Grzeszkiewicz, T. M., Kirschling, D. J., Chen, N., & Lau, L. F. (2001). CYR61 stimulates human skin fibroblast migration through Integrin alpha vbeta 5 and enhances mitogenesis through integrin alpha vbeta 3, independent of its carboxyl-terminal domain. *J Biol Chem, 276*(24), 21943-21950. doi:10.1074/jbc.M100978200

Guiet, R., Van Goethem, E., Cougoule, C., Balor, S., Valette, A., Al Saati, T., . . . Maridonneau-Parini, I. (2011). The process of macrophage migration promotes matrix metalloproteinase-independent invasion by tumor cells. *J Immunol, 187*(7), 3806-3814. doi:10.4049/jimmunol.1101245

Gupte, A. A., Hamilton, D. J., Cordero-Reyes, A. M., Youker, K. A., Yin, Z., Estep, J. D., . . . Hsueh, W. A. (2014). Mechanical unloading promotes myocardial energy recovery in human heart failure. *Circ Cardiovasc Genet, 7*(3), 266-276. doi:10.1161/CIRCGENETICS.113.000404

Haribhai, D., Ziegelbauer, J., Jia, S., Upchurch, K., Yan, K., Schmitt, E. G., . . . Williams, C. B. (2016). Alternatively Activated Macrophages Boost Induced Regulatory T and Th17 Cell Responses during Immunotherapy for Colitis. *J Immunol, 196*(8), 3305-3317. doi:10.4049/jimmunol.1501956

Harman, D. (1965). The Free Radical Theory of Aging: Effect of Age on Serum Copper Levels. *J Gerontol, 20*, 151-153. doi:10.1093/geronj/20.2.151

Hartog, J. W., Voors, A. A., Bakker, S. J., Smit, A. J., & van Veldhuisen, D. J. (2007). Advanced glycation end-products (AGEs) and heart failure: pathophysiology and clinical implications. *Eur J Heart Fail, 9*(12), 1146-1155. doi:10.1016/j.ejheart.2007.09.009

Hautamaki, R. D., Kobayashi, D. K., Senior, R. M., & Shapiro, S. D. (1997). Requirement for macrophage elastase for cigarette smoke-induced emphysema in mice. *Science, 277*(5334), 2002-2004. doi:10.1126/science.277.5334.2002

Heath, E., Tahri, D., Andermarcher, E., Schofield, P., Fleming, S., & Boulter, C. A. (2008). Abnormal skeletal and cardiac development, cardiomyopathy, muscle atrophy and cataracts in mice with a targeted disruption of the Nov (Ccn3) gene. *BMC Dev Biol, 8*, 18. doi:10.1186/1471-213X-8-18

Heck, T., Faccio, G., Richter, M., & Thony-Meyer, L. (2013). Enzyme-catalyzed protein crosslinking. *Appl Microbiol Biotechnol, 97*(2), 461-475. doi:10.1007/s00253-012-4569-z

Hein, S., & Schaper, J. (2001). The extracellular matrix in normal and diseased myocardium. *J Nucl Cardiol, 8*(2), 188-196. doi:10.1067/mnc.2001.113331

Hekimi, S., Lapointe, J., & Wen, Y. (2011). Taking a "good" look at free radicals in the aging process. *Trends Cell Biol, 21*(10), 569-576. doi:10.1016/j.tcb.2011.06.008

Henderson, N. C., Mackinnon, A. C., Farnworth, S. L., Kipari, T., Haslett, C., Iredale, J. P., . . . Sethi, T. (2008). Galectin-3 expression and secretion links macrophages to the promotion of renal fibrosis. *Am J Pathol, 172*(2), 288-298. doi:10.2353/ajpath.2008.070726

Henderson, N. C., Mackinnon, A. C., Farnworth, S. L., Poirier, F., Russo, F. P., Iredale, J. P., . . . Sethi, T. (2006). Galectin-3 regulates myofibroblast activation and hepatic fibrosis. *Proc Natl Acad Sci U S A, 103*(13), 5060-5065. doi:10.1073/pnas.0511167103

Herum, K. M., Choppe, J., Kumar, A., Engler, A. J., & McCulloch, A. D. (2017). Mechanical regulation of cardiac fibroblast profibrotic phenotypes. *Mol Biol Cell, 28*(14), 1871-1882. doi:10.1091/mbc.E17-01-0014

Herum, K. M., Romaine, A., Wang, A., Melleby, A. O., Strand, M. E., Pacheco, J., . . . Christensen, G. (2020). Syndecan-4 Protects the Heart From the Profibrotic Effects of Thrombin-Cleaved Osteopontin. *J Am Heart Assoc, 9*(3), e013518. doi:10.1161/JAHA.119.013518

Hilfiker-Kleiner, D., Kaminski, K., Kaminska, A., Fuchs, M., Klein, G., Podewski, E., . . . Drexler, H. (2004). Regulation of proangiogenic factor CCN1 in cardiac muscle: impact of ischemia, pressure overload, and neurohumoral activation. *Circulation, 109*(18), 2227-2233. doi:10.1161/01.CIR.0000127952.90508.9D

Ho, M. K., & Springer, T. A. (1982). Mac-2, a novel 32,000 Mr mouse macrophage subpopulation-specific antigen defined by monoclonal antibodies. *J Immunol, 128*(3), 1221-1228.

Hodge-Dufour, J., Noble, P. W., Horton, M. R., Bao, C., Wysoka, M., Burdick, M. D., . . . Pure, E. (1997). Induction of IL-12 and chemokines by hyaluronan requires adhesion-dependent priming of resident but not elicited macrophages. *J Immunol, 159*(5), 2492-2500.

Hoeffel, G., Chen, J., Lavin, Y., Low, D., Almeida, F. F., See, P., . . . Ginhoux, F. (2015). C-Myb(+) erythro-myeloid progenitor-derived fetal monocytes give rise to adult tissue-resident macrophages. *Immunity, 42*(4), 665-678. doi:10.1016/j.immuni.2015.03.011

Hoeffel, G., & Ginhoux, F. (2018). Fetal monocytes and the origins of tissue-resident macrophages. *Cell Immunol, 330*, 5-15. doi:10.1016/j.cellimm.2018.01.001

Hoeffel, G., Wang, Y., Greter, M., See, P., Teo, P., Malleret, B., . . . Ginhoux, F. (2012). Adult Langerhans cells derive predominantly from embryonic fetal liver monocytes with a minor contribution of yolk sac-derived macrophages. *J Exp Med, 209*(6), 1167-1181. doi:10.1084/jem.20120340

Horiuchi, K., Amizuka, N., Takeshita, S., Takamatsu, H., Katsuura, M., Ozawa, H., . . . Kudo, A. (1999). Identification and characterization of a novel protein, periostin, with restricted expression to periosteum and periodontal ligament and increased expression by transforming growth factor beta. *J Bone Miner Res, 14*(7), 1239-1249. doi:10.1359/jbmr.1999.14.7.1239

Horn, M. A., Graham, H. K., Richards, M. A., Clarke, J. D., Greensmith, D. J., Briston, S. J., . . . Trafford, A. W. (2012). Age-related divergent remodeling of the cardiac extracellular matrix in heart failure: collagen accumulation in the young and loss in the aged. *J Mol Cell Cardiol, 53*(1), 82-90. doi:10.1016/j.yjmcc.2012.03.011

Horn, M. A., & Trafford, A. W. (2016). Aging and the cardiac collagen matrix: Novel mediators of fibrotic remodelling. *J Mol Cell Cardiol, 93*, 175-185. doi:10.1016/j.yjmcc.2015.11.005

Horton, M. R., McKee, C. M., Bao, C., Liao, F., Farber, J. M., Hodge-DuFour, J., . . . Noble, P. W. (1998). Hyaluronan fragments synergize with interferon-gamma to induce the C-X-C chemokines mig and interferon-inducible protein-10 in mouse macrophages. *J Biol Chem, 273*(52), 35088-35094. doi:10.1074/jbc.273.52.35088

Horton, M. R., Olman, M. A., Bao, C., White, K. E., Choi, A. M., Chin, B. Y., . . . Lowenstein, C. J. (2000). Regulation of plasminogen activator inhibitor-1 and urokinase by hyaluronan fragments in mouse macrophages. *Am J Physiol Lung Cell Mol Physiol, 279*(4), L707-715. doi:10.1152/ajplung.2000.279.4.L707

Horton, M. R., Olman, M. A., & Noble, P. W. (1999). Hyaluronan fragments induce plasminogen activator inhibitor-1 and inhibit urokinase activity in mouse alveolar macrophages: a potential mechanism for impaired fibrinolytic activity in acute lung injury. *Chest, 116*(1 Suppl), 17S.

Horton, M. R., Shapiro, S., Bao, C., Lowenstein, C. J., & Noble, P. W. (1999). Induction and regulation of macrophage metalloelastase by hyaluronan fragments in mouse macrophages. *J Immunol, 162*(7), 4171-4176.

Hoshino-Negishi, K., Ohkuro, M., Nakatani, T., Kuboi, Y., Nishimura, M., Ida, Y., . . . Imai, T. (2019). Role of Anti-Fractalkine Antibody in Suppression of Joint Destruction by Inhibiting Migration of Osteoclast Precursors to the Synovium in Experimental Arthritis. *Arthritis Rheumatol, 71*(2), 222-231. doi:10.1002/art.40688

Houghton, A. M., Quintero, P. A., Perkins, D. L., Kobayashi, D. K., Kelley, D. G., Marconcini, L. A., . . . Shapiro, S. D. (2006). Elastin fragments drive disease progression in a murine model of emphysema. *J Clin Invest, 116*(3), 753-759. doi:10.1172/JCI25617

Hulsmans, M., Clauss, S., Xiao, L., Aguirre, A. D., King, K. R., Hanley, A., . . . Nahrendorf, M. (2017). Macrophages Facilitate Electrical Conduction in the Heart. *Cell, 169*(3), 510-522.e520. doi:10.1016/j.cell.2017.03.050

Ieda, M., Tsuchihashi, T., Ivey, K. N., Ross, R. S., Hong, T. T., Shaw, R. M., & Srivastava, D. (2009). Cardiac fibroblasts regulate myocardial proliferation through beta1 integrin signaling. *Dev Cell, 16*(2), 233-244. doi:10.1016/j.devcel.2008.12.007

Igarashi, A., Okochi, H., Bradham, D. M., & Grotendorst, G. R. (1993). Regulation of connective tissue growth factor gene expression in human skin fibroblasts and during wound repair. *Mol Biol Cell, 4*(6), 637-645. doi:10.1091/mbc.4.6.637

Imanaka-Yoshida, K., Hiroe, M., Nishikawa, T., Ishiyama, S., Shimojo, T., Ohta, Y., . . . Yoshida, T. (2001). Tenascin-C modulates adhesion of cardiomyocytes to extracellular matrix during tissue remodeling after myocardial infarction. *Lab Invest, 81*(7), 1015-1024. doi:10.1038/labinvest.3780313

Inai, K., Norris, R. A., Hoffman, S., Markwald, R. R., & Sugi, Y. (2008). BMP-2 induces cell migration and periostin expression during atrioventricular valvulogenesis. *Dev Biol, 315*(2), 383-396. doi:10.1016/j.ydbio.2007.12.028

Irwin, E. F., Saha, K., Rosenbluth, M., Gamble, L. J., Castner, D. G., & Healy, K. E. (2008). Modulus-dependent macrophage adhesion and behavior. *J Biomater Sci Polym Ed, 19*(10), 1363-1382. doi:10.1163/156856208786052407

Isenberg, J. S., Qin, Y., Maxhimer, J. B., Sipes, J. M., Despres, D., Schnermann, J., . . . Roberts, D. D. (2009). Thrombospondin-1 and CD47 regulate blood pressure and cardiac responses to vasoactive stress. *Matrix Biol, 28*(2), 110-119. doi:10.1016/j.matbio.2009.01.002

Ishida, Y., Kimura, A., Nosaka, M., Kuninaka, Y., Hemmi, H., Sasaki, I., . . . Kondo, T. (2017). Essential involvement of the CX3CL1-CX3CR1 axis in bleomycin-induced pulmonary fibrosis via regulation of fibrocyte and M2 macrophage migration. *Sci Rep, 7*(1), 16833. doi:10.1038/s41598-017-17007-8

Ito, K., Kon, S., Nakayama, Y., Kurotaki, D., Saito, Y., Kanayama, M., . . . Uede, T. (2009). The differential amino acid requirement within osteopontin in alpha4 and alpha9 integrin-mediated cell binding and migration. *Matrix Biol, 28*(1), 11-19. doi:10.1016/j.matbio.2008.10.002

Ivkovic, S., Yoon, B. S., Popoff, S. N., Safadi, F. F., Libuda, D. E., Stephenson, R. C., . . . Lyons, K. M. (2003). Connective tissue growth factor coordinates chondrogenesis and angiogenesis during skeletal development. *Development, 130*(12), 2779-2791. doi:10.1242/dev.00505

Iwanciw, D., Rehm, M., Porst, M., & Goppelt-Struebe, M. (2003). Induction of connective tissue growth factor by angiotensin II: integration of signaling pathways. *Arterioscler Thromb Vasc Biol, 23*(10), 1782-1787. doi:10.1161/01.ATV.0000092913.60428.E6

Jakubzick, C. V., Randolph, G. J., & Henson, P. M. (2017). Monocyte differentiation and antigen-presenting functions. *Nat Rev Immunol, 17*(6), 349-362. doi:10.1038/nri.2017.28

Jellis, C., Martin, J., Narula, J., & Marwick, T. H. (2010). Assessment of nonischemic myocardial fibrosis. *J Am Coll Cardiol, 56*(2), 89-97. doi:10.1016/j.jacc.2010.02.047

Jeong, D., Lee, M. A., Li, Y., Yang, D. K., Kho, C., Oh, J. G., . . . Park, W. J. (2016). Matricellular Protein CCN5 Reverses Established Cardiac Fibrosis. *J Am Coll Cardiol, 67*(13), 1556-1568. doi:10.1016/j.jacc.2016.01.030

Jiang, D., Liang, J., & Noble, P. W. (2011). Hyaluronan as an immune regulator in human diseases. *Physiol Rev, 91*(1), 221-264. doi:10.1152/physrev.00052.2009

Jones, P. L., & Jones, F. S. (2000). Tenascin-C in development and disease: gene regulation and cell function. *Matrix Biol, 19*(7), 581-596. doi:10.1016/s0945-053x(00)00106-2

Jugdutt, B. I. (2003). Ventricular remodeling after infarction and the extracellular collagen matrix: when is enough enough? *Circulation, 108*(11), 1395-1403. doi:10.1161/01.CIR.0000085658.98621.49

Kadler, K. E., Holmes, D. F., Trotter, J. A., & Chapman, J. A. (1996). Collagen fibril formation. *Biochem J, 316 (Pt 1)*, 1-11. doi:10.1042/bj3160001

Katsuragi, N., Morishita, R., Nakamura, N., Ochiai, T., Taniyama, Y., Hasegawa, Y., . . . Sugimura, K. (2004). Periostin as a novel factor responsible for ventricular dilation. *Circulation, 110*(13), 1806-1813. doi:10.1161/01.CIR.0000142607.33398.54

Kawara, T., Derksen, R., de Groot, J. R., Coronel, R., Tasseron, S., Linnenbank, A. C., . . . de Bakker, J. M. (2001). Activation delay after premature stimulation in chronically diseased human myocardium relates to the architecture of interstitial fibrosis. *Circulation, 104*(25), 3069-3075. doi:10.1161/hc5001.100833

Keane, T. J., Londono, R., Turner, N. J., & Badylak, S. F. (2012). Consequences of ineffective decellularization of biologic scaffolds on the host response. *Biomaterials, 33*(6), 1771-1781. doi:10.1016/j.biomaterials.2011.10.054

Keene, D. R., Engvall, E., & Glanville, R. W. (1988). Ultrastructure of type VI collagen in human skin and cartilage suggests an anchoring function for this filamentous network. *J Cell Biol, 107*(5), 1995-2006. doi:10.1083/jcb.107.5.1995

Kielty, C. M., Baldock, C., Lee, D., Rock, M. J., Ashworth, J. L., & Shuttleworth, C. A. (2002). Fibrillin: from microfibril assembly to biomechanical function. *Philos Trans R Soc Lond B Biol Sci, 357*(1418), 207-217. doi:10.1098/rstb.2001.1029

Kielty, C. M., Sherratt, M. J., & Shuttleworth, C. A. (2002). Elastic fibres. *J Cell Sci, 115*(Pt 14), 2817-2828.

Kierdorf, K., Erny, D., Goldmann, T., Sander, V., Schulz, C., Perdiguero, E. G., . . . Prinz, M. (2013). Microglia emerge from erythromyeloid precursors via Pu.1- and Irf8-dependent pathways. *Nat Neurosci, 16*(3), 273-280. doi:10.1038/nn.3318

Kii, I., Nishiyama, T., & Kudo, A. (2016). Periostin promotes secretion of fibronectin from the endoplasmic reticulum. *Biochem Biophys Res Commun, 470*(4), 888-893. doi:10.1016/j.bbrc.2016.01.139

Kii, I., Nishiyama, T., Li, M., Matsumoto, K., Saito, M., Amizuka, N., & Kudo, A. (2010). Incorporation of tenascin-C into the extracellular matrix by periostin underlies an extracellular meshwork architecture. *J Biol Chem, 285*(3), 2028-2039. doi:10.1074/jbc.M109.051961

Kisling, A., Lust, R. M., & Katwa, L. C. (2019). What is the role of peptide fragments of collagen I and IV in health and disease? *Life Sci, 228*, 30-34. doi:10.1016/j.lfs.2019.04.042

Klotz, S., Barbone, A., Reiken, S., Holmes, J. W., Naka, Y., Oz, M. C., . . . Burkhoff, D. (2005). Left ventricular assist device support normalizes left and right ventricular beta-adrenergic pathway properties. *J Am Coll Cardiol, 45*(5), 668-676. doi:10.1016/j.jacc.2004.11.042

Koga, H., Kaushik, S., & Cuervo, A. M. (2011). Protein homeostasis and aging: The importance of exquisite quality control. *Ageing Res Rev, 10*(2), 205-215. doi:10.1016/j.arr.2010.02.001

Kolatsi-Joannou, M., Price, K. L., Winyard, P. J., & Long, D. A. (2011). Modified citrus pectin reduces galectin-3 expression and disease severity in experimental acute kidney injury. *PLoS One, 6*(4), e18683. doi:10.1371/journal.pone.0018683

Krady, M. M., Zeng, J., Yu, J., MacLauchlan, S., Skokos, E. A., Tian, W., . . . Kyriakides, T. R. (2008). Thrombospondin-2 modulates extracellular matrix remodeling during physiological angiogenesis. *Am J Pathol, 173*(3), 879-891. doi:10.2353/ajpath.2008.080128

Kroemer, G., Galluzzi, L., & Brenner, C. (2007). Mitochondrial membrane permeabilization in cell death. *Physiol Rev, 87*(1), 99-163. doi:10.1152/physrev.00013.2006

Kruithof, E. K., Mestries, J. C., Gascon, M. P., & Ythier, A. (1997). The coagulation and fibrinolytic responses of baboons after in vivo thrombin generation--effect of interleukin 6. *Thromb Haemost, 77*(5), 905-910.

Kruzynska-Frejtag, A., Machnicki, M., Rogers, R., Markwald, R. R., & Conway, S. J. (2001). Periostin (an osteoblast-specific factor) is expressed within the embryonic mouse heart during valve formation. *Mech Dev, 103*(1-2), 183-188. doi:10.1016/s0925-4773(01)00356-2

Kudo, A., & Kii, I. (2018). Periostin function in communication with extracellular matrices. *J Cell Commun Signal, 12*(1), 301-308. doi:10.1007/s12079-017-0422-6

Kuilman, T., Michaloglou, C., Mooi, W. J., & Peeper, D. S. (2010). The essence of senescence. *Genes Dev, 24*(22), 2463-2479. doi:10.1101/gad.1971610

Kupprion, C., Motamed, K., & Sage, E. H. (1998). SPARC (BM-40, osteonectin) inhibits the mitogenic effect of vascular endothelial growth factor on microvascular endothelial cells. *J Biol Chem, 273*(45), 29635-29640. doi:10.1074/jbc.273.45.29635

Kurata, K., Uemura, T., Nemoto, A., Tateishi, T., Murakami, T., Higaki, H., . . . Iwamoto, Y. (2001). Mechanical strain effect on bone-resorbing activity and messenger RNA expressions of marker enzymes in isolated osteoclast culture. *J Bone Miner Res, 16*(4), 722-730. doi:10.1359/jbmr.2001.16.4.722

Lacaud, G., Gore, L., Kennedy, M., Kouskoff, V., Kingsley, P., Hogan, C., . . . Keller, G. (2002). Runx1 is essential for hematopoietic commitment at the hemangioblast stage of development in vitro. *Blood, 100*(2), 458-466. doi:10.1182/blood-2001-12-0321

Lakatta, E. G., & Levy, D. (2003a). Arterial and cardiac aging: major shareholders in cardiovascular disease enterprises: Part I: aging arteries: a "set up" for vascular disease. *Circulation, 107*(1), 139-146. doi:10.1161/01.cir.0000048892.83521.58

Lakatta, E. G., & Levy, D. (2003b). Arterial and cardiac aging: major shareholders in cardiovascular disease enterprises: Part II: the aging heart in health: links to heart disease. *Circulation, 107*(2), 346-354. doi:10.1161/01.cir.0000048893.62841.f7

Lake, A. C., Bialik, A., Walsh, K., & Castellot, J. J., Jr. (2003). CCN5 is a growth arrest-specific gene that regulates smooth muscle cell proliferation and motility. *Am J Pathol, 162*(1), 219-231. doi:10.1016/S0002-9440(10)63813-8

Lambeth, J. D. (2004). NOX enzymes and the biology of reactive oxygen. *Nat Rev Immunol, 4*(3), 181-189. doi:10.1038/nri1312

Laplante, M., & Sabatini, D. M. (2012). mTOR signaling in growth control and disease. *Cell, 149*(2), 274-293. doi:10.1016/j.cell.2012.03.017

Lavasani, M., Robinson, A. R., Lu, A., Song, M., Feduska, J. M., Ahani, B., . . . Huard, J. (2012). Muscle-derived stem/progenitor cell dysfunction limits healthspan and lifespan in a murine progeria model. *Nat Commun, 3*, 608. doi:10.1038/ncomms1611

Lavine, K. J., Epelman, S., Uchida, K., Weber, K. J., Nichols, C. G., Schilling, J. D., . . . Mann, D. L. (2014). Distinct macrophage lineages contribute to disparate patterns of cardiac recovery and remodeling in the neonatal and adult heart. *Proc Natl Acad Sci U S A, 111*(45), 16029-16034. doi:10.1073/pnas.1406508111

Lawler, J., Duquette, M., Whittaker, C. A., Adams, J. C., McHenry, K., & DeSimone, D. W. (1993). Identification and characterization of thrombospondin-4, a new member of the thrombospondin gene family. *J Cell Biol, 120*(4), 1059-1067. doi:10.1083/jcb.120.4.1059

Leask, A., & Abraham, D. J. (2004). TGF-beta signaling and the fibrotic response. *FASEB J, 18*(7), 816-827. doi:10.1096/fj.03-1273rev

Leask, A., & Abraham, D. J. (2006). All in the CCN family: essential matricellular signaling modulators emerge from the bunker. *J Cell Sci, 119*(Pt 23), 4803-4810. doi:10.1242/jcs.03270

Lerma, J., Zukin, R. S., & Bennett, M. V. (1991). Interaction of Mg2+ and phencyclidine in use-dependent block of NMDA channels. *Neurosci Lett, 123*(2), 187-191. doi:10.1016/0304-3940(91)90927-l

Levin, H. R., Oz, M. C., Catanese, K. A., Rose, E. A., & Burkhoff, D. (1996). Transient normalization of systolic and diastolic function after support with a left ventricular assist device in a patient with dilated cardiomyopathy. *J Heart Lung Transplant, 15*(8), 840-842.

Levy, D., Anderson, K. M., Savage, D. D., Kannel, W. B., Christiansen, J. C., & Castelli, W. P. (1988). Echocardiographically detected left ventricular hypertrophy: prevalence and risk factors. The Framingham Heart Study. *Ann Intern Med, 108*(1), 7-13. doi:10.7326/0003-4819-108-1-7

Li, G., Oparil, S., Sanders, J. M., Zhang, L., Dai, M., Chen, L. B., . . . Sarembock, I. J. (2006). Phosphatidylinositol-3-kinase signaling mediates vascular smooth muscle cell expression of periostin in vivo and in vitro. *Atherosclerosis, 188*(2), 292-300. doi:10.1016/j.atherosclerosis.2005.11.002

Li, L., Fan, D., Wang, C., Wang, J. Y., Cui, X. B., Wu, D., . . . Wu, L. L. (2011). Angiotensin II increases periostin expression via Ras/p38 MAPK/CREB and ERK1/2/TGF-beta1 pathways in cardiac fibroblasts. *Cardiovasc Res, 91*(1), 80-89. doi:10.1093/cvr/cvr067

Li, Y. Y., Feng, Y., McTiernan, C. F., Pei, W., Moravec, C. S., Wang, P., . . . Feldman, A. M. (2001). Downregulation of matrix metalloproteinases and reduction in collagen damage in the failing human heart after support with left ventricular assist devices. *Circulation, 104*(10), 1147-1152. doi:10.1161/hc3501.095215

Liaw, L., Birk, D. E., Ballas, C. B., Whitsitt, J. S., Davidson, J. M., & Hogan, B. L. (1998). Altered wound healing in mice lacking a functional osteopontin gene (spp1). *J Clin Invest, 101*(7), 1468-1478. doi:10.1172/JCI2131

Lin, C. G., Leu, S. J., Chen, N., Tebeau, C. M., Lin, S. X., Yeung, C. Y., & Lau, L. F. (2003). CCN3 (NOV) is a novel angiogenic regulator of the CCN protein family. *J Biol Chem, 278*(26), 24200-24208. doi:10.1074/jbc.M302028200

Lin, J., Lopez, E. F., Jin, Y., Van Remmen, H., Bauch, T., Han, H. C., & Lindsey, M. L. (2008). Age-related cardiac muscle sarcopenia: Combining experimental and mathematical modeling to identify mechanisms. *Exp Gerontol, 43*(4), 296-306. doi:10.1016/j.exger.2007.12.005

Lin, J. D., Nishi, H., Poles, J., Niu, X., McCauley, C., Rahman, K., . . . Loke, P. (2019). Single-cell analysis of fate-mapped macrophages reveals heterogeneity, including stem-like properties, during atherosclerosis progression and regression. *JCI Insight, 4*(4). doi:10.1172/jci.insight.124574

Lindsey, M. L., Iyer, R. P., Zamilpa, R., Yabluchanskiy, A., DeLeon-Pennell, K. Y., Hall, M. E., . . . de Castro Bras, L. E. (2015). A Novel Collagen Matricryptin Reduces Left Ventricular Dilation Post-Myocardial Infarction by Promoting Scar Formation and Angiogenesis. *J Am Coll Cardiol, 66*(12), 1364-1374. doi:10.1016/j.jacc.2015.07.035

Litvin, J., Blagg, A., Mu, A., Matiwala, S., Montgomery, M., Berretta, R., . . . Margulies, K. (2006). Periostin and periostin-like factor in the human heart: possible therapeutic targets. *Cardiovasc Pathol, 15*(1), 24-32. doi:10.1016/j.carpath.2005.09.001

Liu, C. Y., Liu, Y. C., Wu, C., Armstrong, A., Volpe, G. J., van der Geest, R. J., . . . Lima, J. A. C. (2013). Evaluation of age-related interstitial myocardial fibrosis with cardiac magnetic resonance contrast-enhanced T1 mapping: MESA (Multi-Ethnic Study of Atherosclerosis). *J Am Coll Cardiol, 62*(14), 1280-1287. doi:10.1016/j.jacc.2013.05.078

Liu, H., & Jiang, D. (2011). Fractalkine/CX3CR1 and atherosclerosis. *Clin Chim Acta, 412*(13-14), 1180-1186. doi:10.1016/j.cca.2011.03.036

Loffredo, F. S., Nikolova, A. P., Pancoast, J. R., & Lee, R. T. (2014). Heart failure with preserved ejection fraction: molecular pathways of the aging myocardium. *Circ Res, 115*(1), 97-107. doi:10.1161/CIRCRESAHA.115.302929

Lopez-Otin, C., Blasco, M. A., Partridge, L., Serrano, M., & Kroemer, G. (2013). The hallmarks of aging. *Cell, 153*(6), 1194-1217. doi:10.1016/j.cell.2013.05.039

Lumeng, C. N., Bodzin, J. L., & Saltiel, A. R. (2007). Obesity induces a phenotypic switch in adipose tissue macrophage polarization. *J Clin Invest, 117*(1), 175-184. doi:10.1172/JCI29881

Madigan, J. D., Barbone, A., Choudhri, A. F., Morales, D. L., Cai, B., Oz, M. C., & Burkhoff, D. (2001). Time course of reverse remodeling of the left ventricle during support with a left ventricular assist device. *J Thorac Cardiovasc Surg, 121*(5), 902-908. doi:10.1067/mtc.2001.112632

Malek, M. H., & Olfert, I. M. (2009). Global deletion of thrombospondin-1 increases cardiac and skeletal muscle capillarity and exercise capacity in mice. *Exp Physiol, 94*(6), 749-760. doi:10.1113/expphysiol.2008.045989

Mamalis, A., Markopoulou, C., Lagou, A., & Vrotsos, I. (2011). Oestrogen regulates proliferation, osteoblastic differentiation, collagen synthesis and periostin gene expression in human periodontal ligament cells through oestrogen receptor beta. *Arch Oral Biol, 56*(5), 446-455. doi:10.1016/j.archoralbio.2010.11.001

Mao, Y., & Schwarzbauer, J. E. (2005). Fibronectin fibrillogenesis, a cell-mediated matrix assembly process. *Matrix Biol, 24*(6), 389-399. doi:10.1016/j.matbio.2005.06.008

Martinez-Martinez, E., Rodriguez, C., Galan, M., Miana, M., Jurado-Lopez, R., Bartolome, M. V., . . . Cachofeiro, V. (2016). The lysyl oxidase inhibitor (beta-aminopropionitrile) reduces

leptin profibrotic effects and ameliorates cardiovascular remodeling in diet-induced obesity in rats. *J Mol Cell Cardiol, 92*, 96-104. doi:10.1016/j.yjmcc.2016.01.012

Maruhashi, T., Kii, I., Saito, M., & Kudo, A. (2010). Interaction between periostin and BMP-1 promotes proteolytic activation of lysyl oxidase. *J Biol Chem, 285*(17), 13294-13303. doi:10.1074/jbc.M109.088864

Matsui, Y., Jia, N., Okamoto, H., Kon, S., Onozuka, H., Akino, M., . . . Uede, T. (2004). Role of osteopontin in cardiac fibrosis and remodeling in angiotensin II-induced cardiac hypertrophy. *Hypertension, 43*(6), 1195-1201. doi:10.1161/01.HYP.0000128621.68160.dd

McKee, C. M., Lowenstein, C. J., Horton, M. R., Wu, J., Bao, C., Chin, B. Y., . . . Noble, P. W. (1997). Hyaluronan fragments induce nitric-oxide synthase in murine macrophages through a nuclear factor kappaB-dependent mechanism. *J Biol Chem, 272*(12), 8013-8018. doi:10.1074/jbc.272.12.8013

McWhorter, F. Y., Davis, C. T., & Liu, W. F. (2015). Physical and mechanical regulation of macrophage phenotype and function. *Cell Mol Life Sci, 72*(7), 1303-1316. doi:10.1007/s00018-014-1796-8

Medugorac, I., & Jacob, R. (1983). Characterisation of left ventricular collagen in the rat. *Cardiovasc Res, 17*(1), 15-21. doi:10.1093/cvr/17.1.15

Merad, M., Manz, M. G., Karsunky, H., Wagers, A., Peters, W., Charo, I., . . . Engleman, E. G. (2002). Langerhans cells renew in the skin throughout life under steady-state conditions. *Nat Immunol, 3*(12), 1135-1141. doi:10.1038/ni852

Merle, B., & Garnero, P. (2012). The multiple facets of periostin in bone metabolism. *Osteoporos Int, 23*(4), 1199-1212. doi:10.1007/s00198-011-1892-7

Mewton, N., Liu, C. Y., Croisille, P., Bluemke, D., & Lima, J. A. (2011). Assessment of myocardial fibrosis with cardiovascular magnetic resonance. *J Am Coll Cardiol, 57*(8), 891-903. doi:10.1016/j.jacc.2010.11.013

Midwood, K. S., & Schwarzbauer, J. E. (2002). Tenascin-C modulates matrix contraction via focal adhesion kinase- and Rho-mediated signaling pathways. *Mol Biol Cell, 13*(10), 3601-3613. doi:10.1091/mbc.e02-05-0292

Mienaltowski, M. J., & Birk, D. E. (2014). Structure, physiology, and biochemistry of collagens. *Adv Exp Med Biol, 802*, 5-29. doi:10.1007/978-94-007-7893-1_2

Miftode, R. S., Serban, I. L., Timpau, A. S., Miftode, I. L., Ion, A., Buburuz, A. M., . . . Costache, II. (2019). Syndecan-1: A Review on Its Role in Heart Failure and Chronic Liver Disease Patients' Assessment. *Cardiol Res Pract, 2019*, 4750580. doi:10.1155/2019/4750580

Mills, C. D., Kincaid, K., Alt, J. M., Heilman, M. J., & Hill, A. M. (2000). M-1/M-2 macrophages and the Th1/Th2 paradigm. *J Immunol, 164*(12), 6166-6173. doi:10.4049/jimmunol.164.12.6166

Mizutani, S., Nishio, J., Kondo, K., Motomura, K., Yamada, Z., Masuoka, S., . . . Nanki, T. (2021). Treatment with an Anti-CX3CL1 Antibody Suppresses M1 Macrophage Infiltration in Interstitial Lung Disease in SKG Mice. *Pharmaceuticals (Basel), 14*(5). doi:10.3390/ph14050474

Mo, F. E., & Lau, L. F. (2006). The matricellular protein CCN1 is essential for cardiac development. *Circ Res, 99*(9), 961-969. doi:10.1161/01.RES.0000248426.35019.89

Mo, F. E., Muntean, A. G., Chen, C. C., Stolz, D. B., Watkins, S. C., & Lau, L. F. (2002). CYR61 (CCN1) is essential for placental development and vascular integrity. *Mol Cell Biol, 22*(24), 8709-8720. doi:10.1128/MCB.22.24.8709-8720.2002

Molawi, K., Wolf, Y., Kandalla, P. K., Favret, J., Hagemeyer, N., Frenzel, K., . . . Sieweke, M. H. (2014). Progressive replacement of embryo-derived cardiac macrophages with age. *J Exp Med, 211*(11), 2151-2158. doi:10.1084/jem.20140639

Molofsky, A. V., Slutsky, S. G., Joseph, N. M., He, S., Pardal, R., Krishnamurthy, J., . . . Morrison, S. J. (2006). Increasing p16INK4a expression decreases forebrain progenitors and neurogenesis during ageing. *Nature, 443*(7110), 448-452. doi:10.1038/nature05091

Moriwaki, H., Stempien-Otero, A., Kremen, M., Cozen, A. E., & Dichek, D. A. (2004). Overexpression of urokinase by macrophages or deficiency of plasminogen activator inhibitor type 1 causes cardiac fibrosis in mice. *Circ Res, 95*(6), 637-644. doi:10.1161/01.RES.0000141427.61023.f4

Moskalev, A. A., Shaposhnikov, M. V., Plyusnina, E. N., Zhavoronkov, A., Budovsky, A., Yanai, H., & Fraifeld, V. E. (2013). The role of DNA damage and repair in aging through the prism of Koch-like criteria. *Ageing Res Rev, 12*(2), 661-684. doi:10.1016/j.arr.2012.02.001

Mossadegh-Keller, N., Gentek, R., Gimenez, G., Bigot, S., Mailfert, S., & Sieweke, M. H. (2017). Developmental origin and maintenance of distinct testicular macrophage populations. *J Exp Med, 214*(10), 2829-2841. doi:10.1084/jem.20170829

Munch, J., & Abdelilah-Seyfried, S. (2021). Sensing and Responding of Cardiomyocytes to Changes of Tissue Stiffness in the Diseased Heart. *Front Cell Dev Biol, 9*, 642840. doi:10.3389/fcell.2021.642840

Murphy-Ullrich, J. E., Schultz-Cherry, S., & Hook, M. (1992). Transforming growth factor-beta complexes with thrombospondin. *Mol Biol Cell, 3*(2), 181-188. doi:10.1091/mbc.3.2.181

Murray, P. J. (2017). Macrophage Polarization. *Annual Review of Physiology, 79*(1), 541-566. doi:10.1146/annurev-physiol-022516-034339

Murray, P. J., Allen, J. E., Biswas, S. K., Fisher, E. A., Gilroy, D. W., Goerdt, S., . . . Wynn, T. A. (2014). Macrophage activation and polarization: nomenclature and experimental guidelines. *Immunity, 41*(1), 14-20. doi:10.1016/j.immuni.2014.06.008

Murry, C. E., Giachelli, C. M., Schwartz, S. M., & Vracko, R. (1994). Macrophages express osteopontin during repair of myocardial necrosis. *Am J Pathol, 145*(6), 1450-1462.

Nabi, I. R., Shankar, J., & Dennis, J. W. (2015). The galectin lattice at a glance. *J Cell Sci, 128*(13), 2213-2219. doi:10.1242/jcs.151159

Nagueh, S. F., Smiseth, O. A., Appleton, C. P., Byrd, B. F., 3rd, Dokainish, H., Edvardsen, T., . . . St. Louis, M. (2016). Recommendations for the Evaluation of Left Ventricular Diastolic Function by Echocardiography: An Update from the American Society of Echocardiography and the European Association of Cardiovascular Imaging. *Eur Heart J Cardiovasc Imaging, 17*(12), 1321-1360. doi:10.1093/ehjci/jew082

Nanki, T., Urasaki, Y., Imai, T., Nishimura, M., Muramoto, K., Kubota, T., & Miyasaka, N. (2004). Inhibition of fractalkine ameliorates murine collagen-induced arthritis. *J Immunol, 173*(11), 7010-7016. doi:10.4049/jimmunol.173.11.7010

Neuman, R. E., & Logan, M. A. (1950). The determination of collagen and elastin in tissues. *J Biol Chem, 186*(2), 549-556.

Nishioka, T., Onishi, K., Shimojo, N., Nagano, Y., Matsusaka, H., Ikeuchi, M., . . . Imanaka-Yoshida, K. (2010). Tenascin-C may aggravate left ventricular remodeling and function after myocardial infarction in mice. *Am J Physiol Heart Circ Physiol, 298*(3), H1072-1078. doi:10.1152/ajpheart.00255.2009

Norris, R. A., Damon, B., Mironov, V., Kasyanov, V., Ramamurthi, A., Moreno-Rodriguez, R., . . . Markwald, R. R. (2007). Periostin regulates collagen fibrillogenesis and the biomechanical properties of connective tissues. *J Cell Biochem, 101*(3), 695-711. doi:10.1002/jcb.21224

Norris, R. A., Kern, C. B., Wessels, A., Moralez, E. I., Markwald, R. R., & Mjaatvedt, C. H. (2004). Identification and detection of the periostin gene in cardiac development. *Anat Rec A Discov Mol Cell Evol Biol, 281*(2), 1227-1233. doi:10.1002/ar.a.20135

Norris, R. A., Moreno-Rodriguez, R., Hoffman, S., & Markwald, R. R. (2009). The many facets of the matricelluar protein periostin during cardiac development, remodeling, and pathophysiology. *J Cell Commun Signal, 3*(3-4), 275-286. doi:10.1007/s12079-009-0063-5

Norris, R. A., Moreno-Rodriguez, R. A., Sugi, Y., Hoffman, S., Amos, J., Hart, M. M., . . . Markwald, R. R. (2008). Periostin regulates atrioventricular valve maturation. *Dev Biol, 316*(2), 200-213. doi:10.1016/j.ydbio.2008.01.003

Norris, R. A., Potts, J. D., Yost, M. J., Junor, L., Brooks, T., Tan, H., . . . Goodwin, R. L. (2009). Periostin promotes a fibroblastic lineage pathway in atrioventricular valve progenitor cells. *Dev Dyn, 238*(5), 1052-1063. doi:10.1002/dvdy.21933

North, B. J., & Sinclair, D. A. (2012). The intersection between aging and cardiovascular disease. *Circ Res, 110*(8), 1097-1108. doi:10.1161/CIRCRESAHA.111.246876

O'Regan, A. W., Nau, G. J., Chupp, G. L., & Berman, J. S. (2000). Osteopontin (Eta-1) in cell-mediated immunity: teaching an old dog new tricks. *Immunol Today, 21*(10), 475-478. doi:10.1016/s0167-5699(00)01715-1

Odai, T., Matsunawa, M., Takahashi, R., Wakabayashi, K., Isozaki, T., Yajima, N., . . . Kasama, T. (2009). Correlation of CX3CL1 and CX3CR1 levels with response to infliximab therapy in patients with rheumatoid arthritis. *J Rheumatol, 36*(6), 1158-1165. doi:10.3899/jrheum.081074

Ohnishi, H., Oka, T., Kusachi, S., Nakanishi, T., Takeda, K., Nakahama, M., . . . Tsuji, T. (1998). Increased expression of connective tissue growth factor in the infarct zone of experimentally induced myocardial infarction in rats. *J Mol Cell Cardiol, 30*(11), 2411-2422. doi:10.1006/jmcc.1998.0799

Oka, T., Xu, J., Kaiser, R. A., Melendez, J., Hambleton, M., Sargent, M. A., . . . Molkentin, J. D. (2007). Genetic manipulation of periostin expression reveals a role in cardiac hypertrophy and ventricular remodeling. *Circ Res, 101*(3), 313-321. doi:10.1161/CIRCRESAHA.107.149047

Ophascharoensuk, V., Giachelli, C. M., Gordon, K., Hughes, J., Pichler, R., Brown, P., . . . Johnson, R. J. (1999). Obstructive uropathy in the mouse: role of osteopontin in interstitial fibrosis and apoptosis. *Kidney Int, 56*(2), 571-580. doi:10.1046/j.1523-1755.1999.00580.x

Oriyanhan, W., Tsuneyoshi, H., Nishina, T., Matsuoka, S., Ikeda, T., & Komeda, M. (2007). Determination of optimal duration of mechanical unloading for failing hearts to achieve bridge to recovery in a rat heterotopic heart transplantation model. *J Heart Lung Transplant, 26*(1), 16-23. doi:10.1016/j.healun.2006.10.016

Ostrowski, S. R., Pedersen, S. H., Jensen, J. S., Mogelvang, R., & Johansson, P. I. (2013). Acute myocardial infarction is associated with endothelial glycocalyx and cell damage and a parallel increase in circulating catecholamines. *Crit Care, 17*(1), R32. doi:10.1186/cc12532

Palao, T., Medzikovic, L., Rippe, C., Wanga, S., Al-Mardini, C., van Weert, A., . . . Bakker, E. N. (2018). Thrombospondin-4 mediates cardiovascular remodelling in angiotensin II-induced hypertension. *Cardiovasc Pathol, 35*, 12-19. doi:10.1016/j.carpath.2018.03.003

Palis, J., Robertson, S., Kennedy, M., Wall, C., & Keller, G. (1999). Development of erythroid and myeloid progenitors in the yolk sac and embryo proper of the mouse. *Development, 126*(22), 5073-5084.

Palis, J., & Yoder, M. C. (2001). Yolk-sac hematopoiesis: the first blood cells of mouse and man. *Exp Hematol, 29*(8), 927-936. doi:10.1016/s0301-472x(01)00669-5

Panek, A. N., Posch, M. G., Alenina, N., Ghadge, S. K., Erdmann, B., Popova, E., . . . Ozcelik, C. (2009). Connective tissue growth factor overexpression in cardiomyocytes promotes cardiac hypertrophy and protection against pressure overload. *PLoS One, 4*(8), e6743. doi:10.1371/journal.pone.0006743

Parisi, M. S., Gazzerro, E., Rydziel, S., & Canalis, E. (2006). Expression and regulation of CCN genes in murine osteoblasts. *Bone, 38*(5), 671-677. doi:10.1016/j.bone.2005.10.005

Park, C. B., & Larsson, N. G. (2011). Mitochondrial DNA mutations in disease and aging. *J Cell Biol, 193*(5), 809-818. doi:10.1083/jcb.201010024

Patel, N. R., Bole, M., Chen, C., Hardin, C. C., Kho, A. T., Mih, J., . . . Koziel, H. (2012). Cell elasticity determines macrophage function. *PLoS One, 7*(9), e41024. doi:10.1371/journal.pone.0041024

Pauwels, A. M., Trost, M., Beyaert, R., & Hoffmann, E. (2017). Patterns, Receptors, and Signals: Regulation of Phagosome Maturation. *Trends Immunol, 38*(6), 407-422. doi:10.1016/j.it.2017.03.006

Pedersen, W. A., Wan, R., & Mattson, M. P. (2001). Impact of aging on stress-responsive neuroendocrine systems. *Mech Ageing Dev, 122*(9), 963-983. doi:10.1016/s0047-6374(01)00250-0

Pfister, R. R., & Haddox, J. L. (1996). A neutrophil chemoattractant is released from cellular and extracellular components of the alkali-degraded cornea and blood. *Invest Ophthalmol Vis Sci, 37*(1), 230-237.

Phillip, J. M., Aifuwa, I., Walston, J., & Wirtz, D. (2015). The Mechanobiology of Aging. *Annu Rev Biomed Eng, 17*, 113-141. doi:10.1146/annurev-bioeng-071114-040829

Pinkert, M. A., Hortensius, R. A., Ogle, B. M., & Eliceiri, K. W. (2018). Imaging the Cardiac Extracellular Matrix. *Adv Exp Med Biol, 1098*, 21-44. doi:10.1007/978-3-319-97421-7_2

Pinsky, D. J., Liao, H., Lawson, C. A., Yan, S. F., Chen, J., Carmeliet, P., . . . Stern, D. M. (1998). Coordinated induction of plasminogen activator inhibitor-1 (PAI-1) and inhibition of plasminogen activator gene expression by hypoxia promotes pulmonary vascular fibrin deposition. *J Clin Invest, 102*(5), 919-928. doi:10.1172/JCI307

Pinto, A. R., Godwin, J. W., Chandran, A., Hersey, L., Ilinykh, A., Debuque, R., . . . Rosenthal, N. A. (2014). Age-related changes in tissue macrophages precede cardiac functional impairment. *Aging (Albany NY), 6*(5), 399-413. doi:10.18632/aging.100669

Porrello, E. R., Mahmoud, A. I., Simpson, E., Hill, J. A., Richardson, J. A., Olson, E. N., & Sadek, H. A. (2011). Transient regenerative potential of the neonatal mouse heart. *Science, 331*(6020), 1078-1080. doi:10.1126/science.1200708

Powers, E. T., Morimoto, R. I., Dillin, A., Kelly, J. W., & Balch, W. E. (2009). Biological and chemical approaches to diseases of proteostasis deficiency. *Annu Rev Biochem, 78*, 959-991. doi:10.1146/annurev.biochem.052308.114844

Previtera, M. L., & Sengupta, A. (2015). Substrate Stiffness Regulates Proinflammatory Mediator Production through TLR4 Activity in Macrophages. *PLoS One, 10*(12), e0145813. doi:10.1371/journal.pone.0145813

Puchner, A., Saferding, V., Bonelli, M., Mikami, Y., Hofmann, M., Brunner, J. S., . . . Bluml, S. (2018). Non-classical monocytes as mediators of tissue destruction in arthritis. *Ann Rheum Dis, 77*(10), 1490-1497. doi:10.1136/annrheumdis-2018-213250

Pugin, J., Dunn, I., Jolliet, P., Tassaux, D., Magnenat, J. L., Nicod, L. P., & Chevrolet, J. C. (1998). Activation of human macrophages by mechanical ventilation in vitro. *Am J Physiol, 275*(6), L1040-1050. doi:10.1152/ajplung.1998.275.6.L1040

Rani, S., Barbe, M. F., Barr, A. E., & Litivn, J. (2010). Role of TNF alpha and PLF in bone remodeling in a rat model of repetitive reaching and grasping. *J Cell Physiol, 225*(1), 152-167. doi:10.1002/jcp.22208

Rath, M., Muller, I., Kropf, P., Closs, E. I., & Munder, M. (2014). Metabolism via Arginase or Nitric Oxide Synthase: Two Competing Arginine Pathways in Macrophages. *Front Immunol, 5*, 532. doi:10.3389/fimmu.2014.00532

Redfern, C. H., Degtyarev, M. Y., Kwa, A. T., Salomonis, N., Cotte, N., Nanevicz, T., . . . Conklin, B. R. (2000). Conditional expression of a Gi-coupled receptor causes ventricular conduction delay and a lethal cardiomyopathy. *Proc Natl Acad Sci U S A, 97*(9), 4826-4831. doi:10.1073/pnas.97.9.4826

Reed, M. J., & Sage, E. H. (1996). SPARC and the extracellular matrix: implications for cancer and wound repair. *Curr Top Microbiol Immunol, 213 (Pt 1)*, 81-94. doi:10.1007/978-3-642-61107-0_6

Refai, A. K., Textor, M., Brunette, D. M., & Waterfield, J. D. (2004). Effect of titanium surface topography on macrophage activation and secretion of proinflammatory cytokines and chemokines. *J Biomed Mater Res A, 70*(2), 194-205. doi:10.1002/jbm.a.30075

Ricard-Blum, S., & Vallet, S. D. (2017). Fragments generated upon extracellular matrix remodeling: Biological regulators and potential drugs. *Matrix Biol*. doi:10.1016/j.matbio.2017.11.005

Riley, H. J., Kelly, R. R., Van Laer, A. O., Neff, L. S., Dasgupta, S., Baicu, C. F., . . . Bradshaw, A. D. (2021). SPARC production by bone marrow-derived cells contributes to myocardial fibrosis in pressure overload. *Am J Physiol Heart Circ Physiol, 320*(2), H604-H612. doi:10.1152/ajpheart.00552.2020

Riser, B. L., Najmabadi, F., Perbal, B., Peterson, D. R., Rambow, J. A., Riser, M. L., . . . Riser, S. C. (2009). CCN3 (NOV) is a negative regulator of CCN2 (CTGF) and a novel endogenous

inhibitor of the fibrotic pathway in an in vitro model of renal disease. *Am J Pathol, 174*(5), 1725-1734. doi:10.2353/ajpath.2009.080241

Ristow, M., & Schmeisser, S. (2011). Extending life span by increasing oxidative stress. *Free Radic Biol Med, 51*(2), 327-336. doi:10.1016/j.freeradbiomed.2011.05.010

Rodriguez-Manzaneque, J. C., Lane, T. F., Ortega, M. A., Hynes, R. O., Lawler, J., & Iruela-Arispe, M. L. (2001). Thrombospondin-1 suppresses spontaneous tumor growth and inhibits activation of matrix metalloproteinase-9 and mobilization of vascular endothelial growth factor. *Proc Natl Acad Sci U S A, 98*(22), 12485-12490. doi:10.1073/pnas.171460498

Rodriguez-Vita, J., Ruiz-Ortega, M., Ruperez, M., Esteban, V., Sanchez-Lopez, E., Plaza, J. J., & Egido, J. (2005). Endothelin-1, via ETA receptor and independently of transforming growth factor-beta, increases the connective tissue growth factor in vascular smooth muscle cells. *Circ Res, 97*(2), 125-134. doi:10.1161/01.RES.0000174614.74469.83

Ross, R. S., & Borg, T. K. (2001). Integrins and the myocardium. *Circ Res, 88*(11), 1112-1119. doi:10.1161/hh1101.091862

Rossi, D. J., Bryder, D., Seita, J., Nussenzweig, A., Hoeijmakers, J., & Weissman, I. L. (2007). Deficiencies in DNA damage repair limit the function of haematopoietic stem cells with age. *Nature, 447*(7145), 725-729. doi:10.1038/nature05862

Rother, M., Krohn, S., Kania, G., Vanhoutte, D., Eisenreich, A., Wang, X., . . . Poller, W. (2010). Matricellular signaling molecule CCN1 attenuates experimental autoimmune myocarditis by acting as a novel immune cell migration modulator. *Circulation, 122*(25), 2688-2698. doi:10.1161/CIRCULATIONAHA.110.945261

Rubinsztein, D. C., Marino, G., & Kroemer, G. (2011). Autophagy and aging. *Cell, 146*(5), 682-695. doi:10.1016/j.cell.2011.07.030

Russell, S. J., & Kahn, C. R. (2007). Endocrine regulation of ageing. *Nat Rev Mol Cell Biol, 8*(9), 681-691. doi:10.1038/nrm2234

Sage, H., Vernon, R. B., Decker, J., Funk, S., & Iruela-Arispe, M. L. (1989). Distribution of the calcium-binding protein SPARC in tissues of embryonic and adult mice. *J Histochem Cytochem, 37*(6), 819-829. doi:10.1177/37.6.2723400

Saili, K. S., Zurlinden, T. J., Schwab, A. J., Silvin, A., Baker, N. C., Hunter, E. S., 3rd, . . . Knudsen, T. B. (2017). Blood-brain barrier development: Systems modeling and predictive toxicology. *Birth Defects Res, 109*(20), 1680-1710. doi:10.1002/bdr2.1180

Sakamoto, S., Yokoyama, M., Aoki, M., Suzuki, K., Kakehi, Y., & Saito, Y. (2004). Induction and function of CYR61 (CCN1) in prostatic stromal and epithelial cells: CYR61 is required for prostatic cell proliferation. *Prostate, 61*(4), 305-317. doi:10.1002/pros.20098

Salminen, A., Kaarniranta, K., & Kauppinen, A. (2012). Inflammaging: disturbed interplay between autophagy and inflammasomes. *Aging (Albany NY), 4*(3), 166-175. doi:10.18632/aging.100444

Sanders, J. E., Bale, S. D., & Neumann, T. (2002). Tissue response to microfibers of different polymers: polyester, polyethylene, polylactic acid, and polyurethane. *J Biomed Mater Res, 62*(2), 222-227. doi:10.1002/jbm.10285

Sasaki, T., Hohenester, E., Gohring, W., & Timpl, R. (1998). Crystal structure and mapping by site-directed mutagenesis of the collagen-binding epitope of an activated form of BM-40/SPARC/osteonectin. *EMBO J, 17*(6), 1625-1634. doi:10.1093/emboj/17.6.1625

Sato, I., & Shimada, K. (2001). Quantitative analysis of tenascin in chordae tendineae of human left ventricular papillary muscle with aging. *Ann Anat, 183*(5), 443-448. doi:10.1016/S0940-9602(01)80202-8

Sawai, C. M., Babovic, S., Upadhaya, S., Knapp, D., Lavin, Y., Lau, C. M., . . . Reizis, B. (2016). Hematopoietic Stem Cells Are the Major Source of Multilineage Hematopoiesis in Adult Animals. *Immunity, 45*(3), 597-609. doi:10.1016/j.immuni.2016.08.007

Scatena, M., Liaw, L., & Giachelli, C. M. (2007). Osteopontin: a multifunctional molecule regulating chronic inflammation and vascular disease. *Arterioscler Thromb Vasc Biol, 27*(11), 2302-2309. doi:10.1161/ATVBAHA.107.144824

Schellings, M. W., Vanhoutte, D., van Almen, G. C., Swinnen, M., Leenders, J. J., Kubben, N., . . . Pinto, Y. M. (2010). Syndecan-1 amplifies angiotensin II-induced cardiac fibrosis. *Hypertension, 55*(2), 249-256. doi:10.1161/HYPERTENSIONAHA.109.137885

Schulman, S. P., Lakatta, E. G., Fleg, J. L., Lakatta, L., Becker, L. C., & Gerstenblith, G. (1992). Age-related decline in left ventricular filling at rest and exercise. *Am J Physiol, 263*(6 Pt 2), H1932-1938. doi:10.1152/ajpheart.1992.263.6.H1932

Schultz-Cherry, S., & Murphy-Ullrich, J. E. (1993). Thrombospondin causes activation of latent transforming growth factor-beta secreted by endothelial cells by a novel mechanism. *J Cell Biol, 122*(4), 923-932. doi:10.1083/jcb.122.4.923

Scott, C. L., Zheng, F., De Baetselier, P., Martens, L., Saeys, Y., De Prijck, S., . . . Guilliams, M. (2016). Bone marrow-derived monocytes give rise to self-renewing and fully differentiated Kupffer cells. *Nat Commun, 7*, 10321. doi:10.1038/ncomms10321

Senior, R. M., Griffin, G. L., Mecham, R. P., Wrenn, D. S., Prasad, K. U., & Urry, D. W. (1984). Val-Gly-Val-Ala-Pro-Gly, a repeating peptide in elastin, is chemotactic for fibroblasts and monocytes. *J Cell Biol, 99*(3), 870-874. doi:10.1083/jcb.99.3.870

Sharma, K., & Kass, D. A. (2014). Heart failure with preserved ejection fraction: mechanisms, clinical features, and therapies. *Circ Res, 115*(1), 79-96. doi:10.1161/CIRCRESAHA.115.302922

Sharma, U. C., Pokharel, S., van Brakel, T. J., van Berlo, J. H., Cleutjens, J. P., Schroen, B., . . . Pinto, Y. M. (2004). Galectin-3 marks activated macrophages in failure-prone hypertrophied hearts and contributes to cardiac dysfunction. *Circulation, 110*(19), 3121-3128. doi:10.1161/01.CIR.0000147181.65298.4D

Sheng, J., Ruedl, C., & Karjalainen, K. (2015). Most Tissue-Resident Macrophages Except Microglia Are Derived from Fetal Hematopoietic Stem Cells. *Immunity, 43*(2), 382-393. doi:10.1016/j.immuni.2015.07.016

Shi-wen, X., Stanton, L. A., Kennedy, L., Pala, D., Chen, Y., Howat, S. L., . . . Leask, A. (2006). CCN2 is necessary for adhesive responses to transforming growth factor-beta1 in embryonic fibroblasts. *J Biol Chem, 281*(16), 10715-10726. doi:10.1074/jbc.M511343200

Shirazi, L. F., Bissett, J., Romeo, F., & Mehta, J. L. (2017). Role of Inflammation in Heart Failure. *Curr Atheroscler Rep, 19*(6), 27. doi:10.1007/s11883-017-0660-3

Sica, A., Erreni, M., Allavena, P., & Porta, C. (2015). Macrophage polarization in pathology. *Cell Mol Life Sci, 72*(21), 4111-4126. doi:10.1007/s00018-015-1995-y

Sicari, B. M., Johnson, S. A., Siu, B. F., Crapo, P. M., Daly, K. A., Jiang, H., . . . Badylak, S. F. (2012). The effect of source animal age upon the in vivo remodeling characteristics of an extracellular matrix scaffold. *Biomaterials, 33*(22), 5524-5533. doi:10.1016/j.biomaterials.2012.04.017

Silver, M. A., Pick, R., Brilla, C. G., Jalil, J. E., Janicki, J. S., & Weber, K. T. (1990). Reactive and reparative fibrillar collagen remodelling in the hypertrophied rat left ventricle: two experimental models of myocardial fibrosis. *Cardiovasc Res, 24*(9), 741-747. doi:10.1093/cvr/24.9.741

Singh, K., Sirokman, G., Communal, C., Robinson, K. G., Conrad, C. H., Brooks, W. W., . . . Colucci, W. S. (1999). Myocardial osteopontin expression coincides with the development of heart failure. *Hypertension, 33*(2), 663-670. doi:10.1161/01.hyp.33.2.663

Singh, M., Foster, C. R., Dalal, S., & Singh, K. (2010). Osteopontin: role in extracellular matrix deposition and myocardial remodeling post-MI. *J Mol Cell Cardiol, 48*(3), 538-543. doi:10.1016/j.yjmcc.2009.06.015

Skurk, T., Lee, Y. M., & Hauner, H. (2001). Angiotensin II and its metabolites stimulate PAI-1 protein release from human adipocytes in primary culture. *Hypertension, 37*(5), 1336-1340. doi:10.1161/01.hyp.37.5.1336

Snider, P., Hinton, R. B., Moreno-Rodriguez, R. A., Wang, J., Rogers, R., Lindsley, A., . . . Conway, S. J. (2008). Periostin is required for maturation and extracellular matrix stabilization of noncardiomyocyte lineages of the heart. *Circ Res, 102*(7), 752-760. doi:10.1161/CIRCRESAHA.107.159517

Socha, M. J., Manhiani, M., Said, N., Imig, J. D., & Motamed, K. (2007). Secreted protein acidic and rich in cysteine deficiency ameliorates renal inflammation and fibrosis in angiotensin hypertension. *Am J Pathol, 171*(4), 1104-1112. doi:10.2353/ajpath.2007.061273

Soon, L. L., Yie, T. A., Shvarts, A., Levine, A. J., Su, F., & Tchou-Wong, K. M. (2003). Overexpression of WISP-1 down-regulated motility and invasion of lung cancer cells through inhibition of Rac activation. *J Biol Chem, 278*(13), 11465-11470. doi:10.1074/jbc.M210945200

Sridharan, R., Cavanagh, B., Cameron, A. R., Kelly, D. J., & O'Brien, F. J. (2019). Material stiffness influences the polarization state, function and migration mode of macrophages. *Acta Biomater, 89*, 47-59. doi:10.1016/j.actbio.2019.02.048

Stansfield, W. E., Andersen, N. M., Tang, R. H., & Selzman, C. H. (2009). Periostin is a novel factor in cardiac remodeling after experimental and clinical unloading of the failing heart. *Ann Thorac Surg, 88*(6), 1916-1921. doi:10.1016/j.athoracsur.2009.07.038

Strait, J. B., & Lakatta, E. G. (2012). Aging-associated cardiovascular changes and their relationship to heart failure. *Heart Fail Clin, 8*(1), 143-164. doi:10.1016/j.hfc.2011.08.011

Strandjord, T. P., Madtes, D. K., Weiss, D. J., & Sage, E. H. (1999). Collagen accumulation is decreased in SPARC-null mice with bleomycin-induced pulmonary fibrosis. *Am J Physiol, 277*(3), L628-635. doi:10.1152/ajplung.1999.277.3.L628

Sugiura, T., Takamatsu, H., Kudo, A., & Amann, E. (1995). Expression and characterization of murine osteoblast-specific factor 2 (OSF-2) in a baculovirus expression system. *Protein Expr Purif, 6*(3), 305-311. doi:10.1006/prep.1995.1040

Sundblad, V., Croci, D. O., & Rabinovich, G. A. (2011). Regulated expression of galectin-3, a multifunctional glycan-binding protein, in haematopoietic and non-haematopoietic tissues. *Histol Histopathol, 26*(2), 247-265. doi:10.14670/HH-26.247

Suthahar, N., Meijers, W. C., Sillje, H. H. W., Ho, J. E., Liu, F. T., & de Boer, R. A. (2018). Galectin-3 Activation and Inhibition in Heart Failure and Cardiovascular Disease: An Update. *Theranostics, 8*(3), 593-609. doi:10.7150/thno.22196

Suzuki, H., Amizuka, N., Kii, I., Kawano, Y., Nozawa-Inoue, K., Suzuki, A., . . . Maeda, T. (2004). Immunohistochemical localization of periostin in tooth and its surrounding tissues in mouse mandibles during development. *Anat Rec A Discov Mol Cell Evol Biol, 281*(2), 1264-1275. doi:10.1002/ar.a.20080

Takayama, G., Arima, K., Kanaji, T., Toda, S., Tanaka, H., Shoji, S., . . . Izuhara, K. (2006). Periostin: a novel component of subepithelial fibrosis of bronchial asthma downstream of IL-4 and IL-13 signals. *J Allergy Clin Immunol, 118*(1), 98-104. doi:10.1016/j.jaci.2006.02.046

Talens, R. P., Christensen, K., Putter, H., Willemsen, G., Christiansen, L., Kremer, D., . . . Heijmans, B. T. (2012). Epigenetic variation during the adult lifespan: cross-sectional and

longitudinal data on monozygotic twin pairs. *Aging Cell, 11*(4), 694-703. doi:10.1111/j.1474-9726.2012.00835.x

Tanaka, K., Wilson, R. M., Essick, E. E., Duffen, J. L., Scherer, P. E., Ouchi, N., & Sam, F. (2014). Effects of adiponectin on calcium-handling proteins in heart failure with preserved ejection fraction. *Circ Heart Fail, 7*(6), 976-985. doi:10.1161/CIRCHEARTFAILURE.114.001279

Tanaka, Y., Hoshino-Negishi, K., Kuboi, Y., Tago, F., Yasuda, N., & Imai, T. (2020). Emerging Role of Fractalkine in the Treatment of Rheumatic Diseases. *Immunotargets Ther, 9*, 241-253. doi:10.2147/ITT.S277991

Tatar, M., Bartke, A., & Antebi, A. (2003). The endocrine regulation of aging by insulin-like signals. *Science, 299*(5611), 1346-1351. doi:10.1126/science.1081447

Teekakirikul, P., Eminaga, S., Toka, O., Alcalai, R., Wang, L., Wakimoto, H., . . . Seidman, J. G. (2010). Cardiac fibrosis in mice with hypertrophic cardiomyopathy is mediated by non-myocyte proliferation and requires Tgf-beta. *J Clin Invest, 120*(10), 3520-3529. doi:10.1172/JCI42028

Tober, J., Koniski, A., McGrath, K. E., Vemishetti, R., Emerson, R., de Mesy-Bentley, K. K., . . . Palis, J. (2007). The megakaryocyte lineage originates from hemangioblast precursors and is an integral component both of primitive and of definitive hematopoiesis. *Blood, 109*(4), 1433-1441. doi:10.1182/blood-2006-06-031898

Tomaru, U., Takahashi, S., Ishizu, A., Miyatake, Y., Gohda, A., Suzuki, S., . . . Kasahara, M. (2012). Decreased proteasomal activity causes age-related phenotypes and promotes the development of metabolic abnormalities. *Am J Pathol, 180*(3), 963-972. doi:10.1016/j.ajpath.2011.11.012

Torre-Amione, G., Stetson, S. J., Youker, K. A., Durand, J. B., Radovancevic, B., Delgado, R. M., . . . Noon, G. P. (1999). Decreased expression of tumor necrosis factor-alpha in failing human myocardium after mechanical circulatory support : A potential mechanism for cardiac recovery. *Circulation, 100*(11), 1189-1193. doi:10.1161/01.cir.100.11.1189

Triantafyllopoulou, A., Franzke, C. W., Seshan, S. V., Perino, G., Kalliolias, G. D., Ramanujam, M., . . . Ivashkiv, L. B. (2010). Proliferative lesions and metalloproteinase activity in murine lupus nephritis mediated by type I interferons and macrophages. *Proc Natl Acad Sci U S A, 107*(7), 3012-3017. doi:10.1073/pnas.0914902107

Trueblood, N. A., Xie, Z., Communal, C., Sam, F., Ngoy, S., Liaw, L., . . . Singh, K. (2001). Exaggerated left ventricular dilation and reduced collagen deposition after myocardial infarction in mice lacking osteopontin. *Circ Res, 88*(10), 1080-1087. doi:10.1161/hh1001.090842

Truett, J., Cornfield, J., & Kannel, W. (1967). A multivariate analysis of the risk of coronary heart disease in Framingham. *J Chronic Dis, 20*(7), 511-524. doi:10.1016/0021-9681(67)90082-3

Tucker, R. P., & Chiquet-Ehrismann, R. (2009). The regulation of tenascin expression by tissue microenvironments. *Biochim Biophys Acta, 1793*(5), 888-892. doi:10.1016/j.bbamcr.2008.12.012

Uchida, Y., Ohba, K., Yoshioka, T., Irie, K., Muraki, T., & Maru, Y. (2004). Cellular carbonyl stress enhances the expression of plasminogen activator inhibitor-1 in rat white adipocytes via reactive oxygen species-dependent pathway. *J Biol Chem, 279*(6), 4075-4083. doi:10.1074/jbc.M304222200

Usher, M. G., Duan, S. Z., Ivaschenko, C. Y., Frieler, R. A., Berger, S., Schutz, G., . . . Mortensen, R. M. (2010). Myeloid mineralocorticoid receptor controls macrophage polarization and cardiovascular hypertrophy and remodeling in mice. *J Clin Invest, 120*(9), 3350-3364. doi:10.1172/JCI41080

Vadon-Le Goff, S., Hulmes, D. J., & Moali, C. (2015). BMP-1/tolloid-like proteinases synchronize matrix assembly with growth factor activation to promote morphogenesis and tissue remodeling. *Matrix Biol, 44-46*, 14-23. doi:10.1016/j.matbio.2015.02.006

Valero-Munoz, M., Li, S., Wilson, R. M., Hulsmans, M., Aprahamian, T., Fuster, J. J., . . . Sam, F. (2016). Heart Failure With Preserved Ejection Fraction Induces Beiging in Adipose Tissue. *Circ Heart Fail, 9*(1), e002724. doi:10.1161/CIRCHEARTFAILURE.115.002724

van de Laar, L., Saelens, W., De Prijck, S., Martens, L., Scott, C. L., Van Isterdael, G., . . . Guilliams, M. (2016). Yolk Sac Macrophages, Fetal Liver, and Adult Monocytes Can Colonize an Empty Niche and Develop into Functional Tissue-Resident Macrophages. *Immunity, 44*(4), 755-768. doi:10.1016/j.immuni.2016.02.017

van den Heuvel, A. F., van Veldhuisen, D. J., van der Wall, E. E., Blanksma, P. K., Siebelink, H. M., Vaalburg, W. M., . . . Crijns, H. J. (2000). Regional myocardial blood flow reserve impairment and metabolic changes suggesting myocardial ischemia in patients with idiopathic dilated cardiomyopathy. *J Am Coll Cardiol, 35*(1), 19-28. doi:10.1016/s0735-1097(99)00499-4

van der Poll, T., Levi, M., Buller, H. R., van Deventer, S. J., de Boer, J. P., Hack, C. E., & ten Cate, J. W. (1991). Fibrinolytic response to tumor necrosis factor in healthy subjects. *J Exp Med, 174*(3), 729-732. doi:10.1084/jem.174.3.729

van Furth, R., Cohn, Z. A., Hirsch, J. G., Humphrey, J. H., Spector, W. G., & Langevoort, H. L. (1972). The mononuclear phagocyte system: a new classification of macrophages, monocytes, and their precursor cells. *Bull World Health Organ, 46*(6), 845-852.

Van Goethem, E., Poincloux, R., Gauffre, F., Maridonneau-Parini, I., & Le Cabec, V. (2010). Matrix architecture dictates three-dimensional migration modes of human macrophages: differential involvement of proteases and podosome-like structures. *J Immunol, 184*(2), 1049-1061. doi:10.4049/jimmunol.0902223

Vanhoutte, D., Schellings, M. W., Gotte, M., Swinnen, M., Herias, V., Wild, M. K., . . . Heymans, S. (2007). Increased expression of syndecan-1 protects against cardiac dilatation and

dysfunction after myocardial infarction. *Circulation, 115*(4), 475-482. doi:10.1161/CIRCULATIONAHA.106.644609

Volpert, O. V., Tolsma, S. S., Pellerin, S., Feige, J. J., Chen, H., Mosher, D. F., & Bouck, N. (1995). Inhibition of angiogenesis by thrombospondin-2. *Biochem Biophys Res Commun, 217*(1), 326-332. doi:10.1006/bbrc.1995.2780

Wang, D., Oparil, S., Feng, J. A., Li, P., Perry, G., Chen, L. B., . . . Chen, Y. F. (2003). Effects of pressure overload on extracellular matrix expression in the heart of the atrial natriuretic peptide-null mouse. *Hypertension, 42*(1), 88-95. doi:10.1161/01.HYP.0000074905.22908.A6

Wang, K. X., & Denhardt, D. T. (2008). Osteopontin: role in immune regulation and stress responses. *Cytokine Growth Factor Rev, 19*(5-6), 333-345. doi:10.1016/j.cytogfr.2008.08.001

Weber, K. T., Sun, Y., Bhattacharya, S. K., Ahokas, R. A., & Gerling, I. C. (2013). Myofibroblast-mediated mechanisms of pathological remodelling of the heart. *Nat Rev Cardiol, 10*(1), 15-26. doi:10.1038/nrcardio.2012.158

Wehner, S., Buchholz, B. M., Schuchtrup, S., Rocke, A., Schaefer, N., Lysson, M., . . . Kalff, J. C. (2010). Mechanical strain and TLR4 synergistically induce cell-specific inflammatory gene expression in intestinal smooth muscle cells and peritoneal macrophages. *Am J Physiol Gastrointest Liver Physiol, 299*(5), G1187-1197. doi:10.1152/ajpgi.00452.2009

Weisberg, A. D., Albornoz, F., Griffin, J. P., Crandall, D. L., Elokdah, H., Fogo, A. B., . . . Brown, N. J. (2005). Pharmacological inhibition and genetic deficiency of plasminogen activator inhibitor-1 attenuates angiotensin II/salt-induced aortic remodeling. *Arterioscler Thromb Vasc Biol, 25*(2), 365-371. doi:10.1161/01.ATV.0000152356.85791.52

Wenstrup, R. J., Florer, J. B., Davidson, J. M., Phillips, C. L., Pfeiffer, B. J., Menezes, D. W., . . . Birk, D. E. (2006). Murine model of the Ehlers-Danlos syndrome. col5a1 haploinsufficiency disrupts collagen fibril assembly at multiple stages. *J Biol Chem, 281*(18), 12888-12895. doi:10.1074/jbc.M511528200

Williams, C., Quinn, K. P., Georgakoudi, I., & Black, L. D., 3rd. (2014). Young developmental age cardiac extracellular matrix promotes the expansion of neonatal cardiomyocytes in vitro. *Acta Biomater, 10*(1), 194-204. doi:10.1016/j.actbio.2013.08.037

Williams, C., Sullivan, K., & Black, L. D., 3rd. (2015). Partially Digested Adult Cardiac Extracellular Matrix Promotes Cardiomyocyte Proliferation In Vitro. *Adv Healthc Mater, 4*(10), 1545-1554. doi:10.1002/adhm.201500035

Wilson, R. M., De Silva, D. S., Sato, K., Izumiya, Y., & Sam, F. (2009). Effects of fixed-dose isosorbide dinitrate/hydralazine on diastolic function and exercise capacity in hypertension-induced diastolic heart failure. *Hypertension, 54*(3), 583-590. doi:10.1161/HYPERTENSIONAHA.109.134932

Wohlschlaeger, J., Levkau, B., Brockhoff, G., Schmitz, K. J., von Winterfeld, M., Takeda, A., . . . Baba, H. A. (2010). Hemodynamic support by left ventricular assist devices reduces cardiomyocyte DNA content in the failing human heart. *Circulation, 121*(8), 989-996. doi:10.1161/CIRCULATIONAHA.108.808071

Wolf, M. T., Daly, K. A., Reing, J. E., & Badylak, S. F. (2012). Biologic scaffold composed of skeletal muscle extracellular matrix. *Biomaterials, 33*(10), 2916-2925. doi:10.1016/j.biomaterials.2011.12.055

Woods, A. (2001). Syndecans: transmembrane modulators of adhesion and matrix assembly. *J Clin Invest, 107*(8), 935-941. doi:10.1172/JCI12802

Wunderlich, K., Senn, B. C., Todesco, L., Flammer, J., & Meyer, P. (2000). Regulation of connective tissue growth factor gene expression in retinal vascular endothelial cells by angiogenic growth factors. *Graefes Arch Clin Exp Ophthalmol, 238*(11), 910-915. doi:10.1007/s004170000199

Xie, Z., Singh, M., & Singh, K. (2004). Osteopontin modulates myocardial hypertrophy in response to chronic pressure overload in mice. *Hypertension, 44*(6), 826-831. doi:10.1161/01.HYP.0000148458.03202.48

Xu, B., & Daimon, M. (2016). Cardiac aging phenomenon and its clinical features by echocardiography. *J Echocardiogr, 14*(4), 139-145. doi:10.1007/s12574-016-0292-6

Yamamoto, K., & Loskutoff, D. J. (1996). Fibrin deposition in tissues from endotoxin-treated mice correlates with decreases in the expression of urokinase-type but not tissue-type plasminogen activator. *J Clin Invest, 97*(11), 2440-2451. doi:10.1172/JCI118691

Yan, Q., Clark, J. I., Wight, T. N., & Sage, E. H. (2002). Alterations in the lens capsule contribute to cataractogenesis in SPARC-null mice. *J Cell Sci, 115*(Pt 13), 2747-2756.

Yang, J. H., Sakamoto, H., Xu, E. C., & Lee, R. T. (2000). Biomechanical regulation of human monocyte/macrophage molecular function. *Am J Pathol, 156*(5), 1797-1804. doi:10.1016/S0002-9440(10)65051-1

Yoon, P. O., Lee, M. A., Cha, H., Jeong, M. H., Kim, J., Jang, S. P., . . . Park, W. J. (2010). The opposing effects of CCN2 and CCN5 on the development of cardiac hypertrophy and fibrosis. *J Mol Cell Cardiol, 49*(2), 294-303. doi:10.1016/j.yjmcc.2010.04.010

Yoshiba, N., Yoshiba, K., Hosoya, A., Saito, M., Yokoi, T., Okiji, T., . . . Ozawa, H. (2007). Association of TIMP-2 with extracellular matrix exposed to mechanical stress and its co-distribution with periostin during mouse mandible development. *Cell Tissue Res, 330*(1), 133-145. doi:10.1007/s00441-007-0439-x

Yoshida, Y., Togi, K., Matsumae, H., Nakashima, Y., Kojima, Y., Yamamoto, H., . . . Tanaka, M. (2007). CCN1 protects cardiac myocytes from oxidative stress via beta1 integrin-Akt pathway. *Biochem Biophys Res Commun, 355*(3), 611-618. doi:10.1016/j.bbrc.2007.01.195

Yu, L., Ruifrok, W. P., Meissner, M., Bos, E. M., van Goor, H., Sanjabi, B., . . . de Boer, R. A. (2013). Genetic and pharmacological inhibition of galectin-3 prevents cardiac remodeling by interfering with myocardial fibrogenesis. *Circ Heart Fail, 6*(1), 107-117. doi:10.1161/CIRCHEARTFAILURE.112.971168

Zafeiridis, A., Jeevanandam, V., Houser, S. R., & Margulies, K. B. (1998). Regression of cellular hypertrophy after left ventricular assist device support. *Circulation, 98*(7), 656-662. doi:10.1161/01.cir.98.7.656

Zhang, G., Li, J., Purkayastha, S., Tang, Y., Zhang, H., Yin, Y., . . . Cai, D. (2013). Hypothalamic programming of systemic ageing involving IKK-beta, NF-kappaB and GnRH. *Nature, 497*(7448), 211-216. doi:10.1038/nature12143

Zhang, Y., Ikeno, Y., Qi, W., Chaudhuri, A., Li, Y., Bokov, A., . . . Van Remmen, H. (2009). Mice deficient in both Mn superoxide dismutase and glutathione peroxidase-1 have increased oxidative damage and a greater incidence of pathology but no reduction in longevity. *J Gerontol A Biol Sci Med Sci, 64*(12), 1212-1220. doi:10.1093/gerona/glp132

Zhu, W., Yu, J., Nie, Y., Shi, X., Liu, Y., Li, F., & Zhang, X. L. (2014). Disequilibrium of M1 and M2 macrophages correlates with the development of experimental inflammatory bowel diseases. *Immunol Invest, 43*(7), 638-652. doi:10.3109/08820139.2014.909456

Zorio, E., Gilabert-Estelles, J., Espana, F., Ramon, L. A., Cosin, R., & Estelles, A. (2008). Fibrinolysis: the key to new pathogenetic mechanisms. *Curr Med Chem, 15*(9), 923-929. doi:10.2174/092986708783955455